Final Report On:

Contract NASW-4336

A Study of Ion Composition and Dynamics at Comet Halley

Prepared by:
E.G. Shelley, Principal Investigator
and
S.A. Fuselier, Co-Investigator
March 31, 1991

Table of Contents

PRIMARY
117925

DQ 574450
BH 790295
L1535051
MQ 700802
ML 78950

P. 70

I. INTRODUCTION AND BACKGROUND

This report details the participation by Lockheed coinvestigators in the reduction, analysis, and interpretation of data obtained by the Ion Mass Spectrometer onboard the Giotto mission to Comet Halley. Lockheed's participation in the data analysis was in conjunction with the IMS science team consisting of members from The University of Bern, The Jet Propulsion Laboratory, Lockheed Palo Alto Research Laboratory, The Massachusetts Institute of Technology and The Max-Planck-Institute for Aeronomy. The data analysis activities and much of the scientific collaboration was shared by this team.

One objective of the effort under this contract was to use data obtained by the Giotto Ion Mass Spectrometer (IMS) during the encounter with comet Halley for the purpose of advancing our understanding of the chemistry and physics of the interaction of the solar wind with comets and obtaining new information on the comet's composition. An additional objective was to make this unique data set available in a format which can be easily used by the rest of the cometary science community for other analyses in the future.

The IMS has two sensors: the High Intensity Spectrometer (HIS) and the High Energy Range Spectrometer (HERS). HIS was designed for investigation of the large fluxes of 68 km/s (relative to the spacecraft) ions expected in the inner coma, whereas HERS was designed to observe much broader ranges of ion energy and direction of incidence. The conceptual design, laboratory testing, detailed design, and construction of HERS was accomplished largely with NASA funding, and the principal objective of the contracted effort was therefore the reduction and analysis of HERS data. Because HERS and HIS had complementary fields of view, joint studies based on both data sets have also been made. END

A. Instrument Description

A detailed description of the IMS has been published by Balsiger et al. (1986a). Only those features most relevant to the data analysis tasks that have been accomplished under this contract are reviewed here.

During each 4-second spin period of the Giotto spacecraft, HERS measured the 3-dimensional velocity distribution functions of ions in one of 4 mass ranges: protons (P mode), light ions (L mode) with mass/charge M/Q in the range 2-4 amu/e, medium ions (M mode) with M/Q = 11 to 26 amu/e, and heavy ions (H mode) with M/Q = 15 to 32 amu/e. During the last 10-

minutes of HERS operation each mode was measured for two spins. The energy range was 10 eV to an M/Q-dependent upper limit of 2.0 to 4.7 keV.

Both HERS and HIS had fan-shaped fields of view in planes which included the spacecraft spin axis (which was closely aligned with the velocity vector of the spacecraft relative to the comet). HERS did not view the ram direction, however; its polar (elevation angle) field of view extended from 15° to 75° from the spin/ram direction. The resolution in elevation was 15° for protons and 7.5° for all other ion species. The HERS azimuth angle resolution was 5.6°.

HIS comprised two separate analyzers: 1) a mass analyzer (MA) with a field of view which included the ram/spin direction and extended down to an elevation angle of 12° and 2) an angle analyzer (AA) with an elevation angle field of view which extended down to 22°. The MA did not measure angles, while the AA had 5° resolution in elevation and 22.5° resolution in azimuth. The AA measured ion energy/charge with 2.5% accuracy but did not distinguish M/Q. The time resolution of HIS was 4 s.

B. Summary of Observations

HERS was first turned on and checked out in space in early September, 1985. The spacecraft orientation and mission operations schedules allowed us to obtain about 20 5-hour intervals of solar-wind observations during cruise. At the Halley encounter, HERS was operated nearly continuously from 0530, March 12, until 0003, March 14, Spacecraft Event Time (SCET), when the experiment ceased to function due to damage by collision with cometary dust and associated disturbances of the spacecraft electrical system.

During the encounter, the IMS provided exciting new data concerning the chemistry and physics of ions at comet Halley. The initial investigation of the quick-look data led to a wide variety of discoveries which were summarized by Balsiger et al. (1986b).

C. Accomplishments, under previous data analysis contract NASW-3729

Since the previous Giotto contract concerned some of the early data analysis activities, we review here some of the accomplishments under that contract.

1. Calibration and Data Reduction

a. We created conveniently formatted data files on computers at JPL, LPARL, and MIT and wrote programs to read them efficiently.

b. We compiled a log book of all the HERS data, including identification of missing, bad or questionable data, and made several different types of survey plots and tabulations of the raw data.

c. We parameterized the background counting rates of the microchannel plate (MCP) and the channel electron multipliers (CEM).

d. We completed analysis of laboratory calibration data to allow more accurate velocity calculations.

e. We developed second-generation, but not final, algorithms for calculating phase space density from the raw data.

f. We developed computer codes, based on the second-generation algorithms, to perform the following operations:

i. Computing moments (i.e., density, velocity and temperature) of the ion distributions.

ii. Fitting simple models (e.g., a convected Maxwell-Boltzmann distribution function) to the data.

iii. Plotting "stacked" spectra.

iv. Plotting 2-dimensional contours of phase space densities in any azimuthal plane or on the surface of a cone swept cut by the field of view of any single detector or group of detectors.

v. Plotting time series of selected parameters.

vi. Calculating and plotting power spectral density of plasma parameters.

g. We created plots of several plasma parameters for selected time intervals at agreed-upon scales; these plots were exchanged with investigators working on other Giotto experiments.

h. We submitted the following data files for submission to NSSDC.:

Particles	Data Type	Time Resolution	Time Span
Protons	Moments	16 sec	Day 72 0523 to end
Protons	MB fit	10-min averages	Day 72 1902 to end
Alphas	Moments	16 sec	Day 72 0511 to end
Alphas	MB fit	10-min averages	Day 72 1902 to end
Other ions	Moments	128 sec	Day 72 2130 to end

2. Data Analysis

a. We compiled all available data on photoionization processes required for analyzing the ion mass spectrum in the M/Q = 24-50 amu/e range in terms of ion composition.

b. We analyzed the HIS data for the M/Q range 15-19 amu/e to deduce the amount of methane and ammonia in the parent gases of the comet.

c. We performed a preliminary survey and interpretation of the vector velocity profiles and distribution functions of different groups of ion species along the encounter trajectory.

d. We analyzed the pickup of cometary protons upstream of the Halley bow shock; we observed increased pitch-angle scattering, and increased radius and thickness of the shell of picked up protons as the shock was approached.

e. We analyzed the properties of an intense burst of very hot ions detected just inside the Halley contact surface and considered their possible origin.

f. We studied the density profile of He^+ ions in the inner coma and discovered that current models are incapable of explaining the amount of He^+ observed.

g. We studied the fine structure of the Halley bow shock and discovered that some plasma parameters change over a broad scale consistent with the gyroradius of picked-up heavy ions, whereas the solar-wind protons and alphas show evidence of a series of narrow subshocks. The observations are not well explained by state-of-the-art models.

h. We studied the foreshock region upstream of the bow shock; we found evidence of enhanced ion-flow fluctuations but no evidence for backstreaming protons, as observed in the Earth's foreshock region.

i. We developed a 1-dimensional model of the forces acting between the cometary ions, the cometary neutrals, and the cometary magnetic field that explains the profile of the magnetic field outside the magnetic cavity. A generalized Ohm's law that includes effects due to velocity differences between ions, neutrals, electrons was a result of this study.

j. We found preliminary evidence for the existence of pick-up H_2^+ ions in the vicinity of the comet.

II. ACCOMPLISHMENTS UNDER ANALYSIS CONTRACT NASW-4336

A. Calibration

At the close of the previous contract, we had accomplished significant scientific results using "first and of second generation" analysis codes. Many of the more important investigations we carried during this contract period out required accurate, quantitative analyses of the data based on the best possible knowledge of the instrument performance. We had to therefore substantially improve our present model of the HERS performance, which was based

on a simplified theoretical model of the instrument with some corrections to take account of the calibration data. The following effects were studied in great detail.

1. HERS mass spectra are constructed from the relative number of counts acquired by each of 40 mass anodes arranged behind a micro-channel plate (MCP) amplifier. We had not taken account of the non-uniformity in the MCP sensitivity and response. Because the angle of incidence and the energy with which ions hit the MCP depend on the ion mass and the instrument mode (P, L, M, or H), the calibration data were studied to find any systematic dependence of sensitivity on mass mode and anode number. It was found that there is no systematic dependence with mode within the uncertainties of the measurements. Also, the calibration data were used to test for a systematic dependence on sensitivity to atomic and molecular species. Again, no dependence was identified within the uncertainties of the measurements.

2. Three to five mass anodes contribute counts to each mass spectral peak. The calibration data show that the positions of the peaks have a weak dependence on elevation angle which had not yet been modeled. The shape of a mass peak depends on how closely it is centered on an anode or on an inter-anode gap. There are also dependences of peak width and shape on anode number (because the focussing properties of the analyzer change slightly as a function of position along the MCP. These latter dependences were crudely taken into account for the presentation of preliminary results, but more accurate and more quantitative modelling of these effects (some of which are quite large) was clearly required to enable accurate calculations of relative abundances. Both preflight calibration data and flight data were used to analyze and develop numerical models of these effects. We then developed a computer program to model the locations, shapes, and heights of mass peaks as a function of relative abundances and ion mass/charge, energy, and angle of incidence.

Understanding and correctly accounting for these effects was an arduous task. We believed, however, that it was possible to achieve satisfactory results through coordinated analyses of in-flight and calibration data with the aid of additional calibration runs on the flight spare unit to resolve any ambiguities or to help interpolate or extrapolate from the masses and energies at which the original calibration data were obtained. There were some internal consistency checks which were applied to ascertain if we had obtained a reasonably good model of the instrument. For example, the abundances and velocity distributions of the water group ions should be the same whether they are calculated from the M or H mode spectra. For some ions at

some energies and some directions it was also be possible to compare our results to simultaneous data acquired by other plasma instruments on Giotto. (Of course, each of them also has its own limited field of view and measurement uncertainties.)

The end result of this lengthy task can best be illustrated in Figure 1. This figure shows the water group ion distribution in the Comet Halley coma from the M mode. The shape of each peak was modeled using a modified gaussian of the form:

$$\text{Counts - Background} = A_i e^{-\left(\frac{x - x_i}{w_i}\right)^N}.$$

The peak center x_i, the peak width w_i, and the exponent N were all determined for each mass peak separately using calibration data. The flight data in Figure 1 were fit using the calibrated peak centers, widths, and exponents and allowing the amplitudes A_i to vary. It is clearly evident in Figure 1 that the fitting procedure provided excellent results and that the relative contributions of the water group ions to the total mass spectrum were well determined. Other intervals had different mixes of the various ions and for most intervals the fitting procedure was well behaved and provided good results. Thus, through the combination of calibration and flight data, we were able to determine the peak shapes of all major ions observed by IMS/HERS and therefore determine the relative mix of the various ion species for the entire HERS data set.

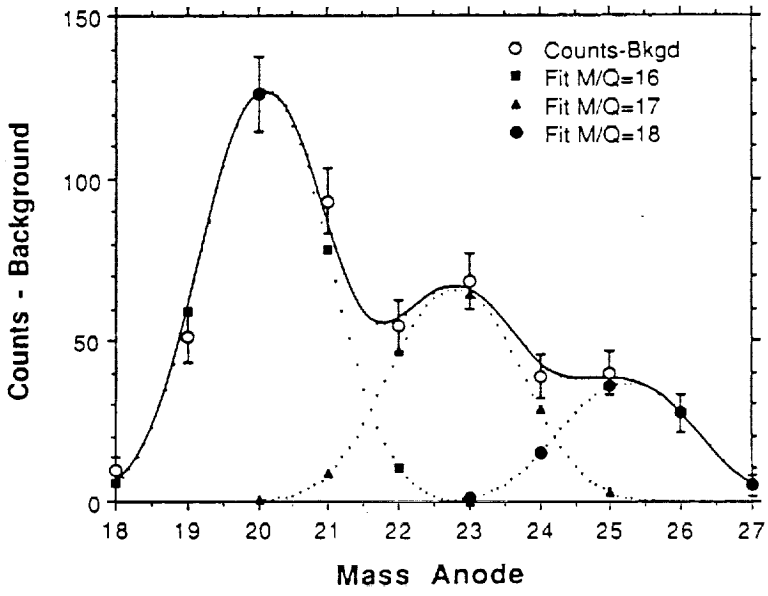

B. Moment Calculations

The improved understanding of the instrument performance discussed above allowed us to determine the relative mix of ions in the coma. To obtain absolute numbers, we modified our first and second generation moments code to take into account our better understanding of the instrument. The calculation of cometary ion moments from the HERS data proceeded as follows:

1. The data were summed over a sufficient number of spacecraft spins to obtain ~ 1000 counts of water-group ions (m/q = 16 to 18 amu/e, using both medium- and heavy-mode data). The lengths of these summation intervals ranged from 128 to 512 seconds, which corresponds to summing over 8 to 32 consecutive spectra for each instrument mode. The 4-kV upper limit of energy/charge and the background counting rates of its microchannel plate (MCP) sensor prevented HERS from detecting the pickup of heavier cometary ions until the spacecraft was ~250,000 km from the nucleus (~2300 SCET). A measurable flux of hot, cometary ions was then observed along the inbound Giotto trajectory until the spacecraft reached a distance of 40,000 km. For the elevation bin closest to the ram direction, the MCP had a "hot spot" at the position of anode 29, which resulted in a very high and very irregular background counting rate for that anode. For this reason, data from anode 29 were not used in the analysis.

2. The count-rate matrices were corrected for detector background counts. The background count-rate corrections, which depended on both elevation angle and mass anode, were determined by averaging several hours of data obtained earlier on the day of the comet encounter when the spacecraft was millions of km from the nucleus and HERS could detect only solar wind ions and picked-up cometary protons.

3. For each of the time intervals selected in Step 1, the vector velocity of the ions with m/q = 16-18 amu/e was obtained by finding the least-squares fit of the observed distribution to a spherically symmetric distribution in velocity space. This process corrected for those parts of the ion distributions outside the HERS field of view. For the part of the distribution that was within the HERS field of view, the data show that isotropy is indeed a good first approximation.

4. The distribution of counts versus mass anode was then modeled using generalized Gaussians to determine the position and width of each mass peak. (This step was

discussed in the previous section). Examination of the flight data showed that the locations of the mass peaks had shifted by a fraction of a mass anode in the year between laboratory calibration of the instrument and the comet encounter. The cause of this shift is not understood. Thus the calibration data were used as a guide to the approximate locations and widths of the mass peaks and least-squares fits of the flight data were performed to determine the best values to use for the data analysis. It was assumed that neither the locations nor the widths of the mass peaks changed during the hour before closest approach to the comet. The positions and shapes of each of the mass peaks were determined for the data set as a whole, while the contributions of different ion species to the counts measured by each anode were separately determined for each time interval by performing a least-squares analysis to determine the height of each peak. Although it was originally intended to use both the medium- and heavy-mode data for calculating the densities of water-group ions, the least-squares fits to the medium-mode data were significantly superior to the heavy-mode data fits (the variances between the data and the fits were smaller and the peak widths determined by the fits were closer to the pre-launch calibration values), so only the medium-mode data were used to calculate the densities for m/q = 16 - 18 amu/e.

5. For each interval, it was then assumed that each ion species had an isotropic distribution and the same bulk velocity vector v_o as the water-group ions (as determined in Step 3). Then, for each value of m/q, the 3-D distribution in elevation -azimuth-energy/charge was transformed into a one-dimensional distribution of phase space density versus $|\Delta v|$, where $\Delta v = v - v_o$. Integration over this 1-D distribution then gave the ion density.

The method used for computing proton and m/q = 2 ion moments was similar except that:

1. The proton counting rate was high enough that the proton density could be calculated on a spin by spin basis to yield 1100 km resolution. The fluxes of ions with m/q = 2 amu/e were great enough to allow 64 sec (4400 km) resolution.

2. A moments technique, rather than a least-squares fit was used to calculate the proton bulk velocity independent of the heavy-ion velocity calculated in Step 2 above.

3. The HERS instrument was able to identify protons unambiguously, with no mass overlap, so Step 4 above was not necessary.

Publications under contract NASW-4336

Neugebauer, M., A. J. Lazarus, H. Balsiger, S. A. Fuselier, B. E. Goldstein, R. Goldstein, F. M. Neubauer, and H. Rosenbauer, The velocity distributions of cometary protons picked up by the solar wind, *J. Geophys. Res., 94,* 5227-5239, 1989.

Goldstein, B. E., K. Altwegg, H. Balsiger, S. A. Fuselier, W. H. Ip, A. Meier, M. Neugebauer, H. Rosenbauer, and R. Schwenn, Observations of a shock and a recombination layer at the contact surface of comet Halley, *J. Geophys. Res., 94,* 17251-17257, 1990.

Kettmann, G., W. H. Ip, H. Balsiger, B. E. Goldstein, A. Meier, H. Rosenbauer, R. Schwenn, and E. G. Shelley, Cometary ion flow variations at comet p/Halley as observed by the u.c. Giotto IMS experiment, *Ann. Geophysical, in press,* 1989.

Ip, W., H. Rosenbauer, R. Schwinn, G. Kettmann, H. Balsiger, J. Geiss, A. J. Meier, B. E. Goldstein, E. G. Shelley, and A. Lazarus, Giotto IMS measurements of the production rate of hydrogen cyanide in the coma of comet Halley, *Anna. Geophys., submitted,* 1989.

Neugebauer, M., R. Goldstein, B. E. Goldstein, S. A. Fuselier, H. Balsiger, and W. Ip, Densities and abundances of hot cometary ions in the coma of P/Halley, *Astrophys. J., in press,* 1991.

Goldstein, B. E., R. Goldstein, M. Neugebauer, S. A. Fuselier, E. G. Shelley, H. Balsiger, G. Kettmann, W. -H.Ip, H. Rosenbauer, and R. Schwenn, Observations of plasma dynamics in the coma of P/Halley by the GIOTTO ion mass spectrometer, *J. Geophys. Res., Submitted,* 1990.

Fuselier, S. A., E. G. Shelley, B. E. Goldstein, R. Goldstein, M. Neugebauer, W. IP, H. Balsiger, and H. Reme, Observations of solar wind ion charge exchange in the comet Halley coma, *Astrophys. J., Submitted,* 1991.

Geiss, J., K. Altwegg, E. Anders, H. Balsiger, W.-H. Ip, A. Meier, M. Neugebauer, H. Rosenbauer, and E. G. Shelley, Interpretation of the ion mass spectra in the mass range 25-35 obtained in the inner coma of Halley's comet by the HIS-sensor of the GIOTTO IMS Experiment, *Astro. and Astrophys., Accepted,* 1990.

Implementation of the above procedure resulted in significant changes in some of the ion moments while others (for example the m/Q = 2 moments) were relatively unchanged from their first generation values. Perhaps the best illustration of the improvement over the first generation moments can be seen in Figure 2. This figure compares the second and generation and final proton densities with the electron densities derived from the Giotto electron experiment. The new proton densities are significantly greater than the old densities after 2100 UT. These new densities agree remarkably well with the electron densities derived from a completely different instrument. The substantially larger new proton densities are primarily the result of the accounting of protons outside the HERS field of view. The discrepancy between the proton and electron densities after 2240 is the result of several known factors. First, the electron density is equivalent to the total ion density, which by 2240 has a significant contribution from heavy cometary ions. Second, when the proton peak moves outside the HERS field of view (after ~ 2350 UT), the total proton density will be underestimated even when we attempt to take into account the protons outside the field of view. Finally, the electron density is underestimated in the inner region because a large fraction of electrons are below the 10eV cutoff of that instrument.

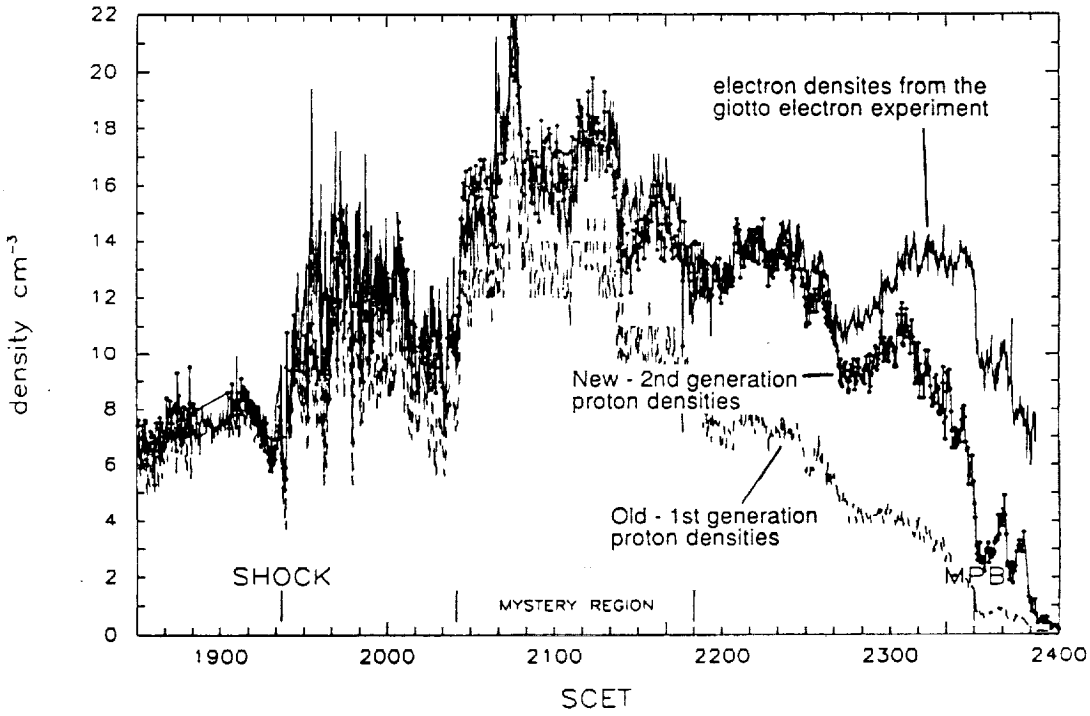

As with the first generation moments, we submitted the revised final moments to the NSSDC and to the International Halley Watch (IHW) archives. Plots and listings of the final moments that were submitted to the NSSDC and IHW archives are given in Appendix A.

C. Science Results

Although the development of final plasma parameters occupied a considerable amount of time under the contract, these efforts were not without reward. We have used these revised plasma parameters in several studies that have either been published, submitted for publication or are presently in press in the scientific literature. We have also presented these results at numerous scientific meetings. Perhaps equally important, we have made these data products available to the general scientific community in an easily interpretable format through the IHW and NSSDC archives.

A list of the papers published, in press, or submitted to scientific journals is in Appendix B. A list of papers presented at scientific meetings is given in Appendix C.

Below, we summarize the results from the scientific studies carried out under this contract. The title of the work is followed by a brief description. Further details may be obtained from Appendix D, which contains copies of the papers listed below and in Appendix B.

1. The velocity distributions of cometary protons picked up by the solar wind
Journal of Geophysical Research, 94, 5227-5239, 1989.

The region upstream from the shock has turned out to be an excellent laboratory for testing many of the theories on the generation of magnetohydrodynamic waves by unstable plasma distributions and the effect these waves have on the distributions. Cometary neutrals can propagate great distances from the nucleus before being ionized. Depending on the orientation of the upstream magnetic field to the solar wind flow, these new born ions picked up by the solar wind and form a ring or a beam in velocity space. Two general conditions can be identified. Ion pickup when the upstream magnetic field orientation is nearly parallel to the upstream flow direction is termed quasi-parallel pickup and ion pickup when the upstream magnetic field orientation is nearly perpendicular to the upstream flow direction is termed quasi-perpendicular pickup. This distincition is very important both for the type of pickup distribution that is expected to be formed and by the type of waves the unstable pickup distribution produces. Quasi-parallel pickup produces a beam-like pickup distribution in that the perpendicular temperature is on the order of or small than the beam drift speed. This type of distribution is unstable to a variety of beam modes, the most important of which is the resonant ion beam instability. The waves generated by this instability will pitch angle scatter the beam distribution from 0 (or 180°) pitch angles toward 90° pitch angles. At the other extreme, quasi-perpendicular pickup produces a ring distribution in that the perpendicular temperature is much larger than the beam drift speed. This type of distribution is unstable to an anisotropy driven instability which will pitch angle scatter the ring distribution away from 90° toward 0 and 180° pitch angles. For both quasi-parallel and quasi-perpendicular pickup, the pitch angle scattering occurs along a shell whose origin is not the center of the proton distribution but is displaced approximately alfven speed along the magnetic field direction. This is because the waves resonant with the ions have velocities equal to the alfven speed and pitch angle scattering represents no net change in energy in the wave frame. Additional evolution of the pickup distribution will occur near the cometary bow shock. In this region, the large amplitude magnetic fluctuations and the presence of the bow shock will result in energy diffusion of the pickup distribution.

The above paper describes the detailed study of the cometary protons picked up by the solar wind upstream from the Halley bow shock. Eleven intervals ranging from 1 to 5 x 10^6 km were selected on the basis that the magnetic field direction remained relatively steady. The three-dimensional proton distribution measured by IMS/HERS was reduced to a pitch angle distribution in the solar wind rest frame by using the computed solar wind flow velocity and the magnetic field direction. For each distribution, the location in pitch angle and energy for the initial pickup ion

distribution was computed. The range of pitch angle scattering about this initial direction and the range of energy diffusion about the initial pickup energy were quantified. Quasi-parallel and quasi-perpendicular pickup intervals were considered separately. For the quasi-parallel intervals, the pickup proton distribution far from the comet was similar to what was expected based on theory. It showed pickup distribution at the local pickup energy that had been scattered partially into a shell. The shell center was located between the center of the proton distribution and the expected location one alfven speed displaced along the magnetic field. Nearer the shock, the pitch angle scattering was greater and some evidence for energy diffusion was seen.

The real surprise came in the quasi-perpendicular pickup regime. Instead of a partially filled shell centered approximately on 90° pitch angles, the distribution for quasi-perpendicular pickup resembled that for quasi-parallel pickup. That is, the partially filled shell was asymetrically centered on 180° rather than 90°. This is a real puzzle because based on the above theoretical concerns, the pitch angle scattering should be peaked at 90° and not 180°. The 180° direction was always the direction for ions traveling away from the comet. Although it is tempting to assume that the 180° pitch angles were filled with protons reflected from the cometary bow shock (much the same as the reflected ions observed at the Earth's bow shock), there are several reasons why this is probably not the case. Probably the most important reason is that at a weak shock like a cometary bow shock, ion reflection does not occur. One possibility raised is that because the turbulence between the spacecraft and the comet is higher than the turbulence between the spacecraft and the sun, there is a net flux of scattered protons traveling along the magnetic field away from the comet. Although this global rather than local view of the problem is a possible solution, further theoretical work is needed to resolve this important issue.

2. Observations of a shock and a recombination layer at the contact surface of comet Halley Journal of Geophysical Research, 94, 17251-17257, 1989.

Before the Giotto encounter with comet Halley, the transition from a collisionless regime to a collisional regime was thought to take place at the contact surface. The IMS/HIS and HERS sensors and their operating modes were designed to detect this transition. HERS was designed to operate mainly in the collisionless regime while HIS was designed to operate mainly in the collisional regime. In fact both sensors have produced interesting results in the regimes they were not specifically optimized for. This overlap is important for the understanding of data from both sensors.

During the encounter, the contact surface was observed about two minutes before closest approach. Many of the characteristics were as expected, namely the exclusion of a solar wind magnetic field and the formation of a field free cavity dominated by cometary ion outflow at ~1 km/s. However, there were some puzzling aspects of this outflow that prompted another look at the contact surface region. Several models described the flow inside the contact surface as radial outward until some distance from the contact surface, where the plasma inside the contact surface is lost down the tail by a change in flow direction from radial to tailward. The initial HIS results showed that this was not the case. The radial flow was observed throughout the region inside the contact surface out to the boundary. This prompted a suggestion that the plasma inside the contact surface was lost by recombination at the contact surface. The model predicted a pileup of plasma just inside the contact surface. This pileup is important because the density increase results in a large increase in the recombination rate and consequently a significant loss of plasma.

The above paper discusses the HIS observations near the contact surface and presents evidence for a plasma pileup region just inside the contact surface. The pileup was observed in the HIS mass analyzer in both the water group fluxes and the "heavy" ion fluxes (ions with mass ~44 amu/q). The density increases were on the order of 4 to 10 times the density prior to the contact surface. This is on the order of what was predicted theoretically. The pileup region was very thin, extending only on the order of 47 km inside the contact surface. However, this thickness was also on the order of that predicted theoretically.

In addition to a density spike at but just inside the contact surface, a density spike was observed somewhat upstream of the contact surface near what was identified in the magnetometer data as an outward propagating fast shock. This density spike was observed in the HIS angle analyzer. Based on where in velocity space the spike occurred, it was concluded that this spike

represented an increase in the suprathermal particle population just upstream from the outward propagating fast shock. Analysis of the data showed that the density of these suprathermal particles was only on the order of 1% of the total plasma density. The density and energy of these particles suggested that they were suprathermal ions accelerated at the shock front through the familiar shock drift acceleration mechanism. In this acceleration process, ions drift along the shock front at the same velocity as the outward propagation of the shock and thus gain energy with each shock encounter. A similar process accelerates ions to suprathermal energies at the Earth's bow shock.

3. Cometary ion flow variations at comet P/Halley as observed by the Giotto IMS experiment. Annales Geophysicae, 8, 229-238, 1990.

The IMS/HERS and HIS sensors were designed with some overlap in field of view. The HERS sensor viewed from 15 to 75° from the ram direction. That is, it was blind along the ram direction. The HIS angle analyzer sensor filled in this blind direction because it viewed from 0 to 22° from the ram direction. Using only the HERS data, we have estimated that the cometary ion distribution moved substantially out of the field of view at around 2340-45 UT or a distance of 8 x 10^4 km from the nucleus. Thus, the continued tracking of the cometary water group velocity inside of this distance required the HIS angle analyzer data.

The angle analyzer data were fit with a Maxwell Boltzmann distribution to determine the velocity and temperature of the total distribution. The velocity profile showed a general decrease from ~25 km/s at 1.5×10^6 km from the comet to ~few km/s near closest approach. This is in contrast to the velocity profiles determined from instruments that did not view in the ram direction. These velocity profiles showed a leveling off in velocity well before closest approach. The discrepancy underscores the need for the ram direction data to determine the true velocity profile near the comet. While the general trend was decreasing, there were relatively large velocity variations, sometimes as much as 50% of the total velocity. These velocity variations are due to the inherently turbulent nature of the comet-solar wind interaction. The temperature profile also showed a general decreasing trend from ~100 eV at 1.6×10^5 km to <1 eV near closest approach.

One of the most interesting results was the sudden appearance of a cold cometary distribution entirely in the ram direction at ~9×10^4 km from the comet. Because it is entirely in the ram direction, it was not detectable from instruments that did not view in that direction. It's relatively sudden appearance showed that the comet-solar wind interaction in the inner regions of the comet coma was not simply described as the gradual slowing of the solar wind due to the pickup of more and more cometary ions. Clearly a rather abrupt change in the interaction occurred when this cold cometary distribution appeared.

In general, comparison of the measured flow velocities and temperatures with MHD models of the comet Halley interaction with the solar wind showed that the modeled flow velocities were too high and the temperatures were too low by as much as a factor of 2 from the measured temperatures and velocities. This discrepancy will be evident in other papers discussed below. It points out the fact that the current cometary models provide good qualitative results but relatively inaccurate quantitative results.

4. Giotto IMS measurements of the production rate of hydrogen cyanide in the coma of comet Halley
Annales Geophysicae, 8, 319-326, 1990.

One of the more important problems in recent cometary research is how to relate the in situ observations with remote observations from the ground. This is an important problem because it is only recently that in situ observations have been made while ground observations have been made for many years. Most ground observations consist of the study of optical emissions from the comet coma. Of the optical emissions, the brightest are the emissions from CN radicals even though the CN production rate has been found to be quite small in comparison to the water production rate in comets.

In the above paper, the M/Q=28 amu/q mass channel of the HIS sensor is used to determine the relative concentration of H_2CN^+ to H_2O^+, thereby deducing the HCN concentration relative to H_2O^+. The M/Q=28 mass channel is important because HCN reacts with water to form H_2CN^+ (M/Q=28) while H_2CN^+ reacts only weakly with water, thereby leaving a significant fraction of H_2CN^+ in the inner coma. The M/Q=28 mass peak can also be contaminated with N_2^+ and CO^+. However, both of these molecules will be preferentially depleted by interaction with the cometary H_2O present in the inner coma. A relatively simple model calculation shows that this is indeed the case and also shows that the H_2CN^+ content is modulated by the NH_3 concentration. Previous study of the IMS/HIS data resulted in an estimated NH_3 concentration relative to H_2O of ~2%. With this estimate, the HCN concentration relative to H_2O in the comet coma is on the order of .02%. Radio observations put the HCN production rate relative to H_2O ~.1-.5%. One possible explanation for this discrepancy is the fact that the HCN production is know to have significant variations. The outgasing from the comet, especially the CN radicals, is know to be highly anisotropic and sporadic at times. The calculations from IMS/HIS are restricted to a steady-state photochemical model.

5. Densities and abundances of hot cometary ions in the coma of P/Halley
The Astrophysical Journal, in press, 1991.

Following the Giotto encounter with comet Halley, a number of models were produced to describe the in situ spacecraft observations. Perhaps the most ambitious model was one that combined a computer simulation of the chemistry inside the contact surface with Magnetohydrodynamic (MHD) computer simulations of the solar wind interaction outside the contact surface. The the chemistry inside the contact surface was used to determine the total amount and relative mix of cometary neutrals. In the MHD simulation, these cometary neutrals were allowed to move outward from the contact surface and interact with an incident solar wind population. Using realistic dissociation, recombination, and ionization rates, the production of cometary ions from the neutrals and the subsequent mass loading of the solar wind were simulated. An imaginary spacecraft was "flown" through the model along the Giotto trajectory and plasma density profiles of a large number of ions were determined.

We felt that the previous IMS/HERS data was not yet suitable for comparison with such an ambitious computer model. However, with the revision of the IMS/HERS densities of cometary and solar wind ions, we were finally in a position to compare in situ observations with the best MHD computer simulations.

In general, HERS detected most of the ions expected to be found in the coma of comet Halley. This much was already known soon after the encounter. What was probably the most surprising result was that the density of cometary ions in the range from 40,000 to 250,000 km was at least an order of magnitude greater than predicted by cometary models. This discrepancy appears to be true for all cometary models produced thus far. It is not the result of a large compression of the plasma since the proton densities in the outer coma, inside the bow shock are about what was expected. It appears that the best explanation for the discrepancy is that the models underestimate the ionization rate for cometary ions. There is evidence from the HERS observations of an anomalously high charge exchange rate for He^{2+} that supports this suggestion. Charge exchange could play an even more important role in the production of cometary ions since the charge exchange cross sections increase with decreasing velocity. This feature was not included in the models but may be very important since the solar wind plasma slows considerably as more and more cometary ions are picked up.

While the absolute densities from in situ measurements and cometary models are in disagreement, the relative densities of the water group ions are in good agreement. The HERS

observations of the density ratios of M/Q=16/M/Q=18, and M/Q=17/M/Q=18 are in good agreement with the MHD models of the cometary coma. This suggests that the dissociation of cometary water molecules in the inner coma is a well understood process. One major discrepancy in the density ratios is the overabundance of C^+ relative M/Q=13, and 14. It has been suggested that the extra C^+ may come from dust grains, whereas the MHD models do not include such a source.

Finally, the new in situ density profiles clearly indicate that the "boundary" at 1.35×10^5 km from the comet is barely discernable in the cometary ion data. It had been suggested that this boundary, which has been called the "cometopause" and the "magnetic pileup boundary", was a "chemical boundary", were solar wind plasma was lost and cometary plasma increased dramatically. It is clear from the HERS data that Giotto did not encounter such a "chemical boundary" as proposed for VEGA observations in a similar region of the Halley coma.

6. Observations of solar wind ion charge exchange in the comet Halley coma
The Astrophysical Journal, submitted, 1990.

Under the previous data analysis contract, we reported anomalously high charge exchange of solar wind He^{2+} to He^{+} in the coma of comet Halley. Charge exchange loss of up to 30% of the solar wind He^{2+} was reported in a region where theorists expected losses of only on the order of 3%. Needless to say, this was quite a surprise and required a follow-up study when the revision of the IMS/HERS moments was completed.

The charge exchange of He^{2+} into He^{+} is by far the easiest to do since both ions were directly observed by IMS/HERS and there is very little initial M/Q=4 ions in the solar wind. However, the large charge exchange rates observed in the comet coma suggested that the effects of charge exchange of other solar wind ions with larger charge exchange cross sections than He^{2+} could be observed. Included in these other solar wind ions were protons and high charge state Oxygen and Carbon ions. Proton charge exchange cannot be observed directly since the product of the charge exchange is a fast neutral that is not detectable by an ion mass spectrometer. However, the higher charge exchange cross section for protons compared to He^{2+} implies that the solar wind He^{2+} to proton density ratio should rise as the comet is approached. Of course, when cometary protons are added in, the density ratio could decrease, increase, or stay the same depending on the relative ratio of solar wind to cometary protons. In addition to the charge exchange of protons, other solar wind ions such as high charge state of Oxygen and Carbon ions have much larger charge exchange cross sections than He^{2+}. One should see a cascade to lower charge states of these ions as the comet is approached.

The revised HERS moments were first used to compute new percentages for the charge exchange of He^{2+}. Also included in this calculation was the removal of H_2^{+} from the M/Q=2 mass peak, using a previous study of H_2^{+} and He^{2+} ions. It was found that the percentage charge exchange of He^{2+} rose to over 40% just inside 10^5 km from the comet. Next, the revised moments were used to compute the He^{2+} to proton density ratio. The average density ratio first rose as the comet was approached and then, at a distance of about 2×10^5 km from the comet, the density ratio leveled out and then decreased rather rapidly. The gradual increase followed by the decrease was modeled using a relatively simple model of the charge exchange process. This model showed that the changes were consistent with an initial loss of solar wind protons at a faster rate than He^{2+}, followed by a rapid increase in the total proton density near the comet due to the addition of cometary protons. These results showed that the relative magnitude of the cross sections for protons and He^{2+} were correct. One possible explanation for the anomalously large

charge exchange of He^{2+} was that the assumed cross section was not correct. The results in this study showed that this is probably not the case.

In general agreement with the proton and He2+ observations, high charge state Carbon and Oxygen ions in the solar wind were observed to charge exchange to lower charge states as the comet was approached. Unfortunately, the densities of these solar wind ions were so low that quantitative studies of the charge exchange process was not possible.

The results of the charge exchange study indicate that we still do not know the origin of the anomalously high charge exchange of He^{2+}. However, we have eliminated several possibilities. One possibility that remains is that the plasma flow near the comet is significantly different from that modeled. If the plasma slowed significantly along the comet-sun line in addition to the deflection away from that line, then there would be significantly more solar wind plasma charge exchange than modeled. The enhanced charge exchange would also result in larger cometary ion densities. Presently, the observed cometary ion densities are about a factor of ten greater than the modeled densities, thus supporting the idea that the cometary ion production through charge exchange is underestimated in the models. Further modeling is required to improve the agreement between theory and observations.

One of the more surprising results from this study was that there was an abrupt change in the He^{2+} to proton density ratio in the so-called "mystery region". This region, between 9 and 5 x 10^5 km from the comet, was known to contain higher solar wind ion densities and enhanced fluxes of energetic (>1 keV) electrons. The enhanced energetic electron fluxes are correlated with the He^{2+} to proton density ratio increase. The density ratio increase and the overall increase in the solar wind density in this region suggest that it is a tube of different solar wind plasma from the surrounding region that has convected into the cometary coma. At present, this is the best explanation of most of the properties. One property it does not explain is the enhanced fluxes of energetic electrons. The enhancement is unique in the Giotto encounter. They suggest that in addition to a different solar wind plasma, the mystery region contains some additional processes related to the comet. At present, we do not know what these processes are.

7. Observations of plasma dynamics in the coma of P/Halley by the Giotto ion mass spectrometer
Journal of Geophysical Research, submitted, 1990.

We have already discussed above the results using the revised cometary and solar wind ion densities. Velocities and temperatures of these ions were also revised. In cometary models, these other moment have a direct effect on the cometary and solar wind ion densities. For example, the cometary pick up process results in the slowing of the solar wind. The more ions picked up, the more the solar wind slows and, since the charge exchange rate is energy dependent, the slowing causes an increase in the loss of solar wind ions. Previous publications included only the ions within the HERS field of view. Near the comet, where the physics becomes interesting, a large fraction of the cometary and solar wind ion distributions are outside the HERS field of view and modeling of the distribution is required to determine the plasma moments. Fortunately, the cometary ion distributions are relatively simple. To first order, they consist of a shell in velocity space centered on the local solar wind flow speed and with radius approximately equal to the local solar wind flow velocity.

The HERS data for the protons, M/Q=2 ions and the entire water group were modeled using an iterative scheme that determined the flow velocity and density of the distribution. This scheme is described in section I of this report. The result was an estimate of the moments and the amount of the distribution outside the HERS field of view. So long as the flow velocity (= center of the distribution) was within the field of view, the modeling produced very good results. They showed a gradual decrease in the flow velocities of all ion species as the comet was approached. No abrupt changes in the flow velocities or temperatures were observed.

Concentrating on the water group ions, they were found to be in the form of a shell distribution with relatively uniform pitch angle coverage. The radius of the shell coincided quite well with the local solar wind speed as expected. As the comet was approached, the shell radius decreased as expected and the water group ion density increased. The density increase was entirely due to the addition of ions at approximately the local pick up speed. In fact, some of the higher energy ions, picked up much earlier and upstream from the spacecraft, were observed to charge exchange away.

There is general agreement with the observed and predicted flow velocities and temperatures. However, predictions from the MHD models generally indicate higher flow velocities and lower cometary ion densities in the inner coma. The two moments are directly

coupled because the lower observed flow velocities are the result of pick up of more cometary material and thus higher cometary ion densities. This disagreement again underscores the need for more work on the modeling of the comet-solar wind interaction.

The HERS flow velocities and the HIS flow velocities show good agreement in the region where the measurements overlap. This is an encouraging result and suggests that further comparison of the HIS and HERS data is possible and will yield a better understanding of the two instruments and the comet environment.

The region described as the "cometopause" or the "magnetic pile up boundary (MPB)" is evident only in the solar wind ions and magnetic field. No distinct change in the cometary ion moments across this boundary was observed. The change in solar wind parameters only is additional strong evidence that the MPB was a rotational discontinuity in the solar wind that had convected into the comet coma.

8. Interpretation of the ion mass spectra in the mass range 25-35 obtained in the inner coma of Halley's comet by the HIS-sensor of the Giotto IMS experiment.
Astronomy and Astrophysics, in press, 1991.

As already pointed out above, the HIS sensor is uniquely suited for the study of the the inner region (inside the contact surface) of the Halley coma. This paper is primarily concerned with the ion mass range from 25 to 35 amu/q. The molecular chemistry in this inner region of the coma is dominated by proton affinity. Molecules having higher proton affinity than water will react with the most abundant ion in the inner coma (H_3O^+) and abstract a proton. These protonated molecules will have much higher densities than their parent molecules Ions with a lower proton affinity than water will either be under-abundant if they react strongly with water or tend to have a high abundance if they do not react with water.

Although the inner coma is dominated by this water reaction process, correct accounting of the ion species requires a model of the inner coma chemistry. Such a model is presented which predicts the relative abundance of the cometary ions. These predictions agree relatively well with the ion mass spectra from HIS inside the contact surface. This agreement indicates the following: 1. H_2CO and CH_3OH dominate the mass range from 25 to 35 amu/q since their parent molecules are most abundant and their proton affinity is the largest. 2) Minimal ion abundances at masses 27, 29, and 34 are consistent with the predictions since most of the ions with this mass per charge react strongly with water. 3) The height of the M/Q=28 mass peak is consistent with the HCN/H_2O abundance ratio of 0.001. CO^+ contributes to this peak but is not dominate. In addition to these results, a molecular abundance profile is determined by fitting the model to the radial variation of the HIS ion data.

9. The evolution of the M/Q=2 ion distribution in the outer coma of comet Halley
To be submitted to the Journal of Geophysical Research, 1991.

Under the previous contract, we did some preliminary analysis of the proton and alpha variations across the bow shock. The protons were analyzed in detail while only the M/Q=2 moments were considered.

Using the revised analysis codes developed under the present contract, we were able to reconstruct the M/Q=2 distribution in pitch angle coordinates in the solar wind proton rest frame. Upstream from the bow shock, we found evidence of a pick up ion distribution with M/Q=2. This distribution is identified as cometary H_2^+ produced primarily through the dissociation of cometary water molecules. Although the picked up distribution is near background, we are confident that it is real because it is at the same velocity as the picked up proton distribution and the distribution is not present prior to just before the bow shock.

Across the bow shock, the solar wind He^{2+} distribution is observed to heat quite rapidly. In contrast, the solar wind proton distribution does not heat until much further downstream. Further downstream from the bow shock, the He^{2+} distribution changes from one that is peaked near zero velocity in the proton rest frame to one that is approximately in the form of a shell in velocity space centered on the proton rest frame. Shell-like He^{2+} distribution have also been observed downstream from the Earth's bow shock. At the Earth's bow shock, the formation of the shell distribution is believed to occur because the differential slowing of He^{2+} and protons across the electrostatic shock potential. We believe that the process is similar at the cometary bow shock. The only difference is that the cometary bow shock is weaker and therefore the relative drift between the protons and He2+ ions (and hence the shell radius) is smaller. Indeed, the He2+ distribution showed no shell like features for the Giotto crossing at the flanks of the cometary bow shock because the shock strength there was relatively weak. Further downstream however, Giotto was sampling plasma that originated nearer the subsolar point. In this region, the shock strength is much greater. In addition, the cometary ion pick up and slowing of the solar wind is faster near the comet-sun line. The more rapid slowing of the solar wind in this region also contributes to the formation of a He^{2+} shell because of a mismatch in the slowing of the solar wind He^{2+} and proton distributions.

III. CONCLUSIONS AND RECOMMENDATIONS

In the proposal for this data analysis contract, we outlined a strategy to go well beyond the initial scientific studies using the IMS/HERS data from the comet Halley encounter. The strategy involved a top to bottom revision of the data analysis codes used to compute physical parameters from the instrument. The revision required a second, more detailed look at the calibration data and careful modeling of the instrument response. We have accomplished all the proposed objectives using this strategy. The revised moments have led to a much improved understanding of the comet-solar wind interaction from the outer regions where the interaction is very weak to the very inner coma where the interaction is very strong. In addition to the science results, we submitted the revised data set to the IHW and the NSSDC in a convenient format for other scientists to use. We expect that this data set will become an invaluable resource for future studies of comets.

With the close of this contract, we feel that we have analyzed to the best of our ability the majority of the IMS/HERS data set. Most of the interactions between the solar wind and the comet have been identified and several, such as cometary proton pick up, are reasonably well understood. Others, such as solar wind ion charge exchange, are not well understood but the observations are well documented. We have also compared the in situ observations with most of the present day cometary models. While the agreement is far from perfect, it is now the responsibility of the cometary modelers to improve the models to agree better with the observations.

Although we feel that we have analyzed the majority of the HERS data set, we do not feel that cometary research is finished. Already pointed out above is the need for better computer models to compare to the data. We have tried, through our submission of the data to the NSSDC and IHW, to provide would be cometary modelers with a data set that was in physical units and easy to handle. In addition to comparison between theory and experiment, we feel that additional inter-experiment comparison will yield better information on the cometary environment. Almost all of the scientific studies performed under this contract were aided by the inter-comparison between data sets from different Giotto instruments. As other experimenters improve their data sets, additional comparisons with the HERS data products are possible. Again, we feel that the NSSDC and IHW archives will provide much of HERS data needed for this inter-comparison.

Finally, we have made preliminary comparisons between the final generation HERS data products and the initial, first generation HIS data products. The comparison between these two instruments is critical to understanding the complex environment sampled by HIS near the comet. There is a significant region where the observations overlap and the preliminary comparisons under

this contract show encouraging agreement between the two sensors. Clearly more work on the HIS data is needed to develop second generation HIS data products and to compare these products with the HERS data and with theoretical predictions of the inner coma of comet Halley.

V. ACKNOWLEDGEMENTS

The accomplishments under this contract would not have been possible without the firm dedication of the entire IMS team. All of the science and data analysis results were obtained through a truly extraordinary collaboration with the other institutes that made up the IMS team. We thank and commend the rest of the IMS team for making the past several years an enjoyable and rewarding experience. In addition, we thank the many members of the other Giotto instrument teams that we have collaborated with. They should certainly share in the successes of the IMS results.

V. APPENDICIES

Appendix A

Listings and Plots of Updated Giotto IMS/HERS Moments Submitted to IHW and NSSDC

LOCKHD::dsk2:[fuselier.giotto.moments]m2_m1_ratio.mom

Final M/Q=2 and proton moments Derived from instrument function fits

Proton moments were averaged over 4 spins to coincide with M/Q=2 moments and ratios of the Density and Temperature were computed.

M/Q=2 moments									Proton Moments							ratio	
doy	SCET hhmmss	SCET minutes	distance km	Density cm-3	HSE Coord Vx	Vy	Vz	Log(T) K	SCET hhmmss	SCET minutes	Density cm-3	HSE Coord Vx	Vy	Vz	Log(T) K	Density ratio	Temp ratio
72	183056.	1110.96	1.36E+06	0.17	-274.	-1.	8.	5.52	183055.	1110.92	6.97	-278.	-15.	-3.	5.42	0.024	1.268
72	183200.	1111.98	1.36E+06	0.19	-279.	-7.	0.	5.45	183151.	1111.84	6.75	-270.	-9.	2.	5.42	0.028	1.065
72	183304.	1113.06	1.35E+06	0.18	-281.	-18.	-9.	5.44	183303.	1113.05	7.04	-277.	-26.	-5.	5.42	0.026	1.046
72	183408.	1114.14	1.35E+06	0.17	-264.	-25.	0.	5.38	183415.	1114.25	6.45	-266.	-23.	-2.	5.41	0.026	0.933
72	183512.	1115.22	1.34E+06	0.19	-286.	-20.	-1.	5.30	183519.	1115.31	7.03	-276.	-30.	-4.	5.43	0.027	0.736
72	183616.	1116.24	1.34E+06	0.19	-277.	-20.	5.	5.27	183614.	1116.24	6.37	-275.	-9.	4.	5.42	0.030	0.708
72	183720.	1117.32	1.34E+06	0.13	-273.	-24.	5.	5.38	183710.	1117.17	7.30	-277.	-28.	4.	5.42	0.018	0.912
72	183824.	1118.40	1.33E+06	0.13	-270.	6.	-26.	5.21	183815.	1118.25	6.68	-273.	-13.	-16.	5.43	0.019	0.602
72	183928.	1119.48	1.33E+06	0.27	-254.	-12.	-5.	5.80	183927.	1119.44	7.20	-254.	-14.	-11.	5.44	0.037	2.267
72	184032.	1120.56	1.32E+06	0.17	-267.	-3.	-26.	5.37	184039.	1120.65	7.45	-269.	-13.	-18.	5.43	0.023	0.876
72	184136.	1121.58	1.32E+06	0.29	-275.	-20.	-17.	5.48	184134.	1121.56	7.80	-286.	-25.	-3.	5.42	0.037	1.157
72	184240.	1122.66	1.31E+06	0.18	-277.	-10.	-13.	5.33	184239.	1122.65	7.72	-275.	-16.	-17.	5.42	0.023	0.809
72	184344.	1123.74	1.31E+06	0.17	-266.	-8.	-4.	5.39	184350.	1123.83	8.07	-272.	-24.	-12.	5.45	0.021	0.881
72	184448.	1124.82	1.31E+06	0.17	-274.	-19.	-16.	5.33	184455.	1124.91	7.97	-270.	-10.	-11.	5.44	0.021	0.770
72	184552.	1125.84	1.30E+06	0.25	-282.	-6.	-7.	5.25	184550.	1125.84	7.53	-270.	-20.	5.	5.42	0.033	0.670
72	184656.	1126.92	1.30E+06	0.19	-277.	-1.	8.	5.36	184646.	1126.77	7.58	-275.	-15.	6.	5.43	0.025	0.851
72	184800.	1128.00	1.29E+06	0.24	-280.	-12.	-20.	5.38	184759.	1127.98	7.40	-275.	-22.	-15.	5.44	0.032	0.867
72	184904.	1129.08	1.29E+06	0.21	-258.	-10.	-2.	5.47	184910.	1129.17	8.15	-259.	-19.	-3.	5.47	0.026	1.005
72	185008.	1130.16	1.28E+06	0.17	-275.	-17.	2.	5.29	185014.	1130.23	7.88	-272.	-18.	-2.	5.45	0.022	0.687
72	185112.	1131.18	1.28E+06	0.19	-286.	-8.	-1.	5.39	185110.	1131.16	7.87	-283.	-26.	-1.	5.43	0.024	0.912
72	190411.	1144.20	1.23E+06	0.22	-287.	-16.	-10.	5.67	190413.	1144.22	8.34	-284.	-13.	-15.	5.45	0.026	1.674
72	190515.	1145.28	1.22E+06	0.19	-269.	-17.	-2.	5.27	190518.	1145.30	8.13	-263.	-22.	-5.	5.42	0.023	0.702
72	190619.	1146.30	1.22E+06	0.22	-268.	-8.	5.	5.44	190614.	1146.24	8.18	-269.	-11.	7.	5.43	0.027	1.017
72	190723.	1147.38	1.21E+06	0.19	-260.	-9.	-1.	5.23	190717.	1147.29	8.35	-260.	-21.	-3.	5.44	0.023	0.620
72	190827.	1148.46	1.21E+06	0.16	-256.	-7.	0.	5.37	190830.	1148.50	8.58	-259.	-18.	-5.	5.42	0.019	0.891
72	190931.	1149.54	1.20E+06	0.19	-276.	-2.	1.	5.38	190941.	1149.69	8.38	-270.	-11.	4.	5.43	0.023	0.891
72	191035.	1150.56	1.20E+06	0.16	-263.	-4.	-1.	5.32	191038.	1150.64	7.97	-265.	-9.	0.	5.42	0.020	0.788
72	191139.	1151.64	1.20E+06	0.15	-269.	-3.	2.	5.25	191133.	1151.55	8.15	-266.	-12.	-3.	5.43	0.018	0.656
72	191243.	1152.72	1.19E+06	0.13	-258.	2.	1.	5.34	191238.	1152.63	7.85	-257.	-14.	-2.	5.44	0.017	0.790
72	191347.	1153.80	1.19E+06	0.16	-277.	-7.	-1.	5.36	191341.	1153.68	7.65	-272.	-19.	-9.	5.44	0.021	0.827
72	191451.	1154.82	1.18E+06	0.21	-275.	9.	-7.	5.28	191446.	1154.76	7.00	-273.	-7.	-7.	5.44	0.030	0.696
72	191555.	1155.90	1.18E+06	0.13	-277.	9.	-13.	5.28	191550.	1155.83	6.97	-282.	-4.	-16.	5.42	0.019	0.733
72	191659.	1156.98	1.17E+06	0.12	-280.	9.	-11.	5.10	191653.	1156.89	7.03	-277.	-7.	-9.	5.43	0.017	0.470
72	191803.	1158.06	1.17E+06	0.12	-287.	4.	-9.	5.33	191805.	1158.08	6.26	-284.	-4.	-10.	5.43	0.019	0.801
72	191907.	1159.14	1.16E+06	0.09	-288.	16.	-8.	5.23	191917.	1159.29	6.18	-284.	-1.	-12.	5.45	0.015	0.602
72	192011.	1160.16	1.16E+06	0.13	-277.	18.	-5.	5.34	192013.	1160.22	6.70	-289.	13.	-14.	5.44	0.019	0.788
72	192115.	1161.24	1.16E+06	0.23	-277.	15.	-24.	5.24	192109.	1161.15	7.40	-283.	3.	-18.	5.44	0.031	0.634
72	192219.	1162.32	1.15E+06	0.18	-261.	24.	30.	5.64	192214.	1162.23	6.72	-264.	9.	13.	5.41	0.027	1.687
72	192323.	1163.40	1.15E+06	0.12	-223.	0.	25.	5.77	192317.	1163.28	5.43	-224.	8.	39.	5.41	0.022	2.266
72	192427.	1164.42	1.14E+06	0.26	-278.	16.	12.	5.55	192422.	1164.36	9.07	-261.	1.	5.	5.53	0.029	1.058
72	192530.	1165.50	1.14E+06	0.28	-253.	31.	20.	5.68	192525.	1165.41	8.15	-268.	19.	22.	5.52	0.034	1.434
72	192635.	1166.58	1.13E+06	0.34	-267.	11.	15.	5.71	192637.	1166.62	9.82	-263.	4.	12.	5.52	0.035	1.536
72	192738.	1167.66	1.13E+06	0.29	-275.	32.	-14.	5.73	192749.	1167.81	10.05	-274.	24.	-5.	5.51	0.029	1.678
72	192842.	1168.68	1.13E+06	0.22	-271.	37.	12.	5.63	192846.	1168.76	9.20	-276.	33.	3.	5.52	0.024	1.298

72	192946.	1169.76	1.12E+06	0.32	-257.	56.	15.	5.41	192941.	1169.69	8.83	-257.	50.	9.	5.50	0.036	0.821
72	193050.	1170.84	1.12E+06	0.25	-240.	39.	22.	5.57	193045.	1170.75	9.85	-245.	39.	6.	5.55	0.025	1.041
72	193154.	1171.92	1.11E+06	0.21	-206.	25.	19.	5.77	193149.	1171.82	9.38	-227.	40.	0.	5.58	0.022	1.564
72	193258.	1172.94	1.11E+06	0.44	-246.	52.	14.	5.68	193301.	1173.02	12.63	-240.	52.	5.	5.57	0.035	1.292
72	193402.	1174.02	1.10E+06	0.28	-230.	59.	-1.	5.61	193405.	1174.08	9.73	-232.	50.	-13.	5.55	0.029	1.148
72	193506.	1175.10	1.10E+06	0.28	-233.	49.	-3.	5.40	193501.	1175.01	9.68	-230.	44.	-3.	5.53	0.029	0.736
72	193610.	1176.18	1.09E+06	0.27	-222.	44.	5.	5.61	193621.	1176.35	9.00	-223.	48.	1.	5.56	0.030	1.122
72	193714.	1177.26	1.09E+06	0.29	-199.	20.	27.	5.61	193732.	1177.54	9.37	-199.	20.	24.	5.55	0.031	1.145
72	193818.	1178.28	1.09E+06	0.24	-177.	43.	11.	5.80	193822.	1178.36	8.87	-192.	22.	16.	5.62	0.027	1.531
72	193922.	1179.36	1.08E+06	0.32	-218.	67.	-6.	5.81	193916.	1179.27	9.82	-218.	57.	-16.	5.64	0.033	1.487
72	194026.	1180.44	1.08E+06	0.37	-243.	45.	-12.	5.72	194021.	1180.35	11.43	-237.	40.	-29.	5.60	0.032	1.315
72	194130.	1181.52	1.07E+06	0.31	-241.	45.	18.	5.88	194124.	1181.40	12.75	-252.	40.	-2.	5.63	0.024	1.798
72	194234.	1182.54	1.07E+06	0.23	-219.	54.	-10.	5.92	194229.	1182.48	12.38	-230.	43.	5.	5.73	0.019	1.565
72	194338.	1183.62	1.06E+06	0.30	-223.	54.	2.	5.99	194333.	1183.55	13.77	-232.	69.	-14.	5.72	0.022	1.851
72	194442.	1184.70	1.06E+06	0.27	-207.	42.	24.	5.94	194429.	1184.48	12.20	-230.	52.	32.	5.73	0.022	1.632
72	194546.	1185.78	1.06E+06	0.24	-193.	72.	-20.	5.92	194549.	1185.81	12.32	-209.	68.	-14.	5.77	0.019	1.428
72	194650.	1186.86	1.05E+06	0.27	-195.	60.	8.	6.00	194653.	1186.88	12.47	-214.	68.	-6.	5.77	0.022	1.711
72	194754.	1187.88	1.05E+06	0.22	-211.	31.	3.	5.68	194748.	1187.81	9.40	-209.	37.	-4.	5.60	0.023	1.197
72	194858.	1188.96	1.04E+06	0.31	-232.	20.	-16.	5.75	194852.	1188.87	12.60	-231.	14.	-6.	5.64	0.025	1.280
72	195002.	1190.04	1.04E+06	0.35	-238.	-4.	-20.	5.65	194949.	1189.82	11.80	-242.	0.	-23.	5.53	0.030	1.321
72	195106.	1191.12	1.03E+06	0.38	-232.	20.	1.	5.81	195052.	1190.86	9.70	-230.	28.	-9.	5.59	0.039	1.644
72	195210.	1192.14	1.03E+06	0.41	-236.	28.	2.	5.74	195202.	1192.04	11.93	-231.	16.	8.	5.58	0.034	1.444
72	195314.	1193.22	1.02E+06	0.33	-224.	35.	-3.	5.64	195308.	1193.13	11.50	-230.	34.	-2.	5.57	0.029	1.188
72	195418.	1194.30	1.02E+06	0.34	-223.	39.	-14.	5.80	195420.	1194.34	10.84	-231.	36.	-23.	5.62	0.031	1.504
72	195521.	1195.32	1.02E+06	0.33	-205.	52.	-21.	5.91	195524.	1195.40	11.27	-215.	43.	-21.	5.66	0.029	1.775
72	195626.	1196.46	1.01E+06	0.39	-210.	51.	-17.	5.93	195628.	1196.47	12.08	-207.	42.	-11.	5.68	0.032	1.768
72	195729.	1197.48	1.01E+06	0.42	-215.	42.	-2.	5.98	195731.	1197.52	11.70	-215.	43.	-6.	5.67	0.036	2.057
72	195833.	1198.56	1.00E+06	0.34	-205.	51.	13.	5.93	195828.	1198.47	12.20	-222.	34.	4.	5.70	0.028	1.706
72	195937.	1199.64	9.98E+05	0.40	-190.	53.	-10.	5.87	195932.	1199.54	12.25	-201.	51.	-19.	5.73	0.033	1.372
72	200041.	1200.66	9.94E+05	0.33	-204.	58.	-5.	6.01	200036.	1200.60	11.60	-206.	53.	-10.	5.73	0.028	1.892
72	200145.	1201.74	9.90E+05	0.30	-199.	52.	-12.	5.91	200140.	1201.67	11.25	-207.	51.	-12.	5.75	0.027	1.453
72	200249.	1202.82	9.85E+05	0.32	-201.	48.	6.	5.90	200244.	1202.73	12.35	-201.	42.	-1.	5.73	0.026	1.469
72	200353.	1203.90	9.81E+05	0.39	-228.	55.	-20.	5.91	200355.	1203.92	13.44	-227.	49.	-8.	5.71	0.029	1.599
72	200457.	1204.98	9.77E+05	0.41	-213.	54.	-5.	5.89	200508.	1205.13	13.33	-222.	44.	-4.	5.72	0.031	1.470
72	200601.	1206.00	9.72E+05	0.34	-201.	49.	-5.	6.03	200605.	1206.08	12.13	-201.	50.	5.	5.71	0.028	2.105
72	200705.	1207.08	9.68E+05	0.37	-207.	47.	-7.	5.85	200659.	1206.99	12.05	-218.	48.	-15.	5.71	0.031	1.379
72	200809.	1208.16	9.64E+05	0.25	-189.	48.	11.	5.82	200804.	1208.07	10.85	-202.	38.	5.	5.70	0.023	1.333
72	200913.	1209.24	9.59E+05	0.28	-196.	59.	5.	5.85	200907.	1209.12	10.15	-203.	51.	5.	5.70	0.028	1.411
72	201017.	1210.26	9.55E+05	0.28	-212.	73.	-1.	5.94	201012.	1210.20	10.63	-210.	57.	-6.	5.68	0.026	1.839
72	201121.	1211.34	9.50E+05	0.30	-199.	79.	-2.	5.92	201115.	1211.25	8.88	-203.	71.	-5.	5.70	0.034	1.669
72	201225.	1212.42	9.46E+05	0.24	-194.	84.	-5.	5.93	201220.	1212.33	10.55	-206.	78.	-10.	5.73	0.023	1.603
72	201329.	1213.50	9.42E+05	0.34	-190.	80.	-4.	5.92	201331.	1213.52	10.54	-199.	72.	-7.	5.73	0.032	1.555
72	201433.	1214.58	9.37E+05	0.36	-199.	77.	5.	5.93	201436.	1214.60	10.07	-206.	69.	11.	5.70	0.036	1.681
72	201537.	1215.60	9.33E+05	0.33	-172.	50.	-4.	5.85	201532.	1215.53	9.20	-183.	39.	-8.	5.67	0.036	1.531
72	201641.	1216.68	9.29E+05	0.34	-182.	57.	8.	5.84	201635.	1216.59	10.73	-193.	46.	-1.	5.69	0.032	1.412
72	201745.	1217.76	9.24E+05	0.31	-161.	72.	8.	5.87	201739.	1217.66	9.30	-170.	54.	2.	5.71	0.033	1.445
72	201849.	1218.84	9.20E+05	0.29	-162.	70.	4.	5.98	201852.	1218.86	10.00	-182.	61.	4.	5.74	0.029	1.724
72	201953.	1219.86	9.16E+05	0.26	-171.	68.	0.	6.03	201944.	1219.74	9.27	-183.	62.	-6.	5.73	0.028	2.009
72	202057.	1220.94	9.11E+05	0.24	-185.	50.	5.	5.87	202059.	1220.98	7.47	-195.	57.	-4.	5.68	0.032	1.567
72	202201.	1222.02	9.07E+05	0.33	-189.	51.	0.	5.70	202203.	1222.06	10.00	-201.	46.	1.	5.68	0.033	1.054
72	202305.	1223.10	9.02E+05	0.30	-194.	48.	10.	5.92	202315.	1223.25	10.65	-203.	44.	3.	5.68	0.028	1.725
72	202411.	1224.18	8.98E+05	0.27	-185.	52.	9.	5.79	202412.	1224.20	10.20	-196.	47.	9.	5.71	0.026	1.193

72	202517.	1225.26	8.93E+05	0.28	-194.	22.	-7.	5.93	202507.	1225.11	10.65	-203.	29.	0.	5.73	0.026	1.602
72	202620.	1226.34	8.89E+05	0.57	-203.	2.	6.	5.98	202611.	1226.19	12.85	-204.	8.	3.	5.70	0.044	1.893
72	202725.	1227.42	8.85E+05	0.43	-210.	34.	-1.	5.95	202731.	1227.51	15.50	-223.	30.	-4.	5.73	0.028	1.659
72	202829.	1228.50	8.80E+05	0.42	-214.	44.	8.	5.93	202835.	1228.59	15.20	-227.	40.	-6.	5.73	0.028	1.594
72	202932.	1229.52	8.76E+05	0.47	-190.	54.	-5.	5.97	202938.	1229.64	14.80	-212.	37.	-11.	5.73	0.032	1.738
72	203036.	1230.60	8.71E+05	0.42	-186.	36.	16.	5.96	203040.	1230.66	16.10	-207.	27.	6.	5.77	0.026	1.564
72	203140.	1231.68	8.67E+05	0.46	-190.	33.	17.	5.92	203143.	1231.72	16.03	-215.	30.	22.	5.75	0.029	1.489
72	203244.	1232.76	8.63E+05	0.45	-197.	49.	19.	5.94	203251.	1232.85	15.80	-217.	43.	11.	5.78	0.028	1.445
72	203348.	1233.78	8.58E+05	0.50	-198.	46.	3.	6.04	203347.	1233.78	16.40	-213.	38.	-10.	5.79	0.030	1.777
72	203452.	1234.86	8.54E+05	0.43	-207.	38.	9.	6.01	203446.	1234.76	16.70	-212.	26.	-3.	5.78	0.026	1.696
72	203556.	1235.94	8.50E+05	0.52	-206.	42.	-1.	6.03	203555.	1235.92	16.28	-220.	31.	2.	5.80	0.032	1.705
72	203700.	1237.02	8.45E+05	0.48	-211.	33.	15.	6.02	203707.	1237.11	14.98	-223.	32.	10.	5.70	0.032	2.078
72	203804.	1238.04	8.41E+05	0.49	-215.	50.	-1.	5.87	203804.	1238.06	14.80	-227.	39.	5.	5.67	0.033	1.572
72	203908.	1239.12	8.37E+05	0.67	-223.	29.	-7.	5.83	203906.	1239.11	15.78	-225.	35.	-14.	5.65	0.042	1.519
72	204012.	1240.20	8.32E+05	0.62	-229.	24.	-24.	5.84	204011.	1240.18	16.43	-228.	20.	-20.	5.61	0.038	1.698
72	204116.	1241.28	8.28E+05	0.77	-213.	5.	-22.	5.89	204115.	1241.24	17.18	-219.	13.	-21.	5.66	0.045	1.706
72	204220.	1242.36	8.23E+05	0.62	-207.	27.	-19.	5.88	204227.	1242.45	17.20	-214.	18.	-22.	5.66	0.036	1.678
72	204324.	1243.38	8.19E+05	0.61	-228.	33.	-16.	5.86	204323.	1243.38	17.87	-225.	26.	-15.	5.68	0.034	1.525
72	204438.	1244.64	8.14E+05	0.83	-221.	21.	-26.	5.87	204436.	1244.60	20.00	-224.	23.	-26.	5.73	0.041	1.367
72	204552.	1245.84	8.09E+05	0.91	-228.	23.	-21.	5.87	204554.	1245.90	21.50	-228.	22.	-25.	5.69	0.042	1.520
72	204656.	1246.92	8.05E+05	0.85	-214.	39.	-33.	5.89	204659.	1246.98	19.58	-224.	33.	-33.	5.69	0.043	1.593
72	204800.	1248.00	8.00E+05	0.63	-228.	36.	-25.	5.95	204802.	1248.03	18.20	-224.	26.	-31.	5.70	0.035	1.777
72	204904.	1249.08	7.96E+05	0.67	-229.	42.	-1.	5.97	204907.	1249.11	16.60	-227.	26.	-17.	5.70	0.040	1.861
72	205008.	1250.16	7.91E+05	0.60	-224.	42.	10.	5.87	205011.	1250.18	16.83	-225.	32.	-4.	5.70	0.036	1.487
72	20511. .	1251.18	7.87E+05	0.59	-209.	40.	-2.	5.93	205114.	1251.24	17.15	-223.	31.	-5.	5.72	0.034	1.612
72	205216.	1252.26	7.83E+05	0.58	-213.	30.	-3.	5.88	205218.	1252.31	16.55	-219.	30.	1.	5.70	0.035	1.513
72	205320.	1253.34	7.78E+05	0.63	-204.	35.	1.	5.97	205322.	1253.37	16.00	-216.	39.	5.	5.70	0.039	1.851
72	205424.	1254.42	7.74E+05	0.50	-194.	44.	15.	5.93	205424.	1254.40	16.10	-203.	35.	8.	5.71	0.031	1.659
72	205528.	1255.44	7.70E+05	0.63	-203.	40.	-1.	6.04	205538.	1255.64	17.37	-210.	36.	-8.	5.73	0.036	2.057
72	205632.	1256.52	7.65E+05	0.58	-209.	42.	-11.	6.02	205634.	1256.57	16.70	-215.	40.	-16.	5.74	0.035	1.926
72	205735.	1257.60	7.61E+05	0.69	-206.	30.	4.	5.98	205731.	1257.51	17.65	-214.	33.	-8.	5.74	0.039	1.737
72	205840.	1258.68	7.56E+05	0.58	-194.	39.	1.	6.03	205843.	1258.71	17.40	-206.	38.	-3.	5.80	0.033	1.698
72	205943.	1259.70	7.52E+05	0.51	-188.	33.	-1.	6.09	205946.	1259.76	16.63	-204.	38.	7.	5.79	0.031	2.007
72	210047.	1260.78	7.48E+05	0.60	-193.	41.	9.	6.09	210050.	1260.84	17.45	-207.	42.	3.	5.80	0.034	1.972
72	210152.	1261.86	7.43E+05	0.54	-193.	40.	-8.	6.05	210153.	1261.89	16.18	-202.	40.	-10.	5.81	0.033	1.748
72	210255.	1262.94	7.39E+05	0.56	-181.	37.	7.	6.06	210258.	1262.97	16.33	-198.	35.	-9.	5.80	0.034	1.830
72	210359.	1263.96	7.35E+05	0.54	-203.	38.	15.	6.05	210402.	1264.04	16.40	-202.	40.	-1.	5.79	0.033	1.819
72	210503.	1265.04	7.30E+05	0.57	-201.	35.	11.	6.03	210506.	1265.10	16.05	-211.	35.	-2.	5.77	0.036	1.809
72	210607.	1266.12	7.26E+05	0.52	-192.	40.	0.	6.04	210610.	1266.17	16.40	-207.	31.	-14.	5.78	0.032	1.840
72	210711.	1267.20	7.21E+05	0.54	-201.	46.	-4.	6.08	210714.	1267.23	16.73	-212.	47.	-1.	5.78	0.032	1.984
72	210815.	1268.28	7.17E+05	0.56	-198.	34.	-4.	6.09	210816.	1268.26	17.27	-214.	42.	8.	5.76	0.032	2.121
72	210919.	1269.30	7.13E+05	0.62	-188.	20.	-11.	5.98	210922.	1269.36	18.67	-197.	24.	-9.	5.74	0.033	1.737
72	211023.	1270.38	7.08E+05	0.63	-202.	32.	-11.	6.01	211023.	1270.38	18.43	-204.	26.	-12.	5.72	0.034	1.949
72	211127.	1271.46	7.04E+05	0.57	-195.	38.	-11.	6.01	211129.	1271.49	17.18	-203.	38.	-17.	5.74	0.033	1.872
72	211231.	1272.54	6.99E+05	0.60	-192.	25.	-11.	6.00	211226.	1272.44	18.73	-208.	35.	-5.	5.75	0.032	1.792
72	211335.	1273.56	6.95E+05	0.54	-190.	30.	-26.	6.00	211337.	1273.62	18.45	-201.	27.	-22.	5.73	0.029	1.861
72	211439.	1274.64	6.91E+05	0.60	-200.	38.	-12.	5.98	211442.	1274.70	18.10	-206.	32.	-8.	5.71	0.033	1.851
72	211543.	1275.72	6.86E+05	0.63	-186.	27.	-4.	6.01	211553.	1275.88	18.27	-199.	20.	-8.	5.72	0.034	1.935
72	211647.	1276.80	6.82E+05	0.59	-190.	36.	-19.	5.97	211650.	1276.83	17.60	-194.	34.	-18.	5.74	0.034	1.688
72	211751.	1277.82	6.78E+05	0.64	-185.	38.	-20.	6.01	211754.	1277.90	18.33	-201.	25.	-13.	5.73	0.035	1.927
72	211855.	1278.90	6.73E+05	0.64	-178.	25.	-17.	5.95	211906.	1279.10	17.00	-189.	24.	-21.	5.72	0.038	1.710
72	211959.	1279.98	6.69E+05	0.71	-187.	23.	-26.	5.97	212004.	1280.06	17.67	-193.	24.	-30.	5.71	0.040	1.833

72	212103.	1281.06	6.64E+05	0.70	-197.	34.	-27.	5.85	212105.	1281.09	16.93	-197.	25.	-31.	5.67	0.041	1.529
72	212207.	1282.14	6.60E+05	0.65	-181.	38.	-23.	5.76	212209.	1282.16	16.20	-192.	35.	-24.	5.65	0.040	1.302
72	212311.	1283.16	6.56E+05	0.75	-185.	42.	-22.	5.83	212313.	1283.22	14.18	-192.	33.	-32.	5.61	0.053	1.658
72	212415.	1284.24	6.51E+05	0.56	-193.	36.	-24.	5.75	212417.	1284.29	13.45	-197.	31.	-29.	5.60	0.042	1.404
72	212519.	1285.32	6.47E+05	0.62	-194.	41.	-28.	5.79	212521.	1285.35	13.85	-192.	32.	-34.	5.60	0.045	1.539
72	212623.	1286.40	6.43E+05	0.58	-182.	37.	-38.	5.81	212626.	1286.43	13.35	-192.	31.	-31.	5.61	0.043	1.602
72	212726.	1287.42	6.38E+05	0.60	-203.	39.	-19.	5.81	212729.	1287.48	13.13	-206.	35.	-19.	5.62	0.046	1.539
72	212847.	1288.80	6.33E+05	0.67	-203.	38.	-18.	5.81	212857.	1288.96	14.16	-204.	33.	-24.	5.62	0.047	1.534
72	212951.	1289.82	6.29E+05	0.57	-201.	39.	-23.	5.83	213001.	1290.02	13.37	-202.	33.	-20.	5.63	0.043	1.573
72	213054.	1290.90	6.24E+05	0.65	-194.	32.	-11.	5.85	213058.	1290.96	14.05	-197.	30.	-10.	5.63	0.046	1.678
72	213158.	1291.98	6.20E+05	0.66	-176.	31.	-9.	5.80	213201.	1292.01	14.08	-189.	25.	-10.	5.63	0.047	1.478
72	213302.	1293.06	6.15E+05	0.53	-177.	29.	-8.	5.88	213305.	1293.09	14.40	-184.	22.	-9.	5.68	0.037	1.584
72	213406.	1294.08	6.11E+05	0.55	-173.	28.	-12.	5.92	213409.	1294.16	14.70	-187.	21.	-11.	5.69	0.037	1.698
72	213510.	1295.16	6.07E+05	0.61	-174.	32.	-13.	5.91	213522.	1295.36	15.20	-185.	18.	-16.	5.67	0.040	1.724
72	213614.	1296.24	6.02E+05	0.58	-174.	29.	-6.	5.96	213608.	1296.14	15.67	-182.	29.	-12.	5.67	0.037	1.964
72	213718.	1297.32	5.98E+05	0.58	-179.	19.	-9.	5.88	213721.	1297.35	14.73	-181.	25.	-14.	5.65	0.039	1.687
72	213822.	1298.34	5.94E+05	0.67	-172.	26.	-10.	5.86	213825.	1298.42	14.10	-187.	23.	-15.	5.63	0.048	1.708
72	213942.	1299.72	5.88E+05	0.69	-174.	20.	-12.	5.75	213937.	1299.61	14.02	-182.	22.	-13.	5.65	0.049	1.270
72	214046.	1300.74	5.84E+05	0.61	-172.	25.	-12.	5.82	214049.	1300.82	14.63	-188.	23.	-11.	5.64	0.042	1.531
72	214150.	1301.82	5.79E+05	0.65	-183.	25.	1.	5.83	214153.	1301.88	14.18	-187.	21.	-1.	5.62	0.046	1.631
72	214254.	1302.90	5.75E+05	0.60	-180.	34.	-1.	5.71	214257.	1302.94	13.73	-186.	31.	-1.	5.61	0.044	1.259
72	214358.	1303.98	5.70E+05	0.62	-178.	32.	-7.	5.68	214401.	1304.01	13.82	-188.	27.	-6.	5.63	0.045	1.135
72	214502.	1305.06	5.66E+05	0.70	-173.	22.	4.	5.79	214505.	1305.09	13.80	-184.	21.	7.	5.62	0.051	1.479
72	214606.	1306.08	5.62E+05	0.44	-175.	31.	7.	5.84	214608.	1306.14	12.25	-183.	22.	7.	5.65	0.036	1.548
72	214710.	1307.16	5.57E+05	0.55	-177.	20.	10.	5.87	214712.	1307.21	13.88	-185.	20.	15.	5.68	0.040	1.548
72	214816.	1308.24	5.53E+05	0.58	-183.	28.	5.	6.01	214816.	1308.27	13.13	-188.	23.	5.	5.70	0.044	2.041
72	214922.	1309.38	5.48E+05	0.48	-182.	3.	12.	5.94	214913.	1309.22	13.63	-189.	15.	0.	5.70	0.035	1.751
72	215026.	1310.46	5.44E+05	0.42	-166.	14.	10.	6.07	215024.	1310.40	12.85	-182.	24.	8.	5.72	0.033	2.248
72	215130.	1311.48	5.40E+05	0.39	-167.	25.	8.	6.02	215137.	1311.62	13.17	-179.	34.	11.	5.74	0.030	1.905
72	215250.	1312.86	5.34E+05	0.38	-144.	18.	5.	5.99	215256.	1312.93	12.78	-164.	28.	5.	5.73	0.030	1.809
72	215410.	1314.18	5.29E+05	0.41	-149.	16.	2.	6.02	215417.	1314.28	12.82	-164.	21.	9.	5.77	0.032	1.785
72	215514.	1315.26	5.24E+05	0.30	-157.	17.	4.	5.95	215520.	1315.34	12.73	-168.	21.	-1.	5.80	0.024	1.423
72	215618.	1316.28	5.20E+05	0.39	-152.	12.	2.	6.13	215617.	1316.28	12.15	-168.	17.	-2.	5.78	0.032	2.250
72	215722.	1317.36	5.16E+05	0.37	-143.	13.	-15.	6.10	215720.	1317.33	12.95	-159.	25.	-12.	5.81	0.029	1.950
72	215826.	1318.44	5.11E+05	0.36	-147.	27.	-17.	6.09	215825.	1318.41	12.93	-157.	23.	-23.	5.81	0.028	1.905
72	215930.	1319.52	5.07E+05	0.36	-139.	29.	-14.	6.11	215928.	1319.46	12.40	-155.	23.	-21.	5.81	0.029	2.006
72	220034.	1320.54	5.03E+05	0.34	-136.	19.	-26.	6.05	220032.	1320.54	12.55	-148.	21.	-25.	5.82	0.027	1.717
72	220137.	1321.62	4.98E+05	0.36	-127.	19.	-18.	6.11	220135.	1321.59	12.68	-147.	20.	-17.	5.81	0.028	1.995
72	220242.	1322.70	4.94E+05	0.34	-136.	13.	-5.	6.06	220240.	1322.67	12.83	-148.	25.	-15.	5.81	0.027	1.768
72	220346.	1323.78	4.89E+05	0.31	-125.	20.	-26.	6.00	220344.	1323.73	12.60	-146.	23.	-20.	5.82	0.025	1.505
72	220449.	1324.80	4.85E+05	0.36	-129.	27.	-21.	6.07	220448.	1324.80	13.85	-143.	24.	-24.	5.84	0.026	1.698
72	220553.	1325.88	4.81E+05	0.38	-117.	34.	-24.	6.10	220552.	1325.87	14.15	-140.	29.	-30.	5.85	0.027	1.777
72	220657.	1326.96	4.76E+05	0.39	-125.	30.	-18.	6.08	220656.	1326.93	13.63	-141.	28.	-28.	5.84	0.029	1.728
72	220801.	1328.04	4.72E+05	0.41	-122.	33.	-18.	6.08	220801.	1328.01	13.40	-142.	28.	-21.	5.83	0.031	1.799
72	220905.	1329.06	4.68E+05	0.39	-130.	27.	-12.	6.05	220904.	1329.06	13.78	-145.	27.	-17.	5.82	0.028	1.717
72	221009.	1330.14	4.63E+05	0.40	-125.	21.	0.	6.06	221008.	1330.14	13.93	-146.	27.	-14.	5.81	0.029	1.778
72	221113.	1331.22	4.59E+05	0.42	-130.	22.	-10.	6.08	221111.	1331.19	13.68	-144.	24.	-10.	5.82	0.031	1.841
72	221217.	1332.30	4.54E+05	0.44	-128.	22.	-12.	6.09	221216.	1332.27	14.07	-145.	26.	-5.	5.83	0.031	1.809
72	221321.	1333.32	4.50E+05	0.52	-129.	13.	-1.	6.18	221319.	1333.32	13.97	-148.	28.	-7.	5.86	0.037	2.113
72	221425.	1334.40	4.46E+05	0.46	-125.	15.	-18.	6.21	221424.	1334.40	14.30	-144.	27.	-11.	5.85	0.032	2.278
72	221529.	1335.48	4.41E+05	0.45	-121.	21.	-17.	6.16	221527.	1335.45	13.30	-140.	29.	-17.	5.86	0.034	1.995
72	221633.	1336.56	4.37E+05	0.45	-129.	3.	-12.	6.13	221632.	1336.53	13.18	-137.	26.	-24.	5.85	0.034	1.905

72	221737.	1337.64	4.32E+05	0.39	-129.	23.	-17.	6.14	221736.	1337.60	13.05	-139.	25.	-22.	5.86	0.030	1.916
72	221841.	1338.66	4.28E+05	0.40	-119.	26.	-24.	6.20	221840.	1338.66	13.07	-141.	22.	-18.	5.85	0.031	2.251
72	221945.	1339.74	4.24E+05	0.38	-123.	18.	-8.	6.14	221944.	1339.73	13.35	-141.	23.	-19.	5.85	0.028	1.961
72	222049.	1340.82	4.19E+05	0.46	-123.	13.	-12.	6.15	222047.	1340.79	13.68	-139.	24.	-16.	5.84	0.034	2.030
72	222153.	1341.90	4.15E+05	0.42	-128.	21.	-13.	6.10	222152.	1341.87	13.75	-141.	28.	-10.	5.83	0.031	1.861
72	222257.	1342.92	4.11E+05	0.37	-125.	30.	-19.	6.11	222255.	1342.92	13.38	-140.	23.	-11.	5.81	0.028	2.006
72	222401.	1344.00	4.06E+05	0.44	-120.	33.	3.	6.12	222400.	1344.00	13.58	-139.	24.	-1.	5.81	0.032	2.041
72	222505.	1345.08	4.02E+05	0.40	-119.	30.	-9.	6.04	222503.	1345.05	13.03	-141.	27.	-3.	5.80	0.031	1.726
72	222609.	1346.16	3.97E+05	0.40	-130.	19.	-7.	6.14	222608.	1346.13	13.13	-147.	23.	-9.	5.82	0.030	2.089
72	222713.	1347.24	3.93E+05	0.40	-130.	21.	10.	6.11	222711.	1347.18	13.70	-140.	26.	5.	5.80	0.029	2.029
72	222817.	1348.26	3.89E+05	0.44	-119.	12.	-5.	6.11	222816.	1348.26	12.85	-139.	20.	1.	5.80	0.034	2.041
72	222921.	1349.34	3.84E+05	0.38	-116.	24.	-13.	6.02	222919.	1349.31	12.40	-137.	20.	-7.	5.80	0.031	1.659
72	223025.	1350.42	3.80E+05	0.32	-115.	18.	-3.	6.06	223023.	1350.39	11.53	-134.	20.	-7.	5.80	0.028	1.819
72	223129.	1351.50	3.76E+05	0.31	-107.	24.	4.	6.03	223127.	1351.45	11.78	-136.	18.	-3.	5.80	0.026	1.706
72	223233.	1352.52	3.71E+05	0.42	-105.	22.	-12.	6.10	223231.	1352.52	11.83	-135.	18.	-8.	5.80	0.036	1.983
72	223337.	1353.60	3.67E+05	0.40	-119.	22.	-2.	6.04	223335.	1353.59	12.00	-137.	24.	-7.	5.80	0.033	1.748
72	223440.	1354.68	3.62E+05	0.39	-124.	15.	0.	6.07	223439.	1354.65	12.38	-139.	21.	-7.	5.81	0.032	1.840
72	223545.	1355.76	3.58E+05	0.43	-120.	16.	-4.	6.11	223544.	1355.73	12.53	-132.	23.	-4.	5.82	0.034	1.972
72	223648.	1356.78	3.54E+05	0.31	-121.	27.	-12.	6.09	223647.	1356.78	11.70	-131.	23.	-5.	5.82	0.026	1.862
72	223800.	1357.98	3.49E+05	0.40	-124.	5.	-11.	6.12	223752.	1357.86	11.60	-130.	24.	-7.	5.83	0.034	1.961
72	223912.	1359.18	3.44E+05	0.37	-119.	21.	-10.	6.11	223911.	1359.18	11.15	-133.	24.	-8.	5.84	0.033	1.883
72	224016.	1360.26	3.40E+05	0.36	-111.	21.	-7.	6.15	224015.	1360.25	10.63	-130.	28.	-11.	5.84	0.034	2.053
72	224120.	1361.34	3.35E+05	0.42	-109.	8.	-5.	6.21	224119.	1361.31	10.33	-129.	27.	-2.	5.84	0.041	2.342
72	224224.	1362.42	3.31E+05	0.34	-107.	24.	2.	6.10	224223.	1362.39	9.30	-128.	26.	-3.	5.84	0.037	1.819
72	224328.	1363.44	3.27E+05	0.34	-110.	18.	-6.	6.18	224326.	1363.44	9.25	-133.	26.	-8.	5.83	0.037	2.238
72	224432.	1364.52	3.22E+05	0.30	-97.	28.	0.	6.09	224431.	1364.52	9.35	-126.	30.	0.	5.85	0.032	1.726
72	224536.	1365.60	3.18E+05	0.33	-100.	16.	5.	6.12	224534.	1365.57	8.93	-119.	25.	1.	5.83	0.037	1.938
72	224640.	1366.68	3.13E+05	0.31	-99.	35.	-2.	6.03	224639.	1366.65	9.45	-119.	25.	-5.	5.83	0.033	1.575
72	224744.	1367.76	3.09E+05	0.31	-89.	16.	-1.	6.05	224743.	1367.72	9.10	-117.	28.	-2.	5.82	0.034	1.717
72	224848.	1368.78	3.05E+05	0.40	-93.	32.	2.	6.19	224847.	1368.78	9.50	-116.	27.	4.	5.85	0.042	2.199
72	224952.	1369.86	3.00E+05	0.28	-104.	25.	1.	6.19	224951.	1369.84	9.18	-120.	27.	1.	5.83	0.031	2.275
72	225056.	1370.94	2.96E+05	0.39	-99.	23.	7.	6.12	225055.	1370.91	9.20	-115.	26.	5.	5.85	0.042	1.883
72	225200.	1372.02	2.91E+05	0.31	-83.	27.	6.	6.04	225159.	1371.99	9.60	-107.	29.	7.	5.86	0.032	1.530
72	225304.	1373.04	2.87E+05	0.36	-89.	32.	2.	6.18	225302.	1373.04	9.15	-112.	29.	4.	5.84	0.039	2.213
72	225408.	1374.12	2.83E+05	0.30	-92.	28.	-13.	6.08	225406.	1374.11	9.60	-106.	28.	-2.	5.84	0.031	1.737
72	225512.	1375.20	2.78E+05	0.37	-80.	30.	-1.	6.11	225510.	1375.17	9.95	-104.	27.	0.	5.86	0.037	1.799
72	225616.	1376.28	2.74E+05	0.37	-89.	25.	15.	6.03	225615.	1376.25	10.00	-106.	29.	0.	5.84	0.037	1.556
72	225720.	1377.36	2.69E+05	0.37	-86.	22.	0.	6.06	225718.	1377.30	10.60	-100.	25.	6.	5.83	0.035	1.698
72	225824.	1378.38	2.65E+05	0.33	-81.	28.	11.	6.08	225823.	1378.38	10.25	-105.	26.	3.	5.85	0.032	1.698
72	225928.	1379.46	2.61E+05	0.34	-71.	20.	2.	6.16	225926.	1379.43	10.10	-101.	28.	4.	5.85	0.034	2.029
72	230032.	1380.54	2.56E+05	0.33	-88.	20.	-10.	6.09	230031.	1380.51	10.45	-102.	26.	1.	5.86	0.032	1.708
72	230136.	1381.62	2.52E+05	0.43	-81.	15.	15.	6.14	230135.	1381.58	9.88	-102.	25.	-1.	5.84	0.044	1.994
72	230240.	1382.64	2.48E+05	0.42	-79.	1.	-7.	6.09	230238.	1382.64	10.48	-96.	23.	-3.	5.84	0.040	1.777
72	230344.	1383.72	2.43E+05	0.39	-70.	12.	-2.	6.12	230341.	1383.69	11.03	-91.	23.	2.	5.84	0.035	1.894
72	230448.	1384.80	2.39E+05	0.43	-70.	4.	1.	6.16	230446.	1384.77	10.88	-89.	24.	4.	5.84	0.040	2.112
72	230552.	1385.88	2.34E+05	0.43	-67.	6.	21.	6.13	230550.	1385.84	11.15	-84.	24.	7.	5.84	0.039	1.938
72	230655.	1386.90	2.30E+05	0.38	-63.	-2.	-1.	6.06	230654.	1386.90	10.60	-89.	22.	-1.	5.85	0.036	1.612
72	230759.	1387.98	2.26E+05	0.38	-51.	19.	-4.	6.10	230750.	1387.84	10.83	-76.	25.	6.	5.87	0.035	1.711
72	230903.	1389.06	2.21E+05	0.50	-70.	-15.	16.	6.24	230902.	1389.03	10.00	-85.	27.	11.	5.87	0.050	2.357
72	231007.	1390.14	2.17E+05	0.33	-76.	23.	5.	6.06	231007.	1390.11	9.20	-95.	29.	9.	5.85	0.036	1.612
72	231111.	1391.16	2.13E+05	0.34	-80.	24.	11.	6.12	231110.	1391.16	9.18	-90.	27.	11.	5.84	0.037	1.926
72	231215.	1392.24	2.08E+05	0.33	-75.	13.	8.	6.09	231214.	1392.24	9.23	-93.	26.	14.	5.84	0.036	1.778

72	231319.	1393.32	2.04E+05	0.43	-77.	12.	17.	6.14	231317.	1393.29	9.60	-88.	25.	7.	5.86	0.045	1.927
72	231423.	1394.40	2.00E+05	0.40	-82.	0.	4.	6.13	231422.	1394.37	9.03	-90.	25.	13.	5.86	0.044	1.883
72	231527.	1395.42	1.95E+05	0.39	-63.	-2.	15.	6.19	231526.	1395.43	8.30	-85.	27.	12.	5.87	0.047	2.089
72	231631.	1396.50	1.91E+05	0.32	-72.	16.	2.	6.14	231630.	1396.50	8.93	-85.	26.	8.	5.86	0.036	1.926
72	231735.	1397.58	1.86E+05	0.36	-72.	16.	2.	6.14	231733.	1397.55	8.10	-91.	29.	11.	5.88	0.044	1.840
72	231839.	1398.66	1.82E+05	0.34	-68.	32.	8.	6.09	231838.	1398.63	8.60	-83.	29.	8.	5.87	0.040	1.649
72	231943.	1399.74	1.78E+05	0.31	-54.	22.	0.	6.14	231942.	1399.70	7.68	-78.	28.	7.	5.85	0.040	1.937
72	232047.	1400.76	1.73E+05	0.29	-39.	10.	-8.	6.15	232046.	1400.76	9.15	-63.	23.	-15.	5.86	0.032	1.950
72	232151.	1401.84	1.69E+05	0.22	-42.	20.	-22.	5.92	232150.	1401.83	7.60	-63.	21.	-17.	5.82	0.029	1.257
72	232315.	1403.28	1.63E+05	0.24	-53.	12.	-10.	6.04	232318.	1403.29	6.94	-62.	19.	-19.	5.81	0.035	1.706
72	232419.	1404.30	1.59E+05	0.31	-27.	-2.	-12.	6.13	232422.	1404.36	7.10	-60.	21.	-19.	5.79	0.044	2.169
72	232523.	1405.38	1.54E+05	0.25	-37.	-5.	-14.	6.05	232517.	1405.29	7.40	-60.	21.	-19.	5.82	0.034	1.698
72	232627.	1406.46	1.50E+05	0.30	-43.	-10.	-19.	6.18	232622.	1406.37	7.48	-58.	21.	-20.	5.81	0.040	2.330
72	232731.	1407.54	1.46E+05	0.21	-39.	21.	-9.	5.95	232725.	1407.42	6.30	-60.	20.	-11.	5.79	0.033	1.444
72	232835.	1408.56	1.41E+05	0.22	-29.	6.	-12.	5.99	232830.	1408.50	5.88	-61.	21.	-6.	5.78	0.037	1.640
72	232939.	1409.64	1.37E+05	0.18	-15.	24.	3.	5.94	232933.	1409.55	5.40	-65.	21.	-10.	5.74	0.033	1.583
72	233043.	1410.72	1.33E+05	0.12	-44.	15.	5.	5.96	233038.	1410.63	3.15	-73.	18.	-2.	5.66	0.038	1.982
72	233147.	1411.80	1.28E+05	0.15	-39.	4.	3.	5.98	233149.	1411.81	2.78	-69.	16.	-5.	5.69	0.054	1.961
72	233251.	1412.82	1.24E+05	0.11	-44.	18.	-12.	5.78	233254.	1412.90	2.63	-68.	18.	-2.	5.67	0.042	1.278
72	233355.	1413.90	1.20E+05	0.09	-56.	13.	4.	5.79	233352.	1413.86	2.70	-63.	17.	-6.	5.68	0.033	1.275
72	233459.	1414.98	1.15E+05	0.13	-28.	17.	-3.	5.88	233453.	1414.89	2.88	-64.	19.	-11.	5.66	0.045	1.679
72	233603.	1416.06	1.11E+05	0.08	-53.	15.	-5.	5.65	233557.	1415.96	2.85	-64.	20.	-7.	5.67	0.028	0.954
72	233707.	1417.14	1.06E+05	0.10	-44.	15.	-8.	5.73	233701.	1417.02	3.05	-64.	18.	-1.	5.63	0.033	1.250
72	233811.	1418.16	1.02E+05	0.13	-32.	15.	1.	5.70	233805.	1418.09	3.78	-60.	17.	7.	5.61	0.034	1.243
72	233915.	1419.24	9.76E+04	0.12	-31.	1.	-12.	5.71	233909.	1419.15	3.97	-56.	17.	1.	5.63	0.030	1.209
72	234018.	1420.32	9.32E+04	0.15	-19.	1.	8.	5.93	234021.	1420.36	4.26	-56.	17.	-1.	5.65	0.035	1.916
72	234123.	1421.40	8.87E+04	0.13	-25.	8.	5.	5.78	234133.	1421.55	2.70	-65.	16.	-1.	5.56	0.048	1.666
72	234227.	1422.48	8.43E+04	0.04	-42.	8.	0.	5.44	234238.	1422.63	2.08	-61.	18.	1.	5.55	0.019	0.781
72	234330.	1423.50	8.01E+04	0.08	-34.	17.	8.	5.69	234332.	1423.54	2.17	-63.	17.	-1.	5.52	0.037	1.477
72	234434.	1424.58	7.57E+04	0.05	-29.	-2.	2.	5.20	234429.	1424.49	2.60	-62.	14.	-3.	5.51	0.019	0.489
72	234538.	1425.66	7.13E+04	0.09	-31.	22.	2.	5.64	234541.	1425.68	3.13	-53.	15.	-10.	5.56	0.029	1.211
72	234642.	1426.68	6.71E+04	0.11	-18.	-2.	-19.	5.94	234629.	1426.48	3.00	-55.	16.	-7.	5.54	0.037	2.509
72	234752.	1427.88	6.22E+04	0.07	-8.	20.	-6.	5.85	234717.	1427.28	3.60	-44.	13.	-11.	5.53	0.019	2.089
72	234902.	1429.02	5.75E+04	0.09	-26.	-6.	-6.	5.92	234916.	1429.26	1.30	-47.	18.	-7.	5.54	0.069	2.399
72	235006.	1430.10	5.31E+04	0.02	-22.	6.	-3.	5.01	235004.	1430.07	0.95	-52.	18.	-3.	5.50	0.021	0.321
72	235110.	1431.18	4.86E+04	0.03	-23.	11.	-7.	4.96	235105.	1431.09	1.20	-50.	19.	-3.	5.50	0.025	0.291
72	235214.	1432.26	4.42E+04	0.03	-23.	6.	-5.	4.85	235210.	1432.17	0.55	-57.	21.	11.	5.47	0.055	0.242
72	235318.	1433.28	4.00E+04	0.01	-20.	13.	-3.	4.63	235315.	1433.25	0.50	-53.	18.	2.	5.38	0.020	0.177
72	235422.	1434.36	3.56E+04	0.01	-25.	14.	0.	4.89	235420.	1434.33	0.50	-53.	20.	-7.	5.38	0.020	0.324
72	235526.	1435.44	3.11E+04	0.01	-30.	13.	5.	4.80	235523.	1435.38	0.60	-52.	16.	-7.	5.40	0.017	0.251
72	235630.	1436.52	2.67E+04	0.08	-48.	31.	-50.	6.94	235626.	1436.43	0.40	-45.	23.	-3.	5.46	0.200	30.168
72	235734.	1437.54	2.25E+04	0.05	-78.	44.	-5.	7.10	235714.	1437.24	0.20	-45.	24.	1.	5.47	0.250	42.658
72	235838.	1438.62	1.81E+04	0.04	-112.	49.	33.	6.78	235835.	1438.59	0.30	-24.	26.	-9.	5.35	0.133	26.802

M/Q =12 Final moments computed from model calculations

doy	SCET hhmmss	SCET minutes	distance km	Density cm-3	HSE Coord Vx	Vy	Vz	Log(T) K	Total seconds
72	230105.	1381.08	2.54E+05	0.80	-59.	-26.	4.	6.28	1024
72	230513.	1385.22	2.37E+05	0.90	-62.	-21.	4.	6.23	496
72	231337.	1393.62	2.03E+05	1.60	-44.	-6.	-6.	5.97	1520
72	231337.	1393.62	2.03E+05	1.20	-38.	3.	-13.	5.99	512
72	232219.	1402.32	1.67E+05	3.00	-33.	0.	-9.	5.86	512
72	232747.	1407.78	1.45E+05	4.70	-29.	1.	-2.	5.72	128
72	232953.	1409.88	1.36E+05	4.90	-31.	0.	-1.	5.65	128
72	233202.	1412.04	1.27E+05	5.50	-27.	2.	-4.	5.63	640
72	233202.	1412.04	1.27E+05	5.80	-26.	4.	-5.	5.70	128
72	233408.	1414.14	1.19E+05	6.30	-23.	3.	-6.	5.50	128
72	233618.	1416.30	1.10E+05	5.70	-24.	1.	-3.	5.44	128
72	233824.	1418.40	1.01E+05	8.90	-20.	-1.	0.	5.47	128
72	234034.	1420.56	9.22E+04	9.50	-20.	-3.	1.	5.49	128
72	234240.	1422.66	8.36E+04	10.80	-16.	-2.	0.	5.41	640
72	234240.	1422.66	8.36E+04	12.30	-18.	-3.	1.	5.40	128
72	234449.	1424.82	7.47E+04	11.70	-13.	-4.	-2.	5.44	128
72	234655.	1426.92	6.61E+04	12.80	-13.	-3.	-3.	5.33	128
72	234923.	1429.38	5.60E+04	7.80	-14.	-4.	-1.	5.31	160
72	235201.	1432.02	4.52E+04	8.40	-10.	-1.	0.	5.29	160

M/C =13 Final moments computed from mode calculation.

doy	SCET hhmmss	SCET minutes	distance km	Density cm-3	HSE Coord Vx	Vy	Vz	Log(T) K	Total seconds
72	230105.	1381.08	2.54E+05	0.20	-59.	-26.	4.	6.40	1024
72	230513.	1385.22	2.37E+05	0.10	-62.	-21.	4.	6.33	496
72	234034.	1420.56	9.22E+04	0.50	-20.	-3.	1.	5.34	128
72	234240.	1422.66	8.36E+04	0.50	-16.	-2.	0.	5.46	640
72	234240.	1422.66	8.36E+04	0.50	-18.	-3.	1.	5.59	128
72	234449.	1424.82	7.47E+04	0.50	-13.	-4.	-2.	5.57	128
72	234655.	1426.92	6.61E+04	0.70	-13.	-3.	-3.	5.30	128
72	234923.	1429.38	5.60E+04	0.40	-14.	-4.	-1.	5.39	160
72	235201.	1432.02	4.52E+04	0.10	-10.	-1.	0.	5.32	160

M C =14 Final moments computed from model calculations

doy	SCET hhmmss	SCET minutes	distance km	Density cm-3	HSE Coord Vx	Vy	Vz	Log(T) K	Total seconds
72	231337.	1393.62	2.03E+05	0.30	-38.	3.	-13.	6.05	512
72	232953.	1409.88	1.36E+05	0.70	-31.	0.	-1.	5.66	128
72	233202.	1412.04	1.27E+05	0.50	-27.	2.	-4.	5.88	640
72	233202.	1412.04	1.27E+05	0.60	-26.	4.	-5.	5.49	128
72	233618.	1416.30	1.10E+05	0.70	-24.	1.	-3.	5.66	128
72	233824.	1418.40	1.01E+05	1.10	-20.	-1.	0.	5.57	128
72	234034.	1420.56	9.22E+04	1.00	-20.	-3.	1.	5.71	128
72	234240.	1422.66	8.36E+04	0.90	-16.	-2.	0.	5.50	640
72	234449.	1424.82	7.47E+04	1.30	-13.	-4.	-2.	5.49	128
72	234655.	1426.92	6.61E+04	0.80	-13.	-3.	-3.	5.31	128

M/Q =15 Final moments computed from model calculations

doy	SCET hhmmss	SCET minutes	distance km	Density cm-3	HSE Coord Vx	Vy	Vz	Log(T) K	Total seconds
72	232219.	1402.32	1.67E+05	0.20	-33.	0.	-9.	5.85	512
72	234034.	1420.56	9.22E+04	0.60	-20.	-3.	1.	5.45	128
72	234240.	1422.66	8.36E+04	0.80	-16.	-2.	0.	5.34	640
72	234240.	1422.66	8.36E+04	1.10	-18.	-3.	1.	5.30	128
72	234449.	1424.82	7.47E+04	1.40	-13.	-4.	-2.	5.32	128
72	234923.	1429.38	5.60E+04	1.30	-14.	-4.	-1.	4.86	160
72	235201.	1432.02	4.52E+04	2.00	-10.	-1.	0.	5.25	160

M.G =lt Final moments computed from model calculations

doy	SCET hhmmss	SCET minutes	distance km	Density cm-3	HSE Coord Vx	Vy	Vz	Log(T) K	Total seconds
72	230105.	1381.08	2.54E+05	4.40	-59.	-26.	4.	6.81	1024
72	230513.	1385.22	2.37E+05	4.30	-62.	-21.	4.	6.51	512
72	231337.	1393.62	2.03E+05	6.70	-44.	-6.	-6.	6.14	1528
72	231337.	1393.62	2.03E+05	5.30	-38.	3.	-13.	6.11	512
72	232219.	1402.32	1.67E+05	11.70	-33.	0.	-9.	6.01	512
72	232747.	1407.78	1.45E+05	17.20	-29.	1.	-2.	5.79	128
72	232956.	1409.94	1.36E+05	18.70	-31.	0.	-1.	5.77	128
72	233202.	1412.04	1.27E+05	16.90	-27.	2.	-4.	5.68	640
72	233202.	1412.04	1.27E+05	19.80	-26.	4.	-5.	5.69	128
72	233412.	1414.20	1.18E+05	19.30	-23.	3.	-6.	5.63	128
72	233618.	1416.30	1.10E+05	16.60	-24.	1.	-3.	5.56	128
72	233828.	1418.46	1.01E+05	23.30	-20.	-1.	0.	5.60	128
72	234034.	1420.56	9.22E+04	29.30	-20.	-3.	1.	5.56	128
72	234243.	1422.72	8.33E+04	24.10	-16.	-2.	0.	5.51	640
72	234243.	1422.72	8.33E+04	28.40	-18.	-3.	1.	5.47	128
72	234449.	1424.82	7.47E+04	28.90	-13.	-4.	-2.	5.46	128
72	234655.	1426.92	6.61E+04	23.30	-13.	-3.	-3.	5.40	128
72	234926.	1429.44	5.58E+04	9.90	-14.	-4.	-1.	5.29	160
72	235205.	1432.08	4.49E+04	8.80	-10.	-1.	0.	5.33	160

M/O =17 Final moments computed from model calculations

doy	SCET hhmmss	SCET minutes	distance km	Density cm-3	HSE Coord Vx	Vy	Vz	Log(T) K	Total seconds
72	230105.	1381.08	2.54E+05	4.50	-59.	-26.	4.	6.84	1024
72	230513.	1385.22	2.37E+05	2.20	-62.	-21.	4.	6.42	512
72	231337.	1393.62	2.03E+05	4.60	-44.	-6.	-6.	6.03	1528
72	231337.	1393.62	2.03E+05	4.10	-38.	3.	-13.	6.11	512
72	232219.	1402.32	1.67E+05	9.90	-33.	0.	-9.	5.93	512
72	232747.	1407.78	1.45E+05	17.50	-29.	1.	-2.	5.73	128
72	232956.	1409.94	1.36E+05	16.10	-31.	0.	-1.	5.80	128
72	233202.	1412.04	1.27E+05	18.70	-27.	2.	-4.	5.78	640
72	233202.	1412.04	1.27E+05	19.80	-26.	4.	-5.	5.64	128
72	233412.	1414.20	1.18E+05	23.70	-23.	3.	-6.	5.58	128
72	233618.	1416.30	1.10E+05	22.40	-24.	1.	-3.	5.55	128
72	233828.	1418.46	1.01E+05	34.10	-20.	-1.	0.	5.62	128
72	234034.	1420.56	9.22E+04	34.30	-20.	-3.	1.	5.55	128
72	234243.	1422.72	8.33E+04	30.30	-16.	-2.	0.	5.48	640
72	234243.	1422.72	8.33E+04	38.20	-18.	-3.	1.	5.47	128
72	234449.	1424.82	7.47E+04	34.90	-13.	-4.	-2.	5.44	128
72	234655.	1426.92	6.61E+04	34.70	-13.	-3.	-3.	5.43	128
72	234926.	1429.44	5.58E+04	18.30	-14.	-4.	-1.	5.25	160
72	235205.	1432.08	4.49E+04	12.90	-10.	-1.	0.	5.30	160

M/C =18 Final moments computed from model calculations

doy	SCET hhmmss	SCET minutes	distance km	Density cm-3	HSE Coord Vx	Vy	Vz	Log(T) K	Total seconds
72	230105.	1381.08	2.54E+05	0.80	-59.	-26.	4.	6.46	1024
72	230513.	1385.22	2.37E+05	1.60	-62.	-21.	4.	6.75	512
72	231337.	1393.62	2.03E+05	2.70	-44.	-6.	-6.	6.04	1528
72	231337.	1393.62	2.03E+05	2.30	-38.	3.	-13.	6.06	512
72	232219.	1402.32	1.67E+05	5.70	-33.	0.	-9.	5.95	512
72	232747.	1407.78	1.45E+05	15.10	-29.	1.	-2.	5.85	128
72	232956.	1409.94	1.36E+05	13.80	-31.	0.	-1.	5.77	128
72	233202.	1412.04	1.27E+05	16.90	-27.	2.	-4.	5.81	640
72	233202.	1412.04	1.27E+05	16.60	-26.	4.	-5.	5.62	128
72	233412.	1414.20	1.18E+05	18.20	-23.	3.	-6.	5.65	128
72	233618.	1416.30	1.10E+05	18.70	-24.	1.	-3.	5.59	128
72	233828.	1418.46	1.01E+05	27.20	-20.	-1.	0.	5.59	128
72	234034.	1420.56	9.22E+04	26.70	-20.	-3.	1.	5.52	128
72	234243.	1422.72	8.33E+04	32.90	-16.	-2.	0.	5.45	640
72	234243.	1422.72	8.33E+04	32.70	-18.	-3.	1.	5.39	128
72	234449.	1424.82	7.47E+04	39.30	-13.	-4.	-2.	5.46	128
72	234655.	1426.92	6.61E+04	44.50	-13.	-3.	-3.	5.40	128
72	234926.	1429.44	5.58E+04	21.70	-14.	-4.	-1.	5.22	160
72	235205.	1432.08	4.49E+04	22.70	-10.	-1.	0.	5.34	160

M C =28 Final moments computed from model calculations

doy	SCET hhmmss	SCET minutes	distance km	Density cm-3	HSE Coord Vx	Vy	Vz	Log(T) K	Total seconds
72	231341.	1393.68	2.02E+05	1.70	-44.	-6.	-6.	6.21	1536
72	232223.	1402.38	1.67E+05	2.70	-33.	0.	-9.	6.10	512
72	232750.	1407.84	1.44E+05	5.90	-29.	1.	-2.	5.95	128
72	232956.	1409.94	1.36E+05	9.00	-31.	0.	-1.	6.10	128
72	233206.	1412.10	1.27E+05	6.00	-27.	2.	-4.	5.96	640
72	233828.	1418.46	1.01E+05	18.90	-20.	-1.	0.	5.85	128
72	234037.	1420.62	9.19E+04	19.80	-20.	-3.	1.	5.72	128
72	234243.	1422.72	8.33E+04	15.50	-16.	-2.	0.	5.73	640
72	234243.	1422.72	8.33E+04	13.70	-18.	-3.	1.	5.72	128
72	234453.	1424.88	7.45E+04	11.40	-13.	-4.	-2.	5.77	128
72	234659.	1426.98	6.59E+04	13.10	-13.	-3.	-3.	5.69	128
72	234930.	1429.50	5.55E+04	8.90	-14.	-4.	-1.	5.34	160

M C =32 Final moments computed from model calculations

doy	SCET hhmmss	SCET minutes	distance km	Density cm-3	HSE Coord Vx	Vy	Vz	Log(T) K	Total seconds
72	231341.	1393.68	2.02E+05	2.50	-44.	-6.	-6.	6.37	1536
72	233206.	1412.10	1.27E+05	5.50	-27.	2.	-4.	6.01	640
72	234243.	1422.72	8.33E+04	6.80	-16.	-2.	0.	5.66	640

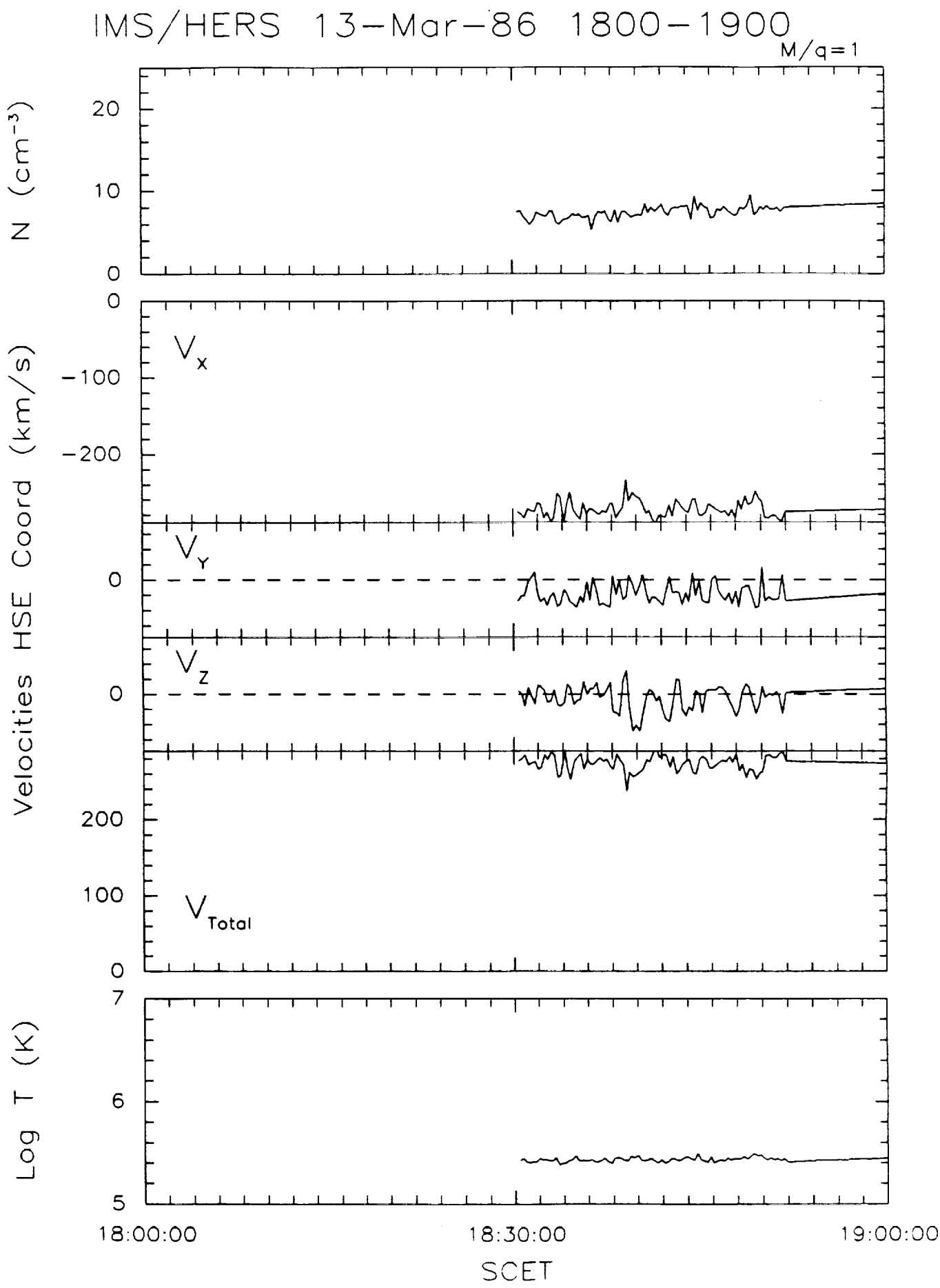
IMS/HERS 13-Mar-86 1800-1900
M/q=1
N (cm⁻³)
20
10
0
Velocities HSE Coord (km/s)
0
-100
-200
V_X
V_Y
0
V_Z
0
200
100
V_Total
0
Log T (K)
7
6
5
18:00:00
18:30:00
19:00:00
SCET

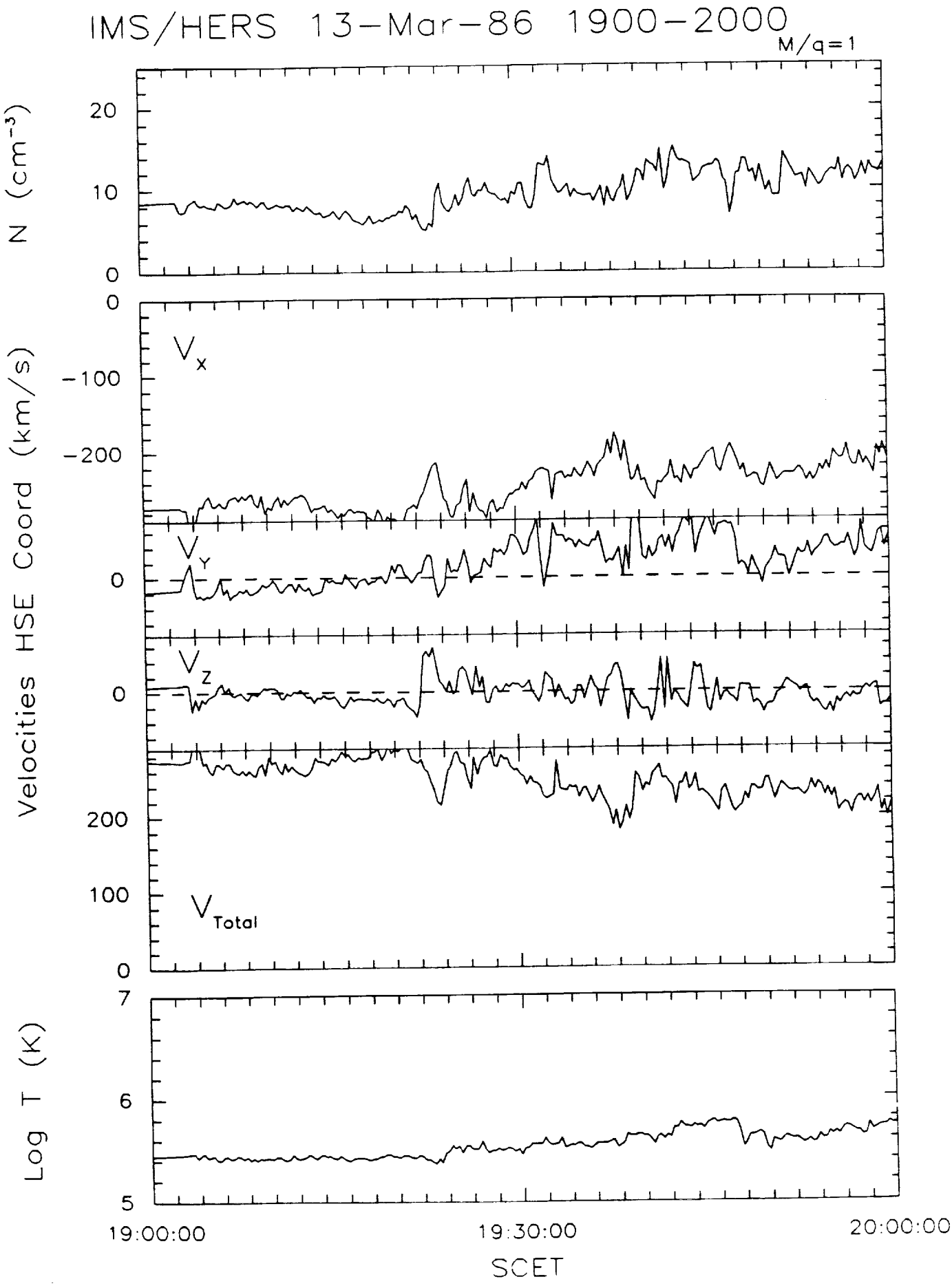
IMS/HERS 13-Mar-86 1900-2000
M/q=1
N (cm⁻³)
20
10
0
Velocities HSE Coord (km/s)
0
-100
-200
V_X
V_Y
0
V_Z
0
200
100
V_Total
0
Log T (K)
7
6
5
19:00:00
19:30:00
20:00:00
SCET

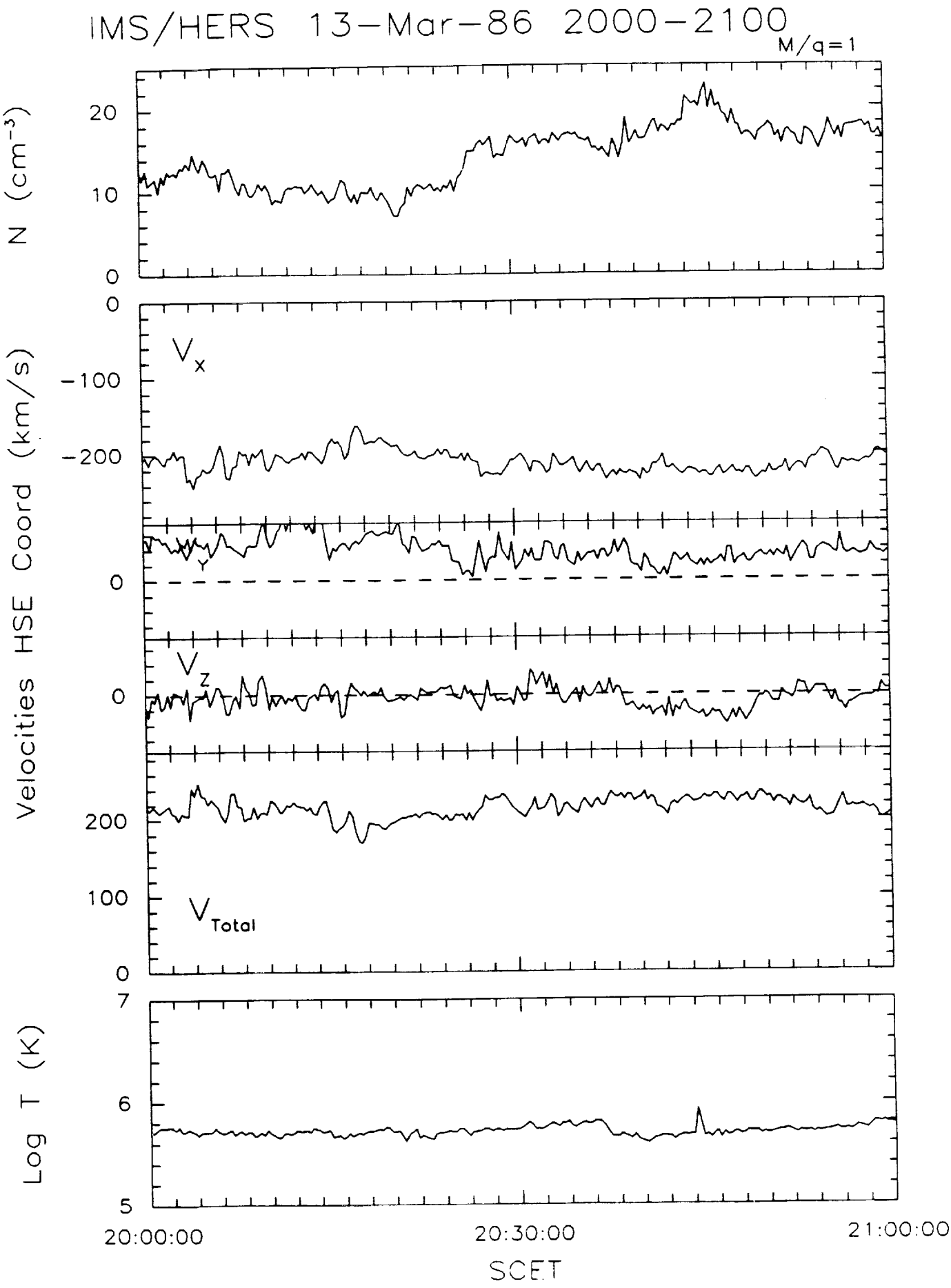
IMS/HERS 13-Mar-86 2000-2100
M/q=1
N (cm⁻³)
20
10
0
Velocities HSE Coord (km/s)
0
-100
-200
Vx
Y
0
Vz
0
200
100
VTotal
0
Log T (K)
7
6
5
20:00:00
20:30:00
21:00:00
SCET

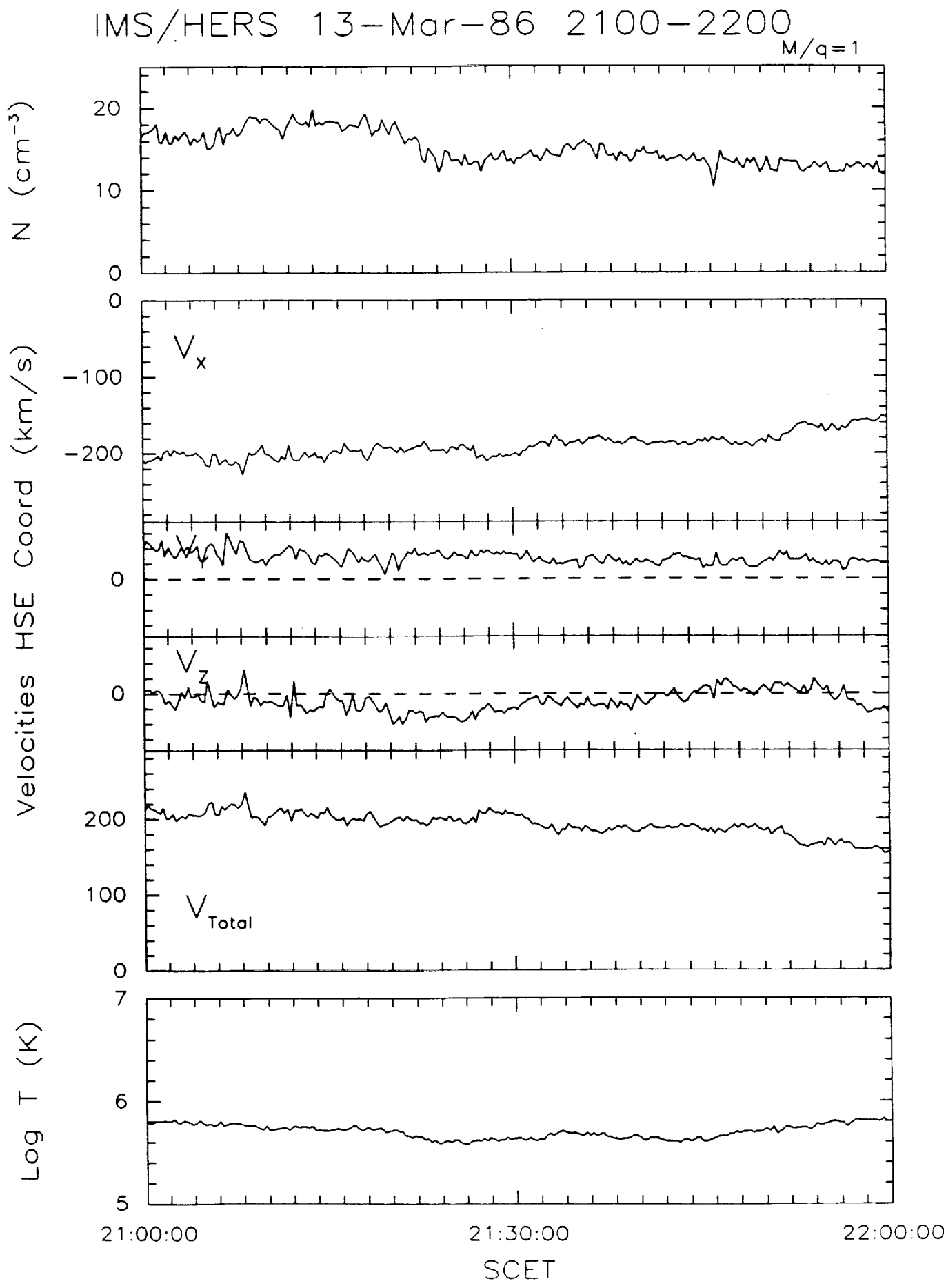
IMS/HERS 13-Mar-86 2100-2200
M/q=1
N (cm⁻³)
20
10
0
Velocities HSE Coord (km/s)
0
-100
-200
Vx
0
Vz
0
200
100
VTotal
0
Log T (K)
7
6
5
21:00:00
21:30:00
22:00:00
SCET

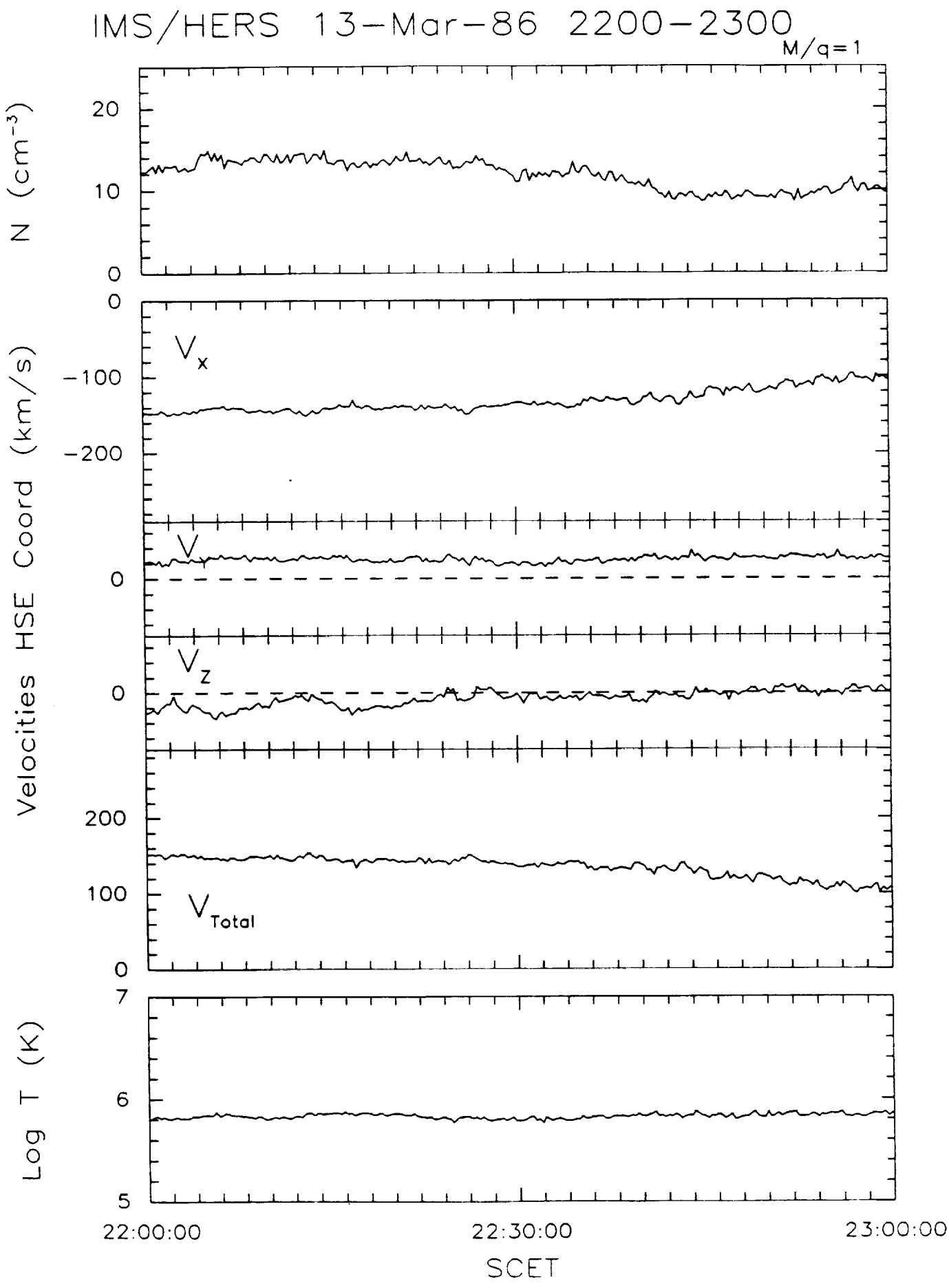
IMS/HERS 13-Mar-86 2200-2300
M/q=1
N (cm⁻³)
20
10
0
Velocities HSE Coord (km/s)
0
-100
-200
Vx
V
0
Vz
0
200
100
V Total
0
Log T (K)
7
6
5
22:00:00
22:30:00
23:00:00
SCET

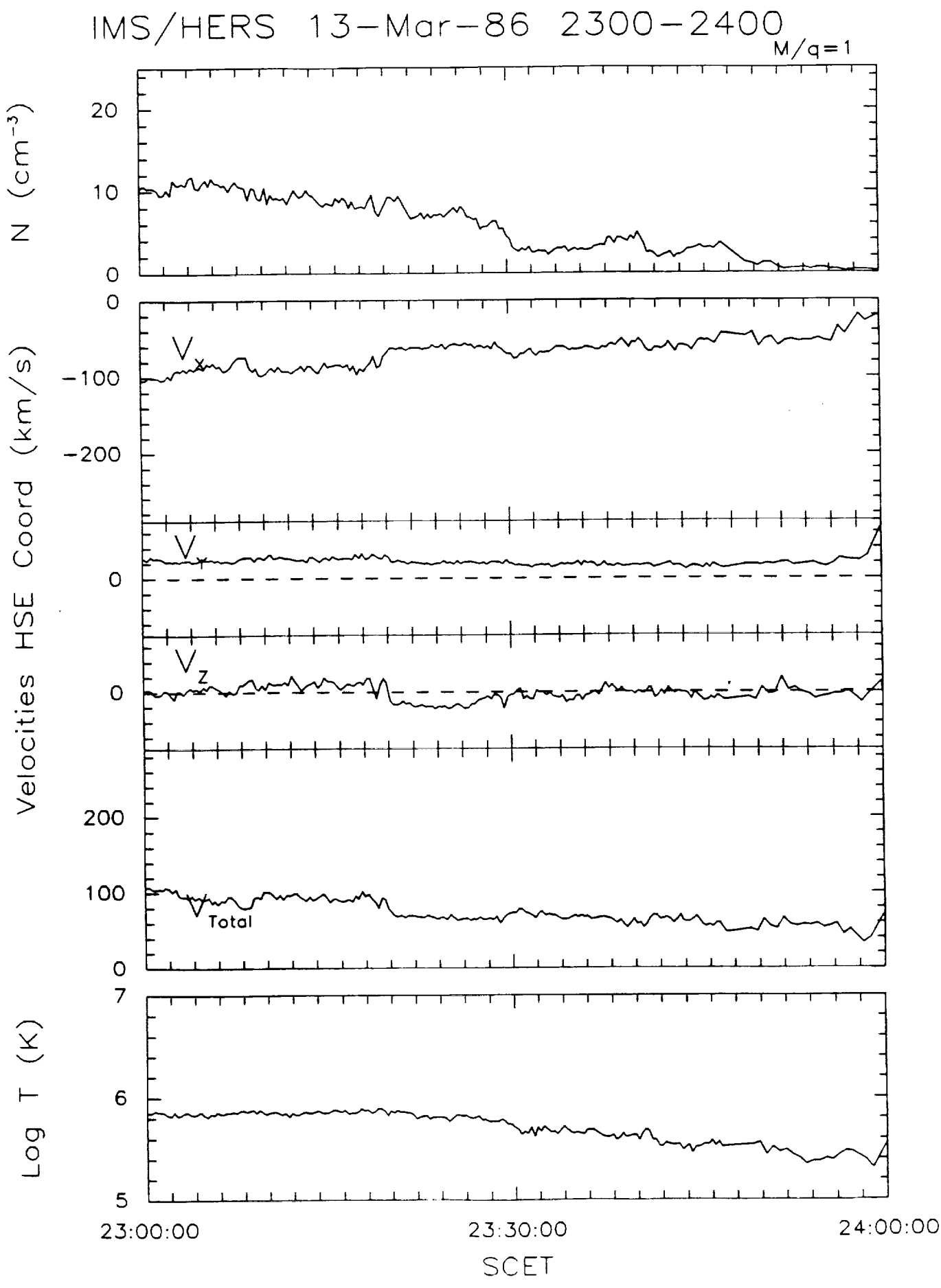
IMS/HERS 13-Mar-86 2300-2400
M/q=1
N (cm⁻³)
20
10
0
Velocities HSE Coord (km/s)
0
-100
-200
Vx
Vy
0
Vz
0
200
100
Total
0
Log T (K)
7
6
5
23:00:00
23:30:00
24:00:00
SCET

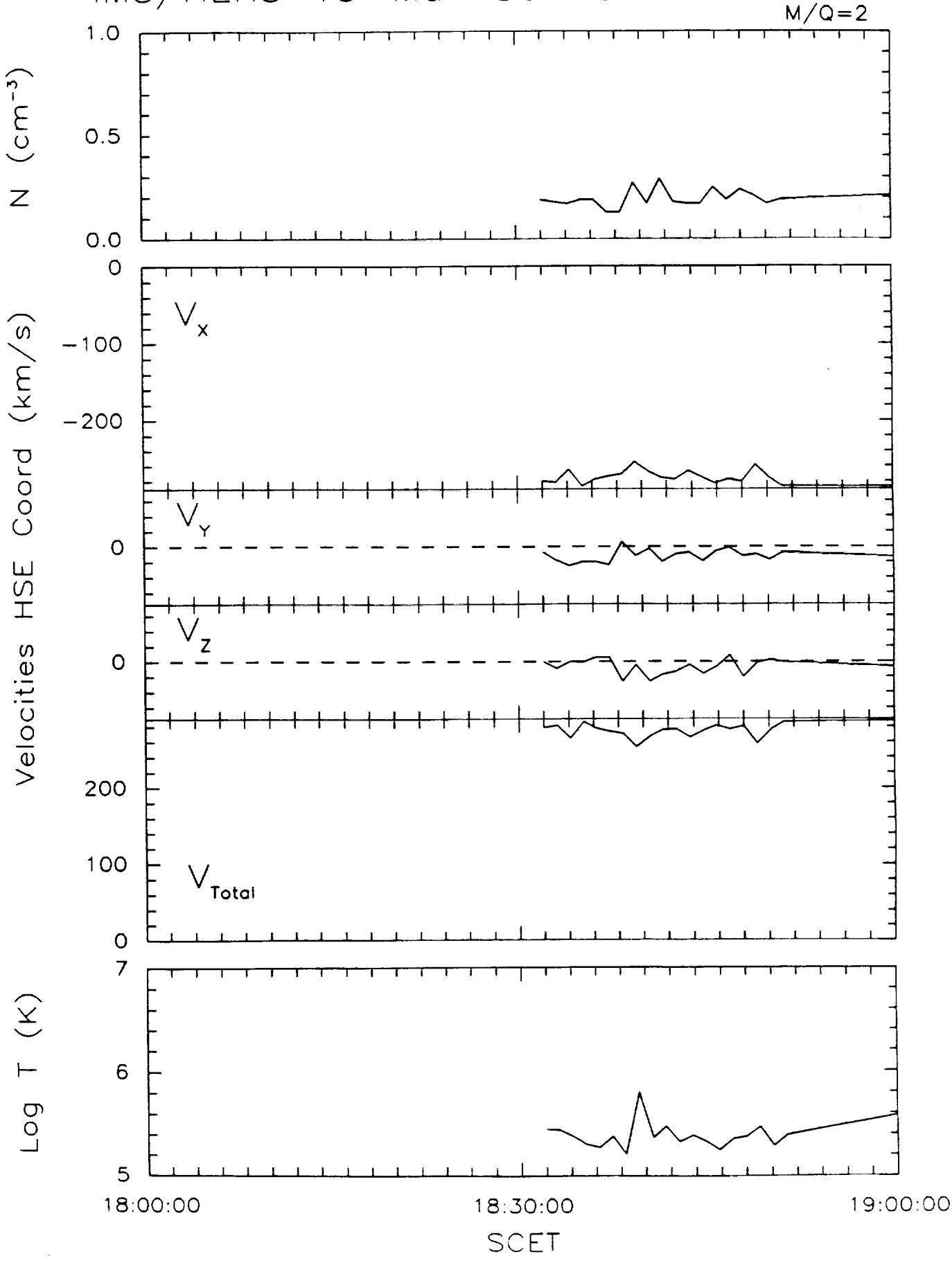
IMS/HERS 13-Mar-86 1800-1900
M/Q=2
N (cm⁻³)
1.0
0.5
0.0
Velocities HSE Coord (km/s)
0
−100
−200
Vx
Vy
0
Vz
0
200
100
VTotal
0
Log T (K)
7
6
5
18:00:00
18:30:00
19:00:00
SCET

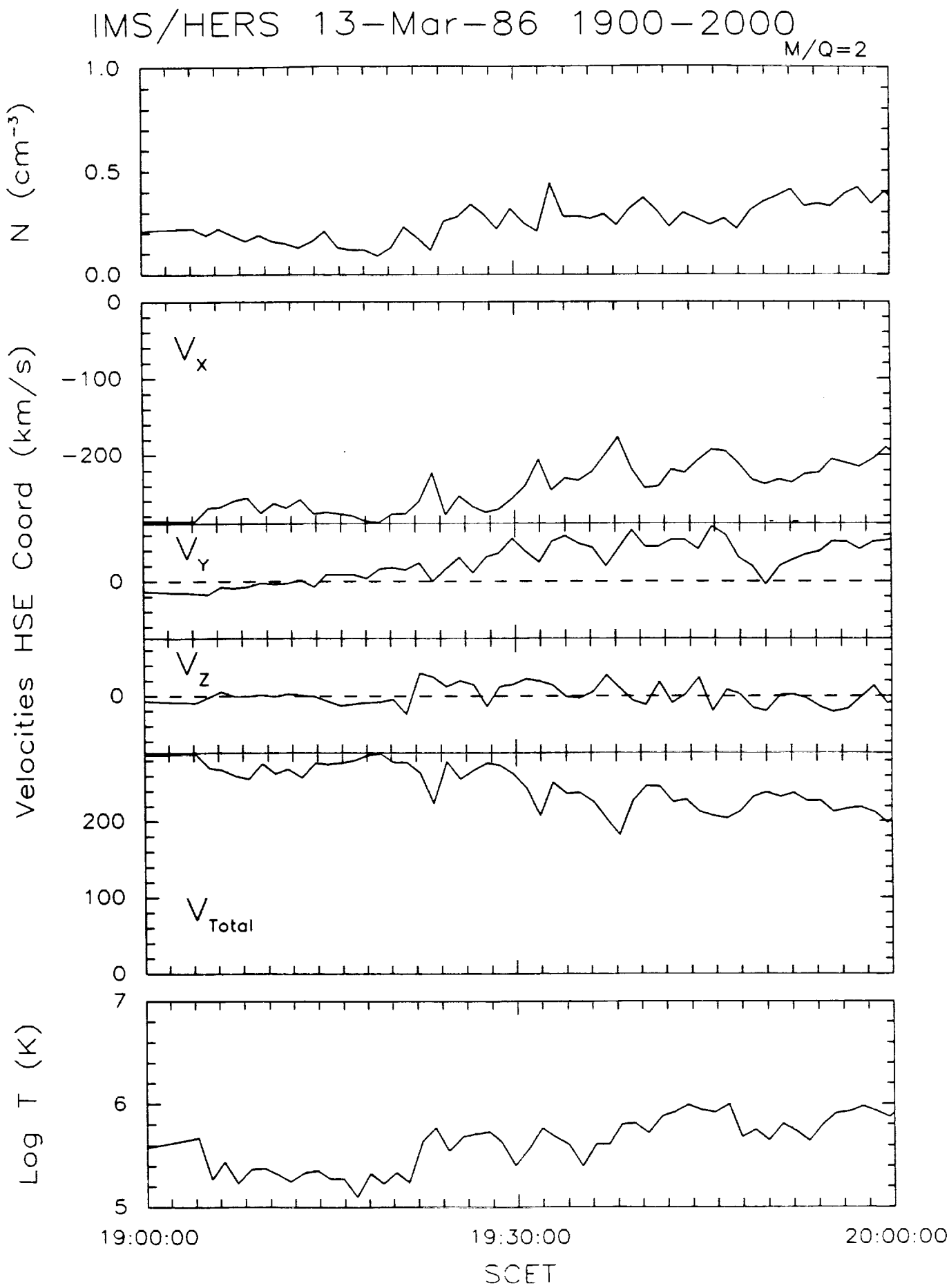
IMS/HERS 13-Mar-86 1900-2000
M/Q=2
N (cm⁻³)
1.0
0.5
0.0
Velocities HSE Coord (km/s)
0
−100
−200
Vx
Vy
0
Vz
0
200
100
VTotal
0
Log T (K)
7
6
5
19:00:00
19:30:00
20:00:00
SCET

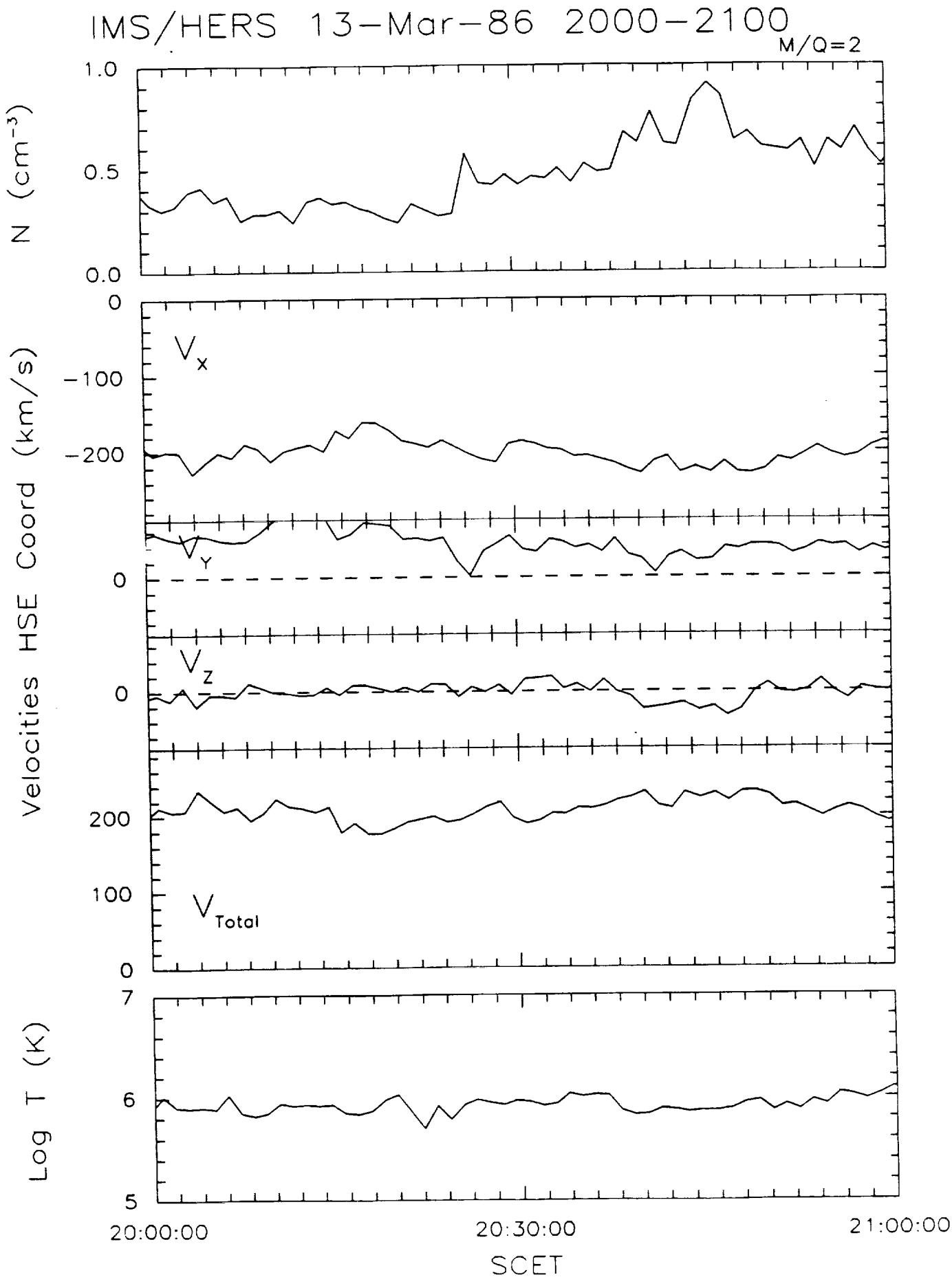
IMS/HERS 13-Mar-86 2000-2100
M/Q=2
N (cm⁻³)
1.0
0.5
0.0
Velocities HSE Coord (km/s)
0
-100
-200
Vx
Vy
0
Vz
0
200
100
VTotal
0
Log T (K)
7
6
5
20:00:00
20:30:00
21:00:00
SCET

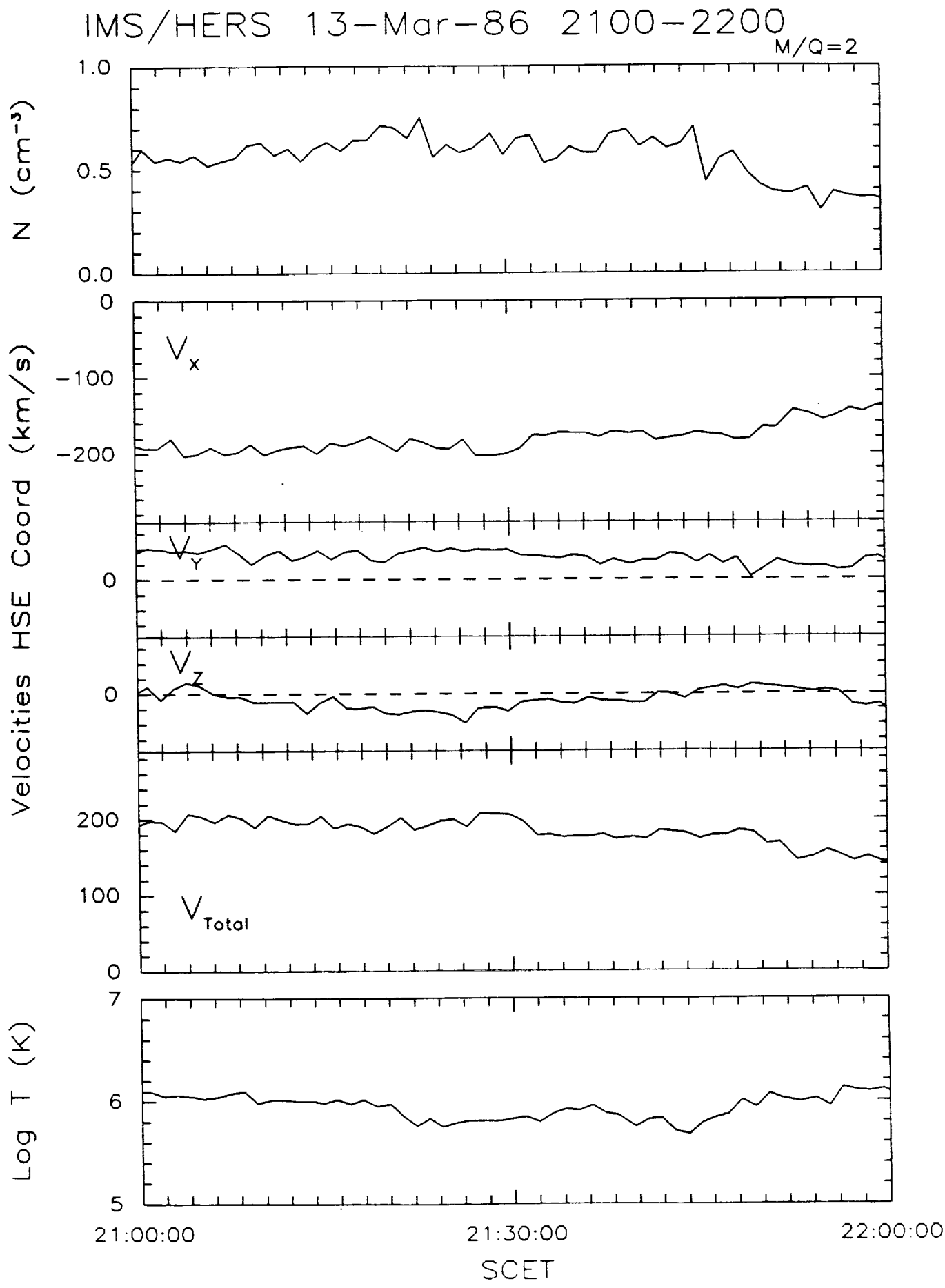
IMS/HERS 13-Mar-86 2100-2200
M/Q=2
N (cm⁻³)
1.0
0.5
0.0
Velocities HSE Coord (km/s)
0
-100
-200
V_X
V_Y
0
V_Z
0
200
100
V_{Total}
0
Log T (K)
7
6
5
21:00:00
21:30:00
22:00:00
SCET

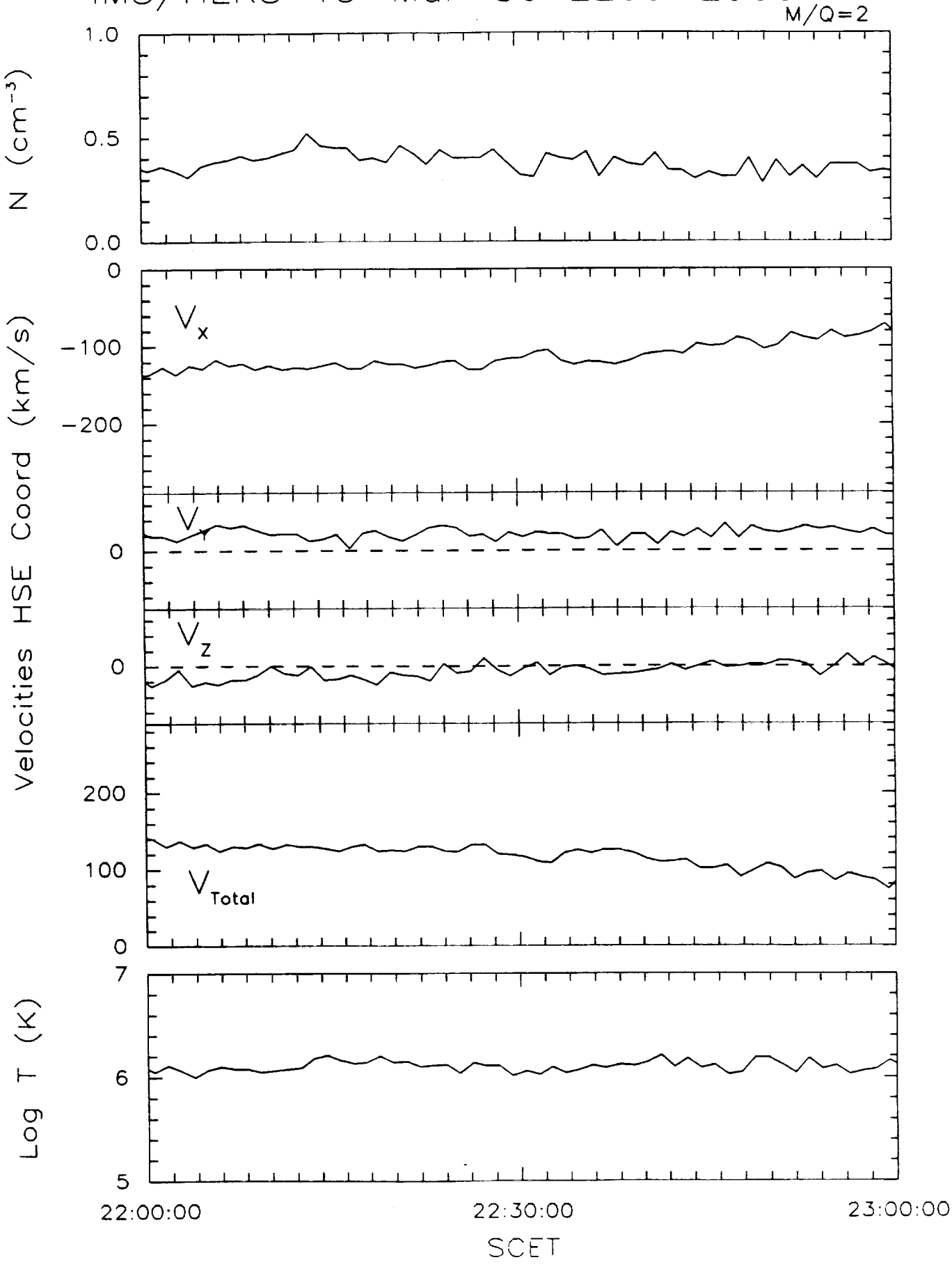
IMS/HERS 13-Mar-86 2200-2300
M/Q=2
N (cm⁻³)
1.0
0.5
0.0
Velocities HSE Coord (km/s)
0
−100
−200
Vx
Vy
0
Vz
0
200
100
VTotal
0
Log T (K)
7
6
5
22:00:00
22:30:00
23:00:00
SCET

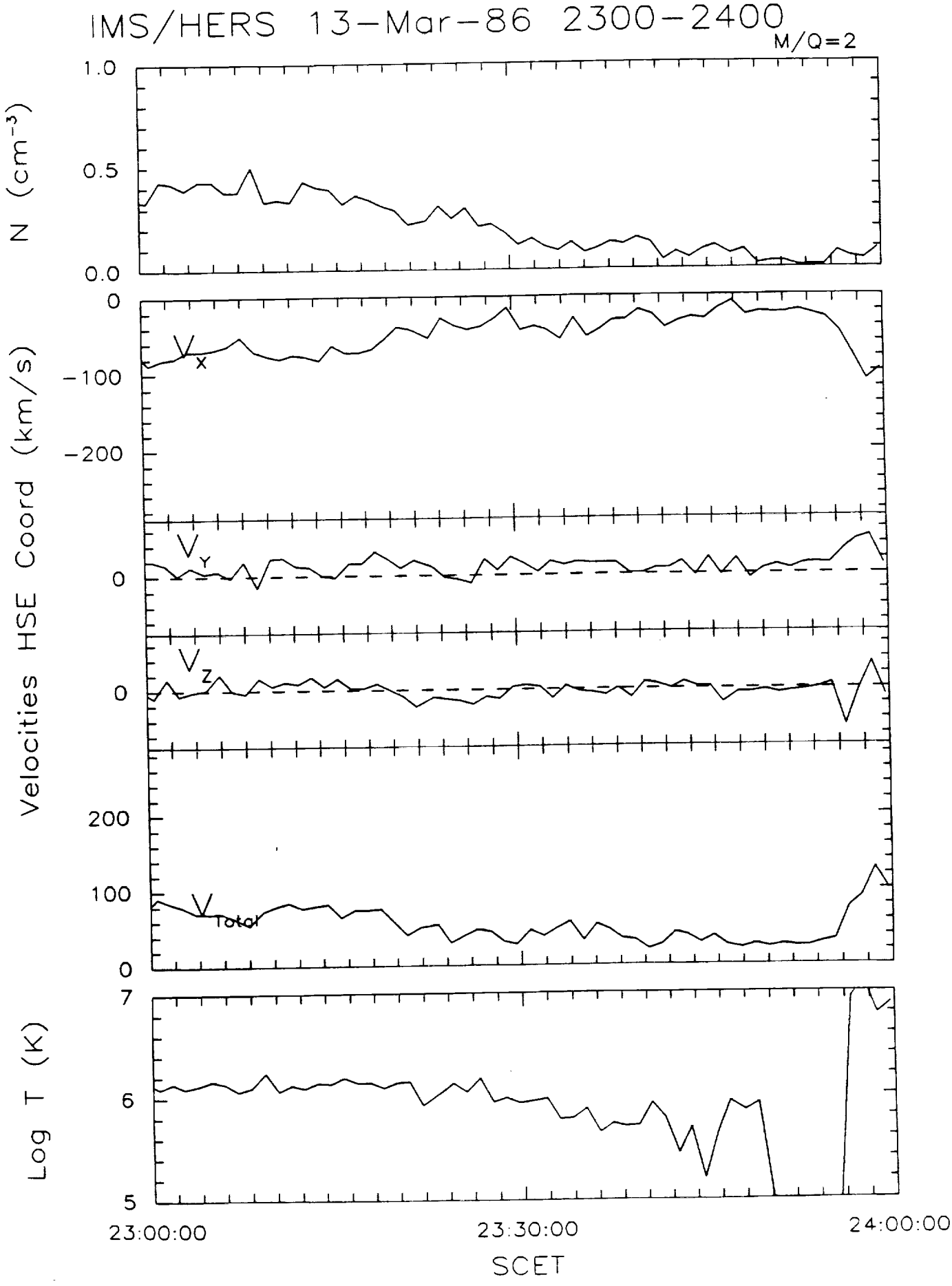
IMS/HERS 13-Mar-86 2300-2400
M/Q=2
N (cm⁻³)
1.0
0.5
0.0
Velocities HSE Coord (km/s)
0
-100
-200
V_X
V_Y
0
V_Z
0
200
100
V_Total
0
Log T (K)
7
6
5
23:00:00
23:30:00
24:00:00
SCET

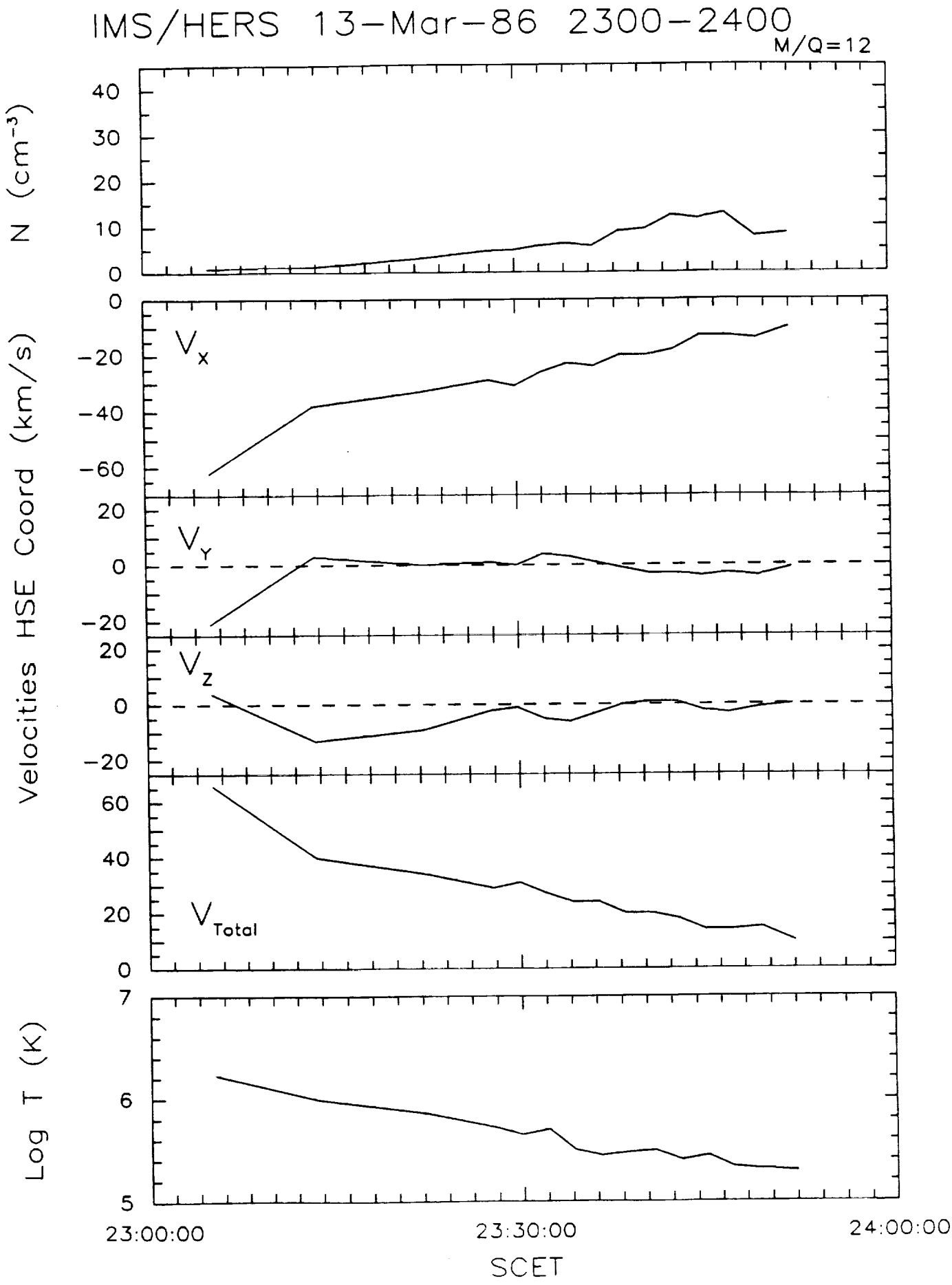
IMS/HERS 13-Mar-86 2300-2400
M/Q=12
N (cm⁻³)
40
30
20
10
0
Velocities HSE Coord (km/s)
0
-20
-40
-60
V_X
20
0
-20
V_Y
20
0
-20
V_Z
60
40
20
0
V_Total
Log T (K)
7
6
5
23:00:00
23:30:00
24:00:00
SCET

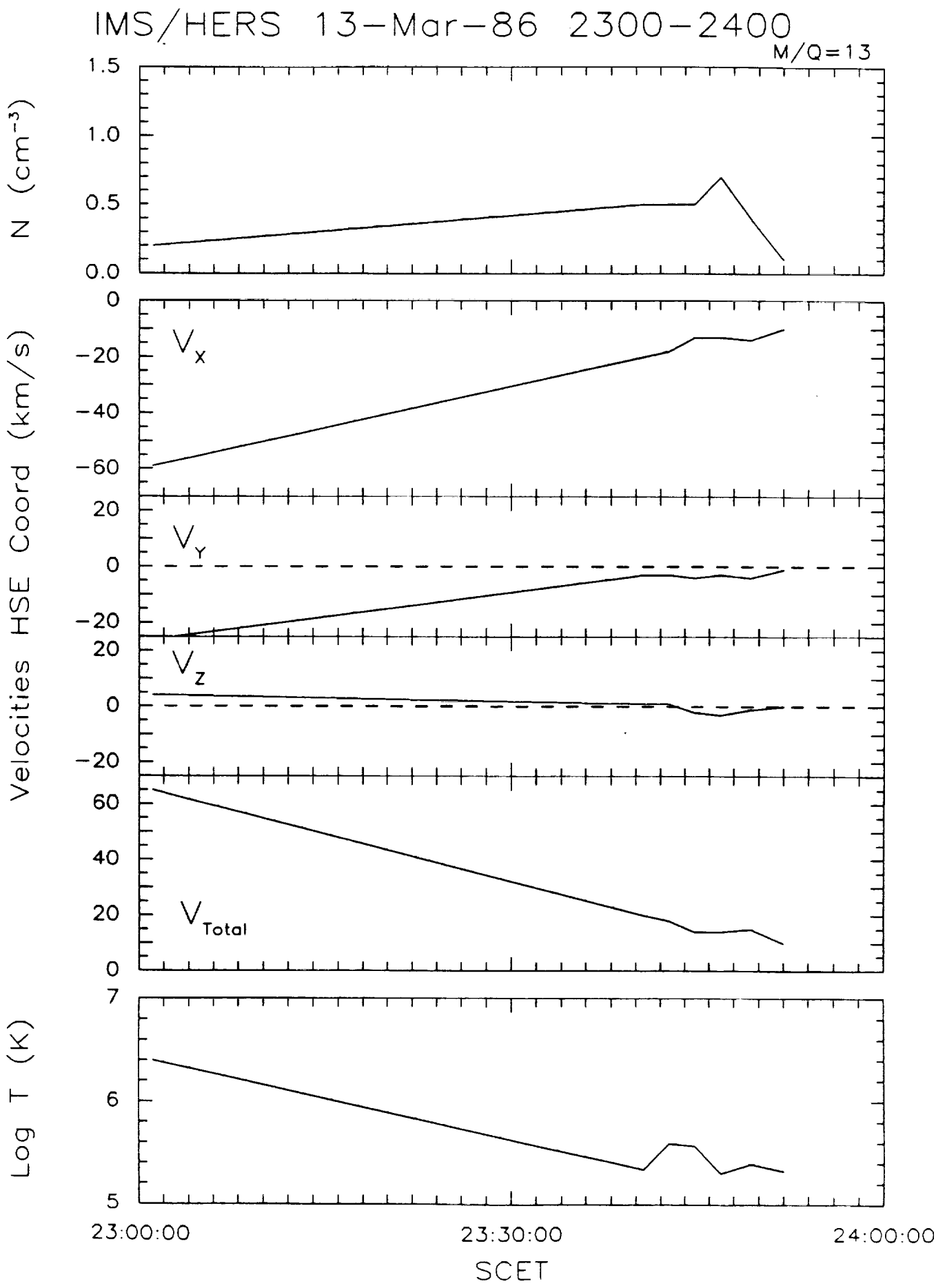
IMS/HERS 13-Mar-86 2300-2400
M/Q=13
N (cm^{-3})
1.5
1.0
0.5
0.0
Velocities HSE Coord (km/s)
V_X
0
-20
-40
-60
V_Y
20
0
-20
V_Z
20
0
-20
V_{Total}
60
40
20
0
Log T (K)
7
6
5
23:00:00
23:30:00
24:00:00
SCET

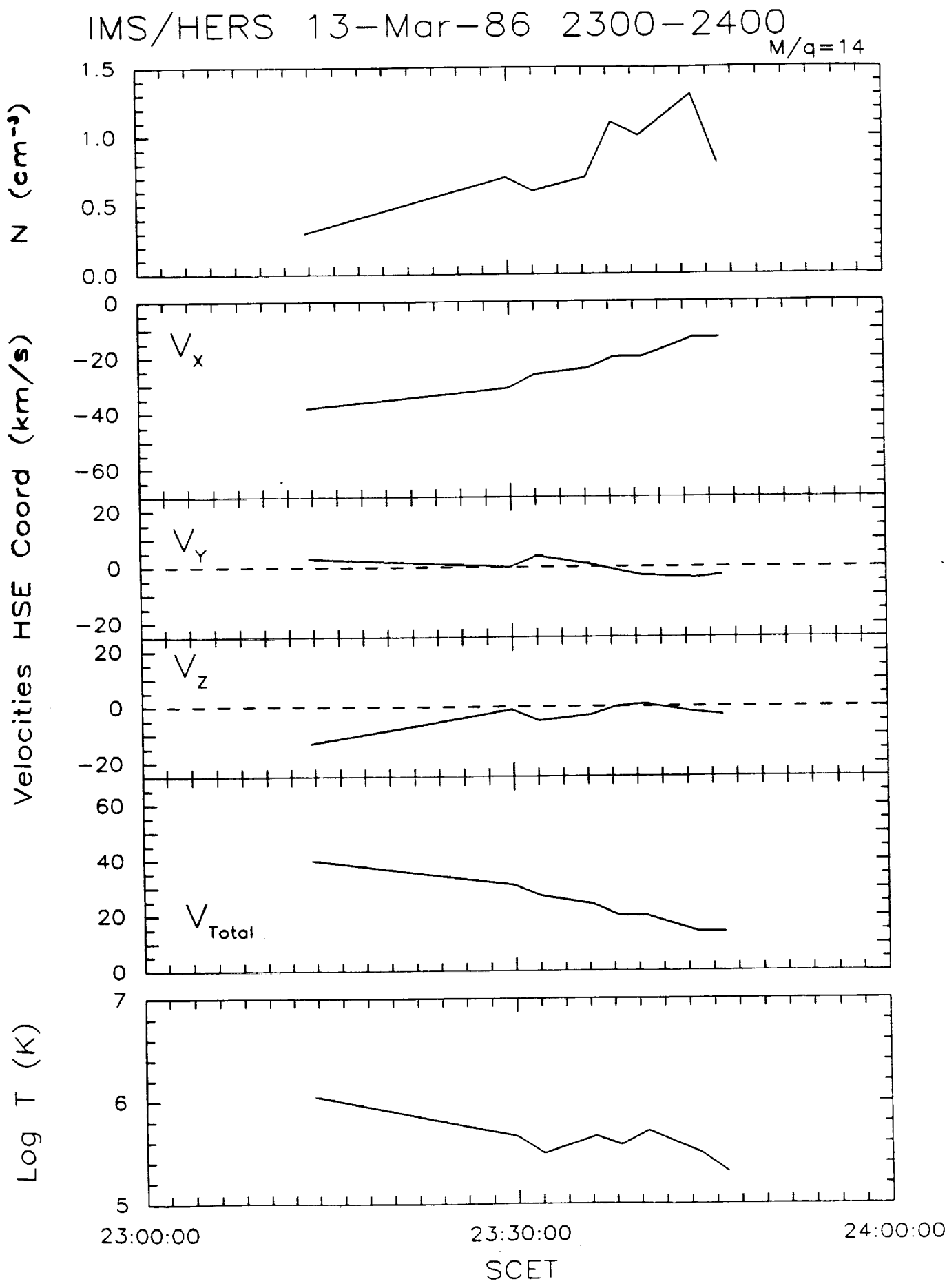
IMS/HERS 13-Mar-86 2300-2400
M/q=14
N (cm⁻³)
1.5
1.0
0.5
0.0
Velocities HSE Coord (km/s)
0
−20
−40
−60
V_X
20
0
−20
V_Y
20
0
−20
V_Z
60
40
20
0
V_{Total}
Log T (K)
7
6
5
23:00:00
23:30:00
24:00:00
SCET

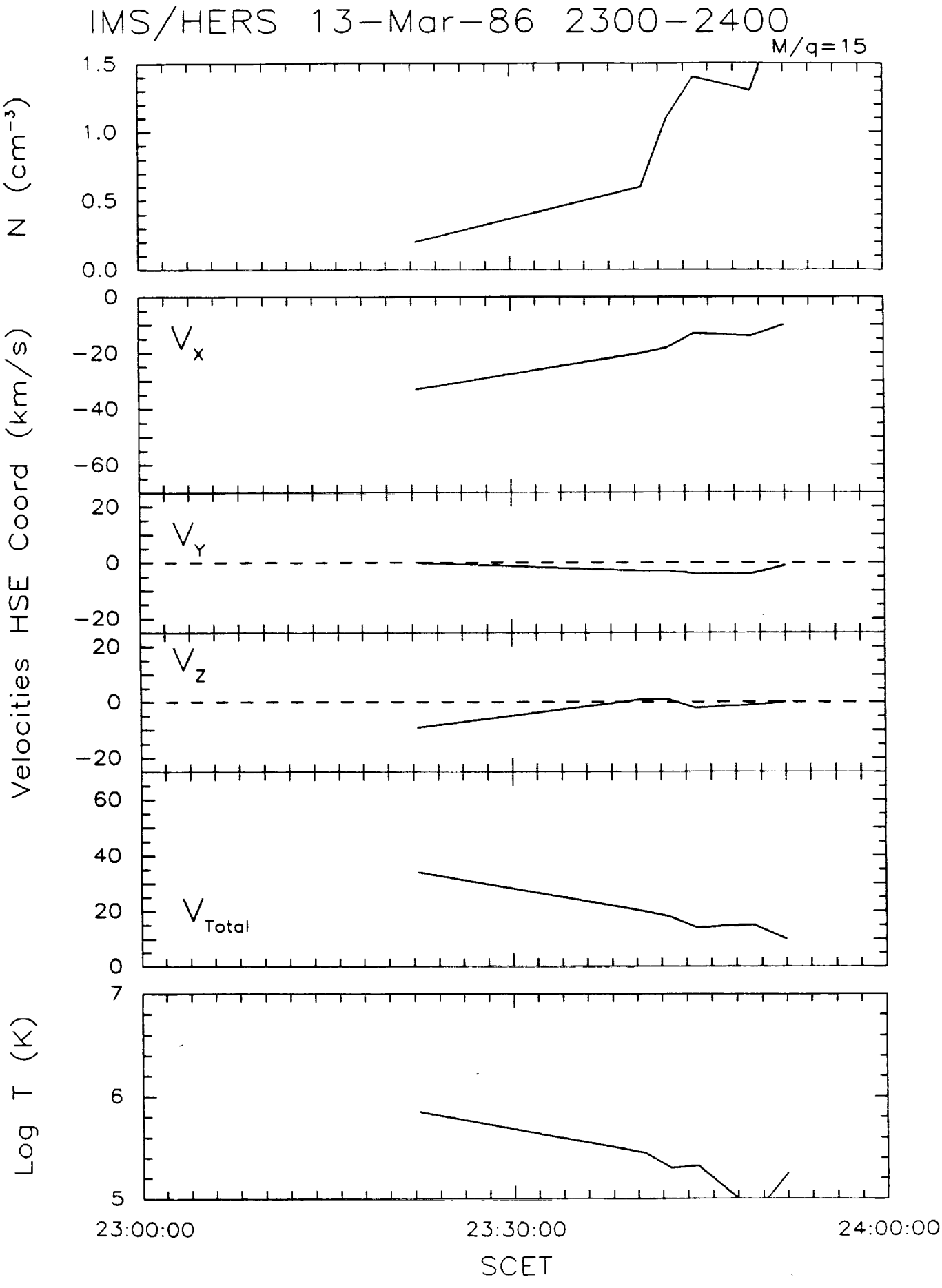
IMS/HERS 13-Mar-86 2300-2400
M/q=15
N (cm⁻³)
1.5
1.0
0.5
0.0
Velocities HSE Coord (km/s)
0
-20
-40
-60
V_X
20
0
-20
V_Y
20
0
-20
V_Z
60
40
20
0
V_Total
Log T (K)
7
6
5
23:00:00
23:30:00
24:00:00
SCET

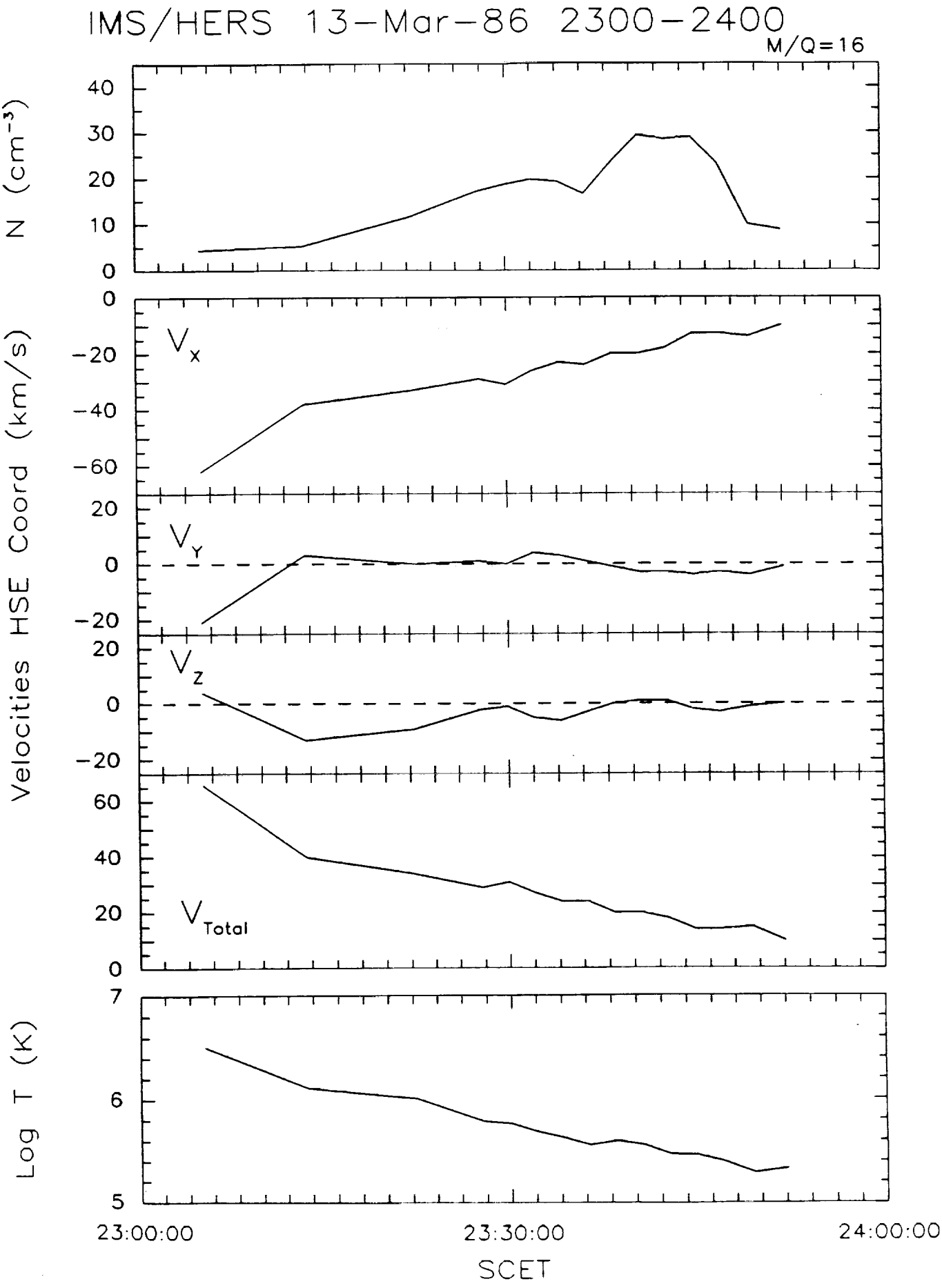
IMS/HERS 13-Mar-86 2300-2400
M/Q=16
N (cm⁻³)
40
30
20
10
0
Velocities HSE Coord (km/s)
0
-20
-40
-60
V_X
20
0
-20
V_Y
20
0
-20
V_Z
60
40
20
0
V_Total
Log T (K)
7
6
5
23:00:00
23:30:00
24:00:00
SCET

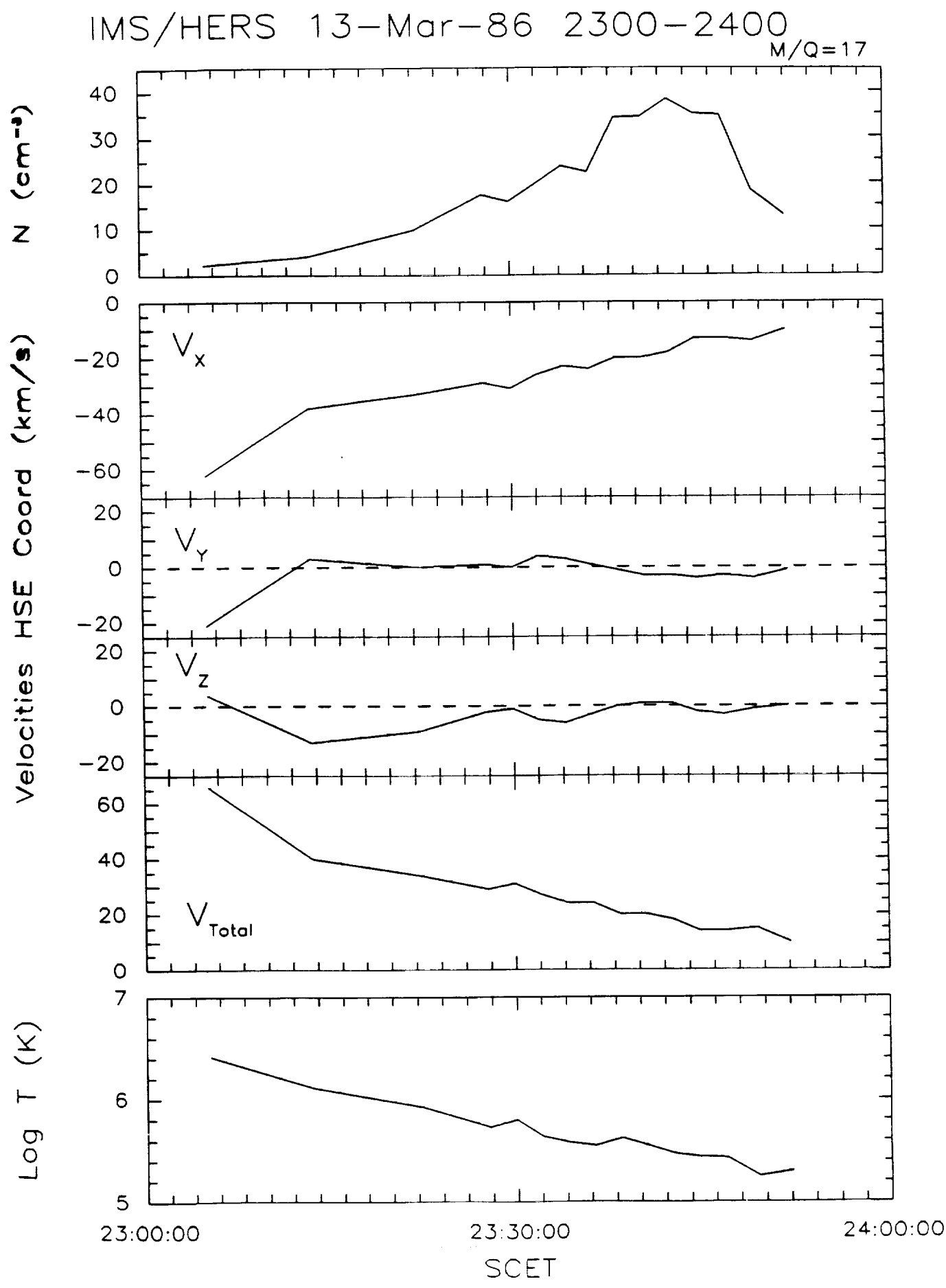
IMS/HERS 13-Mar-86 2300-2400
M/Q=17
N (cm⁻³)
40
30
20
10
0
Velocities HSE Coord (km/s)
0
-20
-40
-60
V_X
20
0
-20
V_Y
20
0
-20
V_Z
60
40
20
0
V_{Total}
Log T (K)
7
6
5
23:00:00
23:30:00
24:00:00
SCET

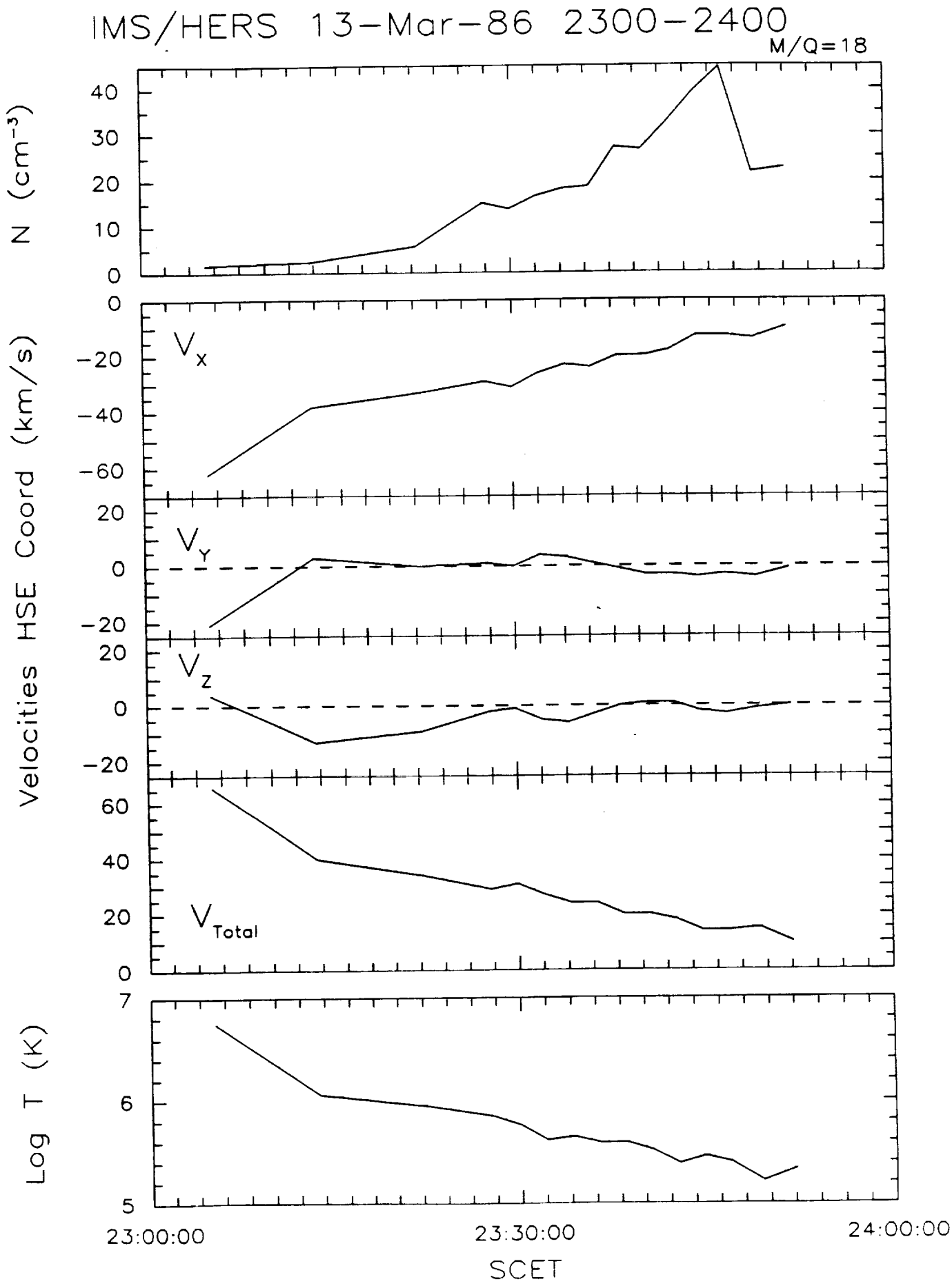
IMS/HERS 13-Mar-86 2300-2400
M/Q=18
N (cm⁻³)
40
30
20
10
0
Velocities HSE Coord (km/s)
0
-20
-40
-60
Vx
20
0
-20
VY
20
0
-20
VZ
60
40
20
0
VTotal
Log T (K)
7
6
5
23:00:00
23:30:00
24:00:00
SCET

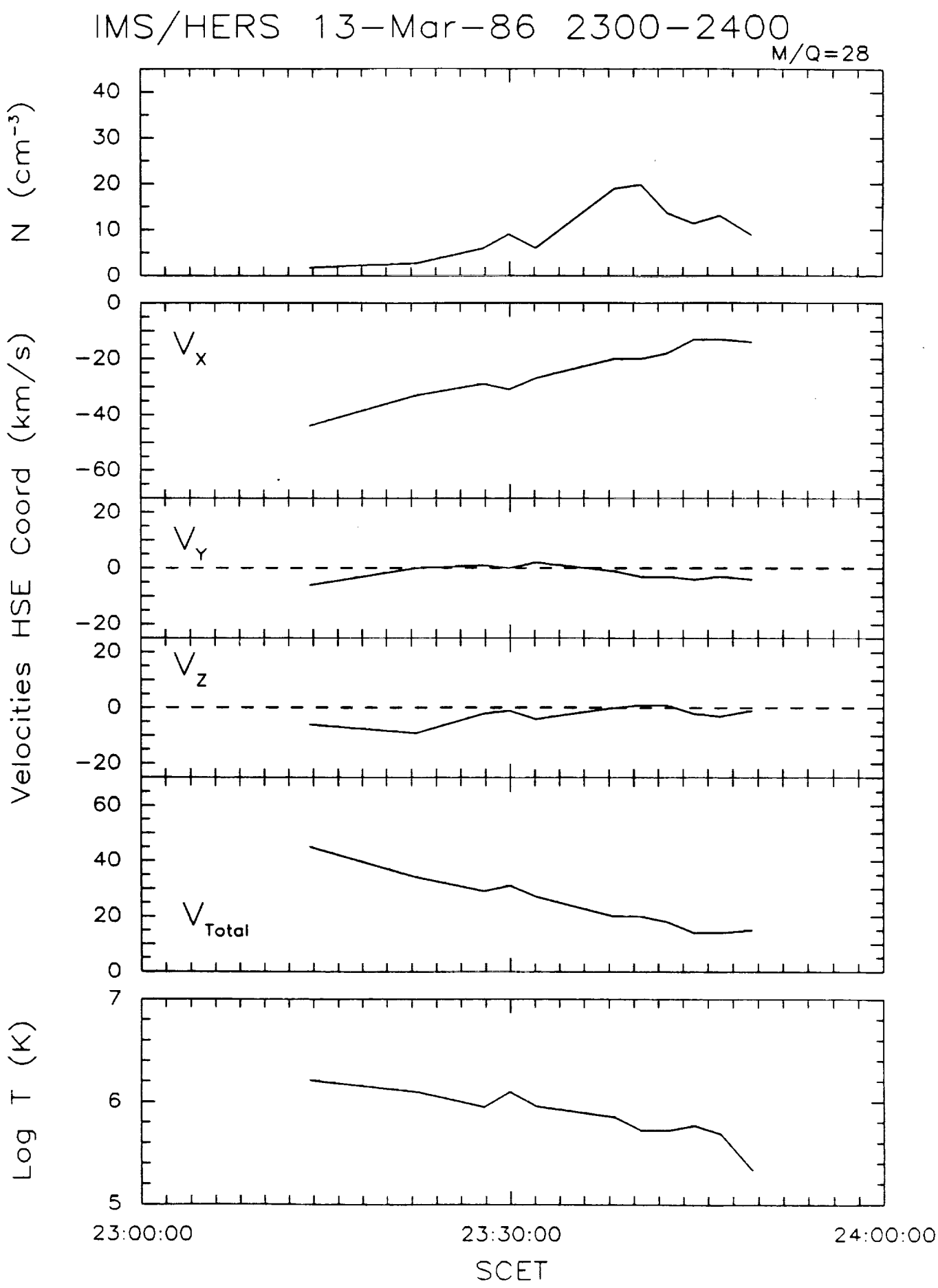
IMS/HERS 13-Mar-86 2300-2400
M/Q=28
N (cm⁻³)
40
30
20
10
0
Velocities HSE Coord (km/s)
0
-20
-40
-60
V_X
20
0
-20
V_Y
20
0
-20
V_Z
60
40
20
0
V_Total
Log T (K)
7
6
5
23:00:00
23:30:00
24:00:00
SCET

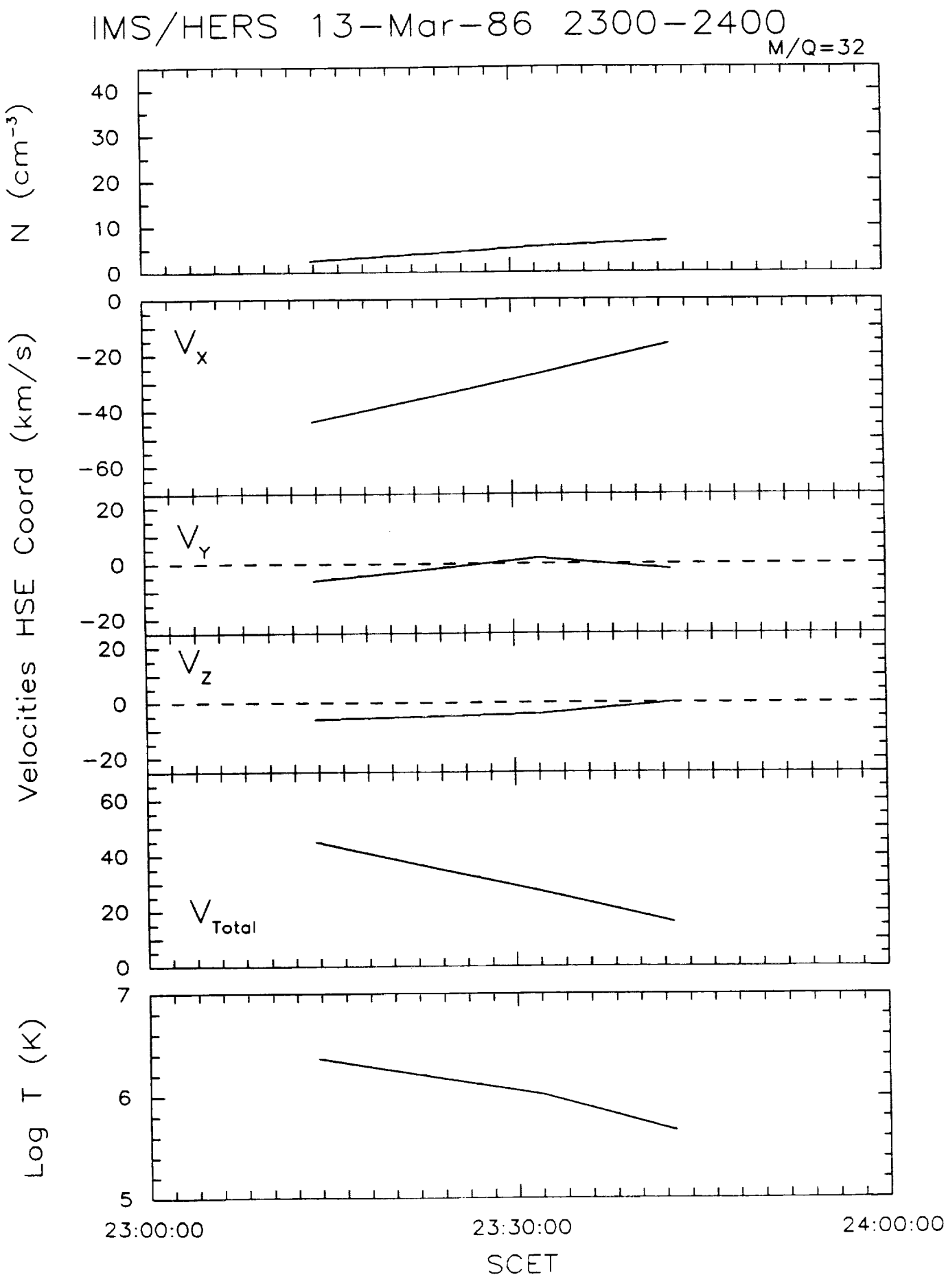
IMS/HERS 13-Mar-86 2300-2400
M/Q=32
N (cm⁻³)
40
30
20
10
0
Velocities HSE Coord (km/s)
0
-20
-40
-60
Vx
20
0
-20
VY
20
0
-20
VZ
60
40
20
0
VTotal
Log T (K)
7
6
5
23:00:00
23:30:00
24:00:00
SCET

Appendix B

Presentations under contract NASW-4336

Presentations under contract NASW-4336

Fuselier, S. A., E. G. Shelley, R. Goldstein, M. Neugebauer, W. H. Ip, H. Balsiger, and H. Rème, Observations of charge exchange of solar wind ions in the comet Halley coma, *Chapman Conference on Cometary Plasma Processes, Guildford, Surrey, England,* July 17-21, 1989.

Glassmeier, K. H., F. M. Neubauer, C. Mazelle, S. A. Fuselier, C. W. Carlson, and M. H. Acuna, Fast magneto-acoustic waves at the pile-up boundary of comet p/Halley, *Chapman Conference on Cometary Plasma Processes, Guildford, Surrey, England,* July 17-21, 1989.

Goldstein, B. E., M. Neugebauer, K. Altwegg, H. Balsiger, A. Meier, W. H. Ip, H. Rosenbauer, R. Schwenn, and S. A. Fuselier, Observations of a shock and a recombination layer at the contact surface of comet Halley, *Chapman Conference on Cometary Plasma Processes, Guildford, Surrey, England,* July 17-21, 1989.

Ip, W. H., H. Rosenbauer, R. Schwenn, G. Kettmann, H. Balsiger, J. Geiss, A. J. Meier, B. E. Goldstein, E. G. Shelley, and A. Lazarus, Giotto IMS measurements of the production rate of hydrogen cyanide in the coma of comet Halley, *Chapman Conference on Cometary Plasma Processes, Guildford, Surrey, England,* July 17-21, 1989.

Kettmann, G., W. H. Ip, R. Schwenn, H. Rosenbauer, H. Balsiger, A. Meier, B. E. Goldstein, and E. G. Shelley, Cometary ion flow variations at comet halley as observed by the giotto IMS experiment, *Champman Conference on Cometary Plasma Processes, Guildford, Surrey, England,* July 17-21, 1989.

Mazelle, C., H. Reme, J. A. Sauvaud, C. d'Uston, D. Lequeau, G. Belmont, K. H. Glassmeier, S. A. Fuselier, C. W. Carlson, K. A. Anderson, R. P. Lin, A. Korth, and D. A. Mendis, Analysis of plasma and magnetic features in the magnetic pile-up region of comet p/Halley, *Chapman Conference on Comentary Plasma Processes, Guildford, Surrey, England,* July 17-21, 1989.

Neugebauer, M., R. Goldstein, B. E. Goldstein, S. A. Fuselier, H. Balsiger, and W.-H. Ip, Densities and abundances of hot cometary ions in the coma of P/Halley, *EOS, Trans. Am. Geophys. U., 71,* 1520, 1990.

Reme, H., C. d'Uston, C. Mazelle, J. A. Sauvaud, K. A. Anderson, C. W. Carlson, R. P. Lin, A. Korth, D. A. Mendis, A. Coates, K. H. Glassmeier, and S. A. Fuselier, Properties of the mystery region and the mystery transition at comet halley, *Champman Conference on Comentary Plasma Processes, Guildford, Surrey, England,* July 17-21, 1989.

Appendix C

Publications under contract NASW-4336

Publications under contract NASW-4336

Neugebauer, M., A. J. Lazarus, H. Balsiger, S. A. Fuselier, B. E. Goldstein, R. Goldstein, F. M. Neubauer, and H. Rosenbauer, The velocity distributions of cometary protons picked up by the solar wind, *J. Geophys. Res., 94,* 5227-5239, 1989.

Goldstein, B. E., K. Altwegg, H. Balsiger, S. A. Fuselier, W. H. Ip, A. Meier, M. Neugebauer, H. Rosenbauer, and R. Schwenn, Observations of a shock and a recombination layer at the contact surface of comet Halley, *J. Geophys. Res., 94,* 17251-17257, 1990.

Kettmann, G., W. H. Ip, H. Balsiger, B. E. Goldstein, A. Meier, H. Rosenbauer, R. Schwenn, and E. G. Shelley, Cometary ion flow variations at comet p/Halley as observed by the u.c. Giotto IMS experiment, *Ann. Geophysical, in press,* 1989.

Ip, W., H. Rosenbauer, R. Schwinn, G. Kettmann, H. Balsiger, J. Geiss, A. J. Meier, B. E. Goldstein, E. G. Shelley, and A. Lazarus, Giotto IMS measurements of the production rate of hydrogen cyanide in the coma of comet Halley, *Anna. Geophys., submitted,* 1989.

Neugebauer, M., R. Goldstein, B. E. Goldstein, S. A. Fuselier, H. Balsiger, and W. Ip, Densities and abundances of hot cometary ions in the coma of P/Halley, *Astrophys. J., in press,* 1991.

Goldstein, B. E., R. Goldstein, M. Neugebauer, S. A. Fuselier, E. G. Shelley, H. Balsiger, G. Kettmann, W. -H.Ip, H. Rosenbauer, and R. Schwenn, Observations of plasma dynamics in the coma of P/Halley by the GIOTTO ion mass spectrometer, *J. Geophys. Res., Submitted,* 1990.

Fuselier, S. A., E. G. Shelley, B. E. Goldstein, R. Goldstein, M. Neugebauer, W. IP, H. Balsiger, and H. Reme, Observations of solar wind ion charge exchange in the comet Halley coma, *Astrophys. J., Submitted,* 1991.

Geiss, J., K. Altwegg, E. Anders, H. Balsiger, W.-H. Ip, A. Meier, M. Neugebauer, H. Rosenbauer, and E. G. Shelley, Interpretation of the ion mass spectra in the mass range 25-35 obtained in the inner coma of Halley's comet by the HIS-sensor of the GIOTTO IMS Experiment, *Astro. and Astrophys., Accepted,* 1990.

Fuselier, S. A., E. G. Shelley, B. E. Goldstein, R. Goldstein, and M. Neugebauer, The evolution of the M/Q=2 ion distribution in the outer coma of comet Halley, *J. Geophys. Res.*, to be submitted, 1991.

Appendix D

Reprints and Preprints of Publications under contract NASW-4336

JOURNAL OF GEOPHYSICAL RESEARCH, VOL. 94, NO. A5, PAGES 5227-5239, MAY 1, 1989

THE VELOCITY DISTRIBUTIONS OF COMETARY PROTONS PICKED UP BY THE SOLAR WIND

M. Neugebauer,[1] A. J. Lazarus,[2] H. Balsiger,[3] S. A. Fuselier,[4]
F. M. Neubauer,[5] and H. Rosenbauer[6]

Abstract. Velocity space distributions of picked up cometary protons were measured by the ion mass spectrometer on the Giotto spacecraft upstream of the Halley bow shock. Large pitch angle anisotropies were observed at all distances $>1.2 \times 10^6$ km from the comet. As expected, pitch angle diffusion was much more rapid than energy diffusion. When the field was quasi-parallel to the solar wind velocity vector, it was possible to discern the effect of pitch angle scattering by sunward propagating, field-aligned hydromagnetic waves, but there is evidence for other scattering modes as well. For quasi-perpendicular geometries, the pitch angle distribution was very asymmetric with phase space density peaks near pitch angles of 180°. It is suggested that the asymmetric pitch angle distribution may be caused by global rather than local wave-particle interactions. Just outside the shock, the pitch angle distribution was nearly isotropic and the radius of the pickup shell increased significantly.

Introduction

The outermost parts of cometary comae have turned out to be excellent sites for the study of a wide variety of wave-particle interactions of importance to space plasma physics. The comet-solar wind interaction offers an excellent opportunity to analyze waves excited by the pickup of cometary ions by the solar wind as well as the effect of those waves back on the plasma. Data obtained by six spacecraft at P/Giacobini-Zinner and P/Halley have inspired a great number of theoretical and observational papers. The present paper is of the latter type. We present observations of the velocity distribution functions of picked-up cometary protons measured by the ion mass spectrometer (IMS) on the Giotto spacecraft over the distance range of 1 to 5 Mkm (1 Mkm = 10^6 km) from the nucleus of comet Halley. The velocity space distributions of the picked-up protons are found to depend on both the direction of the interplanetary magnetic field and proximity to the Halley bow shock. Just as Glassmeier et al. [1987, 1989] found very different wave modes and magnetic power spectra for quasi-parallel and quasi-perpendicular conditions, we find very different pitch angle distributions for those two situations.

[1]Jet Propulsion Laboratory, California Institute of Technology, Pasadena, California
[2]Center for Space Research, Massachusetts Institute of Technology, Cambridge, Massachusetts.
[3]Physikalisches Institut, University of Bern, Bern, Switzerland
[4]Lockheed Palo Alto Research Laboratory, Palo Alto, California.
[5]Institut für Geophysik und Meteorologie, Universität zu Köln, Köln, Federal Republic of Germany
[6]Max-Planck-Institut für Aeronomie, Katlenburg-Lindau, Federal Republic of Germany.

Paper number 88JA04270.
0148-0227/89/88JA-04270$05.00

Instrumentation and Data Selection and Reduction

The design and operation of the Giotto IMS has been described by Balsiger et al. [1987]. The IMS consisted of two sensors named HIS and HERS. The data presented here were obtained outside the Halley bow shock by the high energy range spectrometer (HERS). HERS was a true mass spectrometer capable of mapping velocity distributions as a function of ion mass/charge so the proton distributions could be studied without contamination or confusion by other ion species.

The HERS energy range for protons extended from 10 to 4500 eV. The field of view for proton detection extended from 15° to ~70° from the spacecraft spin axis, which was aligned with the velocity vector of the spacecraft relative to the comet. The geometry is illustrated in the inset in Figure 1. The instrument mapped out 349° in azimuth during a spacecraft spin. The angular bins used for the present analysis were 15° in elevation by 11.25° in azimuth. A three-dimensional proton velocity distribution was measured every fourth spacecraft spin (spin period equal to 4 s).

The present analysis uses 64-s averages of the direction of the interplanetary magnetic field as measured by the Giotto magnetometer, which has been described by Neubauer et al. [1987]. This instrument measured the vector field every 0.035 s. The magnetometer data have been corrected for the spacecraft field and interferences.

Eleven upstream intervals, lettered a through k, were selected for detailed study on the basis that the direction of the interplanetary magnetic field remained relatively steady for a sufficiently long time to accumulate data concerning the three-dimensional distribution of picked-up protons relative to the magnetic field direction. In general, the farther from the comet, the lower the density of picked-up protons, and the longer the interval required to obtain statistically significant results. The locations of the selected intervals relative to the bow shock of comet Halley are shown in Figure 1. The shock was encountered at 1922 UT at a cometocentric distance of 1.14 Mkm; thus the data in intervals k were obtained just outside the shock.

Table 1 lists pertinent information for each interval. From

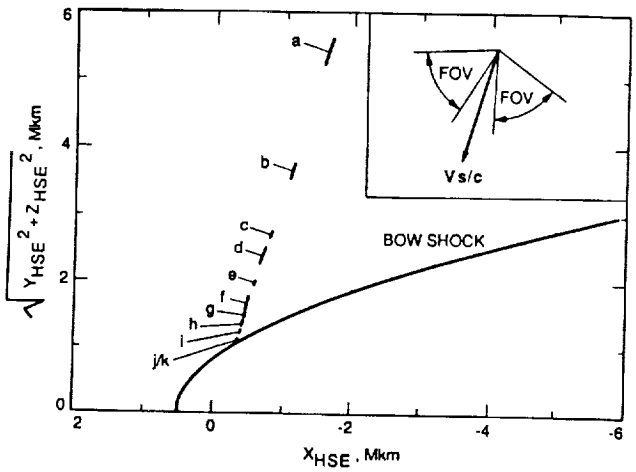

Fig. 1. Locations of the intervals analyzed relative to the bow shock of comet Halley, in Halley-centered solar ecliptic coordinates (HSE). The inset shows the HERS field of view (FOV) relative to the spacecraft velocity vector, Vs/c, and the solar direction X_{HSE}. The field of view is rotationally symmetric about Vs/c.

left to right, the columns in Table 1 are (1) the letter designation and universal (spacecraft event) time, on March 13, 1986, at which the data were obtained, (2) the solar ecliptic latitude angle of the average interplanetary magnetic field vector (positive to the north), (3) the solar ecliptic longitude angle of the average field vector (0° toward the Sun and positive in the direction opposite to planetary motion), (4) the expected radius of a spherical shell of picked-up protons, calculated from the observed solar wind velocity, taking the velocity of the comet into account and assuming an average outflow speed of neutral H atoms of 11 km/s relative to the comet (see Neugebauer et al. [1989] for a discussion of H atom speeds), (5) the angle α between the field direction and the solar wind velocity vector relative to the H atoms, (6) the angle θ_{Bc} between the average magnetic field vector and the direction from the spacecraft to the comet nucleus, and (7) the angle θ_{beam} between the field and the velocity vector of a field-aligned beam of protons reflected from the Halley bow shock.

Figure 2 summarizes the pickup proton distribution functions for each of the 11 intervals. Time increases and distance to the bow shock decreases from the top to the bottom of the figure. The method of transforming the data from a spacecraft coordinate system (speed relative to the spacecraft, elevation angle, and azimuth angle) to a solar-wind-magnetic (SWB) coordinate system moving with the wind and having the field direction as one of its axes has been described by Neugebauer et al. [1989].

Figure 2 shows two plots for each interval. The plots on the right show one-dimensional speed distributions, in SWB coordinates, averaged over both gyroangle and pitch angle, while the left-hand plots present the pitch angle distributions, averaged over both gyroangle and the thickness (in velocity space) of the shell of picked-up protons. The lower limits used for the integration over speed in the calculation of the left-hand plots were obtained from the minima in the right-hand curves between the solar wind and pickup proton distributions. The upper limits were the speeds at which the phase space densities first reached the instrument background level. For both sets of panels the ordinate is the base 10 logarithm of the phase space density, f, in units of cm^{-3} km^{-3} s^3. The mean distance from the comet in units of 10^6 km (Mkm) and the angle α are given to the right of each pair of panels.

In each panel, the observational data are indicated by circles. The horizontal error bars indicate the 15° widths of the pitch angle bins within which the data were averaged, and the vertical error bars show the uncertainties associated with counting statistics. The range of pitch angles sampled depended on the angle between the magnetic field and the spacecraft spin axis; that dependence accounts for the lack of observations at large pitch angles during interval d, for example, and for poor sampling and large error bars at very large or very small pitch angles in many of the other intervals. Unfortunately, the counting statistics are probably not the most significant source of uncertainty or error. First, there is ~30% uncertainty in the absolute calibration of the instrument which affects the absolute values, but not the shapes, of the curves in Figure 2. Second, computation of the weighted

TABLE 1. Average Parameters for Intervals Used in This Study

Interval, UT	θ_B, deg	ϕ_B, deg	Radius, km/s	α, deg	θ_{Bc}, deg	θ_{beam}, deg
Possible range	±90	±180		0-180	0-180	0, 180
a: 0010-0153	-18	-152	365	30	98	180
b: 0800-0859	28	12	383	150	98	0
c: 1220-1249	2	138	352	49	33	?
d: 1324-1424	-10	108	338	80	2	180
e: 1528-1549	87	-37	338	94	101	?
f: 1633-1724	16	178	318	20	74	180
g: 1731-1747	65	-145	320	70	106	180
h: 1757-1820	38	158	313	48	67	?
i: 1828-1849	18	-172	283	21	84	180
j: 1905-1913	62	-100	274	94	124	180
k: 1915-1922	50	-25	285	51	123	?

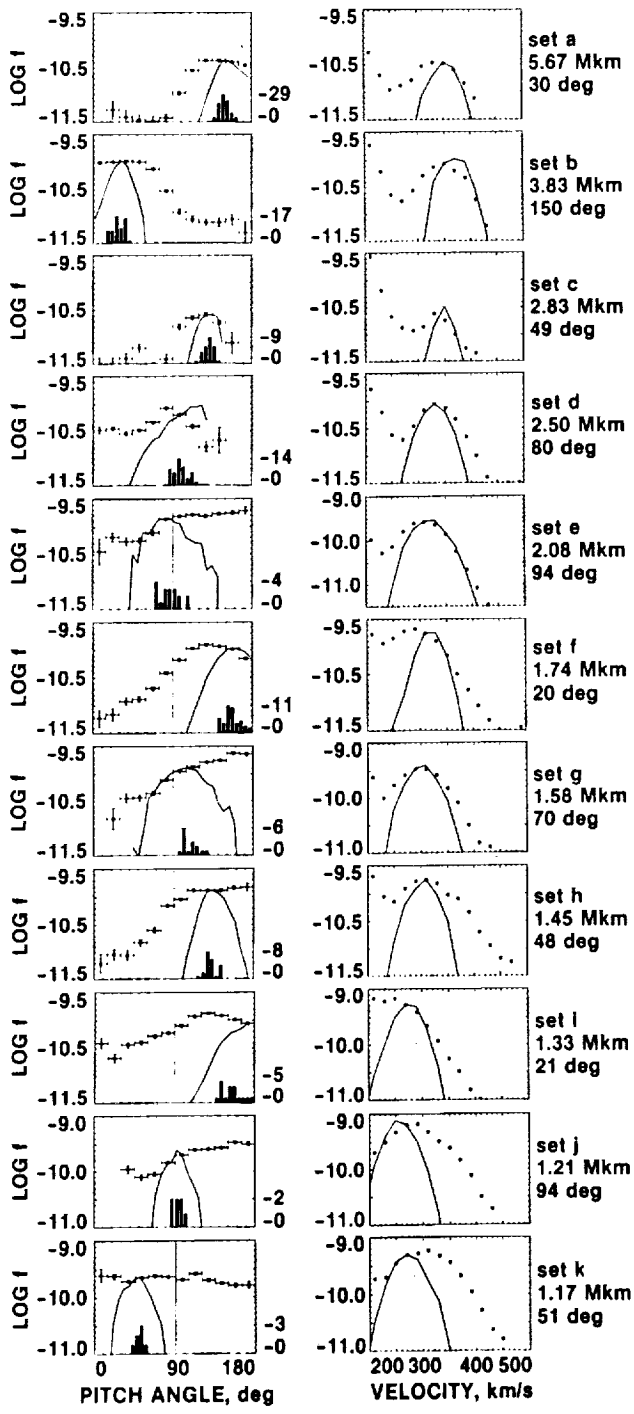

Fig. 2. (Left) Circles: measured pitch angle distributions of picked-up protons. Histograms: distributions of pitch angles expected for a perfect instrument (no uncertainties in angular or energy measurements), indicative of average direction and variations of the interplanetary magnetic field. Smooth curves: calculated cold-ring distributions for model instrument response and measured field directions (see text for explanation). (Right) Circles: measured velocity distributions, averaged over pitch angle. Smooth curves: calculated cold-ring distributions for model instrument response (see text for explanation). The ordinates are $\log_{10}$ (phase space density in units of cm^{-3} km^{-3} s^3).

averages plotted in Figure 2 requires knowledge of both the geometric factor and the volume of three-dimensional phase space covered by each speed-elevation-azimuth bin in which counts were accumulated by the instrument; these factors are neither uniformly well determined by the instrument calibration data nor uniformly well modeled by the data analysis software. In general, the instrument response is very uniform with respect to the azimuthal angle mapped by the spacecraft spin. At the other extreme is a strong and not very well understood or modeled variation with proton energy at any given angle, with the greatest uncertainty at the lowest energies (with respect to the spacecraft). Knowledge and analytical modeling of the elevation response lie between these two extremes. The propagation of these uncertainties into the SWB coordinate system depends on the orientation of the magnetic field and is therefore different for each panel in Figure 2. In the discussions which follow, we will point out which results might possibly be affected by inadequate modeling of the instrument response.

The continuous curves in Figure 2 show the expected response of the instrument to cold rings of picked-up protons. The method of calculating the cold-ring curves requires some explanation. First, there are contributions to the widths of the curves from variations of both the solar wind velocity and the direction of the magnetic field during an averaging interval. Histograms of the expected pitch angles due to those variations alone are shown at the bottom of each panel. The scales for the histograms, in units of the number of 64-s intervals, are linear and are indicated on the right sides of the left panels. The second contribution to the widths of the cold-ring curves is the response function of the instrument. A perfectly cold ring of cometary protons, all picked up at the same velocity and the same field direction, would not result in a delta function in either the pitch angle or the speed distribution because of the finite velocity space acceptance cone of the instrument. The dominant effect arises from the instrument's approximately triangular energy response function which has a full width at half maximum of ~250 eV [Balsiger et al., 1987]. The effects of solar wind variability and the instrumental response were combined by calculating a pitch angle distribution and a velocity spectrum for the cold ring of pickup protons every 64 s, taking the instrument acceptance function into account and using 64 s averages of the solar wind vector velocity and field direction. Each resulting set of 64 s distributions was then summed and normalized to match the peak height of the observed distribution. In other words, the curves in Figure 2 represent convolutions of the instrument acceptance cone in velocity space with the temporal variations of the solar wind and the interplanetary magnetic field during the averaging intervals, ignoring the fluctuations faster than 64 s which Glassmeier et al. [1989] and others have shown to be of small amplitude and to carry only a small fraction of the power.

Results and Discussion

The processes responsible for the different types of pitch angle and velocity profiles shown in Figure 2 are most easily discussed in three separate groups: quasi-parallel pickup, quasi-perpendicular pickup, and phenomena associated with proximity to the bow shock.

Quasi-Parallel Pickup

First consider the pitch angle distributions on the left side of Figure 2. As previously reported for the region well upstream of the bow shock [Terasawa et al., 1986; Neugebauer et al., 1986, 1987; Wilken et al., 1987], the pitch angle distributions are very anisotropic, except for interval k just outside the bow shock. On the other hand, comparison of the observed phase space density to the instrument noise level of $\sim 10^{-11.6}$ cm^{-3} km^{-3} s^{3} [Neugebauer et al., 1989] leads to the conclusion that there was a measurably large flux of picked-up protons at all observable pitch angles for all intervals except perhaps intervals a and c, which were more than 2.5 Mkm from the comet.

For the quasi-parallel intervals (intervals a, b, c, f, h, and i, with $\alpha < 50°$ or $> 130°$), there was a fairly good, but not perfect, correlation between the pitch angle at which the maximum phase space density was observed and the pitch angle at the peak of the distribution expected for the ensemble of cold-ring distributions (continuous curves).

For every interval, the observed pitch angle peak was wider than the calculated cold-ring peak. Such peak widening is expected to be caused by (1) protons picked up upstream of the spacecraft where the field direction may have differed slightly from the locally measured direction due to the propagation of waves through the plasma and (2) pitch angle scattering by either preexisting waves in the solar wind or by waves created by the unstable distribution of the picked-up ions. The general trend was for the pitch angle distribution to broaden as the comet was approached. Far from the comet, at 3.8 and 5.7 Mkm, the ratio of the peak to the minimum phase space density exceeded an order of magnitude. Closer to the comet, in interval i, the ratio of maximum to minimum phase space density was reduced to a factor of ~3, while just outside the bow shock, in interval k, the distribution was nearly isotropic, indicating that pitch angle scattering had filled the shell nearly completely. Intervals i-k were in the region identified as the cometary foreshock by Rème et al. [1986].

Next consider the speed distributions on the right side of Figure 2. Note that the plots cover only the range 200-500 km/s, so that the solar wind peak at zero speed has been excluded. The high-speed tail of the solar wind distribution can be seen at the low-speed end of each spectrum. More complete speed distributions have been presented by Neugebauer et al. [1989].

For all the quasi-parallel intervals except interval h ($\alpha = 48°$), the observed peak was at a slightly lower speed than the cold-ring peak. The probable explanation of this effect can be understood with the aid of Plates 1 and 2, which show phase space density contours of the velocity space distributions for quasi-parallel intervals b and f, respectively. These two-dimensional contour plots have been averaged over gyroangle. The vertical and horizontal axes are the components of velocity perpendicular and parallel to the average magnetic field, respectively. (Note that a proton with zero pitch angle, i.e., one moving parallel to **B**, would be at the extreme left side of Figure 2 but to the right of the origin in Plates 1 and 2.) The contours were calculated from data which had been binned by 20 km/s in speed and by 15° in pitch angle. The symbols L and H in these figures denote local minima or maxima in log f, respectively. There are four contours per decade of phase space density. In both Plates 1 and 2, the solar wind peak is readily distinguishable at v_{par}, v_{perp} coordinates of (0, 0). From the peak of the solar wind distribution, the phase space density dropped approximately 5 orders of magnitude before increasing again due to the presence of the pickup protons. The two highest density contour intervals in the pickup shell have been color coded, as have the corresponding intervals in the solar wind peak. The peaks of the expected cold-ring populations are indicated by the circled asterisks. Arcs of elevated log f stretch out in a direction roughly consistent with that expected for pitch angle scattering. It is apparent from Plates 1 and 2, and from all the other contour plots we have examined, that pitch angle scattering is much more rapid than energy diffusion, consistent with current theoretical understanding of the pickup process [e.g., Gaffey et al., 1988].

The dashed line in Plate 1 represents a surface of constant speed centered on (0, 0). At negative values of v_{par} (pitch angles greater than 90°), this dashed line lies considerably outside the shell of picked-up protons. The dotted curve in Plate 1 is a circle passing through the cold-ring peak and centered at the point (v_A, 0), where v_A is the local value of the Alfvén speed; that point is indicated by a circled point on the abscissa. The dotted curve is the locus of points expected to be occupied by picked-up protons which have been pitch angle scattered from the initial ring by Alfvén waves propagating along the magnetic field toward the Sun [e.g., Wu et al., 1973; Lee and Ip, 1987; Price et al., 1988; Lee, 1989]. The observed shell of scattered pickup protons is located about midway between the dashed and the dotted circles, perhaps slightly closer to the dotted circle.

A similar phenomenon is apparent in Plate 2 for interval f. The magnetic geometry was such that the ring had v_{par}, v_{perp} coordinates of approximately (-300, 100) km/s, and waves propagating along the field toward the Sun would be located on the negative v_{par} axis. Once again, the observed shell of scattered pickup protons is between the two circles. Glassmeier et al. [1989] have made a detailed study of the upstream waves observed by Giotto for two particular intervals. Our interval f nearly coincides with the quasi-parallel interval (1620-1730 UT) in their study. They concluded that during this period, the observed turbulence clearly exhibited an Alfvénic character with sunward wave propagation, consistent with the dotted circle drawn in Plate 2.

The postulated effect of pitch angle scattering by waves traveling along the field toward the Sun can be readily discerned in each of the six quasi-parallel intervals. We interpret the fact that the picked-up protons tend to occupy a surface which lies between a sphere centered on the solar wind velocity and a sphere offset by an amount corresponding to sunward propagation of Alfvén waves as evidence for the existence of additional scattering modes or sources, such as scattering by antisunward propagating waves intrinsic to the solar wind or by nonparallel propagating, locally generated waves.

Quasi-Perpendicular Pickup

In addition to the dependence on distance from the comet, there is an inverse correlation between the pickup proton anisotropy and the angle α between the velocity and the

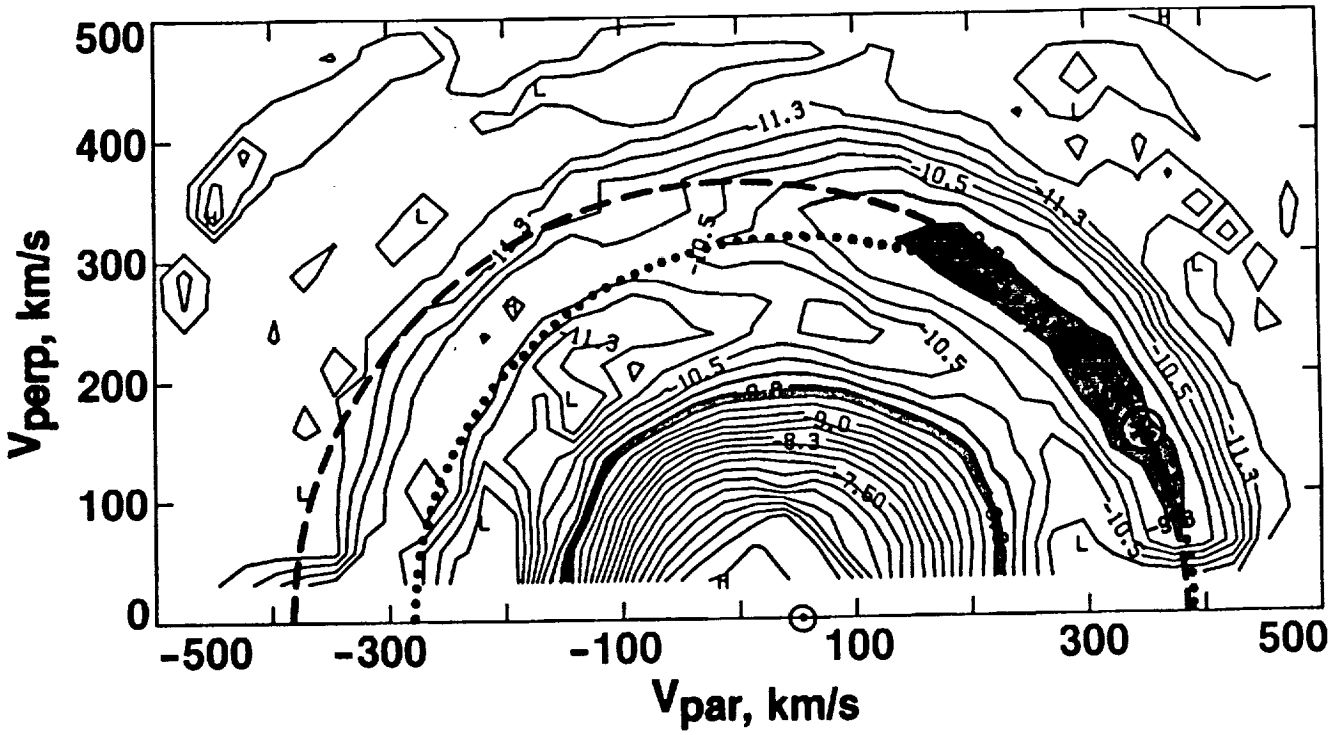

Plate 1. Contours of proton phase space density for quasi-parallel interval b from 0800-0859 UT, March 13, 1986, when the spacecraft was 3.8 Mkm from the nucleus of comet Halley. There are four contours/decade, with f measured in units of cm^{-3} km^{-3} s^3. See text for further explanations.

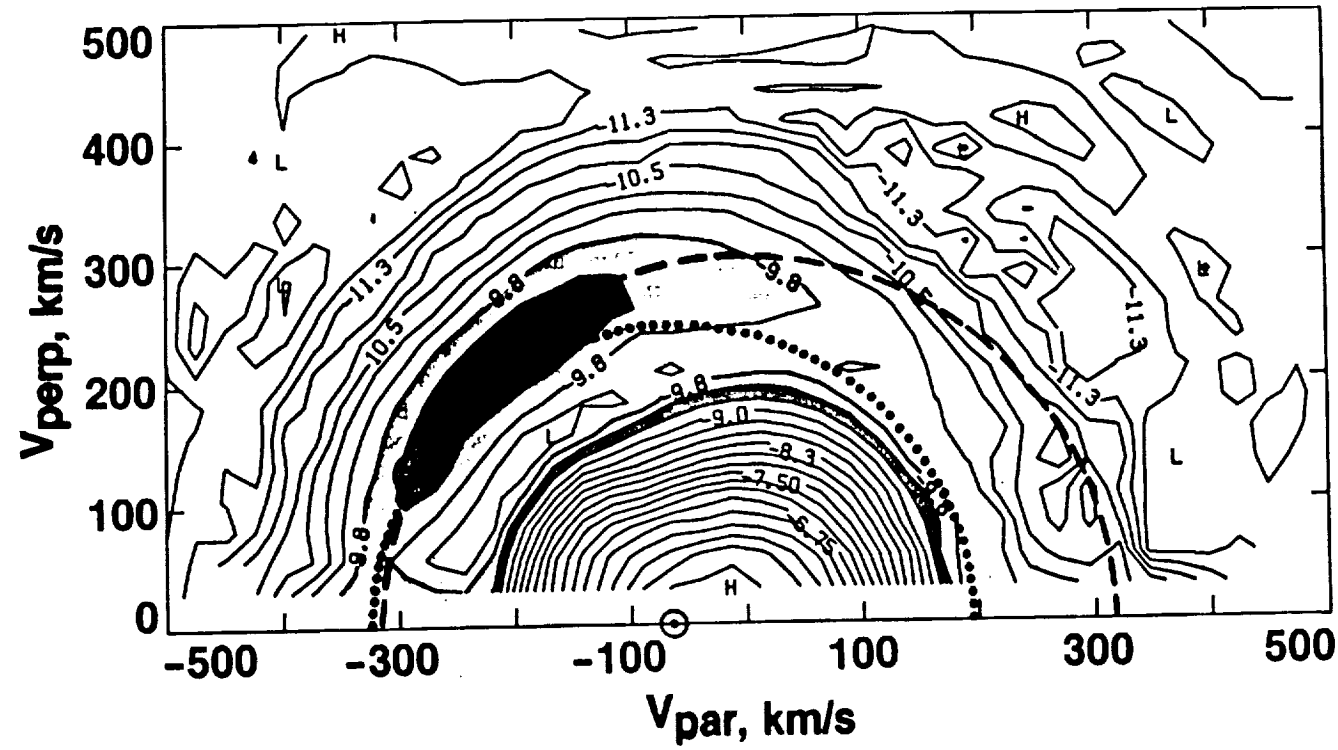

Plate 2. Contours of proton phase space density for quasi-parallel interval f from 1633-1724 UT, March 13, 1986, when the spacecraft was 1.7 Mkm from the nucleus of comet Halley. There are four contours/decade, with f measured in units of cm^{-3} km^{-3} s^3. See text for further explanations.

magnetic field. This effect is evident by comparison of the quasi-perpendicular intervals d, e, g, and j with their nearest quasi-parallel neighbors in Figure 2. The pitch angle distributions are more sharply peaked for the quasi-parallel intervals than for the quasi-perpendicular. The observed correlations of pitch angle peak widths with cometary distance and with α are qualitatively consistent with the theoretical and numerical calculations by Price et al. [1988] who showed that the growth rate of waves excited by freshly created ions in the solar wind increases with both newborn ion density and the angle α over the range $0 \leq \alpha \leq 60°$. Gary et al. [1989], on the other hand, have shown that a high growth rate of waves does not necessarily imply strong effects on the distribution functions.

But there are other peculiarities about the quasi-perpendicular intervals which bear further scrutiny. First note the very similar asymmetric pitch angle distributions for intervals e, g, and j. Also note that in all those cases the highest density was observed near a pitch angle of 180° rather than at the pitch angle predicted by the cold ring model calculations. Interval d might, or might not, have had a similar asymmetry, but the large pitch angle part of phase space was not visible to the instrument for the direction of the field experienced during that particular interval. The apparent drop-off at large pitch angles for interval d may not be real; as indicated by the error bars, there were very few counts, and those which were recorded came from the very edge of the field of view where the geometric factor is not well known or modeled.

Plates 3 - 5 show two-dimensional contour plots of phase space density for intervals e, g and j. In all three cases the asterisks denoting the peaks of the cold-ring distributions lie at the low pitch angle end of a ridge of high phase space density which stretches out along or near the dashed line; for intervals e and j, the ridges were inside and outside the dashed line, respectively. The pitch angle scattering was apparently very asymmetric for all three intervals with little scattering toward smaller pitch angles. The pitch angle distributions for the quasi-perpendicular intervals are so counter to our expectations that we have studied these distribution functions in great detail to search for instrumental effects which might possibly be responsible. Examination of the origin of the counts used to construct the pitch angle distribution in Figure 2g and in Plate 4 reveals that (1) the observed asymmetry between pitch angles greater than and less than the cold-ring pitch angle is almost certainly real because these two groups of pickup protons were incident on the instrument with nearly the same energies and elevation angles but at very different azimuth angles, and (2) a substantial fraction of the pickup protons with pitch angles near the cold ring had low energies in the spacecraft frame, whereas those at larger and smaller pitch angles had higher energies for which the instrument response is better modeled. Thus very poor modeling of the energy response of the instrument might be able to explain the rise in log f in Figure 2g between pitch angles of 90° and 180°. We believe, however, that this is not the correct explanation because the energy dependence of the instrument response has been modeled, albeit somewhat crudely, and because the rise persists when all counts corresponding to proton speeds (relative to the spacecraft) <300 km/s are dropped from the analysis. The shapes of the pitch angle plots in Figures 2e and 2j are similarly little affected by using only protons with speeds over 300 km/s rather than using all proton counts.

For the period 1500-1600 UT, which includes our interval e, Glassmeier et al. [1987, 1989] found a broad, low-amplitude shoulder of excess power in magnetic variations which peaked near 30 mHz and extended from 20 to 90 mHz. The proton cyclotron frequency at that time was ~60 mHz. From cross-spectral analysis, Glassmeier et al. [1989] found that this enhanced wave activity was due to left-hand elliptically polarized waves propagating antiparallel to the field. Theoretically, one would expect waves propagating in the antiparallel direction would arise from instabilities caused by a steep negative slope $df/d\mu$, where μ is the cosine of the pitch angle [e.g., Lee, 1989]. In Plate 3 there is a steep positive slope of log f versus pitch angle near 90°, which corresponds to a negative value of $df/d\mu$. Although most instabilities associated with pickup ions are right handed, the growth of left-hand modes is possible for α near 90° [Gary and Madland, 1988]. We suspect, therefore, that the waves analyzed by Glassmeier et al. [1989] are the result of the asymmetric pitch angle distribution rather than its cause.

Another line of evidence that the waves were caused by the skewed distribution rather than vice versa is that at pitch angles >90°, the ridge of high pickup proton density lies slightly inside the dashed circle in Plate 3. If the protons had been scattered by the observed waves which traveled antiparallel to **B**, they would be found along a circle centered to the left of the origin and would thus lie outside, rather than inside, the dashed line.

Thus the problem is to find a plausible cause of the distributions shown in Plates 3-5. One possibility is that the protons observed at large pitch angles during intervals e, g, and j were reflected from the bow shock. Rème et al. [1987] have used the electron heat flux ratio (defined as the ratio of the minimum to maximum heat flux parallel and antiparallel to the field direction, which was taken as the axis of symmetry of the electron momentum flux tensor) as a diagnostic of magnetic connection to the Halley bow shock. Values of the heat flux ratio close to unity are interpreted as evidence for electrons streaming back along the interplanetary magnetic field in a direction opposite to the heat flux from the Sun. On this basis, Figure 1 of Rème et al. [1987] would imply that the spacecraft was magnetically connected to the bow shock during all of intervals e and j and for most of interval g. The right-hand column of Table 1 gives the probable direction relative to the field of a beam of protons reflected from the shock. For intervals g and j, reflected protons would have pitch angles near 180°, which is where excess densities were observed. During interval e, the interplanetary magnetic field had a large northward component while its projection in the ecliptic was nearly parallel to the shock surface, making it difficult to guess which direction along the field line might lead to the comet.

The Rème et al. [1987] heat flux data suggest that intervals b, i, and k might also be periods of magnetic connection to the bow shock. Interval b is the quasi-parallel interval for which the phase space density contours are plotted in Plate 1. Few reflected protons would be expected at interval b's cometocentric distance of 3.8 Mkm. Furthermore, any field-aligned reflected protons would have had nearly the same

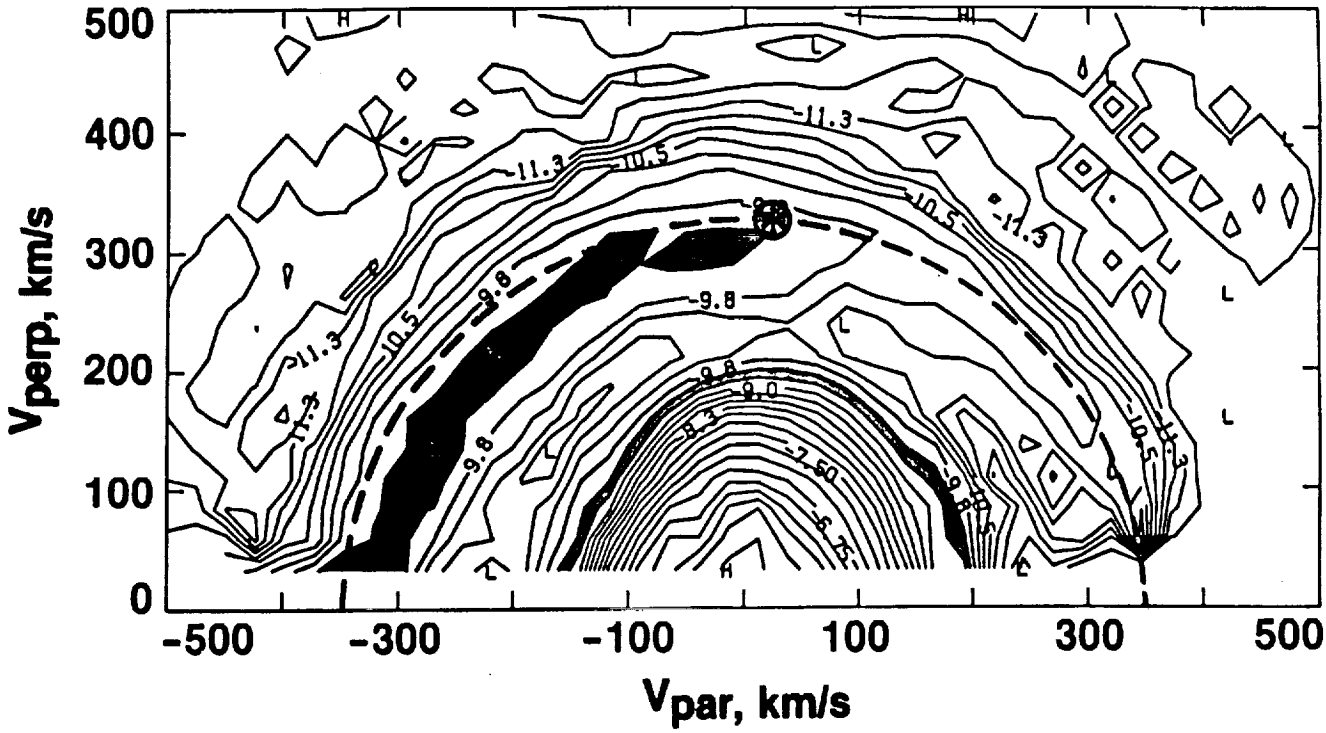

Plate 3. Contours of proton phase space density for quasi-perpendicular interval e from 1528-1549 UT, March 13, 1986, when the spacecraft was 2.1 Mkm from the nucleus of comet Halley. There are four contours/decade, with f measured in units of cm^{-3} km^{-3} s^3. See text for further explanations.

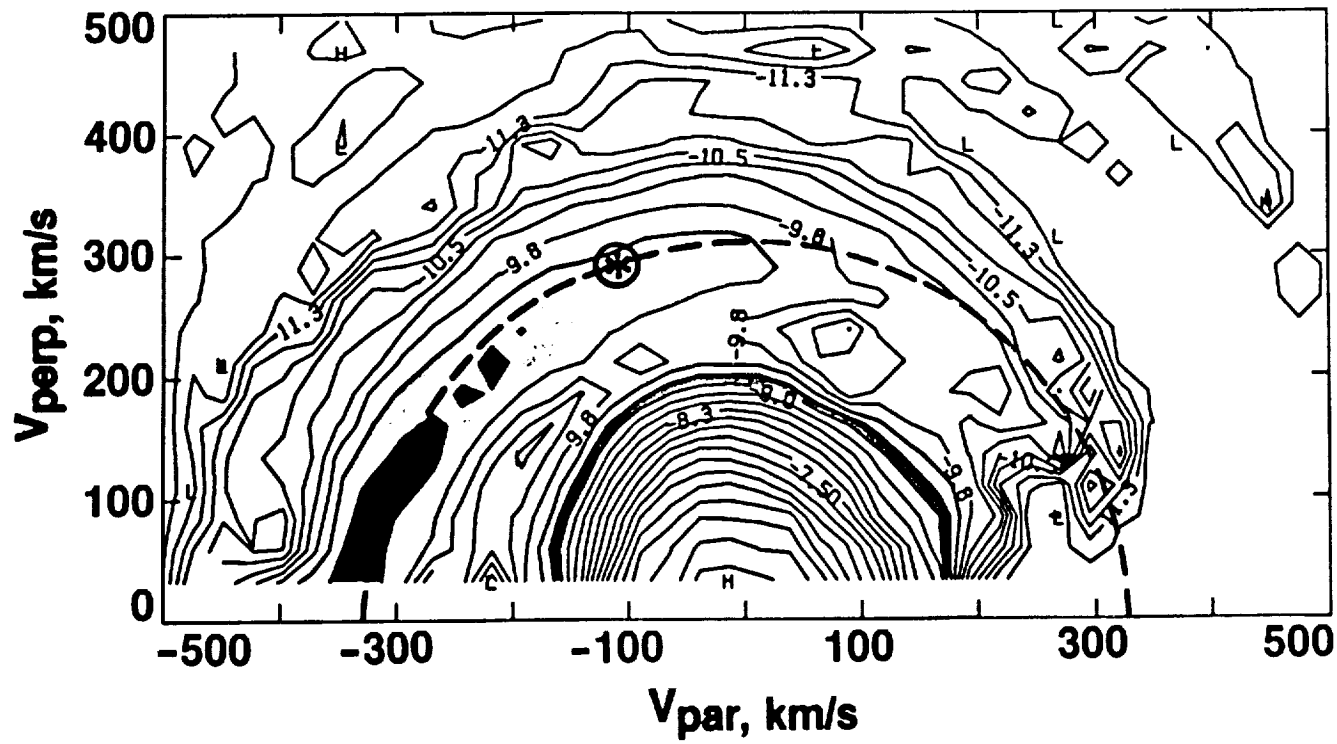

Plate 4. Contours of proton phase space density f for quasi-perpendicular interval g from 1731-1747 UT, March 13, 1986, when the spacecraft was 1.6 Mkm from the nucleus of comet Halley. There are four contours/decade, with f measured in units of cm^{-3} km^{-3} s^3. See text for further explanations.

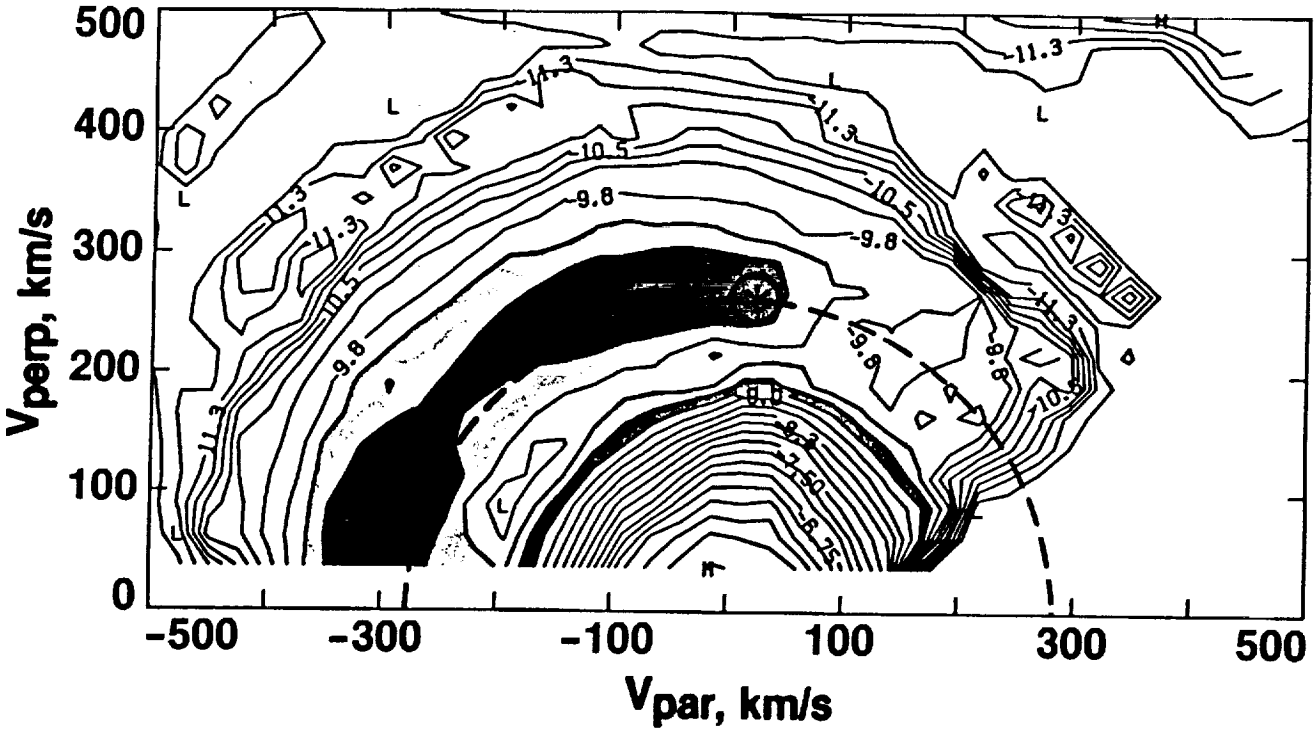

Plate 5. Contours of proton phase space density for quasi-perpendicular interval j from 1905-1913 UT, March 13, 1986, when the spacecraft was 1.21 Mkm from the nucleus of comet Halley. There are four contours/decade, with f measured in units of cm^{-3} km^{-3} s^3. See text for further explanations.

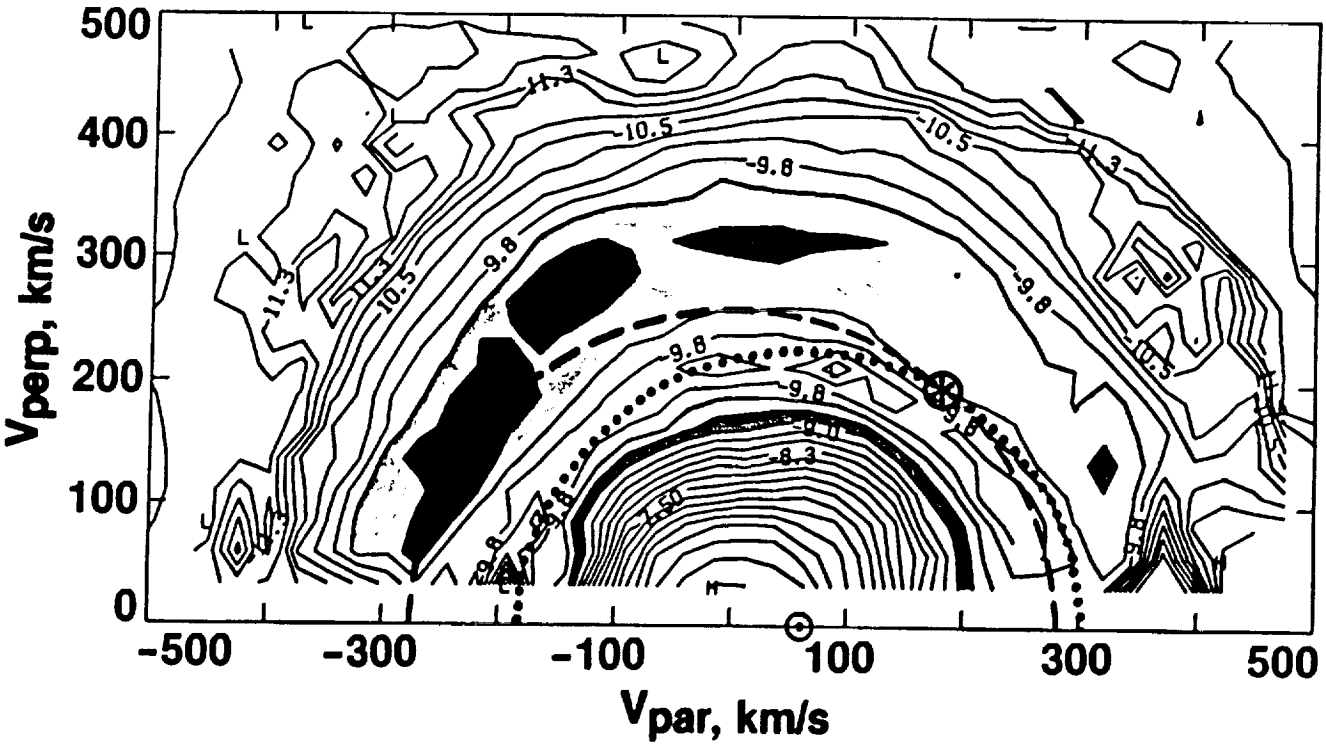

Plate 6. Contours of proton phase space density for interval k from 1915-1922 UT, March 13, 1986, when the spacecraft was just outside the bow shock of comet Halley. There are four contours/decade, with f measured in units of cm^{-3} km^{-3} s^3. See text for further explanations.

pitch angle as the cold-ring pickup protons, thus making the distinction between the two groups of protons impossible. Intervals i and k are discussed in the next section.

The properties of superthermal ions upstream from planetary bow shocks and interplanetary shocks have been reviewed by Paschmann et al. [1981] and by Thomsen [1985]. To be consistent with the Giotto interval e, g, and j observations, shock-generated particles would have properties similar to what Paschmann et al. called "reflected ions" and Thomsen called "field-aligned beams." Such particles are observed only for nearly perpendicular shocks and are scattered into more diffuse distributions with increasing distance from the shock. If (1) the distance the reflected protons traveled from the shock to the spacecraft equaled the distance along the spacecraft trajectory from the spacecraft to the shock (which could be an underestimate if the particles came from a closer part of the shock surface or an overestimate if they came from a more distant part or took a circuitous route), (2) the field direction at the shock was the same as that observed at the spacecraft at the appropriate earlier times, and (3) the shock normal direction was the same when the reflected protons left it as it was when Giotto crossed the shock, then the angle between the field and the shock normal would have been 122°, 126°, and 132°, respectively, at the times the protons detected during intervals e, g, and j were reflected from the shock. There is therefore some reason to believe that the shock might have been sufficiently perpendicular at the appropriate times, but the above calculation cannot be taken very seriously because of all the unprovable assumptions.

We are very skeptical of the bow shock reflection explanation of the 180°-pitch-angle protons for several reasons. First, in neither interval e, g, nor j was the local interplanetary magnetic field pointed toward the shock. This does not rule out a shock connection because large kinks and turns in the field are certainly possible, but it makes connection less likely. The observed correlation of excess field-aligned protons is with α, rather than with θ_{Bc} or with the likelihood of intersection of the local field direction with the shock.

Another difficulty with the reflected ion scenario is that the speed of ions reflected from Earth's bow shock ranges from 1 to 5 times the solar wind speed (in the spacecraft coordinate system) [Paschmann et al., 1981], whereas for intervals e, g, and j the 180°-pitch-angle protons had speeds suspiciously close to the speed expected for picked-up cometary protons. Still another consideration is that there was a great deal of turbulence in the region between the spacecraft and the shock. The fact that picked-up cometary protons are strongly pitch angle scattered before they reach the shock, as illustrated by Figure 2k, suggests that protons traveling upstream from the shock would be similarly scattered and no longer form a field-aligned beam by the time they reached the spacecraft, which was 2.1 and 0.4 Mkm distant from the Giotto shock crossing point during intervals e and g, respectively.

There is also a question whether or not a weak cometary shock is able to produce a field-aligned beam. Such beams have not been observed upstream of interplanetary shocks [Gosling et al., 1984], but it is not known whether this difference between interplanetary and bow shocks is due to a difference of Mach number or to a difference of the shock's scale size and the duration of connection of a flux tube to the shock [Thomsen, 1985].

Finally, there are arguments [Sharma et al., 1988; Hizanidis et al., 1988] that it is not appropriate to refer to the slowing and heating of the solar wind and the generation of turbulence by cometary ion pickup as a shock. If, as argued in those papers, there is no shock at a comet, there would also be no reflection of protons by a shock, in the sense with which we are familiar from the study of planetary bow shocks.

In summary, there are many reasons why we do not believe the excess field-aligned protons originated at a cometary bow shock. This agrees with the conclusion reached by Fuselier et al. [1987] who unsuccessfully searched for backstreaming ions in the cometary foreshock region. Although Glassmeier et al. [1987] originally suggested the presence of reflected protons during an interval which includes our interval e, they have since concluded [Glassmeier et al., 1989] that reflected protons were probably not responsible for the principal features of the observed wave spectra.

Another consideration in the search for a cause of the asymmetric pitch angle profiles for the quasi-perpendicular intervals is the possible difficulty of scattering picked-up protons across a pitch angle of 90°. Some models of wave-particle interactions lack a mechanism for scattering particles across a pitch angle of 90°. Ip's [1988] numerical models of pitch angle scattering show a drop in density at 90° when the pitch-angle-scattering coefficient is very small. Observationally, the pitch angle profiles for intervals a and c (see Figure 2) do show sharp drops in log f at pitch angles of 90°, but many other intervals do not. The principal stumbling block for invoking such an effect for explaining the pitch angle distributions for our quasi-perpendicular intervals is that we obtain essentially the same pitch angle distribution, with a peak near 180°, for interval e whether we use all the data acquired during that time interval or only the subset of data for which the instantaneous (with 64-s resolution) field direction corresponded to pitch angles <90°. For that subset, the protons observed near 180° pitch angles would all have been picked up at pitch angles <90° if the field had not changed since the time and place of their pickup (which, of course, may not be true).

Our final suggestion is that the systematically asymmetric pitch angle distributions during the quasi-perpendicular intervals might be a macroscopic or global rather than a local effect. The picked-up protons might have been in a magnetic configuration which allowed escape in one direction but not the other. The global magnetic configuration was not uniform. The field between the spacecraft and the comet was stronger and more turbulent than the field between the spacecraft and the Sun. Protons picked up with near-90° pitch angles would have been readily mirrored by either compressional waves or the increase in field strength as the solar wind was slowed down by mass loading near the comet.

The observed asymmetry would be consistent with mirroring of particles into the upstream direction if the direction northward along the field line, parallel to **B**, led downstream and the direction southward along the field line, antiparallel to **B**, led upstream and back toward the Sun.

This was in fact probably the situation for each of the intervals e, g, and j. Both the interplanetary magnetic field and the electron heat flux vector pointed outward from the Sun with a northward component during most of the day prior to the time Giotto crossed the Halley bow shock. The small net electron heat flux remained northward and parallel to the field during each of our quasi-perpendicular intervals (D. Larson, personal communication, 1988). Thus the large-scale magnetic configuration may have been responsible for the north-south, or parallel-antiparallel, asymmetry of the pickup proton distributions during the quasi-perpendicular intervals. It is more difficult to imagine why the quasi-perpendicular pitch angle distributions continued to increase toward larger pitch angles with a maximum at 180°. Explanation of that phenomenon is left as an exercise for theoreticians.

Bow Shock Effects

Plate 6 shows the v_{par}, v_{perp} contours for interval k, during which the spacecraft moved through the 30,000-km region just upstream of the bow shock. Once again, the circled asterisk denotes the expected location in velocity space of locally picked up protons, the dashed circle is the trace of a spherical shell passing through this point and centered on the solar wind bulk flow at (0, 0), and the dotted circle is again centered on (v_A, 0) for field-aligned, sunward propagating waves.

From the left-hand side of Figure 2k and from Plate 6 one can see that the shell was well filled at all observed pitch angles. Pitch angle scattering was much more nearly complete than in any of the other intervals studied.

The highest values of log f for picked-up protons on the shell were found at large pitch angles (negative v_{par}). This is reminiscent of the quasi-perpendicular intervals discussed above, with an excess of particles flowing antiparallel to the field, in a generally southward direction, probably in the direction in which the field line connected to the Sun.

In Plate 6, the peak phase space density of the shell of picked-up protons was located well outside both the dashed and dotted circles at all pitch angles; i.e., the picked-up protons had higher speeds than expected on the basis of the locally measured solar wind velocity. At pitch angles near the expected local pickup angle, the shell radius was ~340 km/s, compared to an expected radius of 272 km/s. The same phenomenon can be discerned, to a lesser extent, in Plate 5 for interval j which immediately preceded interval k.

There are three possible explanations for an increase of the shell radius near the shock: (1) the majority of the protons may have been picked up farther upstream before mass loading by water group ions had significantly slowed the solar wind flow, (2) the picked-up protons may have been heated by adiabatic compression in the decelerating solar wind, or (3) Fermi acceleration may have been important in this region.

The first possibility is probably not the most important. There are several reasons which argue against the proposition that most of the picked-up protons observed in intervals j and k were relics of the region upstream of the foreshock. First, log f was much higher for intervals j and k than for intervals g and h, consistent with an abundance of freshly picked-up

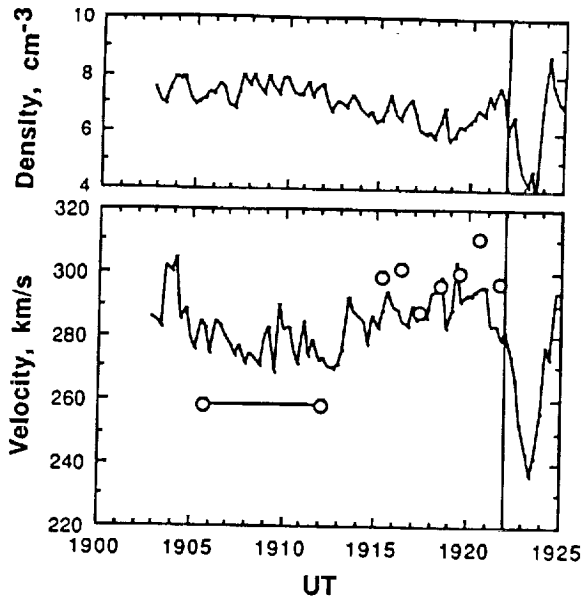

Fig. 3. Top: Solar wind proton density. Bottom: Cometocentric solar wind speed (solid trace) and pickup proton speed (open circles). The line at 1922 UT denotes the outer boundary of the cometary bow shock.

particles. Second, the total density of picked-up protons increased rapidly through the foreshock region as the spacecraft approached the bow shock [Neugebauer et al., 1989]. Third, the velocity at the pickup proton peak for interval k was greater than for the preceding intervals i and j.

The problem with these arguments, as well as with the arguments below concerning adiabatic compression, is that it is not possible to study the temporal variation of a particular parcel of plasma. The Giotto spacecraft approached the comet at a phase angle of 107°, cutting across solar wind streamlines with different velocities, densities, and magnetic field directions, rather than along a single streamline. The problem was especially severe because of the solar wind variability associated with the nearby interplanetary current sheet [Acuna et al., 1986]. If the spacecraft had approached the comet along a streamline, one would expect mass loading to decrease the solar wind speed slowly while the density increased. Figure 3 shows the variations of the solar wind density and velocity relative to the comet for the last 20 min before the spacecraft encountered the bow shock. Rather than a monotonic decrease in speed and a monotonic increase in density, the Giotto profiles were quite jagged. In fact, the speed was lower during interval j (1905 - 1912 UT) than during interval k (1915 - 1922 UT). The sharp discontinuity in speed between intervals j and k was accompanied by a large change in the direction of the interplanetary magnetic field; intervals j and k are clearly samples of different solar wind flows. Neubauer et al. [1988] have presented additional evidence for features due to solar wind structures convected into the shock transition region.

The pickup speeds (i.e., the radii of the peaks of the shells of pickup protons) are indicated by open circles in Figure 3. The average pickup speed for interval j is indicated by two connected circles. Interval j shows the commonly observed

offset of the pickup speed below the solar wind speed in the comet-centered coordinate system; this offset is probably caused by the outflow of atomic H from the nucleus at speeds up to 20 km/s [Neugebauer et al., 1989]. Note that the dashed circles in Plates 1-6 were calculated on the assumption of an 11-km/s outflow speed.

The pickup speeds for each of the seven 64-s intervals which make up interval k are shown as individual circles, which are henceforth referred to as points k1 through k7. Points k1 - k7 were near or above rather than below the observed cometocentric solar wind speed, consistent with the peak of the pickup distribution lying outside the dashed circle in Plate 6. There is no obvious explanation for the jump in pickup speed relative to the solar wind speed between intervals j and k1.

The only hint of compression in Figure 3 is the rise in density from 1919 to 1922 UT. The average solar wind densities for intervals k5 and k6 were 6.2 and 6.8 cm^{-3}, respectively. If this increase in density were attributed to adiabatic compression (which is admittedly inconsistent with the solar wind speed profile during this time), one would expect the radius of the shell to increase by an amount $(6.8/6.2)^{1/3} = 1.03$ for a specific heat ratio of 5/3. The pickup speeds for intervals k5 and k6 were 300 and 311 km/s, respectively, which corresponds to a k5-to-k6 increase of a factor of 1.04. This is better agreement than can be justified by the accuracy of the data. We conclude that the data contain some weak evidence for adiabatic acceleration just outside the shock, but that the principal increase in shell radius at approximately 1914 UT was accompanied by a change in the solar wind and cannot be explained with the data available from HERS.

Second-order, or stochastic, Fermi acceleration by pickup-ion-produced turbulence can result in a pickup ion spectrum whose peak shifts in energy and broadens with time [Ip and Axford, 1986]. A stochastic process is consistent with the observation that the level of plasma turbulence was much greater in the foreshock region than it was farther upstream [Johnstone et al., 1987]. There is also theoretical expectation [Amata and Formisano, 1985] and some observational evidence [Ip, 1988] for first-order Fermi acceleration close to cometary bow shocks. The nature of the HERS data obtained just upstream of the bow shock makes it difficult, however, to draw any firm conclusions about Fermi acceleration or heating. The widths of the pickup peaks in intervals j, k5, and k6 were all similar, while the peak in interval k1 was narrower. Quantitative modeling of the Fermi acceleration processes and comparison to the velocity distributions observed by the Giotto IMS are beyond the scope of this paper, and may not be a fruitful exercise in any case.

Summary and Conclusions

The principal conclusions that we have reached from the data and the analyses presented in the previous section can be summarized as follows:

First, under all conditions studied, pitch angle scattering was considerably more rapid than changes in energy, as expected.

Second, for quasi-parallel conditions: (1) The pitch angle at which the maximum phase space density of picked-up protons was observed was close to the pitch angle at which the protons were picked up. (2) Outside the foreshock region, the pitch angle anisotropy was substantial, with more than an order of magnitude difference between the maximum and minimum phase space densities. (3) The pitch angle distribution became more isotropic inside the foreshock and was nearly isotropic in the region 30,000 km upstream of the bow shock. (4) The shell of pitch-angle-scattered picked-up protons was centered between the origin (equal to the solar wind bulk velocity) and a point on the v_{par} axis offset from the origin by an amount equal to the Alfvén speed and in the direction of wave propagation with a sunward component.

Third, for quasi-perpendicular conditions: (1) The pitch angle scattering was very asymmetric, with protons preferentially scattered antiparallel to the field. It is believed that the spacecraft was in an "away" interplanetary sector at the time of these observations, so that the direction antiparallel to the field led back to the Sun while the direction parallel to the field led downstream. (2) The pitch angle at which the maximum phase space density of picked-up protons was observed was close to 180°, independent of whether the pickup occurred at angles greater than or less than 90°. (3) The ratio of phase space density at the pickup pitch angle to the minimum phase space density on the pickup proton shell was smaller than for quasi-parallel conditions; i.e., pitch angle scattering was more intense. (4) Waves with frequency near the proton cyclotron frequency observed for one of the quasi-perpendicular intervals may have been caused by the gradient in the pitch angle distribution near the pickup pitch angle; i.e., we suggest that the observed, asymmetric pitch angle distribution was the cause of rather than the result of locally generated waves. (5) The asymmetric pitch angle distributions were probably not caused by protons reflected from the cometary bow shock, even though the electron heat flux observations have been interpreted to infer bow shock connection at the time. (6) We suggest that the observed pitch angle distributions may have been caused by the global effect of higher field strength and greater turbulence between the spacecraft and the comet than between the spacecraft and the Sun.

Fourth, the radius of the pickup shell is larger than expected within 70,000 km of the bow shock. There is inconclusive evidence that adiabatic acceleration may account for some of this energization of the pickup protons, but there are other, discontinuous changes in the pickup proton speed that are associated with changes in the solar wind and that cannot be explained from the present data set.

The observations thus confirm many of the predictions from theoretical studies or numerical models and corroborate some of the phenomena discovered by analysis of data acquired at comet Giacobini-Zinner. This is particularly true of the quasi-parallel intervals, where pitch angle scattering by sunward propagating, field-aligned waves could be discerned.

The biggest surprise in these observations was the pitch angle distribution for quasi-perpendicular intervals, which may require global rather than local theoretical modeling. Our arguments against reflection of protons from the cometary bow shock as the cause of the asymmetric distributions for quasi-perpendicular intervals are based on the conventional view of a relatively sharp quasi-perpendicular shock

structure. Our interpretation in terms of global effects is in many respects consistent with the view of Hizanidis et al. [1988] that the entire turbulent interaction region serves the function of a distributed shock.

We also wish to suggest that the decrease in the net electron heat flux observed during quasi-perpendicular intervals [Rème et al., 1987] may be related to the process responsible for the asymmetric pitch angle distributions and not necessarily require connection to the bow shock. Fuselier et al. [1986] have interpreted electron heat flux signatures observed near comet Giacobini-Zinner as evidence of backscattering of the solar wind electron heat flux by turbulence upstream of the comet's bow shock.

The results presented in this paper clearly call for further analyses. It will probably be informative, for example, to compare the picked-up proton velocity distributions presented here to simultaneous velocity distributions of picked-up water-group ions measured by the Giotto implanted ion sensor [Wilken et al., 1987]. More detailed comparisons of proton and electron distribution functions would probably also prove to be fruitful.

Acknowledgments. We gratefully acknowledge the many and substantial contributions by all members of the Giotto ion mass spectrometer and magnetometer teams, without which there would have been no data. B. E. Goldstein and R. Goldstein made essential contributions to the development of numerical models of the HERS response, while R. Sakurai provided valuable assistance with software development. M.N. also wishes to thank A. L. Brinca, M. A. Lee, and B. T. Tsurutani for helpful discussions. A.J.L. wishes to acknowledge the substantial contributions to the development of the cold ring model made by C. K. Clark. The research described in this paper was carried out, in part, by the Jet Propulsion Laboratory of the California Institute of Technology under contract with the U.S. National Aeronautics and Space Administration. Work at MIT was supported in part by NASA grant 22-009-015 and JPL contract 957906. Research at Lockheed was supported by NASA under contract NASW-3729 and the work by F.M.N. was supported by the FRG Bundesministerium für Forschung und Technologie.

The Editor thanks M.A. Lee and another referee for their assistance in evaluating this paper.

References

Acuna, M.H., K.H. Glassmeier, L.F. Burlaga, F.M. Neubauer, and N.F. Ness, Upstream waves of cometary origin detected by the Giotto magnetic field experiment, Proceedings of 20th ESLAB Symposium on Exploration of Halley's Comet, edited by B. Battrick, E.J. Rolfe, and R. Reinhard, *Eur. Space Agency Spec. Publ. SP-250*, (III), 447-449, 1986.

Amata, E., and V. Formisano, Energization of positive ions in the cometary foreshock region, *Planet. Space Sci., 33*, 1243, 1985.

Balsiger, H., et al., The Giotto ion mass spectrometer, *J. Phys. E., 20*, 759, 1987.

Fuselier, S.A., W.C. Feldman, S.J. Bame, E.J. Smith, and F.L. Scarf, Heat flux observations and the location of the transition region boundary of Giacobini-Zinner, *Geophys. Res. Lett., 13*, 247, 1986.

Fuselier, S.A., K.A. Anderson, H. Balsiger, K.H. Glassmeier, B. E. Goldstein, M. Neugebauer, H. Rosenbauer, and E.G. Shelley, The foreshock region upstream from the comet Halley bow shock, Proceedings of the Symposium on Diversity and Similarity of Comets, edited by E. J. Rolfe and B. Battrick, *Eur. Space Agency Spec. Publ. 278*, 77, 1987.

Gaffey, J. D., Jr., D. Winske, and C. S. Wu, Time scales for formation and spreading of velocity shells of pickup ions in the solar wind, *J. Geophys. Res., 93*, 5470, 1988.

Gary, S. P., and C. D. Madland, Electromagnetic ion instabilities in a cometary environment, *J Geophys. Res., 93*, 235, 1988.

Gary, S. P., K. Akimoto, and D. Winske, Computer simulations of cometary-pickup-ion/ion instabilities and wave growth, *J. Geophys. Res.*, in press, 1989.

Glassmeier, K.H., F.M. Neubauer, A.D. Johnstone, M.H. Acuna, and H. Rème, Pick-up waves and reflected ion waves at comet Halley: a case study, in *Proceedings of the Chapman Conference on Plasma Waves and Instabilities in Magnetospheres and at Comets*, pp. 19-22, Sendai, Japan, 1987.

Glassmeier, K.H., A.J. Coates, M.H. Acuna, M.L. Goldstein, A.D. Johnstone, F.M. Neubauer, and H. Rème, Spectral characteristics of low-frequency plasma turbulence upstream of comet P/Halley, *J. Geophys. Res., 94*, 37, 1989.

Gosling, J. T., S. J. Bame, W. C. Feldman, G. Paschmann, N. Sckopke, and C. T. Russell, Suprathermal ions upstream from interplanetary shocks, *J. Geophys. Res., 89*, 5409, 1984.

Hizanidis, K., P.J. Cargill, and K. Papadopoulos, Lower hybrid waves upstream of comets and their implications for the comet Halley "bow wave," *J. Geophys. Res., 93*, 9577, 1988.

Ip, W.-H., Cometary ion acceleration processes, *Comput. Phys. Commun., 49*, 1, 1988.

Ip, W.-H., and W. I. Axford, The acceleration of particles in the vicinity of comets, *Planet. Space Sci, 34*, 1061, 1986.

Johnstone, A.D., A.J. Coates, J. Heath, M.F. Thomsen, B. Wilken, K. Jockers, V. Formisano, E. Amata, J. D. Winningham, H. Borg, and D. A. Bryant, Alfvénic turbulence in the solar wind flow during the approach to comet P/Halley, *Astron. Astrophys., 187*, 25, 1987.

Lee, M. A., ULF waves at comets, in *Plasma Waves and Instabilities at Comets and in Magnetospheres, Geophys. Monogr. Ser.*, edited by B. T. Tsurutani and H. Oya, AGU, Washington, D.C., in press, 1989.

Lee, M. A., and W.-H. Ip, Hydromagnetic wave excitation by ionized interstellar hydrogen and helium in the solar wind, *J. Geophys. Res., 92*, 11041, 1987.

Neubauer, F.M., M.H. Acuna, L.F. Burlaga, B. Franke, B. Gramkow, F. Mariani, G. Musmann, N. F. Ness, H.U. Schmidt, R. Terenzi, E. Ungstrup, and M. Wallis, The Giotto magnetometer experiment, *J. Phys. E: 20*, 714, 1987.

Neubauer, F. M., K. H. Glassmeier, M. H. Acuna, F. Mariani, G. Musmann, and M. Neugebauer, Magnetic

field structure of the inbound bow shock of comet P/Halley observed by Giotto (abstract), *Eos, Trans. AGU 69*, 396, 1988.

Neugebauer, M., A. J. Lazarus, K. Altwegg, H. Balsiger, B. E. Goldstein, R. Goldstein, F. M. Neubauer, H. Rosenbauer, R. Schwenn, E. G. Shelley, and E. Ungstrup, The pick-up of cometary protons by the solar wind, Proceedings of 20th ESLAB Symposium on the Exploration of Halley's Comet, edited by B. Battrick, E.J. Rolfe, and R. Reinhard, *Eur. Space Agency Spec. Pub., ESA SP-250*, (I), 19-23, 1986.

Neugebauer, M., A. J. Lazarus, K. Altwegg, H. Balsiger, B. E. Goldstein, R. Goldstein, F. M. Neubauer, H. Rosenbauer, R. Schwenn, E. G. Shelley, and E. Ungstrup, The pickup of cometary protons by the solar wind, *Astron. Astrophys., 187*, 21, 1987.

Neugebauer, M., B.E. Goldstein, H. Balsiger, F.M. Neubauer, R. Schwenn, and E. G. Shelley, The density of cometary protons upstream of comet Halley's bow shock, *J. Geophys. Res.*, 94, 1261, 1989.

Paschmann, G., N. Sckopke, I. Papamastorakis, J. R. Asbridge, S. J. Bame, and J. T. Gosling, Characteristic of reflected and diffuse ions upstream from the Earth's bow shock, *J. Geophys. Res., 86*, 4355, 1981.

Price, C.P., J.D. Gaffey, Jr., and J.Q. Dong, Excitations of low-frequency hydromagnetic waves by freshly created ions in the solar wind, *J. Geophys. Res., 93*, 837, 1988.

Rème, H., J. A. Sauvaud, C. d'Uston, A. Cros, K. A. Anderson, C. W. Carlson, D. W. Curtis, R. P. Lin, A. Korth, A. K. Richter, and D. A. Mendis, General features of the comet Halley-solar wind interaction from plasma measurements, Proceedings of 20th ESLAB Symposium on the Exploration of Halley's Comet, edited by B. Battrick, E. J. Rolfe, and R. Reinhard, *Eur. Space Agency Spec. Publ.* (I), 29-34, 1986.

Rème, H., J. A. Sauvaud, C. d'Uston, A. Cros, K. A. Anderson, C. W. Carlson, D. W. Curtis, R. P. Lin, A. Korth, A. K. Richter, and D. A. Mendis, General features of comet P/Halley: Solar wind interaction from plasma measurements, *Astron. Astrophys, 187*, 33, 1987.

Sharma, A.S., P.J. Cargill, and K. Papadopoulos, Resonance absorption of Alfvén waves at comet-solar wind interaction regions, *Geophys. Res. Lett., 15*, 740, 1988.

Terasawa, T., T. Mukai, W. Miyake, M. Kitayama, and K. Hirao, Detection of cometary pickup ions up to 10^7 km from comet Halley: Suisei observation, *Geophys. Res. Lett., 13*, 837, 1986.

Thomsen, M. F., Upstream suprathermal ions, in *Collisionless Shocks in the Heliosphere: Reviews of Current Research, Geophys. Monogr. Ser.*, vol. 35, edited by B.T. Tsurutani and R.G. Stone, pp. 253-270, AGU, Washington, D.C., 1985.

Wilken, B., A. Johnstone, A. Coates, H. Borg, E. Amata, V. Formisano, K. Jockers, H. Rosenbauer, W. Stüdemann, M.F. Thomsen, and J. K. Winningham, Pick-up ions at comet P/Halley's bow shock: Observations with the IIS spectrometer on Giotto, *Astron. Astrophys., 187*, 153, 1987.

Wu, C.-S., R. E. Hartle, and K. W. Ogilvie, Interaction of singly charged interstellar helium ions with the solar wind, *J.Geophys. Res., 78*, 306, 1973.

H. Balsiger, Physikalisches Institut, University of Bern, Sidlerstrasse 5, CH-3012 Bern, Switzerland.

S.A. Fuselier, Lockheed Palo Alto Research Laboratory, Department 91-20, Building 255, 3251 Hanover Street, Palo Alto, CA 94304.

A.J. Lazarus, Center for Space Research, Massachusetts Institute of Technology, Cambridge, MA 02139

F.M. Neubauer, Institut Für Geophysik und Meteorologie, Universitat zu Köln, Albertus-Magnus-Platz, D-5000 Köln 41, Federal Republic of Germany.

M. Neugebauer, Jet Propulsion Laboratory, California Institute of Technology, MS 169-506, 4800 Oak Grove Drive, Pasadena, CA 91109.

H. Rosenbauer, Max-Planck-Institut für Aeronomie, D-3411 Katlenburg-Lindau, Federal Republic of Germany.

(Received October 17, 1988;
revised December 7, 1988;
accepted December 14, 1988.)

JOURNAL OF GEOPHYSICAL RESEARCH, VOL. 94, NO. A12, PAGES 17,251–17,257, DECEMBER 1, 1989

Observations of a Shock and a Recombination Layer at the Contact Surface of Comet Halley

B. E. GOLDSTEIN,[1] K. ALTWEGG,[2] H. BALSIGER,[2] S. A. FUSELIER,[3] W.-H. IP,[4] A. MEIER,[2] M. NEUGEBAUER,[1] H. ROSENBAUER,[4] AND R. SCHWENN[4]

Observations in the vicinity of the contact surface (ionopause) of comet Halley obtained by the Giotto ion mass spectrometer (IMS) are reported. Two specific events in this region were observed on the inbound pass. Two seconds before the contact surface was encountered, a burst of energized ions (about 20 eV, much greater than thermal energies) was detected by the angle analyzer; the flux of these ions decreased as the contact surface was approached. The burst of energized ions coincided with a pulse in magnetic field strength interpreted by Neubauer (1988) as a fast mode shock traveling away from the contact surface. At the contact surface, a sharp spike in ion densities was observed by the mass analyzer. This pileup region was at least 0.75 s in duration (about 47 km in width); there may also have been a region of less enhanced densities extending inward another 47 km. The spike in densities was centered approximately at the inner edge of the magnetically determined contact surface. The exact magnitude of the density increase is uncertain due to instrumental limitations, but the increase above the ambient external density appears to have been at least a factor of 3.5, and appears to have been more than an order of magnitude for some species. The sharp spike in ion density is interpreted as a boundary layer into which the radial ionospheric flow enters, piles up, and in which the density increase is limited by recombination.

INTRODUCTION

The Giotto ion mass spectrometer (IMS) [*Balsiger et al.*, 1986] obtained measurements of cometary ions on the inbound pass through the coma of comet Halley. Observations by the magnetometer [*Neubauer*, 1988] at 0001:54.35 on March 14, 1986, indicated a very rapid decrease in the magnetic field strength from 20 nT to undetectable magnetic field in 0.3 s. Neubauer interpreted this discontinuity as the contact surface (ionopause) separating the regions where flow lines originate upstream in the solar wind from the region where flow lines originate in the cometary ionosphere. Approximately 2 s before encountering the contact surface, an outward propagating fast mode shock was encountered [*Neubauer*, 1988]. The angle analyzers of the high intensity spectrometer (HIS) of the IMS detected a burst of suprathermal particles coincident with the shock front; the origin of these particles is discussed.

There have been some puzzling aspects concerning the flow pattern within the cometary ionosphere that are related to the properties of the contact surface. *Wallis and Dryer* [1976] and *Houpis and Mendis* [1980] discuss a model of the comet interaction with the solar wind in which within the ionosphere the outflowing cometary ions are supersonic and pass through an inner shock, and then turn and flow tailward. However, at comet Halley no such behavior was observed. Instead, the cometary outflow was radial with a velocity of approximately 1 km/s [*Schwenn et al.*, 1987] all the way out to the contact surface; there was no decrease in radial velocity. Furthermore, no inner shock was observed. *Cravens* [1989] and *Ip and Axford* [1989] have recently proposed a model in which the ionospheric plasma piles up against the contact surface. Because the pile-up causes a plasma density increase, the recombination rate, which is proportional to the square of the density, can be greatly enhanced. The plasma is thus lost by recombination (rather than by flow down the tail). We report here on observations by the mass analyzers of the HIS of the Giotto IMS of a thin, large amplitude, density spike on the inner edge of the contact surface which we interpret as the proposed recombination layer. Finally, we note that, at radial distances of 3000–5000 km from the comet, cometward directed fast heavy ions were detected [*Goldstein et al.*, 1987; *Eviatar et al.*, 1989] by the high energy range spectrometer (HERS) of the IMS. These ions were due to ionization of inward travelling fast neutrals, a different physical phenomenon than those discussed in this paper. *Johnstone et al.* [1986] observed a burst of energetic ions in the energy range up to 400 eV (their Figure 4 at 0009:51 UT ground received time). The duration of the burst appears to be roughly 2 s. This burst may be related to the events described in our paper; further information about timing and direction of fluxes would be required to draw any useful comparisons.

INSTRUMENT OPERATION

The data were obtained by the high intensity spectrometer (HIS) of the Giotto IMS. This experiment was described by *Balsiger et al.*, [1987], and the initial encounter results from this experiment were reported in *Balsiger et al.* [1986]. The HIS sensor consisted of an angle analyzer (AA) and a mass analyzer (MA). The AA had a rotating fan shaped field of view which covered angles from the spin axis to about 22° off the spin axis. The AA was a quadrispherical analyzer, and did not provide mass analysis, but did provide five separate polar angle channels about the spin axis (roughly from 0.7° to 3.3°, 2.8° to 7.3°, 6.8° to 11.3°, 10.8° to 16.6°, and 15.8° to 21.8°; these channels are referred to as W1, W2, W3, W4, and W5, respectively). There were 64 energy steps; the

[1]Jet Propulsion Laboratory, California Institute of Technology, Pasadena.
[2]Physikalisches Institut, University of Bern, Switzerland.
[3]Lockheed Palo Alto Research Laboratory, Palo Alto, California.
[4]Max-Planck-Institut für Aeronomie, Katlenburg-Lindau, Federal Republic of Germany.

Paper number 89JA01558.
0148-0227/89/89JA-01558$02.00

range of energies corresponded to those of singly ionized particles motionless in the cometary frame with masses between 12 and 57 amu. The centers of the channels were spaced ½ amu apart for steps from 12 amu to 26 amu; above 26 amu the steps in most cases were 1 amu apart. For certain of the energy steps (chosen to correspond to energies where abundant species would be observed), these AA channels were sampled 16 times per spin (16 azimuthal measurements). The azimuthally sampled channels that were useful for our study were at energies (m_{amu} 25 eV) corresponding to motionless ions of mass 17, 18, 19, 32, and 44 amu.

The MA had a field of view that covered from the spin axis to about 7° off the spin axis; this did not provide any angular information in the polar direction. The MA consisted of a quadrispherical analyzer followed by a mass analysis section. In the MA, particles were deflected by a magnet and then focused onto a device with nine detection holes (C1 through C9). Two different approaches were used for scanning the distribution. In one program, (N program) particles of specified masses were focussed onto certain holes. In the other program (H program), each mass was focussed in turn onto a specific hole (C6), and only the data from holes C3 through C8 were returned. The objective of this mode was to acquire observations in which different masses could more readily be intercompared. The measurements obtained for all the hole/energy combinations that were expected to be of interest were integrated over a spin. Additionally, to obtain temporal/angular information, representative hole/energy combinations were chosen for a number of species, and for these channels the results were transmitted back 16 times per spin (4 s/spin); these azimuthal channels typically covered a fairly small portion of the distribution (10% to 25%), so that there were problems when the peak of the distribution moved off the azimuthal channel. It is with this 0.25-s time resolution mass analyzer data that a recombination layer at the contact surface has been detected. The width of an energy channel is the same as described for the angle analyzer.

Observations of Energized Particles at a Shock Just Outside the Contact Surface

Giotto magnetometer observations [*Neubauer*, 1988] of the magnitude of the magnetic field are shown as the bottom panel of Figure 1 (partial reproduction of Figure 1 of *Neubauer* [1988]), along with data obtained from the AA channels. The event labeled B has been proposed by Neubauer as a quasi-perpendicular shock propagating away from the contact surface. The W1 detector of the angle analyzer (spin axis aligned) is not operating properly at this time, so results from this channel are not shown. The nature of the difficulty is not well understood, but there should not be any cross talk or problems with the other channels. Data from the other four analyzers are shown. Among the energy bands transmitted back with 16 sector azimuthal resolution were those corresponding to particles of mass 17, 18, 19, 32, and 44 (approximate to ±0.5 amu per charge) traveling at 68.4 km/s (the velocity of the comet in the spacecraft frame). Count rates for energies corresponding to masses 17, 18, and 19 were summed to obtain a low-energy data set (WnLOW), and correspondingly for masses 32 and 44 into a high-energy data set (WnHIGH), where n denotes the angular channel.

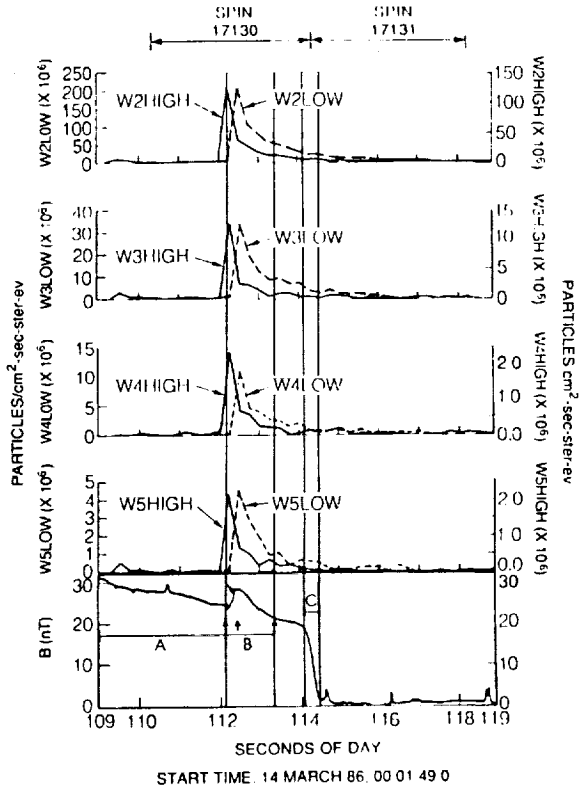

Fig. 1. Data obtained at the contact surface by the angle analyzer of the IMS and magnetometer. The lowest panel is the magnitude of the magnetic field in nanoteslas taken from *Neubauer* [1988]; panels from the top down show particle fluxes from angle analyzers W2, W3, W4, and W5. The WnLOW curves are obtained by summing three energy channels corresponding to particles of mass 17, 18, and 19 that are stationary in the cometary frame; WnHIGH curves are the sums of the corresponding channels for masses 32 and 44. The curves are in units of 10^6 particles/(cm^2 eV sr s).

Low- and high-energy sums for detectors W2, W3, W4, and W5 are shown as the remaining panels of Figure 1. The data are plotted in the center of the angular sector in which they were observed. The instrument voltage sweep proceeds from low masses to high masses, and takes ¼ s (one angular sector). It can be seen that the low-energy fluxes peak for all angles within the sector in which a local maximum in the magnetic field occurs. Correspondingly, the higher-energy channels show a peak one angular sector (0.25 s) earlier. However, because of the timing of the energy sweep, one cannot deduce that the high-energy ions were actually present before the low-energy ions. The dominant contribution to the high-energy data set was from ions of roughly mass 32, which were actually observed 0.015 s after the center of the angular sector in which they are plotted. The low-energy ions are actually observed 0.06 s before the center of the angular sector. Either set of ions could have been present up to 0.25 s before they were actually observed. It can be deduced that the low-energy ions were not present more than 0.105 s ($0.25 + t_{high} - t_{low}$) before the high-energy ions and were present no later than 0.395 s ($t_{low} - t_{high} - 0.25$) after the high-energy ions.

The temperature of ions in the cometosheath just outside the contact surface is roughly around 1500°–2000°K [*Schwenn et al.*, 1987; *Lämmerzahl et al.*, 1987]. For a particle of

mass 19 amu, the thermal speed $(2kT/m_i)^{1/2}$ is about 1.2 km/s. For a spacecraft velocity of 68.4 km/s, this corresponds to an average deviation from the ram direction of 1.0°. Thus particles observed simultaneously over a wide range of angles in detectors W2 through W5 (2.8° through 21.8°) must be suprathermal. To show this in more detail, a "pseudotemperature" for the suprathermal tail is estimated. It is assumed that the velocity is zero in the cometary frame, and that the plasma has a Maxwell-Boltzmann distribution; thermal speeds are estimated based on the decrease in the distribution function with increase in angle. The drop between W2 and W3 would require a pseudotemperature of 5×10^4 °K, the drop between W3 and W4 would require a pseudotemperature of 8×10^3 °K, and the drop between W4 and W5 would require a pseudotemperature of 3×10^5 °K. If a pseudotemperature, T, in the vicinity of 5×10^4 °K is used as an example, the corresponding thermal speed, $v = (2kT/m_i)^{1/2}$, is 6.6 km/s. The actual fluxes observed at the peak of the burst in the W2 analyzer at the water group correspond to a flux of particles of 2×10^8 particles/(cm^2 str eV s), or a local phase space density of 8.3×10^{-2}/cm^3(km/s)^3 for that portion of phase space if the instrument window were uniformly filled. If it is assumed that the accelerated ions form a sphere in phase space of radius 3 km/s centered at the bulk speed of the plasma, the corresponding energetic particle density is 9.4 cm^{-3}. At present, no measurements of the ion density just outside the bow shock have been published; however, theoretical estimates [*Ip et al.*, 1987] suggest values of 1000–2000 cm^{-3}. These various considerations demonstrate that the particles observed are suprathermal in a cometary ionosphere context. No corresponding dramatic changes in counting rates were observed in the mass analyzer channels (which detect the thermal population in the ram direction). The mass analyzer channels are dominated by counts due to the bulk population, and the suprathermal particles would have a negligible impact on the total count rate in these channels.

The fluxes of suprathermal particles decrease with time following the passage of the proposed shock. Assuming a shock velocity of 5 km/s, and assuming that the shock originated at the contact surface, the time for decay of the particle population is considerably less than 30 s. The decrease behind the shock might be due either to conventional plasma processes, or mechanisms involving neutrals such as recombination or collisions. The dissociative recombination rate coefficient, α, is $7 \times 10^{-7} N_i (300/T_e)^{0.5}$ [*Mendis et al.*, 1985], so for an ion number density, N_i, of 1000 cm^{-3} and an electron temperature, T_e, of 1000°K the loss rate would be 3.8×10^{-4}/s, i.e., too slow. Another energy loss mechanism is collisions with neutrals. *Mendis et al.* [1985] calculate an ion-neutral momentum exchange rate of $2.6 \times 10^{-9} N_n(\alpha_0/\mu_A)$, where N_n is the neutral density, α_0 is the neutral polarization in units of 10^{-24} cm^{-3}, and μ_A is the reduced mass in amu. Using a neutral density of 10^6 cm^{-3}, $\mu_A = 9.5$, and $\alpha_0 = 4$, the collision rate is 1.1×10^{-3}/s, and the loss time is 910 s (*Cravens and Körösmezey* [1986] obtain the same loss time). As the observed loss is much faster than the rates for neutral interactions, the decrease with distance behind the shock can not be attributed to interactions with neutrals.

The suprathermal particles, because of their low density, provide insufficient energy density to drive a moderate amplitude (B increased by 20%) shock. Additionally, because the ions are observed closely confined to the vicinity of the shock, they must be accelerated locally rather than having been transported into the region of the shock. What mechanism has heated the ions? For a 6.6-km/s mass 19 ion in a 27-nT field, the ion gyroradius is 48 km; the spacecraft traverses a distance of 48 km/s in 0.71 s. Keeping in mind the 0.25-s time for the instrument voltage sweep, the more energetic ions precede the shock by at most 0.5 s, whereas the lower-energy ions precede the shock by at most 0.3 s. Thus the ions are not accelerated upstream of the shock; instead, they are apparently accelerated by the transverse electric field in the foot of the shock. The burst of energetic ions is seen in angular sectors 9 and 10 of the HIS AA detector. For the W2 analyzer, this corresponds roughly to particles coming with normalized velocity components in the solar ecliptic x-z plane of roughly (−0.98, 0.20); for the W3 the components were (−0.88, 0.46), and for both W4 and W5 detectors the components were (−0.82, 0.57). The convection electric field calculated using the direction of the magnetic field has components of (0.77, −0.63); thus the direction from which the ions are seen is approximately perpendicular to the direction in which ions will be accelerated by the induced electric field. It is possible that if the instrument had been pointed along the induced electric field that even greater fluxes would have been observed; the particles being detected must presumably have been deflected in some fashion by partial gyrations in the magnetic field gradient.

Are the particle energies observed consistent with direct (nonresonant) acceleration of the particles by the electric field? The Alfven speed, V_A, is 5.0 km/s. Using this speed, and a magnetic increase, ΔB, of 5 nT (from 25 nT to 30 nT), the induced electric field, E, as the shock front swept by was $V_A \Delta B = 2.5 \times 10^{-5}$ V/m. The maximum velocity an initially motionless particle can gain in constant electric and magnetic fields is determined by the sum of convection plus gyration velocities: $v = 2E/B$. Thus the maximum velocity to which a particle is directly accelerated is $v = 2V_A \Delta B/B = 2$ km/s. The fluxes of particles observed in the W3, W4, and W5 detectors cannot be explained in this fashion. Resonant acceleration of trapped particles at a quasi-perpendicular shock front (also known as shock drift acceleration [*Armstrong et al.*, 1985; *Ohsawa and Sakai*, 1988]) is an attractive explanation. Particles can be trapped between the normal electric field associated with the shock front and the increase in magnetic field strength at the shock. The particles are then accelerated by drifting along the shock front parallel to the transverse electric field. The maximum velocity a particle can obtain through this resonant acceleration mechanism is limited by the escape of the particle from the trap when it becomes too energetic. *Ohsawa and Sakai* [1988] show that particles can be accelerated to a maximum velocity of

$$v = V_A (m_i/m_e)^{0.5} (M - 1)^{1.5}$$

where M is the Mach number and m_i and m_e are the ion and electron masses. From the increase in magnetic field strength at the shock, we estimate a Mach number of about 1.25. Using ions of mass 19 amu, the maximum energization velocity is about 120 km/s. This mechanism is thus more than sufficient to explain the presence of high-energy particles. Furthermore, one would expect to find greatly enhanced fluxes of energized particles trapped at the shock front, with much lower fluxes at locations more than an ion

gyroradius behind the front. This is what is indicated by the observations. Other models for acceleration of particles at quasi-perpendicular shocks have also been proposed [*Chiueh*, 1988]. The Chiueh model does not trap resonant particles in the shock, but rather scatters particles along and across field lines in the downstream region, and thus recycles a portion of the particles back into the shock for further acceleration. This model would require energized particles in the downstream region; such particles are not observed.

The cause of the shock is unknown. *Neubauer* [1988] has speculated that a reconnection or heating event in the tail of the comet might result in a pressure pulse traveling towards the front of the coma, which would then launch a shock into the cometosheath region. If the occurrence of the shock so close to the contact surface is not just an accident, there might be some cause related to the contact surface. *Ip and Axford* [1989] conclude that the magnetic cavity boundary should be stable. However, as will be seen in the next section, the structure of the boundary is quite different than was analyzed theoretically. There is an outward flow into the boundary from the ionospheric side; the sink for this flow is recombination. Additionally, there are sharp gradients in the magnetic field and the plasma distribution functions at the boundary. For these reasons, further investigation of possibilities for instabilities and surface waves at the boundary might be justified.

Observations of a Recombination Layer at the Contact Surface

A pileup layer was discovered at the contact surface using data from the mass analyzer channels that were transmitted back azimuth by azimuth. Our goal is to find believable limits as to the variations of the particle density during the spin in which the contact surface was encountered. Strictly speaking, we cannot prove such limits, because the corrections for the azimuthal channels depend strongly upon the velocity and temperature of the plasma, these parameters are estimated only once per spin, and inside the pileup region these parameters were not the same as those on either side of this region. A number of important instrumental effects must be taken into account that cause uncertainty in the interpretation of the data. These include observationally determined corrections required to account for the differences between H and N programs (HN correction), for the efficiency of the integral channels relative to the azimuthal channel (IA correction), and for the spin modulation (SP correction). Using these corrections, we then estimate the width of the contact surface, and the density profile encountered passing through the contact surface. These corrections are important, and are subject to rather large uncertainties because the azimuthally transmitted channels are detecting only a moderate fraction (10% to 25% based on the more detailed spectra transmitted back once per spin) of the total distribution for a given species. Since the correction factors are empirically determined from the data, using different sets of spins for their determination will result in different correction factor estimates. Therefore to obtain some idea as to the uncertainty of our procedure, we used several sets of spins for this purpose. The spin covering the time period 114.13 to 118.11 s UT (spin number 17,131) was the spin during which the contact surface was encountered. Corrections were computed from spins 17,100 to 17,129 (correction factors A), from spins 17,122 to 17,129 (correction factors B), from spins 17,133 to 17,136 (correction factors C), and from spins from 17,133 to 17,144 (correction factors D). The first set was to obtain better statistics on the period before the contact surface, the second set was to obtain plasma characteristics before the contact surface possibly more similar to those occurring in spin 17,131, and the third and fourth sets were for comparable reasons after the contact surface. The correction factors based on spins after the ionopause were larger because the plasma distribution was colder and the channels transmitted back were located in the wings (rather than the center) of the distribution function. As a further check we have tried a different method to estimate the density increase relative to background. The heavy group peak (a channel in the vicinity of mass 44) occurred in angular sector 1 of spin 17,131; the water group peak was in angular sector 2. The data during spin 17,131 were acquired in the N program; the prior spin in the N program was 17,129. By taking ratios of counts in the comparable angular bins of spin 17,131 to those of spin 17,129, further alternative estimates (correction factors E) of the relative density increase at the contact surface were obtained. The values of the adjusted count rates calculated using correction factors obtained inside the ionosphere are all higher than those obtained using corrections from the outside. This is because the distribution is colder within the ionosphere and the instrument is seeing the wing of the distribution; the correction factor is correspondingly larger. We consider the estimates we obtain in this fashion to provide a range of plausible values rather than strict upper and lower limits. Although the estimates cannot be used quantitatively to prove or disprove a theory, the results obtained are highly suggestive.

Figure 2 shows the data with HN, IA, and SP corrections for water group and heavy group (a channel in the vicinity of 44 amu) for the time period beginning 109 s UT after the start of day 73. The data are plotted in the center of the angular sector in which they were observed. The instrument voltage sweep proceeds from low masses to high masses, and takes ¼ s (one angular sector). The heavy group data are actually observed 0.07 s after the center of the angular sector. The water group ions are observed 0.06 s before the center of the angular sector. There is a short dropout in the plasma data beginning at 118.11 s UT. The data prior to spin 17,131 have been plotted using the correction factors B (from spins 17,122 to 17,129). The data from spin 17,131 have been plotted using both correction factors B and C (from spins 17,133 to 17,136). For this reason, there are two curves plotted during spin 17,131 (from 114.13 to 118.11 s UT). The water group peak falls either at 114.45, or from 114.20 to 114.45, depending on which of the curves one believes. The heavy group peak falls at 114.33 s UT. *Neubauer* [1988] found the contact surface, as indicated by a rapid drop in magnetic field strength to zero, to be from 114.1 to 114.4 s UT. There appears to be a slight increase in ion count rates just outside where Neubauer observed the beginning of the sharp decrease in magnetic field. The locations of the maximum fluxes occur somewhere between 114.2 to 114.5 s UT; this is the region in which the steepest magnetic field gradient occurs, and in which the magnetic field then becomes zero. The plasma flux boundary then extends further inward at least another 17 km. As the boundary layer is crossed, the plasma temperature is presumably rapidly de-

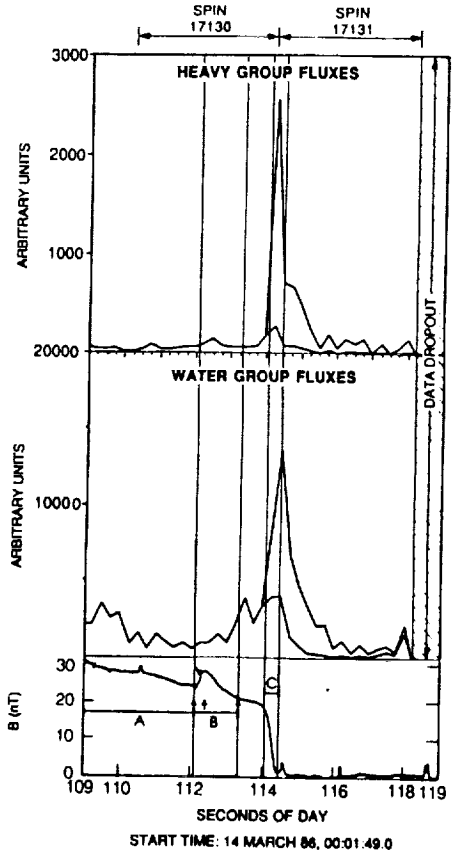

Fig. 2. Data obtained at the contact surface by the mass analyzer of the IMS and magnetometer. The middle panel is the azimuthal mass channel for water group ions. The two curves between 114 and 118 s UT result from two alternate choices for correcting this data. Data are plotted in arbitrary units. The upper panel is the comparable data for heavy group ions (a channel in the vicinity of mass 44). There is a short dropout in the IMS data after 118 s UT. The lower panel is the magnitude of the magnetic field in nanoteslas from *Neubauer* [1988].

creasing to the low temperatures typical of the ionospheric interior. This means that the detection efficiencies of the azimuthal channels were decreasing because the channels detected the wings of the distribution functions. Consequently, the drop-off on the inner edge of the density spike may be less steep than suggested by the plotted curves. It is likely that the lower curve is a good approximation for the beginning of the spin, that the upper curve is a good approximation for the latter part of the spin, but nothing can really be said about how the transition occurs. One can as a rough upper limit take the time at which the maximum curve returns to low values typical of the cometopause or sheath as an estimate of the width of the pileup layer. Using this criterion, we estimate that the water group flux returns to ambient values at about 115.45 to 115.95 s UT, and the heavy group at about 115.57. Taking exit from the pileup layer to occur between 115.5 and 116., we estimate the total width of the transition layer as 1.5 to 2.0 s, or 95 to 136 km. In summary, there appears to be a sharp peak of approximately 0.75 s duration (47 km width), followed by a somewhat more gradual decline to ambient values inside the ionosphere lasting for an additional 0.75 to 1.25 s.

It is also possible to estimate the magnitude by which the densities have increased at the pileup region. To establish a baseline for comparison to the density maximum, we use sums of the count rates over the spin (17,130) preceding the contact surface encounter. The corrected values (estimates using instrument correction factors A, B, C, and D, obtained for four different time periods, are shown) for the densities in the pileup region relative to the ambient (cometosheath) values are then as shown in Table 1. Also shown in Table 1 is an estimate (correction factor E) based on taking as a baseline the comparable angular sector measurements in the prior spin (17,129) that, like spin 17,131, was in the N program.

TABLE 1. Ratios of Maximum Ion Fluxes at the Recombination Layer to Ambient Ion Fluxes

	Water Group	Heavy Group
From correction factors A	6.3	15.0
From correction factors B	4.0	12.7
From correction factors C	10.0	30.7
From correction factors D	15.9	29.6
From correction factors E	3.5	18.0

It should be noted that the estimates of density increase in Table 1 depend on untangling spin modulation effects. The spin modulation in the data is fairly large, roughly a factor of 3. Prior to reaching the contact surface, the raw data show maximum count rates during the middle of a spin, and minimum count rates just about the beginning of the spin. The contact surface observations occur at the beginning of the spin, so that if a plasma velocity change at the contact surface led to a more favorable geometry for detection, the increases at the contact surface might be overestimated by using correction factors A, B, and E. Also, if the temperature within the recombination layer is less than that prior to the contact surface, using correction factors A, B, and E would result in an underestimate the density increase.

Discussion of the Contact Surface Observations

The results obtained here are obviously subject to considerable uncertainty; nonetheless, they furnish some useful information about physical and chemical processes within the contact surface pileup layer. The only useful data concerning the contact surface are from the MA (Figure 2); the AA data (Figure 1) give only a very minor signature in the W2 low-energy channel of a contact surface pileup layer. The AA W1 angular channel, which was looking along the direction to the comet, was not operating properly. The other angular channels were looking at offset angles to the cometary direction, and would only have seen increased fluxes if there were a hot tail on the distribution function, as occurred at the shock. As no such increased fluxes were seen in the AA data, we conclude that no suprathermal heating mechanisms are acting at the contact surface.

The density maximum for the heavy group is considerably larger than for the water group. The peak density estimated for the heavy group was between 12.7 to 30.7 times the ambient external value, whereas the increase for the water group was considerably lower, a factor of 3.5 to 15.9. (Note: at present we cannot quote absolute densities; with further data analysis this should be possible). Thus within the pileup region the ratio of heavy group density to water group

density was enhanced by a factor of from 2 to 3; such an increase might readily be expected due to differing recombination rates of the various species.

The water group accounts for the major portion of the mass, so the water group density increase may be compared to the MHD calculations [*Cravens*, 1989] of the properties of the inner transition layer. In Craven's model, outflowing ionospheric ions approaching the contact surface are reflected by the external magnetic field. A pileup of ions in a relatively thin layer located at and just inside the magnetically defined contact surface results, and enhanced recombination is the primary loss mechanisms for ions trapped within this layer. Cravens considers several cases; of these, his case 4, which has a neutral velocity (or, equivalently, ionospheric outflow velocity) of 0.9 km/s, seem most relevant to the Giotto observations. Case 4 uses a calculated electron temperature profile that is about 220°K at the location (3000 km) where his calculation places the contact surface, and the ion temperature inside the contact surface is estimated from an energy conservation equation as 400°K. The corresponding peak density enhancement over the background value is a factor of 2.4, with a width of 60 km. We have used standard gas dynamic shock theory [*Landau and Lifshitz*, 1959] to predict the density increase within the pileup region, and find that density increases by a factor of 1.5 behind the shock. This shock-based density increase estimate is lower than both our observations and Cravens' numerical model. The shock-based model fails because it does not account for the further decrease of velocity to zero as the contact surface is approached. A better approximate approach therefore is to assume flow into a layer in which the flow stagnates and is recombined. Cravens, using this technique as an alternative to his numerical calculation, and assuming the temperature in the stagnation region, predicts a density increase of 2.4. Without making any temperature assumption, the density increase may be calculated by using conservation of energy flux, by requiring that the energy flux into the stagnation rate is balanced by the recombinative loss of energy; we find that the resulting density increase is similar, a factor of 2.7. Could a further increase in pressure and density within the transition layer beyond that due to pressure balance occur due to ion-neutral drag? Because the pileup boundary is thin, our estimates indicate that the integrated force provided by collisions with neutrals over this region is not especially large; density increases of at most 20% to the analytical estimates mentioned above would be expected. In summary, fluid theory predicts density increases of about 2.4 to 2.7 and can perhaps be stretched a little further, but not to the apparently observed increases of 3.5 or more. In view of the uncertainties of the observations, this should not be considered a problem for the fluid models.

However, it is important to note that the observed length scales are of the same size as the ion mean free path. The mean free path for ion-ion collisions at 300°K is 18 km [*Cravens*, 1989]. As the Coulomb cross section varies inversely with the cube of particle velocity, and as the temperature outside the contact surface is at least 1500°K [*Schwenn et al.*, 1987; *Lämmerzahl et al.*, 1987], the mean free path of the higher energy particles will be about 165 km. Comparable typical gyroradii for 300°K and 1500°K populations in a 20-nT field are 5.0 and 11.1 km, respectively. The more energetic particles will extend further into both the upstream region that is free of magnetic field, and the downstream region of increasing magnetic field. The pressure spike may, from the observations, have a full width at half maximum of perhaps 35–50 km, considerably smaller than the mean free path expected for collisionally heated particles in the recombination layer. Particle kinetic effects are therefore determining the structure around the peak; fluid models are not applicable to determining the structure of the layer. The particle distribution will have substantial deviations from a Maxwell-Boltzmann distribution. In particular, ions entering the region of magnetic field increase experience a $\mathbf{V} \times \mathbf{B}$ force that turns the ions around and reflects them back into the upstream direction. During this reflection, the ions will have a substantial velocity component parallel to the boundary in the direction of the current that causes the increase in **B**. Particles moving parallel to the boundary do not contribute to the pressure balance across the boundary; this might result in densities higher than predicted by fluid models without altering the pressure balance normal to the boundary that is required. Further progress in understanding the structure of the pileup region requires investigation of particle kinetic effects.

Acknowledgments. The portion of this work conducted at the Jet Propulsion Laboratory, California Institute of Technology, was supported under a contract with the National Aeronautics and Space Administration. Funding was also provided by the German Bundesministerium für Forschung und Technologie and the Swiss National Science Foundation. Research at Lockheed was funded by NASA under grant NASW-4336.

The Editor thanks A. J. Coates and another referee for their assistance in evaluating this paper.

REFERENCES

Armstrong, T. P., M. E. Pesses, and R. B. Decker, Shock drift acceleration, in *Collisionless Shocks in the Heliosphere: Reviews of Current Research, Geophys. Monogr. Ser.*, vol. 35, edited by B. T. Tsurutani and R. G. Stone, p. 271, AGU, Washington, D. C., 1985.

Balsiger, H., et al., Ion composition and dynamics at comet Halley, *Nature*, *321*, 330, 1986.

Balsiger, H., et al., The Giotto ion mass spectrometer, *J. Phys. E*, *20*, 759, 1987.

Chiueh, T., Multiple-encounter shock-drift acceleration in nearly perpendicular shocks, *Astrophys. J.*, *333*, 1988.

Cravens, T. E., A magnetohydrodynamical model of the inner coma of comet Halley, *J. Geophys. Res.*, *94*, in press, 1989.

Cravens, T. E., and A. Körösmezey, Vibrational and rotational cooling of electrons by water vapor, *Planet. Space Sci.*, *34*, 961, 1986.

Eviatar, A., R. Goldstein, D. T. Young, H. Balsiger, H. Rosenbauer, and S. A. Fuselier, Energetic ion fluxes in the inner coma of comet P/Halley, *Astrophys. J.*, *339*, 545, 1989.

Goldstein, R., D. T. Young, H. Balsiger, F. Buehler, B. E. Goldstein, M. Neugebauer, H. Rosenbauer, R. Schwenn, and E. G. Shelley, Hot ions observed by the Giotto ion mass spectrometer at the comet P/Halley contact surface, *Astron. Astrophys.*, *187*, 220, 1987.

Houpis, H. L. F., and D. A. Mendis, Physiochemical and dynamical processes in cometary ionospheres, I, The basic flow profile, *Astrophys. J.*, *239*, 1107, 1980.

Ip, W.-H., and I. A. Axford, Cometary plasma processes, in *The Physics and Chemistry of Comets*, edited by W. F. Huebner, Springer-Verlag, New York, in press, 1989.

Ip, W.-H., R. Schwenn, H. Rosenbauer, H. Balsiger, M. Neugebauer, and E. G. Shelley, An interpretation of the ion pile-up region outside the ionospheric contact surface, *Astron. Astrophys.*, *187*, 132, 1987.

Johnstone, A., et al., Ion flow at comet Halley, *Nature*, *321*, 344, 1986.

Lämmerzahl, P., et al., Expansion velocity and temperatures of gas

and ions measured in the coma of comet P/Halley, *Astron. Astrophys.*, *187*, 169, 1987.

Landau, L. D., and E. M. Lifshitz, *Fluid Mechanics*, p. 331, Addison-Wesley, Reading, Mass., 1959.

Mendis, D. A., H. L. F. Houpis, and M. L. Marconi, The physics of comets, *Fundam. Cosmic Phys.*, *10*, 1, 1985.

Neubauer, F. M., The ionopause transition and boundary layers at comet Halley from Giotto magnetic field observations, *J. Geophys. Res.*, *93*, 7272, 1988.

Ohsawa, Y., and J.-I. Sakai, Prompt simultaneous acceleration of protons and electrons to relativistic energies by shock waves in solar flares, *Astrophys. J.*, *332*, 439, 1988.

Schwenn, R., W.-H. Ip, H. Rosenbauer, H. Balsiger, F. Bühler, R. Goldstein, A. Meier, and E. G. Shelley, Ion temperatures and flow profiles in comet P/Halley's close environment, *Astron. Astrophys.*, *187*, 160, 1987.

Wallis, M. K., and M. Dryer, Sun and comets as sources in an external flow, *Astrophys. J.*, *205*, 895, 1976.

K. Altwegg, H. Balsiger, and A. Meier, Physikalisches Institut, University of Bern, CH-3012 Bern, Switzerland.

S. A. Fuselier, Lockheed Palo Alto Research Laboratory, Department 91-20, Building 255, 3251 Hanover Street, Palo Alto, CA 94304.

B. E. Goldstein, W.-H. Ip, and M. Neugebauer, Jet Propulsion Laboratory, California Institute of Technology, 4800 Oak Grove Drive, Pasadena, CA 91109.

H. Rosenbauer and R. Schwenn, Max-Planck-Institut für Aeronomie, D-3411 Katlenburg-Lindau, Federal Republic of Germany.

(Received May 1, 1989;
revised July 17, 1989;
accepted July 18, 1989.)

Cometary ion flow variations at comet P/Halley as observed by the Giotto IMS experiment

G. KETTMANN ([1, *]), W.-H. IP ([1]), H. BALSIGER ([2]), B. E. GOLDSTEIN ([3]), A. MEIER ([2]), H. ROSENBAUER ([1]), R. SCHWENN ([1]), and E. G. SHELLEY ([4])

([1]) *Max-Planck-Institut für Aeronomie, Katlenburg-Lindau, FRG*
([2]) *Physikalisches Institut, University of Bern, Bern, Switzerland*
([3]) *Jet Propulsion Laboratory, California Institute of Technology, Pasadena, USA*
([4]) *Lockheed Palo Alto Research Laboratory, Palo Alto, California, USA*

Received May 19, 1989 ; revised September 7, 1989 ; accepted September 14, 1989.

ABSTRACT. Using the combined data sets from the angle analyzer (AA) and the mass analyzer (MA) of the Giotto IMS-HIS experiment, we have derived the three-dimensional plasma flow properties of cometary ions for masses ≥ 12 AMU. At cometocentric distances larger than 1.3×10^5 km, the cometary ion temperature is very high ($kT \geq 100$ eV), and derivations of the flow parameters are uncertain. After crossing the magnetic pile-up boundary (MPB) at 23 : 30 SCET (Spacecraft Event Time), the ion temperature becomes lower ($kT \geq 50$ eV), and the flow speed can be evaluated to decrease gradually from ~ 20-25 km s^{-1} to ~ 17 km s^{-1} until 23 : 41 SCET (9×10^4 km) at which point an abrupt drop to a value of ~ 13 km s^{-1} occurs. This velocity discontinuity coincides with the appearance of a cold ion population ($kT \approx 10$ eV) mostly in the ram direction of the spacecraft. Around 23 : 49 SCET (5.5×10^4 km), another velocity decrease occurs simultaneously with the disappearance of the hot ion component and an intensification of the colder one. These features are in agreement with the theoretical model of charge exchange loss of the hot cometary ions.

Annales Geophysicae, 1990, **8,** (3), 229-238.

1. INTRODUCTION

The process of solar wind-comet interaction represents a class of plasma effects in which the ionization and pickup of new ions play a dominant role. One unique feature is that, with the free energy available from the peculiar velocity distributions of the newly implanted ions, plasma instabilities could take place leading to various kinds of particle-wave interactions (Wu and Davidson, 1972). Besides the generation of very high level of plasma wave activity and turbulence in the vicinity of a cometary coma — as demonstrated by *in situ* measurements at comet Giacobini-Zinner and comet Halley (Scarf *et al.*, 1986 ; Smith *et al.*, 1986 ; Mogilevsky *et al.*, 1987 ; Klimov *et al.*, 1986 ; Riedler *et al.*, 1986 ; Neubauer *et al.*, 1986) — the determination of the plasma flow properties also can shed light on the issue of momentum coupling between the solar wind plasma and the new cometary ions. The acceleration of the heavy ions (i.e., O^+, H_2O^+, etc.) of cometary origin could be facilitated in several ways. First, collisional Coulomb interaction could be of interest. Second, wave-particle interaction as a result of plasma instabilities could be significant in assimilating the new ions into the ambient plasma flow. Finally, the $\mathbf{E} \times \mathbf{B}$ drift effect would allow the cometary ions to move with an initial speed of $v_i = v_0 \sin \theta$ in the direction perpendicular to the background magnetic field. In the special case when the angle between the plasma flow vector and the local magnetic field orientation is very small, the initial drift velocity will be small as well (i.e., $v_i \ll v_0$).

Since the cometary coma environment varies from a situation where the plasma flow is dominated by the solar wind at large cometocentric distances ($r \geq 10^6$ km) to the situation where the ion composition is mostly cometary at $r \leq 10^5$ km, the three mechanisms identified above might contribute at different levels at different distances. Indeed, the momentum-coupling between the solar wind and the cometary ions might become so inefficient at a certain point that there could be a relative drift between these two components. The cometary ion component could have a non-Maxwellian velocity distribution since it is basically a mixture of new ions accreted at different positions along the plasma flow tubes. There could be even relative drifts among the cometary ions. Furthermore, as the cometary plasma flow enters the dense atmosphere of the comet, charge exchange recombi-

(*) Now at : Los Alamos National Laboratory, University of California, Los Alamos, New Mexico, USA.

Annales Geophysicae, 0992-7689, 90 03, 229 10 $ 3.00 © EGS-Gauthier-Villars

nation *via* collisional interaction with cometary neutrals would deplete energetic ions picked up at larger distances. In place of the hot ions, there would be the build-up of cold cometary ion populations created in the inner coma. Such a scenario of charge exchange cooling was first suggested by Wallis and Ong (1975). After the spacecraft observations at comet Halley, Gombosi (1987) and Ip (1989) have examined similar effects on the formation of the so-called cometopause at $r \approx 10^5$ km (Gringauz *et al.*, 1986 ; d'Uston *et al.*, 1987) separating the fast solar wind dominated plasma on one side from the plasma controlled by the slow, cold heavy ions of cometary origin. The work by Ip, for example, showed that the charge exchange loss of hot cometary ions and the solar wind protons could be used to explain the number density profiles observed by the Ion Mass Spectrometer (IMS) experiment on the Giotto spacecraft. An exponential depletion of the hot ion populations with a scale length of about 10^4 km occurring near $6\text{-}8 \times 10^4$ km was indicated by both 2-dimensional theoretical computations and the IMS measurements. The formation of the cometopause located at about 1.4×10^5 km, however, cannot be directly related to the charge exchange loss process.

Theoretical modellings of these rather complicated processes, so far, have been limited to simple 1-D analytical flow models, or flow field profiles from 2-D MHD simulations assuming complete assimilation of the cometary ions into the solar wind flow. To further our understanding of the actual effects, it would be advantageous to examine the *in situ* measurements of plasma flow parameters at comet Halley. In the present work, we focus our attention on the observations by the High Intensity Spectrometer (HIS) of the IMS experiment. A scheme combining data from different sensors is invoked to compute the three-dimensional velocity distribution of the water group ions. While Formisano *et al.* (1988) have reported study of the flow parameters between the bow shock and the outer coma ($r \approx 1.16 \times 10^6\text{-}4 \times 10^4$ km) using the Implanted Ion Sensor (IIS) observations, our results provide a comprehensive picture of the plasma flow through the whole coma until a distance ($r \approx 10^4$ km) just before the ionospheric contact discontinuity.

The plan of our paper is as follows. A brief instrumental description will be given in Section 2. The method of data analysis is outlined in Section 3. Since there is still work being done on the calibration of the HIS, we will address only ion flow vectors and temperatures but not densities which will be subject of a future paper. The results of the water group ion flow profile will be given in Section 4, which is followed by a summary of the main points. Before proceeding, however, a clarification appears to be necessary. A cometopause boundary as identified in the Vega 1 and 2 observations is not that clear in all the available Giotto data. Although a sharp drop of the proton density is obvious in the data from the Vega as well as from the Giotto spacecraft (Gringauz *et al.*, 1986 ; Goldstein *et al.*, 1987), the Vega data show a sharp increase of the water group ion density in the ram direction that is not apparent in the Giotto data (Rème *et al.*, 1987). Further, the magnetic field changed smoothly across the Vega cometopause while the Giotto magnetometer measured a sharp increase of the field strength at the time of the proton density decrease (Neubauer, 1987). Because it is still unclear whether the Giotto and Vega spacecraft observed the same kind of boundary, we will avoid the term cometopause and refer to the « Magnetic Pile-up Boundary » (MPB) instead which is clearly identified in the Giotto data at 23 : 30 SCET ($r \approx 1.38 \times 10^5$ km) or the cometopause region if a broader region around this distance is implied.

2. DESCRIPTION OF THE EXPERIMENT

The High Intensity Spectrometer (HIS) of the Ion Mass Spectrometer (IMS) on board the Giotto spacecraft has specifically been designed with regard to the expected ion properties in the inner coma, i.e., high densities and low temperatures and bulk speeds in the comet frame of reference. For a full description of the IMS, the reader is referred to the work of Balsiger *et al.* (1987) and the thesis of Meier (1988). Briefly, the HIS consists of two separate sections, the mass analyzer (MA) and the angle analyzer (AA). Both sensors are mounted in such a way that their fields of view include the ram direction. Due to the spin of the spacecraft, the MA covers a cone of ~ 12° half width about the ram direction while the AA field of view is extended to 22° in elevation. As the AA includes only an electrostatic quadrispherical analyzer, mass separation is not possible. On the other hand, in the case of the MA the addition of a sector magnet after the electrostatic analyzer permits the measurement of the temperature distributions of selected ion channels.

2.1. The angle analyzer

2.1.1. *General description*

The AA measurements are subdivided into 64 E/Q (energy per charge) bins. Because the ions are predominantly singly charged, a particular E/Q channel corresponds to a particular ion mass, given a constant ion velocity. For the same reason, total energy is equivalent to energy per charge. Introducing the term « nominal » as referring to the relative speed between Giotto and Halley of 68.4 km s^{-1}, the nominal energy is given by the relation E [eV] = 24.5 × M [AMU], M being the nominal ion mass. The full energy range which is scanned 16 times per spin period (4 seconds) covers the nominal energy of mass 12 up to that of mass 57 (300 eV/e – 1400 eV/e). Because of the above relation between ion mass and energy, a particular E/Q bin which corresponds to nominal mass M is mostly referred to as mass channel M. For example, water ions being at rest in the comet frame of reference are measured in E/Q step 14 which thus is referred to as mass channel 18. Nevertheless, there are contributions from other ion species to this mass channel as well.

For five energy steps (corresponding to approximately the nominal energy of masses 17, 18, 19, 28, and 44 AMU), individual flux distributions are available

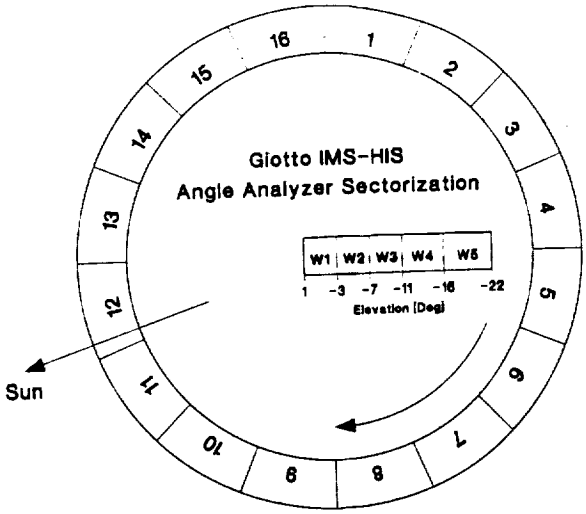

Figure 1
Sector organization of the angle analyzer. The arrow indicates the spin direction; the comet is behind the paper.

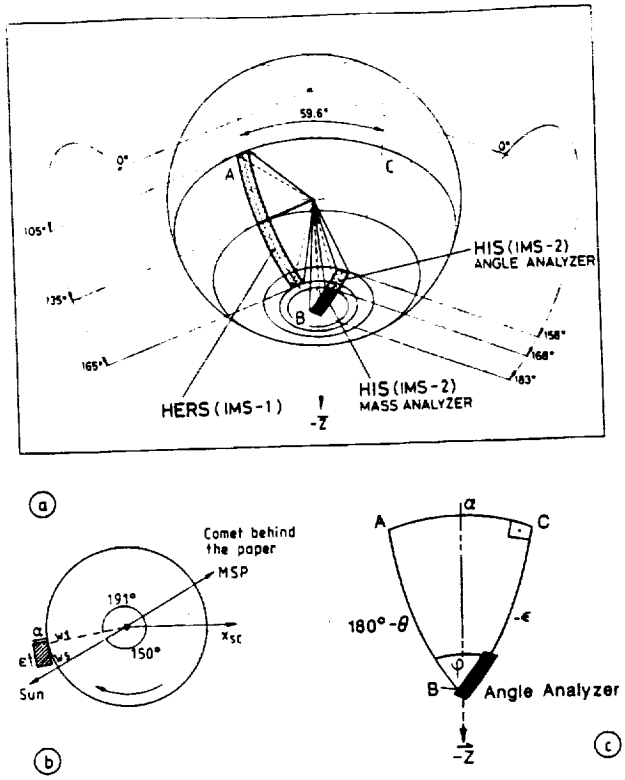

Figure 2
(a) *Angular coverage of the* IMS-HIS *sensor. The* $-z$ *direction corresponds to the Giotto spin axis and points toward the comet. (After Balsiger* et al., 1987).
(b) *Definition of the S/C coordinate system and position of the* IMS-HIS *with respect to the spacecraft skin at the time of the Sun Reference Pulse* (SRP). *Azimuthal sector* 1 *starts at the Mode Sync Pulse* (MSP), *i.e., half a spin period after the* SRP.
(c) *Definition of angles used for the calibration and the calculation of the look direction by means of the spherical triangle ABC from* (a).

in 16 azimuthal sectors (facilitated by the spin of the spacecraft) and 5 contiguous elevation sectors. The sector organization is shown in Figure 1. Elevation angle runs from $+1°$ to $-22°$. Note that the angular width of the two outermost sectors (i.e., W4 and W5) is about 50 % larger. Spin accumulated fluxes are provided for each energy step for the innermost elevation bin (W1, including the ram direction) and the remaining four bins (W2-W5) summed all together (W).

2.1.2. *Calculation of the flow direction*

The calculation of the portion of the ion distribution seen by a particular bin is a non-trivial task. Figure 2*a* shows the IMS angular coverage and field of view, Figure 2*b* sketches the position of the HIS on the instrument platform which is perpendicular to the spin axis. The comet is behind the paper. Let α be the angle in the narrow-angle and ε in the wide-angle direction of the HIS, i.e., α is the angle in the plane perpendicular to the spacecraft skin including the spin axis (positive outward), and ε is in the plane parallel to the spacecraft skin (positive in the direction of the rotation). The direction $\alpha = 0$, $\varepsilon = 0$ coincides with the direction of the spin axis (cf. Balsiger *et al.*, 1987; Meier, 1988).

The calibration of the HIS has been performed using these angles. Let us now introduce a spherical spacecraft frame of reference with θ and φ being the polar and azimuthal angle (see Fig. 2*c*). The analysis of the AA measurements is complicated by the fact that the point α_{max} of the maximum sensitivity (being used for the calculation of the ion fluxes below) deviates considerably from the $\alpha = 0$ direction and depends further on the ion mass. α_{max} can be expressed as (Meier, 1988):

$$\alpha_{max} = \alpha_0 + \frac{19.75}{M_0}\,[\mathrm{deg}] \qquad (1)$$

where α_0 is between 2.3° (W4) and 3.8° (W5), and M_0 is the nominal mass of the measured ions. The total α range covered by the AA is $\alpha_{max} \pm 5.5°$.

Referring to the spherical triangle shown in Figure 2*c*, the transformation from α and ε to the azimuthal angle φ and the polar angle θ is:

$$\cos\theta = -\cos\alpha\cos\varepsilon \qquad (2)$$

$$\tan\varphi = -\frac{\tan\alpha}{\sin\varepsilon}. \qquad (3)$$

Now inserting the results of the HIS calibration into the above equation one finds that, for example, the azimuthal angle of simultaneously measured water ions comprises a φ range of about 55°. Therefore, let us refer to $\alpha = 0$ in order to determine the azimuth φ_i of the HIS look direction (being the $+\varepsilon$ direction) for a given azimuthal sector i. Let φ now be measured with respect to the projection of the sun direction. Since sector 1 starts at the Mode Synch Pulse (MSP), the HIS is located at an angle of 11° from the x_{SC} axis at that time, i.e., at $\varphi = 161°$, and the look direction is $\varphi = 71°$. Thus (note that the spacecraft is spinning in the clockwise direction):

$$\varphi_i = 71° - (i-1)\cdot 22.5°. \qquad (4)$$

As shown in Figure 1, the instrument is looking toward the sun in sector 12.

2.2. The mass analyzer

During the encounter, the MA was operated in two modes with different ways of data accumulation. In the N program used for this study, for each mass between 12 and 45 AMU, the thermal velocity spread is measured in up to 11 steps. The energy per charge range covered by these steps varies with mass. The highest resolution is achieved for the water group ions, e.g., for mass 18 the nominal energy (439 eV/e, corresponding to the Giotto/Halley relative speed of 68.4 km s^{-1}) ± 15 % are included. From the spectra, we can get estimates of the relative abundances of these ions and, in the inner coma, of the temperature and the ion flow speed in the ram direction as well (see below).

3. DATA ANALYSIS

In an earlier study, Schwenn *et al.* (1987) estimated the ion temperature and the component of the bulk speed in the ram direction of the spacecraft directly from the MA data for the last 10 min before closest approach. However, their method applying Maxwellian fits to the MA data would be problematic if the peak of the ion distribution falls outside the MA energy range (in case of higher bulk speed) or if the thermal velocity distribution is too broad (compared with the MA energy band). In principle, this problem can be resolved by including the AA data such that a sufficiently large energy range would be covered. We therefore combine the AA data (which are a composite of all masses) with the MA data to infer the plasma bulk speed and the temperature. Our present approach is to take the MA data as a measure of the relative abundances of the cometary ions and then to find the best approximation of the AA spectra by a three-dimensional Maxwellian ion distribution. The fully resolved directional distributions are needed to obtain the direction of the flow vector.

The basic assumption is that all cometary ion species, being isotropic in their rest frame of reference, share the same temperature and bulk speed, and can be adequately described by a simple Maxwellian distribution. Now let the index i denote the ion species, and take a particular W/W1 elevation bin. As a first order approximation, the count rate C_k^W measured in energy channel k can be written as the sum over the fluxes j_{ik} (dimension : (cm² s ster eV/e)$^{-1}$) of all masses at energy E_k, multiplied with the geometric factor G_W (cm² ster eV/e) taken at a reference energy E_0 and the corresponding width of the energy passband being proportional to the energy E_k in the case of an electrostatic analyzer :

$$C_k^W = G_W \cdot \frac{E_k}{E_0} \cdot \sum_{i=m_1}^{m_2} j_{ik} \,. \tag{5}$$

If the ions follow a Maxwellian distribution with bulk speed $\mathbf{v}_b$ relative to the spacecraft, then the ion flux j_{ik} in a particular azimuthal and polar bin may be written as (e.g., Roelof *et al.*, 1976) :

$$j_{ik} = N_i \cdot \left(\frac{m_i}{2\pi kT} \right)^{3/2} \cdot \frac{v_{ik}^2}{m_i} \times \times \exp\left(-\frac{m_i}{2kT} (\mathbf{v}_{ik} - \mathbf{v}_b)^2 \right) \tag{6}$$

N_i is the number density, T the temperature, and m_i the ion mass. $\mathbf{v}_{ik}$ represents the velocity of the measured particles, and $v_{ik} = |\mathbf{v}_{ik}|$. To fit the W/W1 spectra to a Maxwellian distribution we need to know the relative abundances of the ions. More precisely, we need a quantity being proportional to the pre-exponential factor of the above equation. Such a quantity can be derived from the highest MA count rate C_{ij}^M of species i at energy step j (providing the best statistics) in the following way. Note that, in general, this peak does not correspond to the maximum of the ion distribution.

Since the sensitivity of the MA is strongly mass dependent, we must first introduce the geometric factor G_M of the MA as a function of the ion mass (Meier, 1988). An analytical approximation is given by

$$G_M = 1.13 \cdot 10^{-3} \cdot \begin{cases} (9.5 \cdot 10^{-4} \cdot M)^2 & M \leq 24 \\ -4 \cdot 10^{-5} + (2/M)^3 & M > 24 \end{cases}$$

$$G_M = [\text{cm}^2 \text{ ster eV/e}] \tag{7}$$

M = nominal mass [AMU] corresponding to energy bin j .

As the count rate is the product of ion flux and integral response function, C_{ij}^M can then be expressed as

$$C_{ij}^M = N_i \cdot G_{M,j} \left(\frac{m_i}{2\pi kT} \right)^{3/2} \cdot \frac{v_{ij}^2}{m_i} \times \times \exp\left(-\frac{m_i}{2kT} (\mathbf{v}_{ij} - \mathbf{v}_b)^2 \right) . \tag{8}$$

Now comparing Eq. (6) and Eq. (8) we find

$$j_{ik} = \frac{C_{ij}^M}{G_{M,j}} \cdot \left(\frac{v_{ik}}{v_{ij}} \right)^2 \times \times \exp\left\{ -\frac{m_i}{2kT} \cdot [(\mathbf{v}_{ik} - \mathbf{v}_b)^2 - (\mathbf{v}_{ij} - \mathbf{v}_b)^2] \right\} . \tag{9}$$

At this stage, a computer program performs a least χ^2 fitting of the angle analyzer data in order to evaluate the bulk speed and the temperature. The data base consists of 3 point running averages over single HIS records, with a weight ratio of 1 : 3 : 1. Because of the computer time needed it is not possible to include the complete response function of the AA. Therefore, we calculate the ion fluxes only at the center of each energy-azimuth-polar angle bin. One has to be aware that this might lead to a bias as soon as the ion temperatures become comparable to or even smaller than the width of the energy windows, i.e., in particular in the close environment of the comet. Thus, taking into account the detector response function might improve the results obtained for the last five or ten minutes before closest approach. Further, it turns out that it is difficult to fit a

C-2

complete W/W1 spectrum if it consists of more than one ion group. Starting at around 23 : 45 SCET, the contributions of heavier ions such as CO^+, S^+, and CO_2^+ to the AA count rates become noticeable at higher energy channels. After ~ 23 : 54 SCET, three mass peaks can be clearly identified in the W/W1 spectra. A reasonable explanation for the difficulties might be that G_M suffers relatively high uncertainties (Meier, 1988) in particular around $M/Q = 28$ which in turn severely influence estimates of the abundance ratios of the various ion groups. As a consequence of this, we only included the water group peak of the W/W1 data in our analysis, namely, we discarded all W/W1 measurements beyond the eighth channel on the high energy side of the W water group peak. We point out that the application of Eq. (9) in order to determine the plasma flow speed and temperature does not require exact values of the geometric factors. One only needs relative sensitivities which are quite well known for the water group ions.

4. RESULTS

Figure 3 shows some individual fits approximately every 2.5 min starting at ~ 23 : 25 UT. Note that UT refers to Spacecraft Event Time (SCET) throughout this paper. At the top of each frame, the ion flow bulk speed in the Giotto frame of reference and the ion temperature are indicated. Considerable deviations between the model and the measurements are evident outside the cometopause region which is crossed at ~ 23 : 30 UT (1.35×10^5 km ; d'Uston *et al.*, 1987 ; cf. also Gringauz *et al.*, 1986). They might occur because the count rates are low and, since the plasma is rather hot, show no well developed maximum. Subsequently the W measurements (upper curve) are fit quite well while the W1 data are represented not as well, namely in the bottom row of Figure 3. A remarkable change in the ion spectra is observed between the 23 : 39 : 37 UT and the 23 : 42 : 01 UT frame where the peak of the distribution moves down to lower mass channel numbers (equivalent to energy), and its shape becomes narrower. This indicates a deceleration of the ion flow as well as a cooling. For completeness, Figure 4 provides a comparison of the fitted angular distributions with the measured data. Again there is a good agreement between model and measurements most of the time. Note that the skewed shape of the distributions is an instrumental effect caused by the fact that particles appearing from quite different directions are detected simultaneously (see Sect. 2.1.2).

The reason for the poor agreement between the W1 measurements and the calculated W1 spectra after 23 : 52 UT is still not clear. The laboratory calibration of the instrument indicated that the occurrence of spacecraft charging might reduce the W1 count rate. Another possibility is that the W1 becomes saturated. Therefore, we have also carried out the analysis taking into account only the four outermost elevation bins of the AA for the χ^2 fits after 23 : 52 UT. The results are shown in Figure 5 where the dashed lines represent the calculated W1 spectra. Obviously, the calculated W1 spectra differ considerably from the data while the agreement between the measured and calculated W spectra is enhanced.

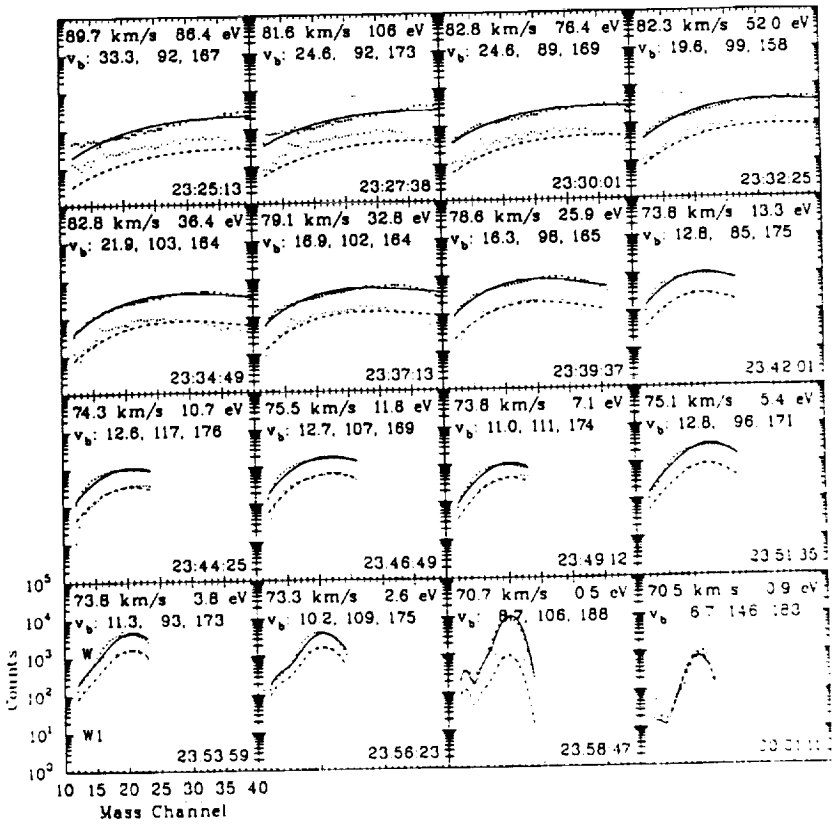

Figure 3
Examples of individual fits of the AA W/W1 *data to a* 3D *Maxwellian distribution. Bulk speed in the spacecraft frame of reference and the plasma temperature are indicated at the top of each frame. The second row represents the magnitude and the polar and azimuthal angle, respectively, of the bulk flow vector in* HSE *coordinates. The dots represent the measured fluxes, the lines correspond to the fits. The upper curves represent the* W, *the lower curves are due to the* W1 *data.*

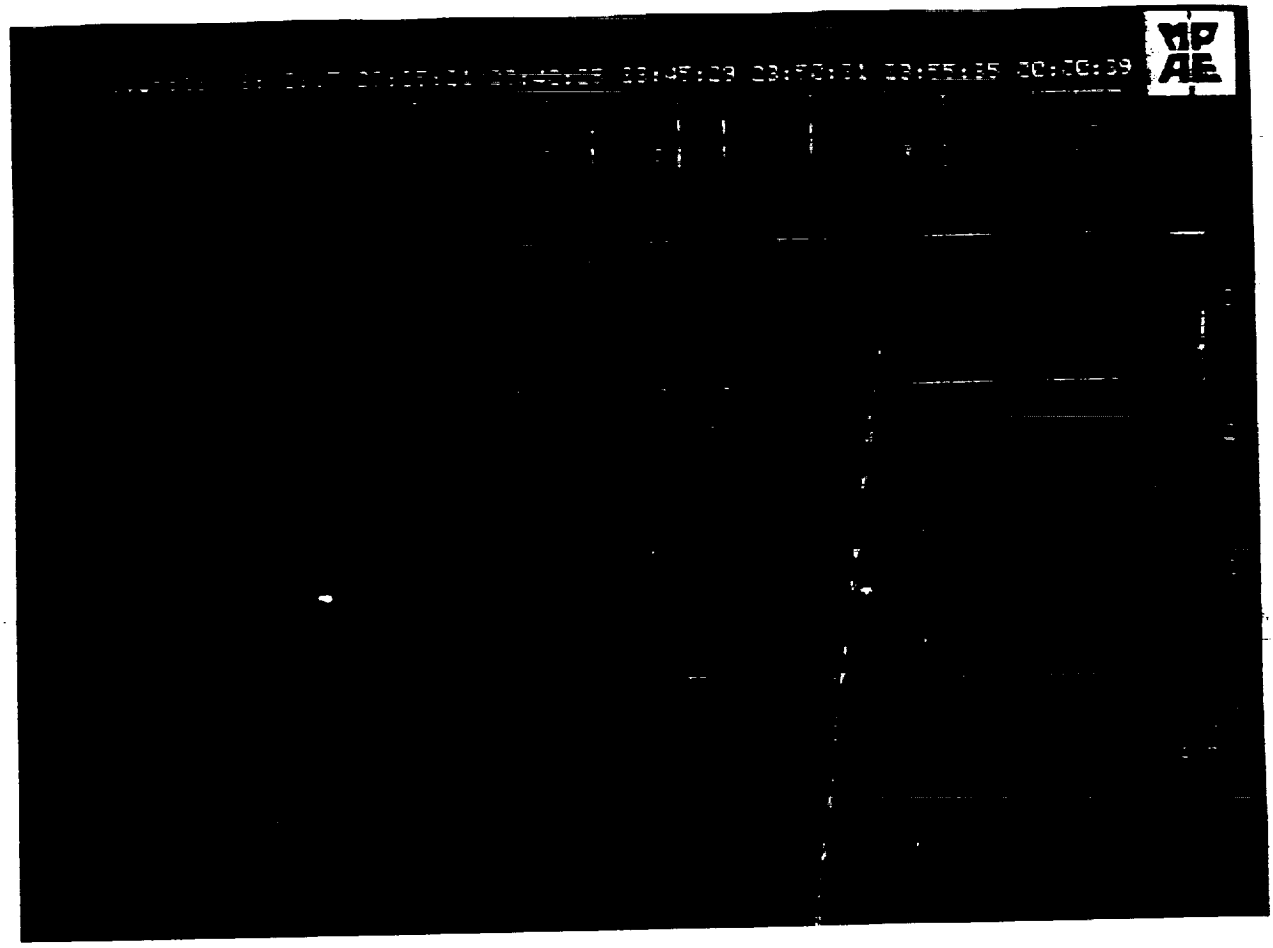

Figure 4
Comparison of the measured (left) and modelled (right) AA *ion distributions in time steps of approximately five minutes. The horizontal axis represents the five elevation sectors (for the corresponding angles* ε *see Fig.* 1), *and the vertical axis the* 16 *azimuthal sectors for each of the five mass channels indicated at the left margin* (17, 18, 19, 28, *and* 44 AMU).

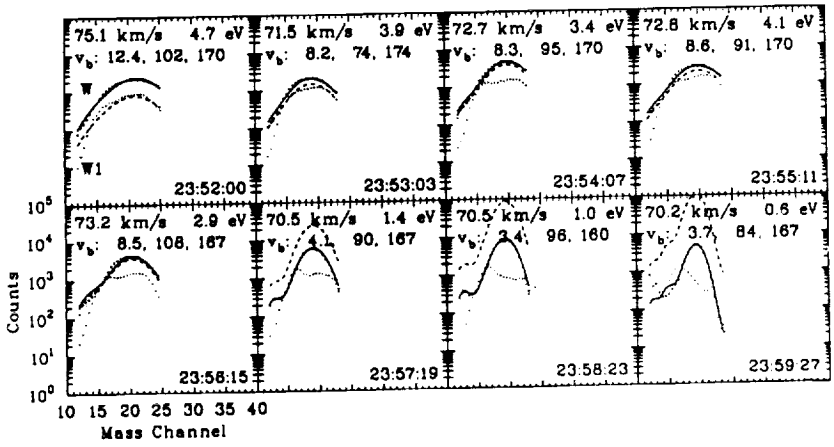

Figure 5
Same as Figure 3, *but for* χ^2 *fits taking the innermost elevation bin not into account. The dashed curves represent the modelled* W1 *count rates.*

Figure 6 summarizes the results of our analysis. The dashed curves after 23 : 52 UT show the plasma moments if the W1 channel is discarded which we assume to be more reliable. In the bottom panel, the count rates of the MA channel with the highest fluxes are drawn for the water group ions as a measure of the number density. At the bottom, an additional axis is included representing the distance from the comet in units of 10^3 km. As mentioned above, the plasma moments before 23 : 30 UT are unsure. During the 5 min following the crossing of the MPB region, the bulk speed trace exhibits relatively high variations, on the average, however, v seems to be constant at $\sim 23\ \mathrm{km\ s^{-1}}$. This value is in good agreement with the work of Formisano *et al.* (1988) who reported the same value. The ion temperature falls off rather smoothly from ~ 60 eV outside the cometopause region to ~ 20 eV at 23 : 41 UT. From 23 : 35 UT to 23 : 40 UT, there is a decrease of v leading to a drop from $17\ \mathrm{km\ s^{-1}}$ down to $13\ \mathrm{km\ s^{-1}}$ within 1 min

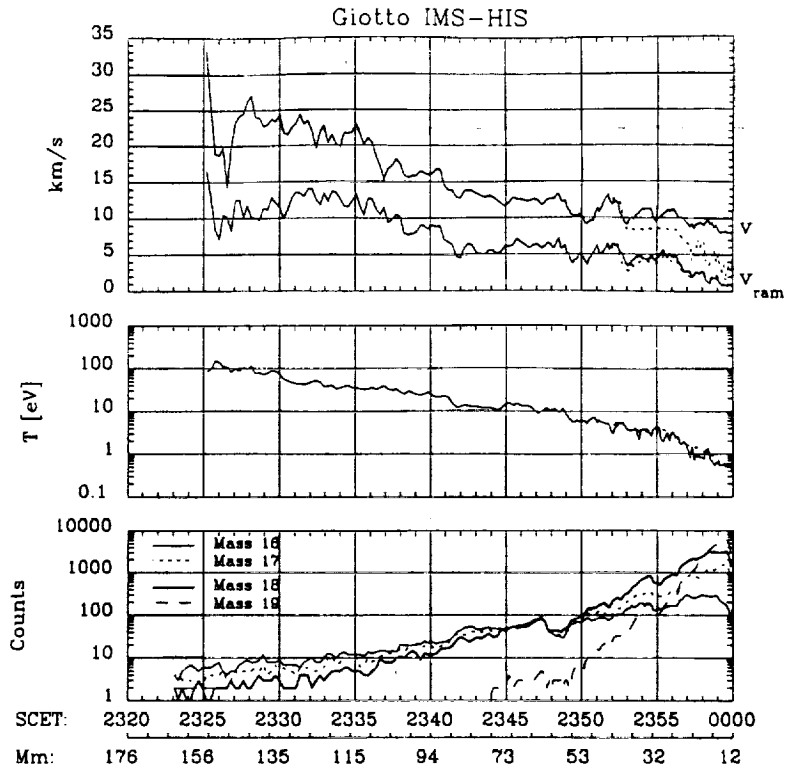

Figure 6
Cometary ion flow parameters as observed by the Giotto IMS-HIS *spectrometer. The top two panels show the total plasma bulk speed in* HSE *coordinates, its component in the ram direction, and the temperature as derived from* 3D χ^2 *fits of the angle analyzer measurements to a flowing Maxwellian. The dashed lines after* 23 : 52 UT *show the results if the* W1 *channel is discarded in the analysis. Since* W1 *measurements close to the encounter are obviously faulty, the dashed curve is most likely more reliable. Mass ratios as derived from the mass analyzer have been applied. In the bottom panel, the peak count rates from the mass analyzer are drawn for the water group ions. Distance from the comet is indicated in units of* 10^3 km.

between 23 : 41 UT and 23 : 42 UT ($r \approx 9 \times 10^4$ km). This is the reason of the spectral change discussed above. The nature of this discontinuous transition is best seen in the ram velocity v_r and the temperature which drop suddenly from 10 km s^{-1} to 6 km s^{-1} and from 22 eV to 12 eV, respectively.

The observed velocity and temperature changes correlate well with the so-called « Discontinuity X » identified earlier by Balsiger (1989). At 23 : 42 UT, Johnstone *et al.* (1986) reported a gradual loss of energetic solar wind ions. Goldstein *et al.* (1987) found a very rapid drop (by a factor of 3) of the proton density. As judged from their Figure 2, the proton density decrease starts and terminates simultaneously with the cometary ion flow transition within only a few seconds. It should be noted that around this time there is also a small increase of the cold ion fluxes (bottom panel of Fig. 6) in addition to the overall rise of the fluxes.

Another interesting feature in the ion flow speed profile is the second decrease starting at 23 : 48 : 30 UT and the bulge centered around 23 : 52 UT. This decrease at $r \approx 5.5 \times 10^4$ km shows a quite similar behaviour with regard to the total ion fluxes as observed at discontinuity X. An enhancement of the ion fluxes is observed in coincidence with the decrease of the ion flow speed while the total ion fluxes are reduced prior to the deceleration of the flow. It seems that the final sharp drop at ~ 23 : 52 : 30 UT carries similar signatures. The results obtained after 23 : 53 UT agree reasonably well with the findings of Schwenn *et al.* (1987). Between 23 : 53 UT and 23 : 56 UT, v_r is around 5 km s^{-1}, as has been found by Schwenn *et al.* (see their Fig. 1) who also reported the sudden decrease at 23 : 56 UT. The only difference is that their values of v_r after 23 : 56 UT are slightly lower than our results. Note that the omission of the W1 measurements leads to bulk speeds being a few km s^{-1} lower. However, since in this case the bulk flow vector is closer to the spin axis of the spacecraft, the ram velocity is almost not affected.

It is worthwhile to compare our data with the work of Wegmann *et al.* (1987). Based on a cometary MHD model including photochemical processes which lead to the production of different ion species in the coma of comet Halley, they published a diagram showing the expected major plasma properties (for example, ion and electron temperatures, plasma flow speed, and ion density) along the trajectory of the Giotto spacecraft. According to their predictions, the plasma flow speed should decrease almost linearly between cometocentric distances of 1.8×10^5 km and 10^4 km. In the cometopause region, the Wegmann *et al.* model predicts a flow speed of $v \approx 60$ km s^{-1} decreasing to a value of about 5 km s^{-1} at 10^4 km from the cometary centre. On the other hand, the measured total flow speed from our experiment is ~ 25 km s^{-1} in the vicinity of the cometopause. Furthermore, the velocity profile is found to be quite jagged reflecting large-scale variations in the cometary plasma flow. The measured ion temperature tends to be slightly higher (up to a factor of 2) than the theoretical value at $r > 9 \times 10^4$ km. At this distance, the trend reverses and the experimental values become consistently smaller than the theoretical values of the ion temperature.

Finally, Figure 7 shows the flow direction of the cometary ions projected into the HSE (Halley-centric Solar Ecliptic) xy plane (positive x toward the sun) along the Giotto path. We have overlaid the presumed position of the MPB (dashed line) and the streamlines

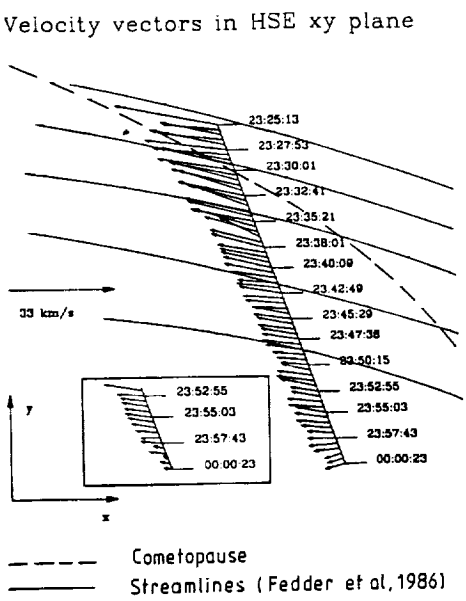

Figure 7

Projection of the cometary ion bulk flow vector into the ecliptic plane centered at comet Halley. The positive x axis points toward the sun. The position of the magnetic pile-up boundary taken from Fuselier et al. (1988) *(dashed line) and the streamlines of a* MHD *model after Fedder* et al, (1986) *are also shown. The insertion shows the flow vectors from the fits omitting the* W1 *channel.*

of a MHD model after Fedder *et al.* (1986). It is seen that the flow direction of the cometary ions is almost anti-sunward and close to the MHD streamlines. A comparison (Fuselier *et al.*, 1988) of H_2^+ velocities with He^{++} velocities, both measured by the HERS sensor of the IMS, showed that in the vicinity of the MPB there was a velocity difference between the H_2^+ ions of cometary origin and the He^{++} ions of solar wind origin. Unfortunately, the published He^{++}/H_2^+ velocities are based on moment calculations. These moment calculations have similar biases (allowing comparison of the H_2^+ with He^{++}), but are not accurate enough at low velocities to allow reliable comparisons with the heavy ion data. Work is in progress fitting the He^{++}/H_2^+ data with simulations of the instrument response to Maxwell-Boltzmann distributions ; these results may be sufficiently accurate to allow such comparisons (B. Goldstein, to be published, 1989).

5. DISCUSSION AND SUMMARY

We have performed a three-dimensional analysis of the Giotto IMS-HIS data to determine the moments of the cometary ion distributions. After crossing the cometopause region, the ions become gradually colder. Further, we found a clear decrease of the flow speed between $\sim 1.15 \times 10^5$ and 8.6×10^4 km from comet Halley. While for the first 5 min inside the MPB our values of the flow speed agree very well with those previously reported by Formisano *et al.* (1988), the subsequent clear decrease appears to be conflicting with their results indicating the water group ion velocity to be constant at ~ 23 km s^{-1} inside the MPB down to 4×10^4 km. The reason for this discrepancy is still unclear and might be subject to speculations. However, we feel that the shape of the angle analyzer spectra (Fig. 3) showing the peak moving to lower energies as well as the high energy resolution of the HIS in the critical range support our results. Fuselier *et al.* (1988) have found some differences between H_2^+ ions of cometary origin and He^{++} ions of solar wind origin using the HERS sensor of the IMS ; however, due to systematic biases that similarly affect the He^{++} and H_2^+ ions, these velocities cannot presently be compared with our heavy ion observations.

It is instructive to trace the temporal development of the angular distribution of the cometary ions. Figure 8 displays a time series of selected fully resolved AA data for two representative mass channels. While the detailed analysis of these data forms the subject of a work in progress, we would like to point out that several episodes can be defined. The comparably high bulk speed and/or temperature shift the peak of the ion distribution toward higher energies (i.e., higher mass channels), thus the highest count rates are found in mass channel 44 at the beginning. Note that the measured particles are water group ions, not CO_2^+. The peak of the distribution lies close to the ram direction only for the last three frames, i.e., after $\sim 23 : 52$ UT. Before this time, at least a large fraction of the ion distribution is clearly located outside the AA field of view. It seems that around 23 : 30 UT, the AA detects two ion populations with distinct velocities and temperatures. Another possibility is that the distribution is shell-like rather than a Maxwellian. Detailed results from shell fits to the HERS water group data will be published in a forthcoming paper. They indicate that the plasma velocities obtained from the shell fits are basically consistent with our HIS analysis which leads to slightly smaller values (B. Goldstein, to be published, 1989).

Briefly before the first sudden drop of the ram velocity, around 23 : 38 UT, a second rather cold ion population appears close to the ram direction. The distributions measured between this time and $\sim 23 : 48$ UT apparently consist of two distinct populations, the cold one around the ram direction, and the rather hot one close to the bounds of the field of view. At this time, as the second discontinuity occurs, the hot distribution seems to move closer to the ram direction. Somewhere around 23 : 53 UT, the hot fraction vanishes leaving behind the rather cold ions observed close to the ram direction.

As outlined in the Introduction, charge exchange effects can lead to replace the hot cometary ions picked up farther upstream by cold ions. Using a MHD model by Fedder *et al.* (1986), model calculations of Ip (1989) showed that the density profile measured by the IMS can qualitatively be explained by charge exchange loss of the hot cometary ions and solar wind protons. By this process, a hot ion and a cold cometary neutral react to produce a fast neutral and a cold ion. Comparing our results with previously published density profiles of the hot and cold O^+ ions (Balsiger, 1989 ; Shelley *et al.*, 1987), it turns out that the « Discontinuity X » at 23 : 41 UT

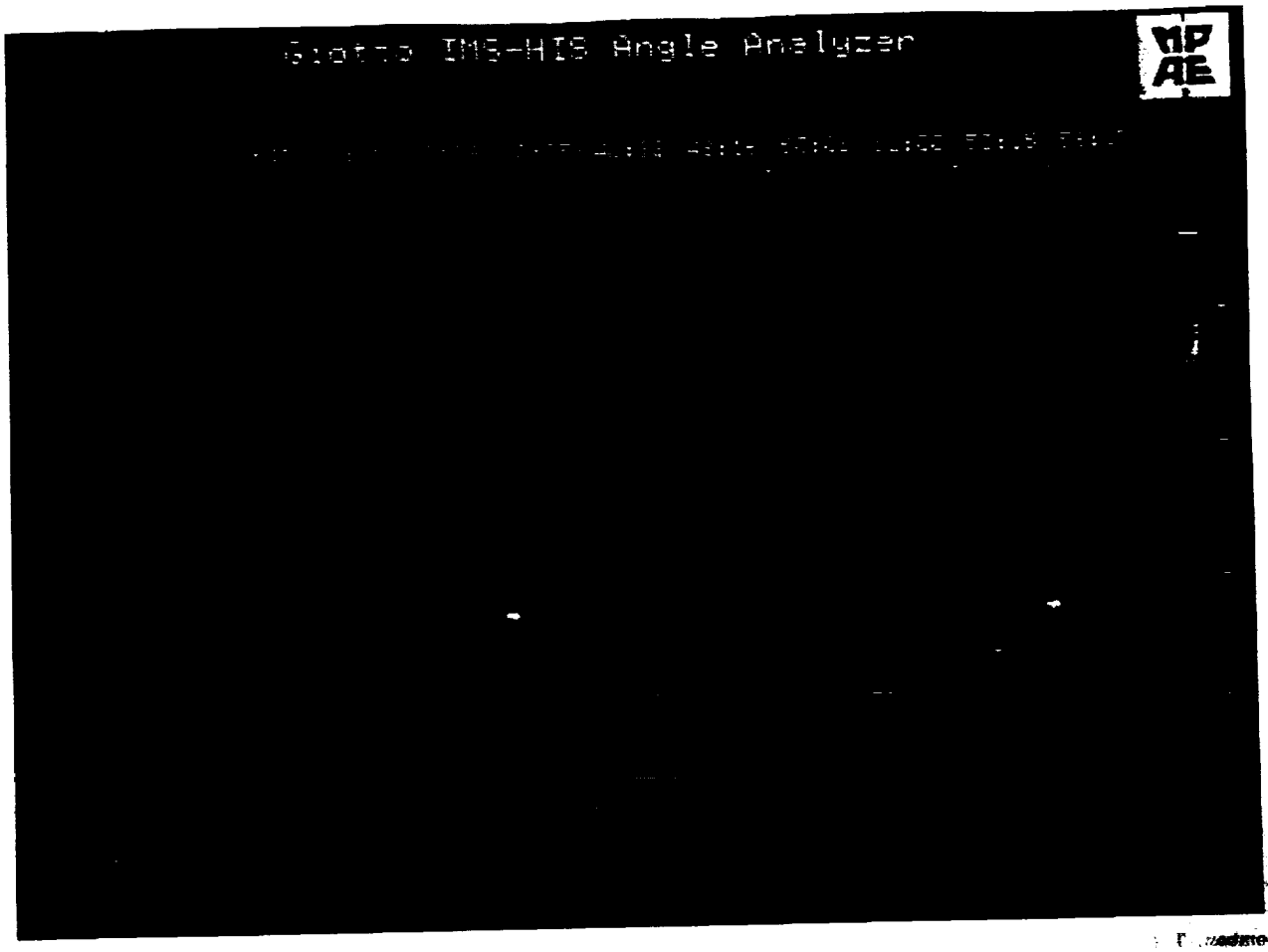

Figure 8
Time series of selected angle analyzer distributions for mass channels 18 *(top row) and* 44 *(bottom). The colour coding is shown at right. Azimuth runs from* 0° *to* 360°, *elevation from* $-1°(0)$ *to* $22°(5)$.

($r \approx 9 \times 10^4$ km) coincides with the maximum density of hot O^+ as measured by the IMS-HERS. Starting at about this distance, an exponential decrease of the hot O^+ is measured while an exponential increase of the cold O^+ begins once the cometopause region is crossed. Note that according to Figure 6 the increase of the water group ion fluxes is stronger at this time than it is on the average. The second discontinuity at 23 : 49 UT ($r \approx 5.5 \times 10^4$ km) is observed at the same time as the cold O^+ density again rises sharply after a brief period where almost no density changes have been observed. These local increases of the ion number density can be understood as being caused by the deceleration of the plasma flow. As a consequence of the continuity equation this would lead to an accumulation of ions picked up farther upstream (Ip, 1989).

In conclusion, the observed velocity and temperature profiles turn out to be explainable on the basis of charge exchange processes although some features remain unclear, e.g., what particular effects cause the flow to be decelerated abruptly at certain distances. However, the plasma moments derived in this work must be treated as an average over distributions which are a composite of two or even more distinct populations of quite different characteristics. Since there is evidence for drifts among the cometary ion species, the velocity discontinuities might be some kind of artifact arising at those radial distances where a particular component starts to dominate. Therefore, to get further insight in the processes involved, it is necessary to find an algorithm being able to separate the various ion populations.

Acknowledgements

The authors wish to thank the other IMS co-investigators for their support, especially S.A. Fuselier for the careful review of the manuscript. The work of G. K. was financed by the Deutsche Forschungsgemeinschaft. The revised version of the manuscript was prepared at the Los Alamos National Laboratory under the auspices of the U.S. Department of Energy. Funding for experimental building and data analysis was provided by the German Bundesministerium für Forschung und Technologie, the Swiss National Science Foundation, and by NASA. Research at Lockheed was funded under NASA grant NASW-4336.

Balsiger, H., *Measurements of Ion Species within the Coma of Comet Halley from Giotto*, Ellis Horwood Ltd., Chichester, England, 1989.

Balsiger, H., K. Altwegg, J. Benson, F. Bühler, J. Fischer, J. Geiss, B. E. Goldstein, R. Goldstein, P. Hemmerich, G. Kulzer, A. J. Lazarus, A. Meier, M. Neugebauer, U. Rettenmund, H. Rosenbauer, K. Säger, T. Sanders, R. Schwenn, E. G. Shelley, D. Simpson, and D. T. Young, The ion mass spectrometer on Giotto, *J. Phys. E : Sci. Instrum.*, **20**, 759-767, 1987.

D'Uston, C., H. Rème, J. A. Sauvaud, A. Cros, K. A. Anderson, C. W. Carlson, D. Curtis, R. P. Lin, A. Korth, A. K. Richter, and A. Mendis, Description of the main boundaries seen by the Giotto electron experiment inside comet P/Halley-solar wind interaction region, *Astron. Astrophys.*, **187**, 137-140, 1987.

Fedder, J. A., J. G. Lyon, and J. L. Guiliani Jr., Numerical simulations of comets : Predictions for comet Giacobini-Zinner, *EOS Trans. AGU*, **67**, 17, 1986.

Formisano, V., E. Amata, M. B. Cattaneo, P. Torrente, A. Johnstone, A. Coates, B. Wilken, K. Jockers,. M. Thomsen, D. Winningham, and H. Borg, Plasma flow inside comet P/Halley, *Astron. Astrophys.*, submitted, 1988.

Fuselier, S. A., E. G. Shelley, H. Balsiger, J. Geiss, B. E. Goldstein, R. Goldstein, and W.-H. Ip, Cometary H_2^+ and solar wind He^{2+} dynamics across the Halley cometopause, *Geophys. Res. Lett.*, **15**, 549-552, 1988.

Goldstein, B. E., M. Neugebauer, H. Balsiger, J. Drake, S. A. Fuselier, R. Goldstein, W.-H. Ip, U. Rettenmund, H. Rosenbauer, R. Schwenn, and E. G. Shelley, Giotto-IMS observations of ion-flow velocities and temperatures outside the magnetic cavity of comet P/Halley, *Astron. Astrophys.*, **187**, 174-178, 1987.

Gombosi, T. I., Charge exchange avalanche at the cometopause, *Geophys. Res. Lett.*, **14**, 1174-1177, 1987.

Gringauz, K. I., T. I. Gombosi, M. Tátralley, M. I. Verigin, A. P. Remizov, A. K. Richter, I. Apáthy, I. Szemerey, A. V. Dyachkov, O. V. Balakina, and A. F. Nagy, Detection of a new « chemical » boundary at comet Halley, *Geophys. Res. Lett.*, **13**, 613-616, 1986.

Ip, W.-H., On charge exchange effect in the vicinity of the cometopause of comet Halley, *Astrophys. J.*, **343**, 946-952, 1989.

Johnstone, A., A. Coates, S. Kellock, B. Wilken, K. Jockers, H. Rosenbauer, W. Stüdemann, W. Weiss, V. Formisano, E. Amata, R. Cerulli-Irelli, M. Dobrowolny, R. Terenzi, A. Egidi, H. Borg, B. Hultquist, J. Winningham, C. Gurgiolo, D. Bryant, T. Edwards, W. Feldman, M. Thomsen, M. K. Wallis, L. Biermann, H. Schmidt, R. Lust, G. Haerendel, and G. Paschmann, Ion flow at comet Halley, *Nature*, **321**, 344-347, 1986.

Klimov, S., S. Savin, Ya. Aleksevich, G. Avanesova, V. Balebanov, M. Balikhin, A. Galeev, B. Gribov, M. Nozdrachev, V. Smirnov, A. Sokolov, O. Vaisberg, P. Oberc, Z. Krawczyk, S. Grzedzielski, J. Juchniewicz, K. Nowak, D. Orlowski, B. Parflanovich, D. Woźniak, Z. Zbyszynski, Ya. Voita, and P. Triska, Extremely-low frequency plasma waves in the environment of comet Halley, *Nature*, **321**, 292-293, 1986.

Meier, A., *Eichung des für die Untersuchung der inneren Koma des Kometen Halley verwendeten Ionenmassenspektrometers Giotto-IMS-HIS*, PhD thesis, Inauguraldissertation, Universität Bern, 1988.

Mogilevsky, M., Y. Mikhailov, O. Molchanov, R. Grard, A. Pedersen, J. G. Trotignon, C. Béghin, V. Formisano, V. Shapiro, and V. Shevchenko, Identification of boundaries in the cometary environment from ac electric field measurements, *Astron. Astrophys.*, **187**, 80-82, 1987.

Neubauer, F. M., Giotto magnetic field results on the magnetic field pile-up region and cavity boundaries, *Astron. Astrophys.*, **187**, 73-79, 1987.

Neubauer, F. M., K. H. Glaßmeier, M. Pohl, J. Raeder, M. H. Acuña, L. F. Burlaga, N. F. Ness, G. Musmann, F. Mariani, M. K. Wallis, E. Ungstrup, and H. U. Schmidt, First results from the Giotto magnetometer experiment at comet Halley, *Nature*, **321**, 352-355, 1986.

Rème, H., J. A. Sauvaud, C. d'Uston, A. Cros, K. A. Anderson, C. W. Carlson, D. W. Curtis, R. P. Lin, A. Korth, A. K. Richter, and D. A. Mendis, General features of comet P/Halley : Solar wind interaction from plasma measurements, *Astron. Astrophys.*, **187**, 33-38, 1987.

Riedler, W., K. Schwingenschuh, Ye. G. Yeroshenko, V. A. Styashkin, and C. T. Russell, Magnetic field observations in comet Halley's coma, *Nature*, **321**, 288-289, 1986.

Roelof, E. C., E. P. Keath, C. O. Bostrom, and D. J. Williams, Fluxes of $\geq$ 50-keV protons and $\geq$ 30-keV electrons at $\sim 35\ R_E$. Velocity anisotropies and plasma flow in the magnetotail, *J. Geophys. Res.*, **81**, 2304-2314, 1976.

Scarf, F. L., F. V. Coroniti, C. F. Kennel, D. A. Gurnett, W.-H. Ip, and E. J. Smith, Plasma wave observations at comet Giacobini-Zinner, *Science*, **232**, 377-381, 1986.

Schwenn, R., W.-H. Ip, H. Rosenbauer, H. Balsiger, F. Bühler, R. Goldstein, A. Meier, and E. G. Shelley, Ion temperature and flow profiles in comet P/Halley's close environment, *Astron. Astrophys.*, **187**, 160-162, 1987.

Shelley, E. G., S. A. Fuselier, H. Balsiger, J. F. Drake, J. Geiss, B. E. Goldstein, R. Goldstein, W.-H. Ip, A. J. Lazarus, and M. Neugebauer, Charge exchange of solar wind ions in the coma of comet P/Halley, *Astron. Astrophys.*, **187**, 304-306, 1987.

Smith, E. J., B. T. Tsurutani, J. A. Slavin, D. E. Jones, G. Siscoe, and D. Mendis, International Cometary Explorer encounter with Giacobini-Zinner : Magnetic field observations, *Science*, **232**, 382-384, 1986.

Wallis, M. K., and R. S. B. Ong, Strongly-cooled ionizing plasma flows with application to Venus, *Planet. Space Sci.*, **23**, 713-721, 1975.

Wegmann, R., H. U. Schmidt, W. F. Huebner, and D. C. Boice, Cometary MHD and chemistry, *Astron. Astrophys.*, **187**, 339-350, 1987.

Wu, C. S., and R. C. Davidson, Electromagnetic instabilities produced by neutral particle ionization in interplanetary space, *J. Geophys. Res.*, **77**, 5399-5406, 1972.

Giotto IMS measurements of the production rate of hydrogen cyanide in the coma of comet Halley

W.-H. IP (1), H. BALSIGER (2), J. GEISS (2), B. E. GOLDSTEIN (3), G. KETTMANN (6), A. J. LAZARUS (4), A. MEIER (2), H. ROSENBAUER (1), R. SCHWENN (1), and E. SHELLEY (5)

(1) *Max-Planck-Institut für Aeronomie, D-3411 Katlenburg-Lindau, FRG*
(2) *Physikalisches Institut, Universität Bern, CH-3012 Bern, Switzerland*
(3) *Jet Propulsion Laboratory, California Institute of Technology, Pasadena, CA 91109, USA*
(4) *Centre for Space Research, Massachusetts Institute of Technology, Cambridge, MA 02139, USA*
(5) *Lockheed Palo Alto Research Laboratory, Palo Alto, CA 94304, USA*
(6) *Los Alamos National Laboratory, Los Alamos, NM 87545, USA*

Received April 25, 1989 ; revised September 11, 1989 ; accepted November 9, 1989.

ABSTRACT. The ion composition measurements in the ionosphere of comet Halley by the ion mass spectrometer (IMS) experiment on the Giotto spacecraft are used to estimate the relative abundance of HCN. From a comparison of the normalized number density of ions with mass-to-charge (M/q) ratio of 28 AMU/e with steady-state photochemical models, it can be determined that the production rate of HCN directly from the central nucleus is $Q(HCN) \leq 2 \times 10^{-4} Q(H_2O)$ at the time of Giotto encounter. The related photo chemical model calculations also indicate that $Q(NH_3)/Q(H_2O) \approx 5 \times 10^{-3}$ in agreement with recent determination from ground-based observations. The estimated value of Q(HCN) is lower than the relative abundance of $Q(HCN)/Q(H_2O) \approx 10^{-3}$ as derived from radio observations of the 88.6 GHz emission of the $J = 1 - 0$ transition of HCN. The difference may be the result of time-variations of the coma composition and dynamics as well as other model-dependent effects.

Annales Geophysicae, 1990, **8**, (5), 319-326.

1. INTRODUCTION

One of the brightest emissions in the optical comae of comets belongs to the CN radicals even though the CN production rate has been found to be quite small in comparison with the water production rate (i.e., $Q(CN) \approx 10^{-3} Q(H_2O)$; see A'Hearn, 1982). The parent molecules of CN have been suggested to be HCN, CH_3CN, C_2N_2 and more complicated molecules such as the cyanopolyynes, $HC_{2n+1}N$. The first two molecules have been detected in interstellar space while the cyanopolyynes were predicted to be the products of ion-molecule reactions in interstellar molecular clouds (Mitchell *et al.*, 1979 ; Kroto *et al.*, 1987). Besides these many possible parent molecules, the CN radicals could be released in several different ways in cometary comae. First, parent molecules like HCN could be emitted directly from the nucleus. The subsequent process of photodissociation would then lead to the injection of the CN radicals as daughters into the expanding atmosphere. (The photodissociation time scale of HCN at a heliocentric distance of 1 AU is 8×10^4 s ; Huebner and Carpenter, 1979). Second, the parent molecules themselves could be first created from a grandparent or released from small dust grains. The latter process might have indeed been indicated by the formation of narrow jets in CN emission in comet Halley's coma (A'Hearn *et al.*, 1986 ; Cosmovici *et al.*, 1988). A suggestion by A'Hearn *et al.* is that the CN radicals (together with C_2, C_3 and other molecules) in the jets could be emitted from sub-micron grains of organic composition. Up to now, there is yet no accurate determination on the proportion of CN emitted in the distributed source region relative to the total CN production rate.

Ground-based radio observations have been successful in monitoring the HCN emission at 88.6 GHz from a number of comets including comet Halley. Among them are comets Kohoutek 1973 XII (Huebner *et al.*, 1974), Bradfield 1978 VII (Schloerb *et al.*, 1979), Bradfield 1979 X (Ekelund *et al.*, 1981), IRAS-Araki-Alcock 1983d (Bockelee-Morvan *et al.*, 1984) and Halley (Despois *et al.*, 1986 ; Schloerb *et al.*, 1986).

Annales Geophysicae, 0992-7689, 90 05, 319 7 $ 2.70

The result of comet IRAS-Araki-Alcock 1983d is of particular interest as the upper limit of the HCN production rate ($< 1.2 \times 10^{25}$ mol.s^{-1}) was shown to be significantly below that of the CN radicals ($Q(CN) \approx 5 \times 10^{25}$ mol.s^{-1}). This is the first indication that HCN might not be the main supplier of the CN radicals in some comets (Bockelee-Morvan *et al.*, 1984 ; Bockelee-Morvan and Crovisier, 1985).

The observations of comet Halley by Despois *et al.* (1986) in 1985 suggested that $Q(HCN) \approx 8 \times 10^{-4} Q(OH)$. In comparison, the corresponding value of Q(CN) was estimated to be on the order of $10^{-3} Q(H_2O)$ by Wyckoff *et al.* (1988). Schloerb *et al.* (1986) thus proposed that HCN could still be the main parent molecule of CN, at least, in the case of comet Halley. The variation in the ratio of Q(HCN)/Q(CN) in different comets (i.e., comet IRAS-Araki-Alcock *vs.* comet Halley) may in fact reflect the variations in their chemical compositions, origins and/or thermal evolutionary histories. A clarification of this point will be an important task of future ground-based observations with a view to establish a data base for as many comets as possible.

Since the production rate of HCN obtained from radio observations depends sensitively on theoretical models of the excitation mechanism (see Bockelee-Morvan *et al.*, 1984), it is important to check this value using an independent method. The Giotto encounter with comet Halley in 1986 provided a unique opportunity in this respect. Several instruments onboard the spacecraft were capable of detecting cometary ions *in situ* by means of mass spectrometer techniques. In the following, we shall discuss how the measurements by the ion mass spectrometer (IMS) experiment can be used to derive the production rate of HCN. In Section 2 the instrumental characteristics and observational procedures will be outlined. This is to be followed by a discussion on the numerical method in getting the value of Q(HCN) from the ion composition measurements. The final section is dedicated to a summary of the main results and its possible implication in cometary physics.

2. OBSERVATIONS

The measurements were carried out by the IMS experiment onboard the Giotto spacecraft during its flyby observations of comet Halley on March 13, 1986 (Balsiger *et al.*, 1986). The experiment consisted of two sensors : (*a*) the high energy range sensor (HERS) which was optimized for measuring hot cometary ions with energy E/q = 10-4500 eV/e, and (*b*) the high intensity sensor (HIS) which was designed specifically to enable measurements of cold cometary ions in the inner coma where the count rates were expected to be very high. Both HERS and HIS are mass spectrometers using variable electric fields and static magnetic fields for simultaneous determination of mass per charge (M/q) and velocity distributions within respective energy ranges. The optical principles of the IMS and its flight configuration can be found in Balsiger *et al.* (1987).

The data taking scheme of the HIS part were divided into two modes, i.e., the N-mode and H-mode. The sharing of the data transmission rate was such that, for cometocentric distance (r) $> 8 \times 10^4$ km, the time resolution for each mode was 16 s (i.e., four spacecraft spin periods) and the corresponding spatial resolution was 1100 km. When $r < 8 \times 10^4$ km, both time and spatial resolutions would be improved by a factor of 2.

The closest approach to the nucleus of comet Halley was at a distance of 610 km ; but the IMS instrument failed to function normally due to dust impact once reaching a cometocentric distance of about 1300 km inbound. In any event, the most interesting region of cometary ionospheric dynamics, namely, the boundary of the magnetic field-free cavity separating the ionospheric plasma of pure cometary origin and the external cometary plasma flow mixed with solar wind was traversed by the spacecraft at r = 4600 km. Reports on the Giotto observations in this region can be found in Balsiger *et al.* (1986), Krankowsky *et al.* (1986), Neubauer *et al.* (1986), and Schwenn *et al.* (1987).

In the present discussion, we shall concentrate on the H-mode data taken by the HIS sensor inside the contact discontinuity where the magnetic field strength is essentially zero. Inside this boundary, the expanding ionospheric flow may be approximated by a spherically symmetric model thus rendering a much simpler way of data analysis. It should be mentioned here that the contact discontinuity represents not just a boundary of plasma dynamics but also two plasma flow regions of different chemical compositions. Certain signatures of compositional variations across this surface can be identified. For example, the number density of the H_3O^+ ions with M/q = 19 AMU/e displays a jump at this location. These features reflect the important influence of flow dynamics on the cometary ionospheric chemistry. A study of the ion compositional changes across the contact surface will be reported in a later work.

The number densities given in Figure 1 were obtained by scaling the total count rate from the M/q = 19 AMU/e channel at the contact discontinuity to a number density of $n_i(H_3O^+) = 10^3$ cm^{-3}. Photochemical models of comet Halley's ionosphere at a heliocentric distance of 0.9 AU generally predict a total ion number density on the order of 10^3 cm^{-3} (Ip, 1986). Only by increasing the solar UV ionizing photon flux by a factor of 10 larger than the nominal value would the ionospheric content be increased by a factor of about 2 (Marconi and Mendis, 1988). But this may be a somewhat extreme example.

With the same scaling factor for the H_3O^+ ions we could obtain the normalized number densities of other ion channels. Shown in Figure 1 are the corresponding values for the M/q = 28 AMU/e and 29 AMU/e ions, respectively, inside the contact surface. Due to the possible presence of complex instrumental effects permitting cross-talk between these two channels the H_2CN^+ ions might in fact be counted mostly in the mass channel with M/q = 29 AMU/e. This trend is supported by preliminary calibration data. Before the final calibration procedure pertinent to these ion masses is completed, we would refer to these values as representing the lower and upper limits.

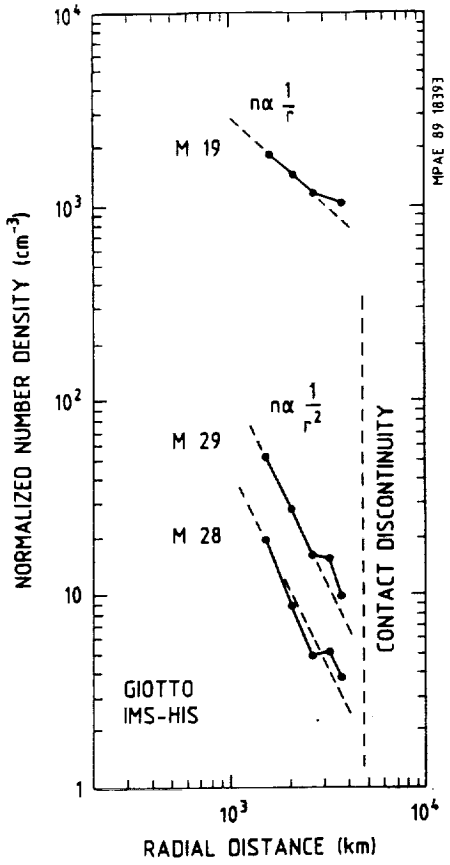

Figure 1

A display of the count rates of the mass channels M19, M28 *and* M29 *from the ion mass spectrometer* (IMS) *onboard Giotto. Each mass channel nominally corresponds to ions with mass-to-charge ratio* (M/q) *as indicated, i.e.,* M/q = 19 AMU/e *for the mass channel* M19. *Because of instrumental effects, ions with certain* M/q *values might be measured in the mass channel above or below. For example, preliminary calibrations suggest that* M/q = 28 AMU/e *ions could be measured in the* M29 *channel. Before the final determination, the count rates from mass channels* M28 *and* M29 *will be adopted as the lower and upper limits corresponding to* M/q = 28 AMU/e *ions. In the present figure the* M19 *(e.g.,* H_3O^+ *ions) count rate is normalized to a value of* $n = 10^3$ cm^{-3} *at the contact discontinuity near* r = 4600 km.

3. THEORETICAL MODELLING

The channel with $M/q = 28/e$ is interesting because of the fact that the HCN molecules could collisionally interact with the H_2O^+ and H_3O^+ ions to form the H_2CN^+ ions, i.e.,

$$HCN + H_3O^+ \rightarrow H_2CN^+ + H_2O\,, \qquad k_1 = 3.5 \times 10^{-9}\ \mathrm{cm^3\,s^{-1}} \quad (1)$$

$$HCN + H_2O^+ \rightarrow H_2CN^+ + OH\,, \qquad k_2 = 1.0 \times 10^{-9}\ \mathrm{cm^3\,s^{-1}}\,. \quad (2)$$

On the other hand, the H_2CN^+ ions only react very weakly with water molecules (rate constant $k \approx 8.8 \times 10^{-13}$ cm^3 s^{-1} ; see Anicich and Huntress, 1986) such that electron dissociative recombination :

$$H_2CN^+ + e \rightarrow \text{products}\,, \qquad \alpha_3 = 2.3 \times 10^{-7}\ \mathrm{cm^3\,s^{-1}} \quad (3)$$

would be its most important loss process in the inner coma. In this manner, H_2CN^+ could become one of the dominant ions within the first 1000 km radius of the inner coma (Ip, 1986). Consequently, in spite of the fact that HCN is a minor species, the chemical enhancement of the H_2CN^+ ions in the inner coma could facilitate its indirect detection.

The $M/q = 28/e$ channel can be contaminated by the CO^+ ions. This possibility must be examined carefully in view of the fact that the CO molecules have been found to be the second most abundant species in comet Halley with $Q(CO) \approx (0.10 - 0.15) \times Q(H_2O)$; see Eberhardt *et al.* (1987) and Krankowsky and Eberhardt (1989). Interestingly enough, the general trend of ion chemistry in the cometary ionosphere is to deplete the CO^+ ions such that within certain cometocentric distance ($r \lesssim 4000$ km, say), the H_2CN^+ ions could still dominate the $M/q = 28/e$ channel with relatively small contamination from the CO^+ ions. This point can be clarified as follows. First, the CO^+ ions from photoionization would react rapidly with the H_2O molecules *via* ion-molecule reaction :

$$CO^+ + H_2O \rightarrow \text{products}\,, \qquad k_4 = 2.5 \times 10^{-9}\ \mathrm{cm^3\,s^{-1}} \quad (4)$$

such that CO^+ itself would be preferentially depleted. At quasi-photochemical equilibrium, the photoionization source term is balanced by the ion-molecule reaction loss :

$$n(CO)/t_i \approx k_4\, n(CO^+) \cdot n(H_2O)\,. \quad (5)$$

In other words, we have

$$n(CO^+) \approx [n(CO)/n(H_2O)]/(k_4\, t_i)\,. \quad (6)$$

According to Eberhardt *et al.* (1987), about half of the CO molecules were released directly from the nucleus and the rest in a distributed source region with a dimension of about 2×10^4 km, we can then assume $n(CO)/n(H_2O) \approx Q(CO)/Q(H_2O) \approx 0.05$. With a photoionization time scale (t_i) of 3×10^6 s (Huebner and Carpenter, 1979) and an ion-molecule reaction rate (k_4) of 2.5×10^{-9} cm^3 s^{-1} (Anicich and Huntress, 1986), we find $n(CO^+) \approx 7$ cm^{-3}. By the same token, the number density of N_2^+ can be determined to be $n(N_2^+) \lesssim 2$ cm^{-3} if $Q(N_2)/Q(H_2O) \lesssim 1\,\%$, taking into account the following ion-molecule reactions (Anicich and Huntress, 1986) :

$$N_2^+ + H_2O \rightarrow H_2O^+ + N_2\,, \qquad k_7 = 1.6 \times 10^{-9}\ \mathrm{cm^3\,s^{-1}} \quad (7)$$

and

$$N_2^+ + H_2O \rightarrow N_2H^+ + OH\,, \qquad k_8 = 5.0 \times 10^{-10}\ \mathrm{cm^3\,s^{-1}}\,. \quad (8)$$

Since the number density of CO^+ in Eq. (6) depends on the ratio of $n(CO)$ to $n(H_2O)$, it is nearly constant throughout the inner coma up to the contact discontinuity. The N_2^+ ion would follow the same pattern. As for the H_2CN^+ ions, the density profile follows

essentially a r^{-2} law (see discussion below and Fig. 1). These different patterns hence provide a means to separate the H_2CN^+ from the N_2^+ and CO^+ ions, provided there are no other ion species contributing to the $M/q = 28$ AMU/e channel.

In order to investigate this point further, we have carried out a simple model calculation for the ionospheric composition of comet Halley during the time period of Giotto flyby. The expansion of the neutral gas and cometary plasma is assumed to be spherically symmetric. The H_2O production rate is taken to be $Q(H_2O) = 7 \times 10^{29}$ mol s^{-1} and the radial expansion velocity is assumed to be a constant value of $V_n = 1$ km s^{-1} (Krankowsky *et al.*, 1986).

The network of photochemical calculations includes the photolytic reactions of H_2O, HCN and NH_3, the electron dissociative recombination reactions of the major ions involved, and ion-molecule reactions of the daughter ions with the parent neutrals. For completeness, the reactions considered are listed in Tables 1-3. NH_3 is considered here because, as a result of protonation, the NH_4^+ ion could become one of the major ions in the inner coma (Aikin, 1974; Allen *et al.*, 1987). This interesting property of cometary ion chemistry has been used to infer the relative abundance of NH_3 in the coma of comet Halley (Allen *et al.*, 1987; Marconi and Mendis, 1988). Furthermore, as will be discussed later, the NH_4^+ ion also tends to modulate the abundance of H_2CN^+ ion in the inner coma.

A more comprehensive photochemical model calculation (Ip, 1986) including H_2O, NH_3, HCN, CO, CO_2, CH_4, and several hydrocarbons has shown that ions such as OH^+, CO^+, HCO^+, and CO_2^+ all have number densities < 10 cm^{-3} (e.g., $< 1\%$ of total ion number density). Their omission in the present computation therefore should not cause serious problems in our investigation specific to the abundance of HCN. Note that a highly simplified photochemical network has the merit of fast-computation thus permitting a more complete study of the relevant parameters. On the other hand, a chemical model including as many species and reactions as possible (cf. Ip, 1986) is extremely time-consuming; the resultant computer program would also lack the flexibility as required here. Our present approach is hence a reasonable compromise.

The radial variations of the ion number densities and ion composition depend on the electron temperature (T_e) profile adopted. This is because electron dissociative recombination, with the rate coefficients following a temperature dependence usually in the form of $T_e^{-0.5}$, is the main loss mechanism therein. The effects of several different temperature profiles have been examined. As shown in Figure 2, use of quantitatively

Table 1

Photolytic reactions.

Reaction		Rate constant	Reference
1. $H_2O + h\nu$	$\rightarrow H + OH$	1.0×10^{-5}	HC
2. $H_2O + h\nu$	$\rightarrow H_2 + O(^1D)$	1.4×10^{-6}	HC
3. $H_2O + h\nu$	$\rightarrow H_2O^+ + e$	3.3×10^{-7}	HC
4. $H_2O + h\nu$	$\rightarrow OH^+ + H + e$	5.5×10^{-8}	HC
5. $H_2O + h\nu$	$\rightarrow O^+ + H_2 + e$	5.8×10^{-9}	HC
6. $H_2O + h\nu$	$\rightarrow H^+ + OH + e$	1.3×10^{-8}	HC
7. $NH_3 + h\nu$	$\rightarrow NH_2 + H$	1.1×10^{-4}	HC
8. $NH_3 + h\nu$	$\rightarrow NH + H_2$	6.3×10^{-5}	HC
9. $NH_3 + h\nu$	$\rightarrow NH_3^+ + e$	6.1×10^{-7}	HC
10. $NH_3 + h\nu$	$\rightarrow NH_2^+ + H + e$	1.9×10^{-7}	HC
11. $NH_3 + h\nu$	$\rightarrow NH^+ + H_2 + e$	6.9×10^{-9}	HC
12. $HCN + h\nu$	$\rightarrow H + CN$	1.3×10^{-5}	HC
13. $HCN + h\nu$	$\rightarrow HCN^+ + e$	3.0×10^{-7}	Guesstimate
14. $HCN + h\nu$	$\rightarrow CN^+ + H + e$	3.0×10^{-7}	Guesstimate

HC = Huebner and Carpenter (1979).

Table 2

Electron dissociative recombination reactions.

Reaction		Rate constant	Reference
101. $H_3O^+ + e$	$\rightarrow H + OH$	$9.1 \times 10^{-8} T_e^{-0.5}$	ADH
102. $H_3O^+ + e$	$\rightarrow O + H_2$	$3.9 \times 10^{-8} T_e^{-0.5}$	ADH
103. $H_3O^+ + e$	$\rightarrow H_2O + H$	$3.4 \times 10^{-8} T_e^{-0.5}$	ADH
104. $NH_3^+ + e$	$\rightarrow NH_2 + H$	$4.1 \times 10^{-8} T_e^{-0.5}$	ADH
105. $NH_3^+ + e$	$\rightarrow NH + H$	$4.1 \times 10^{-8} T_e^{-0.5}$	ADH
106. $H_2CN^+ + e$	$\rightarrow H + HCN$	$4.0 \times 10^{-8} T_e^{-0.5}$	Guesstimate *
107. $HCN^+ + e$	$\rightarrow H + CN$	$4.0 \times 10^{-8} T_e^{-0.5}$	Guesstimate *

ADH = Allen *et al.* (1987).
* K = $3.7 \times 10^{-8} T_e^{-0.5}$ according to Schmidt *et al.* (1988).

Table 3

Ion-molecule reactions.

Reaction		Rate constant	Reference
201. $NH^+ + H_2O$	$\rightarrow H_3O^+ + N$	1.1×10^{-9}	AH
202. $NH^+ + H_2O$	$\rightarrow H_3O^+ + NH$	1.1×10^{-9}	AH
203. $NH^+ + H_2O$	$\rightarrow NH_3^+ + OH$	8.8×10^{-10}	AH
204. $NH^+ + H_2O$	$\rightarrow NH_3^+ + O$	1.8×10^{-9}	AH
205. $NH_3^+ + H_2O$	$\rightarrow H_3O^+ + NH$	2.8×10^{-9}	AH
206. $NH_3^+ + H_2O$	$\rightarrow NH_4^+ + O$	1.5×10^{-10}	AH
207. $NH_3^+ + H_2O$	$\rightarrow NH^+ + OH$	1.1×10^{-9}	AH
208. $NH_3^+ + NH_3$	$\rightarrow NH_4^+ + NH_2$	2.2×10^{-9}	AH
209. $O^+ + H_2O$	$\rightarrow H_2O^+ + O$	3.2×10^{-9}	AH
210. $H^+ + H_2O$	$\rightarrow H_2O^+ + H$	8.2×10^{-9}	AH
211. $OH^+ + H_2O$	$\rightarrow H_2O^+ + OH$	1.5×10^{-9}	AH
212. $OH^+ + H_2O$	$\rightarrow H_3O^+ + O$	1.4×10^{-9}	AH
213. $CN^+ + H_2O$	$\rightarrow H_2O^+ + CN$	3.2×10^{-9}	AH
214. $CN^+ + H_2O$	$\rightarrow HCN^+ + OH$	1.6×10^{-9}	AH
215. $CN^+ + H_2O$	$\rightarrow H_2CN^+ + O$	4.8×10^{-10}	AH
216. $CN^+ + NH_3$	$\rightarrow NH_3^+ + HCN$	1.0×10^{-9}	AH
217. $CN^+ + NH_3$	$\rightarrow NH_4^+ + CN$	1.2×10^{-9}	AH
218. $CN^+ + NH_3$	$\rightarrow HCN^+ + NH_2$	4.0×10^{-10}	AH
219. $CN^+ + NH_3$	$\rightarrow H_2CN^+ + NH$	3.0×10^{-10}	AH
220. $CN^+ + HCN$	$\rightarrow HCN^+ + CN$	2.5×10^{-9}	AH
221. $HCN^+ + NH_3$	$\rightarrow NH_3^+ + HCN$	1.7×10^{-9}	AH
222. $HCN^+ + NH_3$	$\rightarrow H_2^+ + NH_2$	8.4×10^{-10}	AH
223. $HCN^+ + NH_3$	$\rightarrow NH_4^+ + CN$	1.4×10^{-10}	AH
224. $HCN^+ + H_2O$	$\rightarrow H_3O^+ + CN$	1.8×10^{-9}	AH
225. $HCN^+ + H_2O$	$\rightarrow H_3O^+ + HCN$	1.8×10^{-9}	AH
226. $HCN^+ + HCN$	$\rightarrow H_2CN^+ + CN$	1.6×10^{-9}	AH
227. $H_2CN^+ + NH_3$	$\rightarrow NH_4^+ + HCN$	2.4×10^{-9}	AH
228. $H_2O^+ + NH_3$	$\rightarrow NH_4^+ + OH$	1.0×10^{-9}	AH
229. $H_2O^+ + NH_3$	$\rightarrow NH_3^+ + H_2O$	2.0×10^{-9}	AH
230. $H_2O^+ + H_2O$	$\rightarrow H_3O^+ + H_2O$	2.1×10^{-9}	AH
231. $H_2O^+ + HCN$	$\rightarrow H_2CN^+ + OH$	1.0×10^{-9}	AH
232. $H_2O^+ + HCN$	$\rightarrow H_3O^+ + CN$	1.0×10^{-9}	AH
233. $H_3O^+ + NH_3$	$\rightarrow NH_4^+ + H_2O$	2.2×10^{-9}	AH
234. $H_3O^+ + HCN$	$\rightarrow H_2CN^+ + H_2O$	3.5×10^{-9}	AH

AH = Anicich and Huntress (1986).

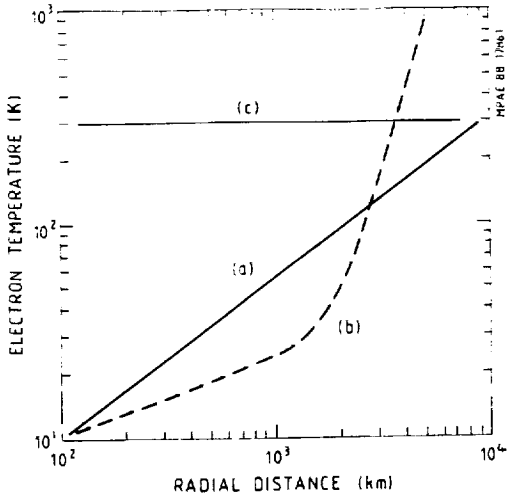

Figure 2

Different possible electron temperature profiles in the inner coma of comet Halley. Curves (a) *and* (b) *represent electron temperature variations with different magnitudes of radial gradients. The very abrupt increase of electron temperature inside the contact surface as illustrated in case* (b) *is not supported by the Giotto* IMS *measurements. Curves* (a) *and* (c) *produce similar results in ion compositions for r between* 10^3 *and* 4.5×10^3 km. *In the present work, the curve* (c) *with a constant value of* T_e (= 300 K) *has been adopted.*

approximates the situation where T_e increases smoothly from a value of about 10 K at $r \approx 100$ km to 300 K at $r \approx 5000$ km. This behaviour has been predicted by thermal model calculations (Mendis *et al.*, 1985). The other case (*b*) is to investigate the situation in which a very steep electron temperature gradient may exist in the inner coma (Körösmezry *et al.*, 1986). Our photochemical calculations show that the sharp increase in T_e as given by case (*b*) would lead to a rapid increase of the H_3O^+ ion number density which reaches a value of about 2000 cm^{-3} near the contact discontinuity. As such upturn of the count rate of ions with M/q = 19 AMU/e was not observed by the IMS experiment, this may be taken as an indication that the electron temperature should have a relatively smooth profile as exemplified by case (*a*). The actual electron temperature profile could be, of course, somewhat different. One extreme limit would be to have a flat temperature profile with $T_e \approx 300$ K (i.e. case (*c*)) as adopted in the model calculations by Allen *et al.* (1987). The main effect would be to have slightly larger ion number densities at $r < 3000$ km because of the reduced effect of electron dissociative recombination. The general behaviour in the radial dependence of the ion number density is maintained, however.

The dependence of the H_2CN^+ content on the relative abundance of HCN can be evaluated by using different values of Q(HCN) in the photochemical calculations. Figure 3 shows the cases with $Q(HCN)/Q(H_2O) = 2 \times 10^{-4}$, 5×10^{-4} and 10^{-3}, respectively. At the same time, five different values of $Q(NH_3)/Q(H_2O)$ are considered. The effect of increasing the NH_3 abundance is to reduce both the H_2CN^+ density and the corresponding radial gradient. In other words, the HCN and NH_3 abundances are coupled.

From an examination of the theoretical H_2CN^+ ion density profiles as a function of the relative abundances of both HCN and NH_3, we could obtain a curve relating the Q(HCN) and $Q(NH_3)$ combinations which provide acceptable fits to the measurements. In Figure 4, we see that such a curve, if incorporating the two determinations of the NH_3 abundance by Allen *et al.* (1987) and by Tegler and Wyckoff (1989), would imply a value between $2\text{-}3 \times 10^{-3}$ for the relative abundance of HCN. A value as high as 10^{-3} for the relative abundance of HCN would require $Q(NH_3)/Q(H_2O) \approx 5$ % which is ruled out by both *in situ* measurements and ground-based optical observations. In fact, if the slope of the density variation as depicted by the IMS observations is taken into consideration, the smaller value appears to be a better fit and in turn points to a relative abundance of NH_3 of about 0.5 ± 0.2 as proposed by Tegler and Wyckoff (1989).

4. DISCUSSION

As mentioned before, the radio observations by Despois *et al.* (1986) and Schloerb *et al.* (1986) reported a HCN production rate on the order of $Q(HCN) \approx 10^{-3}\, Q(H_2O)$. The Giotto IMS measurements in the ionosphere of comet Halley, on the other

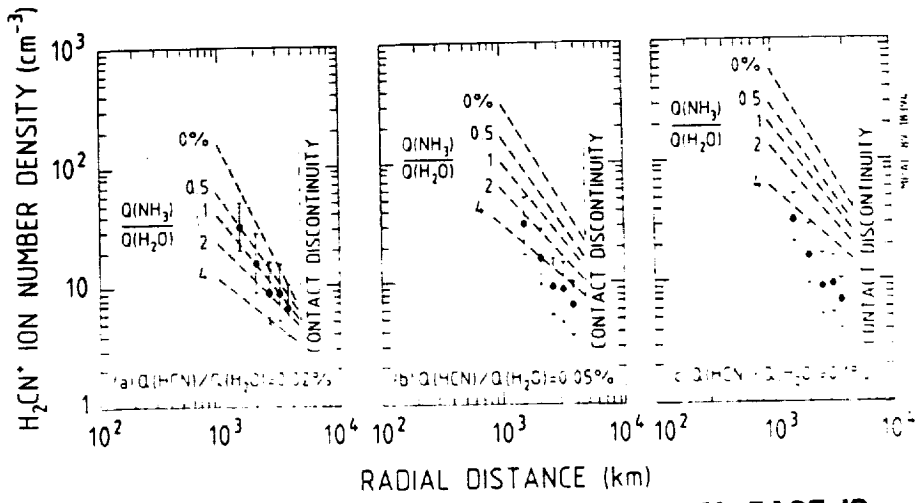

Figure 3

A comparison of the theoretical radial profiles of the H_2CN^+ *ions with different values of the relative abundance of* NH_3 *and of* HCN: (a) $Q(HCN)/Q(H_2O) = 2 \times 10^{-4}$; (b) 5×10^{-4}; *and* (c) 10^{-3}.

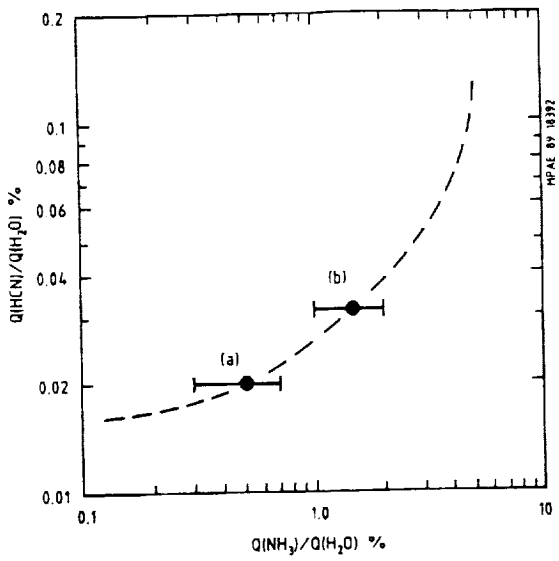

Figure 4

A graphical curve relating the relative abundances of HCN *and* NH_3 *as constrained by the* IMS *measurements of the* H_2CN^+ *density profile. The range of relative abundance of* NH_3 *as given by Tegler and Wyckoff* (1989) *is indicated as* (a) *and that by Allen* et al. (1987) *is indicated as* (b).

hand, pointed to a value about a factor of 4 smaller. Within the context of a steady state photochemical model, the IMS data set an interesting limit on the relative abundance of HCN emitted directly from the central nucleus, i.e., $Q(HCN) \leq 2 \times 10^{-4}\, Q(H_2O)$ as given by the $M/q = 29$ AMU/e channel, at the time of Giotto encounter — in case $Q(NH_3)/Q(H_2O) \approx 5 \times 10^{-3}$ as determined by Tegler and Wyckoff (1989). This difference may be partly due to time-variation in the outgassing process of the comet. For example, Schloeb *et al.* (1986) found significant day-to-day variations in the HCN production rate whilst formation of expanding CN shells was observed in the coma of comet Halley (Schlosser *et al.*, 1986). The infrared fluorescence equilibrium model used to compute the excitation rate of the 88.6 GHz emission of the $J = 1 - 0$ transition of HCN might also contribute to some uncertainties. The possibility thus exists that HCN is only a minor contributor to the CN radicals at different episodes leaving CH_3CN, C_2N_2 and other more complicated molecules as the main suppliers.

Even though CN is only a very minor species in cometary atmosphere, its very strong optical emission can be used as an important tracer for the chemical composition and hydrodynamics of the gaseous coma. This is particularly interesting in view of the observations of CN-jets and expanding CN halos in the coma of comet Halley. The formation of the CN-jets in fact points to a possible dichotomy of the sources of the CN radicals. First, organic solid particles such as the so-called CHON dust grains (Kissel *et al.*, 1986) may be a significant source of the CN-radicals in jet-like structures (A'Hearn *et al.*, 1986). Second, the volatile ice on the surface of the central nucleus must also be a supplier of HCN and other parent molecules of CN. A precise knowledge of the relative importances of these different sources could provide important clues to the condensation history of cometary nuclei in the solar nebula. While further ground-based observations, both in optical, infrared and radio wavelengths would be needed to follow up this issue, *in situ* mass spectrometer measurements to be performed by the CRAF mission at comet Kopff would be equally indispensible in this respect.

Finally, we should point out that we have restricted our consideration to a steady-state photochemical model. Observations of the gas emission and activity of comet Halley have produced ample evidence that its outgassing process could be highly anisotropic and sporadic at times (A'Hearn *et al.*, 1986 ; Larson *et al.*, 1986 ; Feldman *et al.*, 1987). In addition, photoionization might not be the only ionization mechanism. The validity of present calculations is therefore subject to correction once the ionospheric environment of comet Halley during the Giotto encounter is more clarified.

Acknowledgements

We would like to thank our colleagues in the Giotto IMS team for very helpful assistance and useful discussions. Prof. M. A'Hearn and another referee for useful comments. This work was supported by the German Bundesministerium fuer Forschung und Technologie, the Deutsche Forschung Gemeinschaft (Schwerpunkt program : Kleine Körper im Sonnensystem) the Swiss National Science Foundation, and NASA.

REFERENCES

Aikin, A. C., Cometary coma ions. *Astrophys. J.*, **193**, 263-264, 1974.

A'Hearn, M. F., Spectrophotometry of comets at optical wavelengths, in *Comets*, Ed. L. L. Wilkening, University of Arizona Press, pp. 433-460, 1982.

A'Hearn, M. F., S. Hoban, P. V. Birch, C. Bowers, R. Marin, and D. A. Klinglesmith, III., Cyanogen jets in comet Halley, *Nature*, **324**, 649-651, 1986.

Allen, M., M. Delitsky, W. Huntress, Y. L. Yung, W.-H. Ip, R. Schwenn, H. Rosenbauer, E. Shelley, H. Balsiger, and J. Geiss, Evidence for methane and ammonia in the coma of comet P Halley, *Astron. Astrophys.*, **187**, 502-512, 1987.

Anicich, V. G., and W. T. Huntress, A survey of bimolecular ion-molecule reactions for use in modeling the chemistry of planetary atmospheres, cometary comae, and interstellar clouds, Jet Propulsion Lab. Report, Jan. 2, 1986.

Balsiger, H., K. Altwegg, F. Bühler, J. Geiss, A. G. Ghielmetti, B. E. Goldstein, R. Goldstein, W. T. Huntress, W.-H. Ip, A. J. Lazarus, A. Meier, M. Neugebauer, U. Rettenmund, H. Rosenbauer, R. Schwenn, R. D. Sharp, E. G. Shelley, E. Ungstrup, and D. T. Young, Ion composition and dynamics at comet Halley. *Nature*, **321**, 330-335, 1986.

Balsiger, H., K. Altwegg, J. Benson, F. Bühler, J. Fischer, J. Geiss, B. E. Goldstein, R. Goldstein, P. Hemmerich, G. Kulzer, A. J. Lazarus, A. Meier, M. Neugebauer, U. Rettenmund, H. Rosenbauer, K. Säger, T. Sanders, R. Schwenn, E. G. Shelley, D. Simpson, and D. T. Young, The ion mass spectrometer on Giotto. *J. Phys. E : Sci. Instrum.*, **20**, 759-767, 1987.

Bockelee-Morvan, D., J. Crovisier, A. Baudry, D. Despois, M. Perault, W. M. Irvine, F. P. Schoerb, and D. Swade, Hydrogen cyanide in comets : Excitation conditions and radio observations of comet IRAS-Araki-Alcock 1983d, *Astron. Astrophys.*, **141**, 411-418, 1984.

Bockelee-Morvan, D., and J. Crovisier, Possible parents for the cometary CN radical : Photochemistry and excitation conditions. *Astron. Astrophys.*, **151**, 90-100, 1985.

Cosmovici, C. B., G. Schwarz, W.-H. Ip, and P. Mack, Gas and dust jets in the inner coma of comet Halley, *Nature*, **332**, 705-709, 1988.

Despois, D., J. Crovisier, D. Bockelee-Morvan, J. Schraml, T. Forveille, and E. Gerard, Observations of hydrogen cyanide in comet Halley, *Astron. Astrophys.*, **160**, L11-L12, 1986.

Eberhardt, P., D. Krankowsky, W. Schulte, U. Dolder, P. Lämmerzahl, J. J. Berthelier, J. Woweries, U. Stubbemann, R. R. Hodges, J. H. Hoffmann, and J. M. Illiano, The CO and N_2 abundance in comet P/Halley, *Astron. Astrophys.*, **187**, 481-484, 1987.

Ekelund, L., W. M. Irvine, C. Andersson, F. P. Schloerb, and S. E. Robinson, A search for millimeter-wave emission from HCN and other molecules in comet Bradfield (1979l), *Icarus*, **47**, 431-433, 1981.

Feldman, P. D., M. C. Festou, M. F. A'Hearn, C. Arpigny, P. S. Butterworth, C. B. Cosmovici, A. C. Danks, R. Gilmozzi, W. M. Jackson, L. A. McFadden, P. Patriarchi, D. G. Schleicher, G. P. Tozzi, M. K. Wallis, H. A. Weaver, and T. N. Woods, IUE observations of comet P/Halley : evolution of the ultraviolet spectrum between September 1985 and July 1986, *Astron. Astrophys.*, **187**, 325-328, 1987.

Huebner, W. F., and C. W. Carpenter, Solar photon rate coefficients, Los Alamos Scientific Laboratory, Informal Report, LA-8085-MS, 1979.

Huebner, W. F., L. E. Snyder, and D. Buhl, HCN radio emission from comet Kohoutek (1973f), *Icarus*, **23**, 580-585, 1974.

Ip, W.-H., An overview of gas phenomena in comet Halley, *Adv. Space Res.*, **5**, 233-245, 1986.

Kissel, J., R. Z. Sagdeev, J. L. Bertaux, V. N. Angarov, J. Audouze, J. E. Blamont, K. Büchler, E. N. Evlanov, H. Fechtig, M. N. Fomenkova, H. von Hoerner, N. A. Inogamov, V. N. Khromov, W. Knabe, F. R. Krueger, Y. Langevin, V. B. Leonas, A. C. Levasseur-Regourd, G. G. Managadze, S. N. Podkolzin, V. D. Shapiro, S. R. Tabaldyev, and B. V. Zubkov, Composition of comet Halley dust particles from Vega observations. *Nature*, **321**, 280-282, 1986.

Körösmezey, A., T. E. Cravens, T. I. Gombosi, A. F. Nagy, D. A. Mendis, K. Szegö, B. E. Gribov, R. Z. Sagdeev, V. D. Shapiro, and V. I. Shevchenko, A model of inner cometary ionospheres, in *Proc. 20th ESLAB Symp. on the Exploration of Halley's Comet*, ESA SP-250, **1**, 241-246, 1986.

Krankowsky, D., and P. Eberhardt, Evidence for the composition of ices in the nucleus of comet Halley, in *Comet Halley 1986. World Wide Investigations, Results and Interpretations*, Ellis Horwood Limited, Chichester, England, in press, 1989.

Krankowsky, D., P. Lämmerzahl, I. Herrwerth, J. Woweries, P. Eberhardt, U. Dolder, U. Herrmann, W. Schulte, J. J. Berthelier, J. M. Illiano, R. R. Hodges, and J. H. Hoffmann, *In situ* gas and ion measurements at comet Halley, *Nature*, **321**, 326-330, 1986.

Kroto, H. W., J. R. Heath, S. C. O'Brien, R. F. Curl, and R. E. Smalley, Long carbon chain molecules in circumstellar shells, *Astrophys. J.*, **314**, 352-355, 1987.

Larson, H. P., D. S. Davis, M. J. Mumma, and H. A. Weaver, Velocity-resolved observations of water in comet Halley, *Astrophys. J.*, **309**, L95-L99, 1986.

Marconi, M. L., and D. A. Mendis, On the ammonia abundance in the coma of Halley's comet, *Astrophys. J.*, **330**, 513-517, 1988.

Mendis, D. A., H. L. F. Houpis, and M. L. Marconi, The physics of comets, *Fund. Cosmic Phys.*, **10**, 1-380, 1985.

Mitchell, G. F., W. T. Huntress, Jr., and S. S. Prasad, Interstellar synthesis of the cyanopolyynes and related molecules. *Astrophys. J.*, **233**, 102-108, 1979.

Neubauer, F. M., K. H. Glassmeier, M. Pohl, J. Raeder, M. H. Acuna, L. F. Burlaga, N. F. Ness, G. Musmann, F. Mariani, M. K. Wallis, E. Ungstrup, and H. U. Schmidt, First results from the Giotto magnetometer experiment at comet Halley, *Nature*, **321**, 352-355, 1986.

Schloerb, F. P., W. M. Kinzel, D. A. Swade, and W. M. Irvine, HCN production from comet Halley, *Astrophys. J.*, **310**, L55-L60, 1986.

Schloerb, F. P., W. M. Irvine, and S. Robinson, A search for millimeter-wave emission from HCN, CO, and CH_3CN in comet Bradfield (1978c), *Icarus*, **38**, 392-397, 1979.

Schlosser, W., R. Schulz, and P. Koczet, The cyan shells of comet P/Halley, in *Proc. 20th ESLAB Symp. on Exploration of Halley's Comet*, ESA SP-250, **3**, 495-501, 1986.

Schmidt, H. U., R. Wegmann, W. F. Huebner, and D. C. Boice, Cometary gas and plasma flow with detailed chemistry, *Comp. Phys. Comm.*, **49**, 17-59, 1988.

Schwenn, R., W.-H. Ip, H. Rosenbauer, H. Balsiger, F. Bühler, R. Goldstein, A. Meier, and E. G. Shelley, Ion temperature and flow profiles in comet P/Halley's close environment, *Astron. Astrophys.*, **187**, 160-162, 1987.

Tegler, S., and S. Wyckoff, NH_2 fluorescence efficiencies and the NH_2 abundance in comet Halley, *Astrophys. J.*, **343**, 445-449, 1989.

Wyckoff, S., S. Tegler, P. A. Wehinger, H. Spinrad, and M. J. S. Belton, Abundances in comet Halley at the time of the spacecraft encounters, *Astrophys. J.*, **325**, 927-938, 1988.

DENSITIES AND ABUNDANCES OF HOT COMETARY IONS IN THE COMA OF P/HALLEY

M. NEUGEBAUER, R. GOLDSTEIN AND B. E. GOLDSTEIN

Jet Propulsion Laboratory, California Institute of Technology

S. A. FUSELIER

Lockheed Palo Alto Research Laboratory

H. BALSIGER

University of Bern

AND

W.-H. IP

Max-Planck-Institut für Aeronomie

Submitted to *The Astrophysical Journal*

Received: _____

Accepted: Dec. 1990

in press 1991

ABSTRACT

On its flight by P/Halley, the Giotto spacecraft carried a High Energy Range Spectrometer (HERS) for measuring the properties of cometary ions picked up by the solar wind in the nearly collisionless regions of the coma. Preliminary estimates of the ion densities observed by HERS have now been reevaluated and extended; density profiles along the Giotto trajectory are presented for 13 values of ion mass/charge. Comparison with the physical-chemical model of the interaction of sunlight and the solar wind with the comet by Schmidt et al. (1988) reveal that, with the exception of protons and H_2^+, all ion densities were at least an order of magnitude higher than predicted. The high ion densities cannot be explained on the basis of compression of the plasma, but require additional or stronger ionization mechanisms. Ratios of the densities of different ion species reveal an overabundance of carbonaceous material and an underabundance of H_2^+ compared to the predictions of the Schmidt et al. model. While the densities of solar wind ions (H^+ and He^{++}) changed sharply across a magnetic discontinuity located 1.35×10^5 km from the comet, this feature, which has been called both the "cometopause" and the "magnetic pileup boundary" was barely distinguishable in the density profiles of hot cometary ions. This result is consistent with the interpretation that the magnetic pileup boundary detected by Giotto was caused by a discontinuity in the solar wind rather and is not an intrinsic feature of the interaction of the solar wind with an active comet.

Subject headings: comets -- plasmas -- abundances

I. INTRODUCTION

Most cometary plasma falls into one of two categories: (1) Hot plasma consisting of material ionized in the upstream solar wind or in the slower, mass-loaded solar wind in the outer coma. These pickup ions spiral around the magnetic field carried by the solar wind and have a "thermal" speed nearly equal to the speed of the wind at their point of pickup. (2) Cold plasma in the inner coma in collisional equilibrium with the neutral gas flowing out from the nucleus with speed < ~1 km/s and a temperature of ~300 K (Lämmerzahl et al., 1987).

The ion mass spectrometer (IMS) flown through the coma of P/Halley by the Giotto spacecraft in March, 1986, used separate sensors to study hot and cold ions. Preliminary estimates of the densities of different ion species observed by the IMS along the spacecraft track were reported by Balsiger et al. (1986, 1987a), Schwenn et al. (1987), and Balsiger (1990). The significance of those ion measurements has been interpreted by Balsiger et al. (1986), Allen et al. (1987), Geiss (1987), and Ip (1989a), among others. The intervening four years have allowed detailed reexamination of the IMS data together with more realistic analysis and modeling of the instrument's performance. It is the purpose of this paper to present the results of the recomputation of the densities of the hot component of the ion population observed by the IMS. The recomputed densities are generally greater than those presented before. The analysis has also been extended to include more ion species and finer temporal or spatial resolution. Comparison of the hot ion densities and abundances with the predictions of a numerical physical-chemical model by Schmidt et al. (1988) allows some conclusions to be drawn about the dynamics and chemistry of the coma as well as the composition of the volatile material in the nucleus. The comparison shows that some modifications of the model are clearly required.

Revised analyses of the hot-ion dynamics (i.e., distribution functions, velocities, and temperatures) and of the cold-ion densities and abundances will be presented in future papers.

II. INSTRUMENT DESCRIPTION

The IMS had two sensors, named the high-intensity spectrometer (HIS) and the high-energy-range spectrometer (HERS). HIS was optimized for measuring the cold, slow ion flow in the inner coma, whereas HERS was optimized for measuring the hot plasma in the outer coma and in the solar wind. Details of these sensors have been described previously (Balsiger et al., 1987b); only those characteristics pertinent to the discussions of data which follow are repeated here. HIS and HERS both used combinations of electric and magnetic analyzers to map out the three-dimensional velocity distributions as a function of the mass/charge ratio of the ions. Functionally, they differed in that the HIS field of view pointed along the spacecraft spin axis, which was aligned with the velocity vector of the spacecraft relative to the comet, while the HERS field of view extended from ~15° to ~75° from the spin axis. Thus HIS analyzed the dense, slow-moving plasma scooped up by the spacecraft motion, while HERS was sensitive to the hot pickup ions gyrating around the magnetic field. The present paper concentrates on the hot ion data acquired by HERS.

HERS measured ion mass/charge and velocity distributions in a 3° x 60° fan-shaped field of view which swept out a 360° by 60° annulus as the spacecraft spun with a period of 4 seconds. The energy/charge range of the sensor extended from 10 eV/e to a mass-dependent upper limit of ~ 4 keV/e. The sensor mass/charge range changed once per spin period, cycling through four measurement modes: the light mode with m/q = 2 - 4 amu/e, the medium mode with m/q = 12 - 26 amu/e, the heavy mode with m/q = 15 - 35 amu/e, and the proton mode. The time to repeat observations in a given look direction for a

given mass/charge was thus 16 s, which corresponds to a spatial resolution along the spacecraft trajectory of 1100 km. In the inner coma, less than 62,000 km from the nucleus, priority was given to HIS measurements with the consequence that two spins of HERS data were summed for each mass/charge range, thereby changing the time resolution to 32 s (2200 km spatial resolution). Except for the proton mode, HERS registered ions on a microchannelplate (MCP) detector, measuring the energy/charge (64 quasilogarithmic bins), azimuth angle (64 bins denoting the phase of the spin motion), elevation angle relative to the spin axis (8 bins, each 7.5° wide), and mass/charge (denoted by which of 40 mass anodes of the MCP recorded the ion). The output data thus formed a time series of 4-dimensional arrays (counts versus energy/charge, azimuth, elevation, and mass/charge). Proton data were acquired slightly differently; their mass/charge was uniquely determined, there were only four elevation bins (each 15° wide), and they were detected by channel electron multipliers rather than the MCP.

III. METHOD OF CALCULATING DENSITIES

The orientation of the spacecraft spin axis and velocity vector allowed the HERS to observe the solar wind for several days before the encounter with the comet. Beginning ~12×10^6 km from the comet, HERS detected picked-up cometary protons; the cometary proton density upstream of the bow shock (1.14×10^6 km from the nucleus) has been reported by Neugebauer et al. (1989). Once inside the bow shock, the distributions of picked-up cometary protons and the heated solar wind ions overlapped in velocity space, so only the total (cometary plus solar) proton density could be calculated. The light-mode HERS data provided information on helium and other minor ion species in the solar wind, both upstream and downstream of the Halley bow shock.

The 4-kV upper limit of energy/charge and the background counting rates of its microchannelplate (MCP) sensor prevented HERS from detecting the pickup of heavier cometary ions until the spacecraft was ~250,000 km from the nucleus. A measurable flux of hot, cometary ions was then observed along the inbound Giotto trajectory until the spacecraft reached a distance of 40,000 km. The plasma seen in the ram direction by HIS started to increase slowly at 150,000 km; by 50,000 km most of the plasma flux was limited to the HIS field of view. Near closest approach to the nucleus, the HERS ceased operation following a severe electrical disturbance on-board the spacecraft, probably caused by a dust impact near closest approach to the nucleus; thus no HERS data were obtained on the outbound leg of the Giotto trajectory.

The calculation of cometary ion densities from the HERS data proceeded as follows:

1. The data were summed over a sufficient number of spacecraft spins to obtain ~1000 counts of water-group ions (m/q = 16 to 18 amu/e, using both medium- and heavy-mode data). The lengths of these summation intervals ranged from 128 to 512 seconds, which corresponds to summing over 8 to 32 consecutive spectra for each instrument mode.

2. The count-rate matrices were corrected for detector background counts. The background count-rate corrections, which depended on both elevation angle and mass anode, were determined by averaging several hours of data obtained earlier on the day of the comet encounter when the spacecraft was millions of km from the nucleus and HERS could detect only solar wind ions and picked-up cometary protons. Figure 1 shows the distribution of counts versus mass anode number summed over the two elevation-angle bins closest to the ram direction (i.e., elevation angles of 15 to 30°) for the entire interval 220,000 to 40,000 km. The spectra for the medium- and heavy-mode data are displayed

separately, in both linear and logarithmic formats to bring out different features of the data. For the elevation bin closest to the ram direction, the MCP had a "hot spot" at the position of anode 29, which resulted in a very high and very irregular background counting rate for that anode. Due to the time varying nature of the hot spot, the background rate for that anode was overestimated for the interval displayed in Figure 1. Data from anode 29 were not used in the analysis presented below. The numbers printed over the count-rate peaks in Figure 1 indicate the corresponding values of m/q. The count-rate versus mass anode spectra cannot be converted directly into density or flux without detailed modelling of the instrumental response; the most important factor is that the geometric factor of the instrument varied approximately as $(m/q)^{-4}$.

3. For each of the time intervals selected in Step 1, the vector velocity of the ions with m/q = 16-18 amu/e was obtained by finding the least-squares fit of the observed distribution to a spherically symmetric distribution in velocity space. This process corrected for those parts of the ion distributions outside the HERS field of view. For the part of the distribution that was within the HERS field of view, the data show that isotropy is indeed a good first approximation.

4. The distribution of counts versus mass anode was then modeled using generalized Gaussians to determine the position and width of each mass peak. Examination of the flight data showed that the locations of the mass peaks had shifted by a fraction of a mass anode in the year between laboratory calibration of the instrument and the comet encounter. The cause of this shift is not understood. Thus the calibration data were used as a guide to the approximate locations and widths of the mass peaks and least-squares fits of the flight data were performed to determine the best values to use for the data analysis. It was assumed that neither the locations nor the widths of the mass peaks changed during the hour before closest approach to the comet. The positions and shapes of each of the mass

peaks were determined for the data set as a whole, while the contributions of different ion species to the counts measured by each anode were separately determined for each time interval by performing a least-squares analysis to determine the height of each peak. Although it was originally intended to use both the medium- and heavy-mode data for calculating the densities of water-group ions, the least-squares fits to the medium-mode data were significantly superior to the heavy-mode data fits (the variances between the data and the fits were smaller and the peak widths determined by the fits were closer to the pre-launch calibration values), so only the medium-mode data were used to calculate the densities for m/q = 16 - 18 amu/e. Figure 2 illustrates the type of fit that could be obtained; it shows the measured water-group counts in anodes 18-27 for medium-mode measurements. In this example, the measured counts are indicated by circles with error bars representing the uncertainty arising from counting statistics; the upper curve shows the least-squares fit; while the dotted curves show the individual contributions of ions with m/q = 16, 17, and 18 amu/e.

5. For each interval, it was then assumed that each ion species had an isotropic distribution and the same bulk velocity vector $\mathbf{v_0}$ as the water-group ions (as determined in Step 3). Then, for each value of m/q, the 3-D distribution in elevation-azimuth-energy/charge was transformed into a one-dimensional distribution of phase space density versus $|\Delta v|$, where $\Delta \mathbf{v} = \mathbf{v} - \mathbf{v_0}$. Integration over this 1-D distribution then gave the ion density.

The method used for computing proton densities was similar except that:

1. The proton counting rate was high enough that the proton density could be calculated on a spin by spin basis to yield 1100 km resolution. The computed proton densities have been averaged over 6 minutes (25,000 km) for the purposes of this paper, but the full

resolution data have been submitted to the International Halley Watch (IHW) and the US National Space Science Data Center (NSSDC) archives.

2. A moments technique, rather than a least-squares fit was used to calculate the proton bulk velocity independent of the heavy-ion velocity calculated in Step 2 above.

3. The HERS instrument was able to identify protons unambiguously, with no mass overlap, so Step 4 above was not necessary.

The fluxes of ions with m/q = 2 amu/e were great enough to allow 64 sec (4400 km) resolution. As for the protons, 6-minute (25,000 km) averages are presented in this paper, with the full resolution data available from the authors or through the IHW or NSSDC.

IV. RESULTS

The density values computed as described above are listed in Tables 1-13 -- one table for each value of mass/charge. Each table includes a quality index, which ranges from 1 to 5. These indices should be interpreted as follows:

Quality = 1: high count rate and negligible statistical uncertainty. Also no significant overlap with any other mass peak. The only important uncertainty in the density is the absolute calibration of the instrument, which is estimated to be ~ ±30%. Only protons and ions with m/q = 2 and 12 amu/e were assigned Quality = 1.

Quality = 2: high count rate and negligible statistical uncertainty, but ~10% additional uncertainty due to overlapping mass peaks, leading to a total uncertainty of $(.30^2 + .10^2)^{1/2}$ = 32%. Water-group ions (m/q = 16 - 18 amu/e) fall in this category.

Quality = 3: low count rate with an additional uncertainty of ~10% due to counting statistics (32% total uncertainty), but no significant problem due to mass-peak overlaps. Ions with mass/charge 14 and 32 fall in this category despite the use of longer averaging intervals for those ion species.

Quality = 4: moderate count rates and severe problems of overlap with a neighboring mass peak. The additional uncertainty is ~25% (39% total uncertainty). Ions with mass/charge = 28 amu/e have Quality = 4.

Quality = 5: severe problems with low count rates and/or a large neighboring mass peak. The additional uncertainty may be 35%, to yield a total uncertainty of 46%. Ions with Quality = 5 are at 4, 13, 15, and 29 amu/e.

The count-rate spectra in Figure 1 show some evidence for minor ion species for which we have not presented densities. There was clearly some small number of ions with m/q = 19 amu/e present. For the more reliable medium-mode data, the mass/charge peak for m/q = 19 amu/e straddled the hot spot on anode 29, and it showed up as only a small shoulder on the heavy-mode m/q = 18 amu/e peak. The HIS data showed that although ions with m/q = 19 amu/e (presumably mostly H_3O^+) were the dominant species at cometocentric distances <2000 km, they provided less than 10% of the cold ion density outside 35,000 km and less than 1% outside 80,000 km. We conclude that H_3O^+ is an important species only in the collision dominated inner coma.

Figure 1 also shows several small peaks between m/q = 19 and 28 amu/e. None of these peaks was more than 2 standard deviations above background. Further work on limiting the region of phase space examined may allow calculation of a density for the m/q

= 24 amu/e peak which had counts in two adjacent anodes in both the medium and heavy modes.

It must be emphasized that inside 80,000 km the densities given in Tables 1-13 are lower limits to the total ion densities in that they refer only to the hot ions whose velocity distributions overlapped the field of view of the HERS sensor. They are the ions picked up by the mass-loaded solar wind which, at cometocentric distances >40,000 km, still had a flow speed exceeding 10 km/s relative to the comet nucleus. As the spacecraft approached the comet, the density of the hot ions reached a maximum of ~150 cm^{-3} near 75,000 km, and then declined as the hot ions were replaced by cold ions due to collisions with the cometary neutral gas. The hot-ion population was too small to be detected by the IMS by the time the spacecraft reached 40,000 km. This is consistent with the findings of other instruments on Giotto; Krankowsky et al. (1986), for example, reported that evidence for energetic ions persisted in to ~40,000 km from the nucleus, and Korth et al. (1987) reported high temperatures and broad ion distributions outside 43,000 km. Density or flux profiles of the cold ions in the inner coma have been published by Balsiger et al. (1986, 1987a), Balsiger (1990), Schwenn et al. (1987), Kettmann et al. (1990), Korth et al. (1987), and Krankowsky et al. (1986).

The circles and diamonds in Figure 3 show the 6-minute average densities of protons and ions with m/q = 2 amu/e, respectively, from Tables 1 and 2 plotted versus distance from the comet. Although inside 200,000 km H_2^+ contributed to the density of ions with m/q ~ 2 amu/e (Fuselier et al., 1988), at greater distances the m/q = 2 amu/e population consisted almost entirely of He^{++} ions from the solar wind. The measured number-density ratio n_2/n_1 ranged from 0.02 to 0.04, which is quite typical for the low-speed solar wind near interplanetary sector boundaries, such as that observed at the Giotto encounter with P/Halley. Fuselier et al. (1990) consider the ion abundances in the solar

wind and the charge-exchange reactions of solar wind ions with the coma gas in much greater detail. The continuous curve shown in this figure is disussed in the following section. The jump in proton and He^{++} densities at the Halley bow shock is indicated by the vertical line at $1.14x10^6$ km.

The dashed vertical line in Figure 3 at $1.35x10^5$ km marks the crossing of a discontinuity that has been called both the "cometopause" and the "magnetic pileup boundary". Whatever its proper name, its most striking feature was a sudden jump in the strength of the magnetic field from ~10 to ~30 nT (Neubauer et al., 1986). It is clear that on the scale of Figure 3 (one point per 25,000 km), the magnetic pileup boundary marked a sharp decrease in the density of solar-wind ions.

In Figure 4, the circular symbols repeat portions of the proton and m/q = 2 amu/e data from Figure 3 and also show the densities of the other ion species listed in Tables 4-13. The principal difference between the formats of Figures 3 and 4 is that in Figure 4 the distance scale is logarithmic and corresponds to a smaller range -- from 25,000 to 250,000 km (log distances = 4.4 - 5.4, respectively). The dashed vertical line again locates the magnetic pileup boundary; the bow-shock would be located off-scale to the right. Again, discussion of the continuous curves is postponed to the following section.

The distance profiles of the cometary ions (m/q = 12 - 32 amu/e) were markedly different from those of the solar wind ions. The density of each species of hot cometary ion reached a maximum between 60,000 and 100,000 km (log distance = 4.8 - 5.0), and each of their distance profiles had roughly the same shape. Inside the maxima, the hot ions were removed by collisions. Outside the maxima, the densities of the hot cometary ions continued to decrease with increasing distance, barely reacting to the magnetic pileup boundary at all.

Figure 5 displays several ratios of ion densities as a function of distance from the comet in the same format as Figure 4. Again, please ignore the continuous curves until the next section. The increases in the ratios n_{16}/n_{18}, n_{17}/n_{18}, and $n_{12}/(n_{28} + n_{29})$ with distance and the decrease in n_{13}/n_{12} are consistent with expectations of the breakup of molecules into smaller molecules and atoms. The principal reason for the steep rise in n_2/n_{18} with distance is the increasing amount of solar wind He^{++}.

The horizontal line in the panel displaying the ratio n_{13}/n_{12} indicates the value of the ratio that would be observed if all the m/q = 13 amu/e ions were $^{13}C^+$ and if the ratio of $^{12}C/^{13}C = 63$, as reported by Wyckoff and Lindholm (1989) from ground-based observations of $^{13}C^{14}N$ in comet Halley. The observed ratio is above that line, which indicates the presence of CH^+ ions.

V. COMPARISON TO THE THEORETICAL MODEL OF SCHMIDT ET AL.

The most ambitious model of the physics and chemistry of cometary ions is that of Schmidt et al. (1988); we shall hereafter use the acronym SWHB to refer to that paper and model. SWHB produced hydrodynamic and magnetohydrodynamic simulations of the gas and plasma flow around Halley's comet with a detailed photo and chemical reaction network (19 different processes) of 59 neutral and 76 ionized chemical species. Their model assumed that all cometary gas was released directly from the nucleus and did not include dust which is known to be a distributed source of gas (e.g., Eberhardt et al., 1987). The model assumes a composition of 80.0% H_2O, 8.0% CO, 3.0% CO_2, 2.0% CH_4, 2.0% NH_3, 2.0% H_2CO, 1.0% CS_2, 0.68% N_2, 0.67% C_2H_2, 0.05% $H_2C_3H_2$, 0.30% H_2CO_2, 0.16% CH_3CN, 0.08% NH_2CH_3, and 0.06% HCN. SWHB calculated the densities of different ion species expected along the Giotto trajectory, using gas

production rates and solar wind parameters appropriate to the time of the Giotto encounter with P/Halley. Their densities and density ratios are indicated by the continuous curves in Figures 3 through 5.

From Figure 3, it can be seen that outside the magnetic pileup boundary the observed proton density profile is in fairly good agreement with the SWHB model. The disagreement inside the magnetic pileup boundary can be qualitatively accounted for by the fact that the SWHB curve represents the total (both hot and cold) proton density. Although the SWHB model shows substantial cooling of the ions inside 10^5 km, it has no discontinuous jump in temperature anywhere between the contact surface (also called the ionopause or the diamagnetic cavity boundary) observed at 4700 km (Neubauer et al., 1986) and the bow shock. The calculated position of the bow shock (slightly beyond the end of the curve plotted in Figure 3) is slightly farther from the comet than was the observed shock.

The center panel in the top row of Figure 4 compares the model to the observed densities of ions with m/q = 2 amu/e. SWHB did not include solar-wind helium ions in their model; this explains why the model profile drops while the observed density rises with increasing distance. In SWHB, ions with m/q = 2 amu/e are entirely H_2^+, while the observations show a mixture of H_2^+ and He^{++} with an increasing proportion of H_2^+ closer to the comet (Fuselier et al., 1988). What is interesting is that inside the magnetic pileup boundary, the sum of the observed H_2^+ and He^{++} is less than the SWHB density for H_2^+ alone.

The remaining panels in Figure 4 show that all other ion species had significantly higher densities than predicted by the simulation, The differences often exceed an order of magnitude. The observational profiles are generally much more concave downward than

are the SWHB profiles. At small distances, the difference is caused by collisional cooling of the hot ions which removes them from the HERS field of view. For many species (i.e., m/q = 16, 17, 18, 28, and 29 amu/e) the observed slope at large distance is steeper than the slope predicted by SWHB; no simple reason for this discrepancy is apparent. Outside the magnetic pileup boundary, each of these species dropped off more rapidly than r^{-2}.

Figure 5 shows excellent agreement between the data and the SWHB model for the ratios n_{16}/n_{18} and n_{17}/n_{18}, indicating that the simulation does a good job of modeling the dissociation and ionization of water molecules and their products. The ratio of n_{12}/n_{16} indicates that the model underestimates the relative amount of carbonaceous material. The fact that the observed value of the ratio $n_{12}/(n_{28} + n_{29})$ is greater than the model value of this ratio probably indicates that the missing carbonaceous material is not entirely additional CO. The SWHB model does not include any ^{13}C, which can account for some of, but not all the mismatch between the observed and calculated values of n_{13}/n_{12}. Because the photodissociation lifetime of CH molecules is only 100 s, the source of the CH^+ is not obvious.

The ratio n_{14}/n_{16} is also higher than that given by SWHB, by about the same factor as the n_{12}/n_{16} ratio. The ion peak at m/q = 14 amu/e, however, has contributions from both N^+ and CH_2^+, so it is not safe to conclude that the comet must have more nitrogen-bearing material than was included in the SWHB model.

VI. DISCUSSION

HERS did detect most of the ions expected to be found in the coma of comet Halley. The HERS mass/charge spectra had peaks corresponding to each of the ions detected spectroscopically from Earth (C^+, CH^+, NH^+, OH^+, H_2O^+, CN^+, CO^+, N_2^+,

Ca^+, and CO_2^+) except for those heavier than the 35 amu/e range of the instrument. It was no surprize that water-group ions were found to be the most abundant. It is, perhaps, surprizing that the densities of both Na^+ and C_2^+ were below the detection threshold, especially in light of the observation of a major peak at m/q = 23-24 amu/e in the ion spectra obtained by the ICE spacecraft at P/Giacobini-Zinner (Ogilvie et al., 1986). Ip (1989b) has argued that the expected density of Na^+ (m/q = 23 amu/e) is > 10^{-3} times the density of water-group ions, which is close to the detection limit of HERS. Detection of ions with m/q = 23 and 24 amu/e in the inner coma (i.e., in the cold-ion region) of P/Halley has been reported by Krankowsky et al. (1986) and Eviatar et al. (1989).

One of the principal conclusions of the present study is that the density of cometary ions in the distance range 40,000 to 250,000 km is at least an order of magnitude higher than the predicted density. This discrepancy had previously been noted by Ip (1989a) on the basis of preliminary values of ion density. Furthermore, the problem is not unique to the SWHB model. For example, the calculation by Ip (1989b) shows a similar disparity The density of protons is, however, in good agreement with the models. Thus, we can rule out compression of the plasma as the cause of the high density of cometary ions, because the solar-wind protons would have been compressed too. Another argument against significant compression is that the strength of the magnetic field was significantly less than predicted by the model outside the magnetic pileup boundary and roughly the same as the model field inside it (Huebner et al., 1989).

Ip (1989b) and Marconi and Mendis (1988) have suggested that the solar EUV flux at the time of the Giotto encounter may have been significantly greater than the typical solar-minimum values assumed in the models. But Ip (1989b) has argued that even an order-of-magnitude increase in solar EUV would not lead to an order-of-magnitude increase in the ionization rate because of the importance of other mechanisms for creating

cometary ions, such as charge exchange with the solar wind. Furthermore, there is not necessarily a direct relation between ion density and ionization rate.

Perhaps the models underestimate the rate of ionization associated with charge-exchange reactions. The results of the study by Shelley et al. (1987) were consistent with an anomalously high charge-exchange rate of He^{++}. There are several effects associated with charge exchange that have not been included in the models. (1) The velocity dependence of the charge-exchange cross sections was neglected, but it is known that the cross sections increase with decreasing velocity. (2) The SWHB model does not include ionization by or other effects of the fast neutral products of charge-exchange interactions. Ip (1990) has shown, however, that energetic neutral atoms can play an important role in the physics of the coma. (3) In the models, the term accounting for the source of cometary ions due to charge exchange is appropriate for an unmagnetized plasma. It does not include the greater path length traversed by a hot ion which gyrates around the magnetic field. (4) The flow field and the relative velocity between the solar wind and cometery neutrals may differ from that in the models. A comparision of the observed velocities with those predicted by various models is the topic of a future study.

There may have been other sources of "anomalous ionization", which was a topic of great interest many years ago. For example, tail currents closing through the inner coma could be an important source of ionization; Ip (1979) has drawn an analogy with energy deposition during terrestrial substorms. Along this line, Neubauer (1988) suggested that a possible cause of a weak shock observed by the Giotto magnetometer to be propagating radially outward at a distance of ~5000 km might have been caused by a transient injection of hot ions and electrons following magnetic merging in the tail. There are also other spacecraft observations that have been interpreted as evidence for field-line reconnection on the dayside of Halley's coma (Verigin et al., 1987; Kirsch et al., 1989). It is questionable

whether such processes could contribute to the level of ionization on the large scale observed.

Another type of anomalous ionization that has been suggested in connection with comets is the critical ionization velocity (CIV) effect (Formisano et al., 1982; Galeev et al., 1986). In this effect, first postulated by Alfvén (1954), the kinetic energy of the relative flow of a neutral gas across magnetic field lines is collisionlessly transferred to the plasma electrons which then collide with and ionize the gas. The difficulty with invoking CIV to explain the anomalous ionization observed by HERS is the absence of a simultaneous large flux of energetic electrons. The RPA instrument on Giotto had a 10-eV threshold for detecting electrons; it did detect anomalously high fluxes of keV electrons in the so-called "mystery region" at distances from the nucleus between 550,000 and 850,000 km (Reme et al., 1987), but the HERS energy range and sensitivity threshold prevented observations of cometary ions at those distances. The RPA investigators have estimated that even in the sharpest spikes of energetic electron fluxes observed in the mystery region, the rate of ionization due to electron impact was less than twice the photoionization rate (R. P. Lin, personal communication). Such relatively weak and localized sources of ionization probably cannot account for the higher than expected ion densities.

It also cannot be ruled out that temporal variation or anisotropic emission of gas from the comet might have contributed to the excess ionization. Approximately 1 day is required for the neutral gas to travel each 10^5 km from the nucleus. Thus the gas and ions observed at 2×10^5 km left the nucleus approximately a day earlier than the gas and ions detected at 1×10^5 km. IUE observations by Feldman et al. (1987) showed a 25% decrease in brightness during the day prior to the Giotto closest approach to P/Halley. The ground-based observations by Millis and Schleicher (1986), on the other hand, showed very little change in the comet's gas production rate over this same interval.

The ratios of the densities of different ion species put important constraints on cometary chemistry. Comparison of the density ratios n_{16}/n_{18} and n_{17}/n_{18} to ratios computed from the SWHB model might suggest that the major chain of dissociation and ionization of water is well understood. One major discrepancy between observations and the model is the overabundance of C^+ and the higher than predicted ratios of n_{13}/n_{12}, n_{14}/n_{16}, and $n_{12}/(n_{28} + n_{29})$. One suspects that the extra carbonaceous material probably originated in the CHON grains (Kissel et al., 1986) which were a distributed source of gas in the coma (Eberhardt et al., 1987), whereas SWHB did not include any source other than the comet's surface. The underabundance of H_2^+ compared to the model is a much more difficult problem which requires detailed chemical modeling to understand.

Comparison of the SWHB model and the HERS data shows that the model requires iteration before the molecular composition of the volatiles in the nucleus can be deduced. The discrepancy seems to be both of a physical and chemical nature because neither the total nor the relative ion abundances predicted by the model fit the data.

Finally, we wish to comment on the implications of the HERS density data for the nature of the magnetic pileup boundary. That feature was marked by sudden changes in the density of solar wind protons and alphas, in the strength of the magnetic field, and in the density of electrons with energy >10 eV (Reme et al., 1987). Its magnetic structure was consistent with that of a tangential discontinuity (Neubauer, 1987). As pointed out previously (Balsiger et al., 1987a; Balsiger, 1990; d'Uston et al., 1987), it was not accompanied by a discontinuous change in either the density or the chemical composition of hot cometary ions. Thus it was not a "chemical boundary" as proposed by Gringauz et al. (1986) on the basis of observations of a discontinuity in a similar region of the coma by the Vega spacecraft. The HERS data support the conclusion of Raeder et al. (1989) that the

magnetic pileup boundary observed by Giotto was not an intrisic feature of the interaction of an active comet with the solar wind, but rather a response to the passage of an interplanetary discontinuity of a type commonly observed near magnetic sector boundaries in the solar wind.

Acknowledgements. We thank R. Wegmann for providing tables of the model ion densities along the Giotto trajectory in computer readable format. We also thank all members of the IMS team at Lockheed Palo Alto Research Laboratory, the University of Bern, and the Max-Planck-Institut für Aeronomie who made this investigation possible. The work at the Jet Propulsion Laboratory was done under a contract between the California Institute of Technology and the National Aeronautics and Space Administration under the sponsorship of the Planetary Atmospheres program. Research at Lockheed was supported by NASA through contract NASW-4336. This work was also supported by the Swiss National Science Foundation and by the German Bundesministerium für Forschung und Technologie..

TABLE 1. m/q = 1. (Quality = 1)

Decimal Hrs	Distance (km)	Density (cm^{-3})
18.550	0.135E+07	6.90
18.650	0.133E+07	7.14
18.750	0.130E+07	7.75
18.900	0.127E+07	7.83
19.050	0.123E+07	8.13
19.150	0.121E+07	8.30
19.250	0.118E+07	7.20
19.350	0.116E+07	6.59
19.450	0.113E+07	9.18
19.550	0.111E+07	10.07
19.650	0.108E+07	10.36
19.750	0.106E+07	12.09
19.850	0.103E+07	11.48
19.950	0.101E+07	11.80
20.050	0.985E+06	12.43
20.150	0.960E+06	10.64
20.250	0.935E+06	10.08
20.350	0.911E+06	9.64
20.450	0.886E+06	13.34
20.550	0.861E+06	16.21
20.650	0.837E+06	15.94
20.750	0.812E+06	19.27
20.850	0.788E+06	16.73
20.950	0.763E+06	16.93
21.050	0.738E+06	16.44
21.150	0.714E+06	17.52
21.250	0.689E+06	18.15
21.350	0.665E+06	16.43
21.450	0.640E+06	13.59
21.550	0.615E+06	14.42
21.650	0.591E+06	14.47
21.750	0.566E+06	13.52
21.850	0.542E+06	13.04
21.950	0.517E+06	12.67
22.050	0.492E+06	13.02
22.150	0.468E+06	13.75
22.250	0.443E+06	13.63
22.350	0.418E+06	13.45
22.450	0.394E+06	13.07
22.550	0.369E+06	11.99
22.650	0.345E+06	11.14
22.750	0.320E+06	9.23
22.850	0.295E+06	9.32
22.950	0.271E+06	10.12
23.050	0.246E+06	10.63
23.150	0.222E+06	9.93
23.250	0.197E+06	8.85
23.350	0.172E+06	7.94
23.450	0.148E+06	6.57
23.550	0.123E+06	2.84
23.650	0.985E+05	3.52
23.750	0.738E+05	2.62
23.850	0.492E+05	0.86
23.950	0.246E+05	0.40
24.000	0.123E+05	0.20

TABLE 2. m/q = 2. (Quality = 1)

Decimal Hrs	Distance (km)	Density (cm^{-3})
18.550	0.135E+07	0.18
18.650	0.133E+07	0.20
18.750	0.130E+07	0.19
18.900	0.127E+07	0.20
19.050	0.123E+07	0.20
19.150	0.121E+07	0.18
19.250	0.118E+07	0.15
19.350	0.116E+07	0.14
19.450	0.113E+07	0.29
19.550	0.111E+07	0.29
19.650	0.108E+07	0.30
19.750	0.106E+07	0.26
19.850	0.103E+07	0.36
19.950	0.101E+07	0.37
20.050	0.985E+06	0.35
20.150	0.960E+06	0.30
20.250	0.935E+06	0.32
20.350	0.911E+06	0.28
20.450	0.886E+06	0.41
20.550	0.861E+06	0.46
20.650	0.837E+06	0.61
20.750	0.812E+06	0.76
20.850	0.788E+06	0.62
20.950	0.763E+06	0.58
21.050	0.738E+06	0.56
21.150	0.714E+06	0.57
21.250	0.689E+06	0.60
21.350	0.665E+06	0.69
21.450	0.640E+06	0.60
21.550	0.615E+06	0.60
21.650	0.591E+06	0.63
21.750	0.566E+06	0.58
21.850	0.542E+06	0.45
21.950	0.517E+06	0.37
22.050	0.492E+06	0.35
22.150	0.468E+06	0.40
22.250	0.443E+06	0.45
22.350	0.418E+06	0.41
22.450	0.394E+06	0.41
22.550	0.369E+06	0.38
22.650	0.345E+06	0.37
22.750	0.320E+06	0.32
22.850	0.295E+06	0.35
22.950	0.271E+06	0.35
23.050	0.246E+06	0.41
23.150	0.222E+06	0.39
23.250	0.197E+06	0.37
23.350	0.172E+06	0.28
23.450	0.148E+06	0.25
23.550	0.123E+06	0.12
23.650	0.985E+05	0.12
23.750	0.738E+05	0.07
23.850	0.492E+05	0.04
23.900	0.369E+05	0.05

TABLE 3. m/q = 4 (Quality = 5)

Decimal Hrs	Distance (km)	Total Time (s)	Density (cm^{-3})
22.116	0.476E+06	3150	0.014
22.616	0.353E+06	1800	0.016
22.949	0.271E+06	1200	0.015
23.116	0.230E+06	600	0.020
23.283	0.189E+06	600	0.015
23.449	0.148E+06	600	0.014
23.616	0.107E+06	600	0.024
23.783	0.657E+05	600	0.016

TABLE 4. m/q = 12 (Quality = 1)

Decimal Hrs	Distance (km)	Total Time (s)	Density (cm^{-3})
23.087	0.237E+06	496	1.0
23.227	0.203E+06	512	1.1
23.372	0.167E+06	512	2.4
23.463	0.144E+06	128	3.6
23.498	0.136E+06	128	4.4
23.534	0.127E+06	128	5.0
23.569	0.118E+06	128	5.4
23.605	0.110E+06	128	5.1
23.640	0.101E+06	128	8.3
23.676	0.921E+05	128	9.3
23.711	0.834E+05	128	11.0
23.747	0.746E+05	128	10.4
23.782	0.660E+05	128	11.3
23.823	0.559E+05	160	6.6
23.867	0.450E+05	160	11.8

TABLE 5. m/q = 13 (Quality = 5)

Decimal Hrs	Distance (km)	Total Time (s)	Density (cm^{-3})
23.534	0.127E+06	640	0.1
23.710	0.837E+05	640	0.4
23.867	0.450E+05	480	0.2

TABLE 6. m/q = 14 (Quality = 3)

Decimal Hrs	Distance (km)	Total Time (s)	Density (cm^{-3})
23.300	0.185E+06	1056	0.3
23.534	0.127E+06	640	0.4
23.710	0.837E+05	640	0.7
23.867	0.450E+05	480	0.2

TABLE 7 m/q = 15 (Quality = 5)

Decimal Hrs	Distance (km)	Total Time (s)	Density (cm^{-3})
23.534	0.127E+06	640	0.4
23.710	0.837E+05	640	1.1
23.867	0.450E+05	480	0.8

TABLE 8. m/q = 16 (Quality = 2)

Decimal Hrs	Distance (km)	Total Time (s)	Density (cm^{-3})
23.087	0.237E+06	512	3.8
23.227	0.203E+06	512	6.3
23.372	0.167E+06	512	13.0
23.463	0.144E+06	128	16.7
23.499	0.136E+06	128	20.4
23.534	0.127E+06	128	21.2
23.570	0.118E+06	128	17.7
23.605	0.110E+06	128	17.4
23.641	0.101E+06	128	23.5
23.676	0.921E+05	128	31.8
23.712	0.832E+05	128	28.4
23.747	0.746E+05	128	29.8
23.782	0.660E+05	128	23.8
23.824	0.556E+05	160	8.7
23.868	0.448E+05	160	9.5

TABLE 9 m/q = 17 (Quality = 2)

Decimal Hrs	Distance (km)	Total Time (s)	Density (cm^{-3})
23.087	0.237E+06	512	2.2
23.227	0.203E+06	512	3.9
23.372	0.167E+06	512	8.7
23.463	0.144E+06	128	15.2
23.499	0.136E+06	128	14.0
23.534	0.127E+06	128	17.4
23.570	0.118E+06	128	21.2
23.605	0.110E+06	128	18.7
23.641	0.101E+06	128	27.6
23.676	0.921E+05	128	27.5
23.712	0.832E+05	128	31.8
23.747	0.746E+05	128	29.9
23.782	0.660E+05	128	26.8
23.824	0.556E+05	160	12.6
23.868	0.448E+05	160	13.7

TABLE 10. m/q = 18 (Quality = 2)

Decimal Hrs	Distance (km)	Total Time (s)	Density (cm^{-3})
23.087	0.237E+06	512	0.6
23.227	0.203E+06	512	1.6
23.372	0.167E+06	512	5.7
23.463	0.144E+06	128	12.7
23.499	0.136E+06	128	11.8
23.534	0.127E+06	128	13.8
23.570	0.118E+06	128	15.1
23.605	0.110E+06	128	20.2
23.641	0.101E+06	128	28.6
23.676	0.921E+05	128	27.6
23.712	0.832E+05	128	33.9
23.747	0.746E+05	128	38.3
23.782	0.660E+05	128	43.9
23.824	0.556E+05	160	17.2
23.868	0.448E+05	160	32.1

TABLE 11. m/q = 28 (Quality = 4)

Decimal Hrs	Distance (km)	Total Time (s)	Density (cm^{-3})
23.302	0.184E+06	1016	2.6
23.499	0.136E+06	380	7.4
23.677	0.918E+05	380	20.5
23.810	0.591E+05	396	12.1

TABLE 12. m/q = 29 (Quality = 5)

Decimal Hrs	Distance (km)	Total Time (s)	Density (cm^{-3})
23.302	0.184E+06	1016	0.8
23.499	0.136E+06	380	3.7
23.677	0.918E+05	380	5.9
23.810	0.591E+05	396	2.7

TABLE 13. m/q = 32 (Quality = 3)

Decimal Hrs	Distance (km)	Total Time (s)	Density (cm^{-3})
23.302	0.184E+06	1016	2.0
23.499	0.136E+06	380	4.7
23.677	0.918E+05	380	8.8
23.810	0.591E+05	396	6.7

REFERENCES

Alfvén, H. 1954, *On the Origin of the Solar System*, Oxford Univ. Press.

Allen, M., et al. 1987, *Astr. Ap.*, **187**, 502.

Balsiger, H. 1990, in *Comet Halley 1986, World-Wide Investigation, Results, and Interpretations* (Chichester, UK: Ellis Horwood Limited), in press

Balsiger, H., et al. 1986, *Nature*, **321**, 330.

Balsiger, H., et al. 1987a, *Astr. Ap.*, **187**, 163.

Balsiger, H., et al. 1987b, *J. Phys. E*, **20**, 759.

d'Uston, C., et al. 1987, *Astr. Ap.*, **187**, 137.

Eberhardt, P., et al. 1987, *Astr. Ap.*, **187**, 435.

Eviatar, A., et al. 1989, *Ap. J.*, **339**, 545.

Feldman, P. D., et al. 1987, *Astr. Ap.*, **187**, 325.

Formisano, V., Galeev, A. A., and Sagdeev, R. Z. 1982, *Planet. Space Sci.*, **30**, 491.

Fuselier, S. A., et al. 1988, *Geophys. Res. Lett.*, **15**, 549.

Fuselier, S. A., et al. 1990, in preparation.

Geiss, J. 1987, *Astr. Ap.*, **187**, 859.

Galeev, A. A., et al. 1986, *Geophys. Res. Lett.*, **13**, 845.

Gringauz, K. I., et al. 1986, *Geophys. Res. Lett.*, **13**, 613.

Huebner, W. F., et al. 1989, *Adv. Space Res.*, **9**, (3)385.

Ip, W.-H. 1979, *Planet. Space Sci.*, **27**, 121.

Ip, W.-H. 1989a, *Adv. Space Res.*, **9**, (3)141.

Ip, W.-H. 1989b, *Ap. J.*, **343**, 946.

Ip, W.-H. 1990, *Ap. J.*, **353**, 290.

Kettmann, G., et al. 1990, *Ann. Geophys*, **8**, 229.

Kirsch, E., et al. 1989, *Ann. Geophys.*, **7**, 107.

Kissel, J., et al. 1986, *Nature*, **321**, 280.

Korth, A., et al. 1987, *Astr. Ap.*, **187**, 149.

Krankowsky, D., et al. 1986, *Nature*, **321**, 326.

Lämmerzahl, P., et al. 1987, *Astr. Ap.*, **187**, 169.

Marconi, M. L., and Mendis, D. A. 1988, *Ap. J.*, **330**, 513.

Millis, R. L., and Schleicher, D. G. 1986, *Nature*, **324**, 646.

Neubauer, F. M., et al. 1986, *Nature*, **321**, 352.

Neubauer, F. M. 1987, *Astr. Ap.*, **187**, 73.

Neubauer, F. M. 1988, *J. Geophys. Res.*, **93**, 7272.

Neugebauer, M., et al. 1989, *J. Geophys. Res.*, **94**, 1261.

Ogilvie, K. W., Coplan, M. A., Bochsler, P., and Geiss, J. 1986, *Science*, **232**, 374.

Raeder, J., et al. 1989, *Chapman Conf. Cometary Plasma Processes*, in press.

Reme, H., et al. 1987, *Astr. Ap.*, **187**, 33.

Schmidt, H. U., Wegmann, R., Huebner, W. F., and Boice, D. C. 1988, *Computer Phys. Comm.*, **49**, 17.

Schwenn, R., et al. 1987, *Astr. Ap*, **187**, 160.

Shelley, E. G., et al. 1987, *Astr. Ap.*, **187**, 304

Verigin, M. I., Axford, W. I., Gringauz, K. I., and Richter, A. K. 1987, *Geophys. Res. Lett.*, **14**, 987.

Wyckoff, S., and Lindholm, E. 1989, *Adv. Space Res.*, **9**, (3)151.

FIGURE CAPTIONS

Fig. 1. Total counts, after correction for background, versus mass-anode number for the time (distance) interval 2301 - 2353 UT (254,000 - 39,600 km). Only those counts in the two elevation-angle bins closest to the spacecraft ram direction are included. The heavy and medium mode data are plotted separately. The numbers over the count-rate spectra indicate the mass/charge values of each of the peaks. The background correction averaged about 30 counts/anode.

Fig. 2. Illustration of a least-squares fit of the countrate vs mass-anode spectrum for m/q = 16, 17, and 18 amu/e. The observed counts are indicated by circles; the solid curve is the least-squares fit; and the dotted curves indicate the contributions of the individual m/q peaks to the fit. The fitting procedure solved for 3 parameters (the heights of the peaks with m/q = 16, 17, and 18 amu/e, respectively) which gave the best fit to the 10 measured points. The time (distance) interval for the data displayed here was 23.372 UT (167,000 km).

Fig 3. Observed densities of protons (circles) and ions with mass/charge = 2 amu/e (triangles) versus distance. The continuous curve indicates the proton density from the model of Schmidt et al. (1988). The vertical dashed line marks the location of the magnetic pileup boundary.

Fig. 4. Density versus log distance profiles for ions with 12 different values of mass/charge. The circles represent the hot-ion densities observed by HERS. The continuous curves show the densities from the model of Schmidt et al. (1988). The vertical dashed line marks the location of the magnetic pileup boundary.

Fig. 5. Ratios of the densities of ions with different values of mass/charge versus log cometocentric distance. The circles represent the hot-ion densities observed by HERS. The condinuous curves show the densities from the model of Schmidt et al. (1988). The vertical dashed line marks the location of the magnetic pileup boundary.

B. E. GOLDSTEIN, R. GOLDSTEIN, and M. NEUGEBAUER: Mail Stop 169-506, Jet Propulsion Laboratory, 4800 Oak Grove Drive, Pasadena, CA 91109

S. A. FUSELIER: Dept. 91-20, Bldg. 255, Lockheed Palo Alto Research Laboratory, 3251 Hanover St., Palo Alto, CA 94304

H. BALSIGER: Physikalisches Institut, University of Bern, Sidlerstrasse 5, CH-3012 Bern, Switzerland

W.-H. IP: Max-Planck-Institut für Aeronomie, D-3411 Katlenburg-Lindau, Federal Republic of Germany

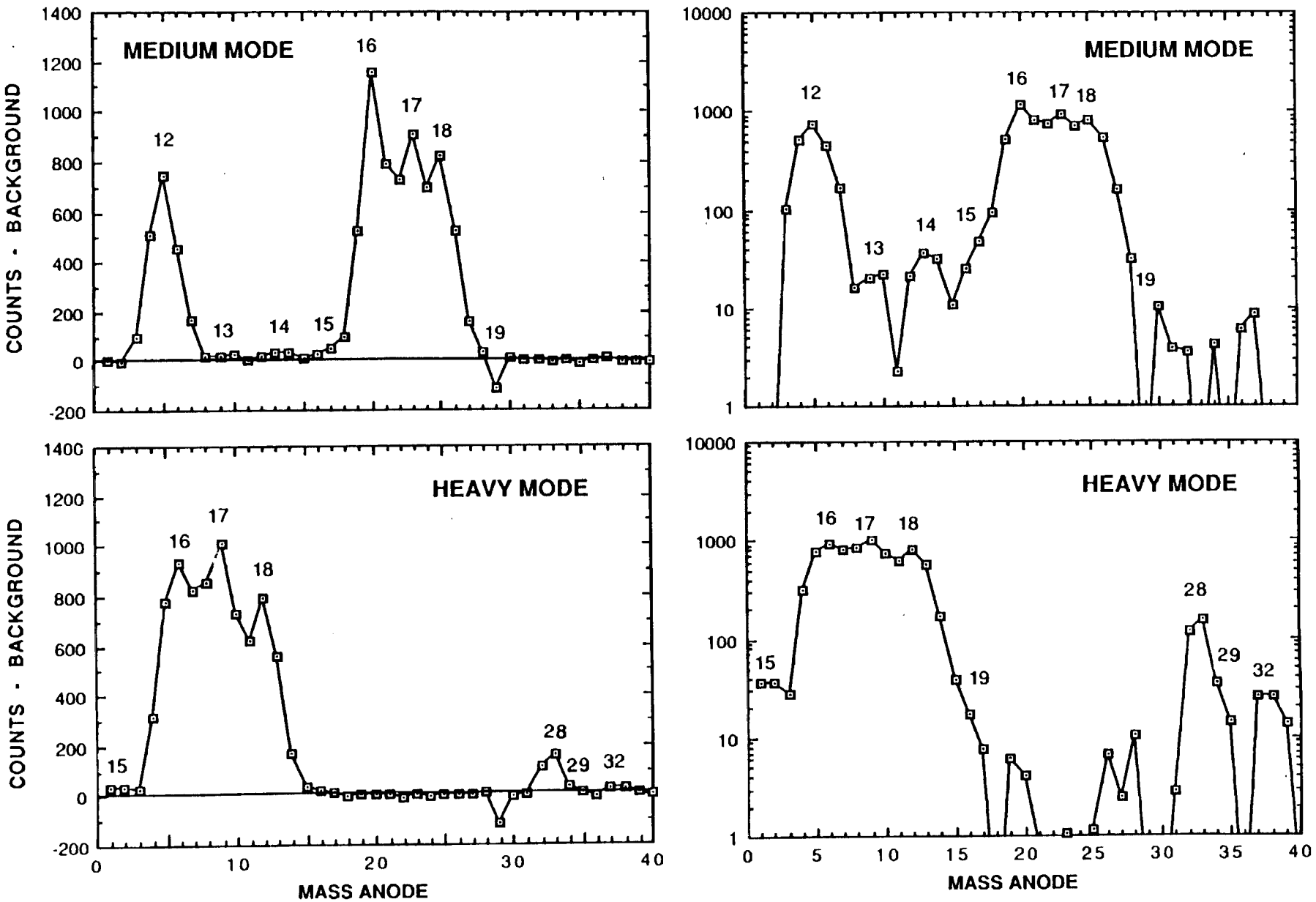
MEDIUM MODE
HEAVY MODE
COUNTS - BACKGROUND
MASS ANODE
12
13
14
15
16
17
18
19
28
29
32

Figure 1

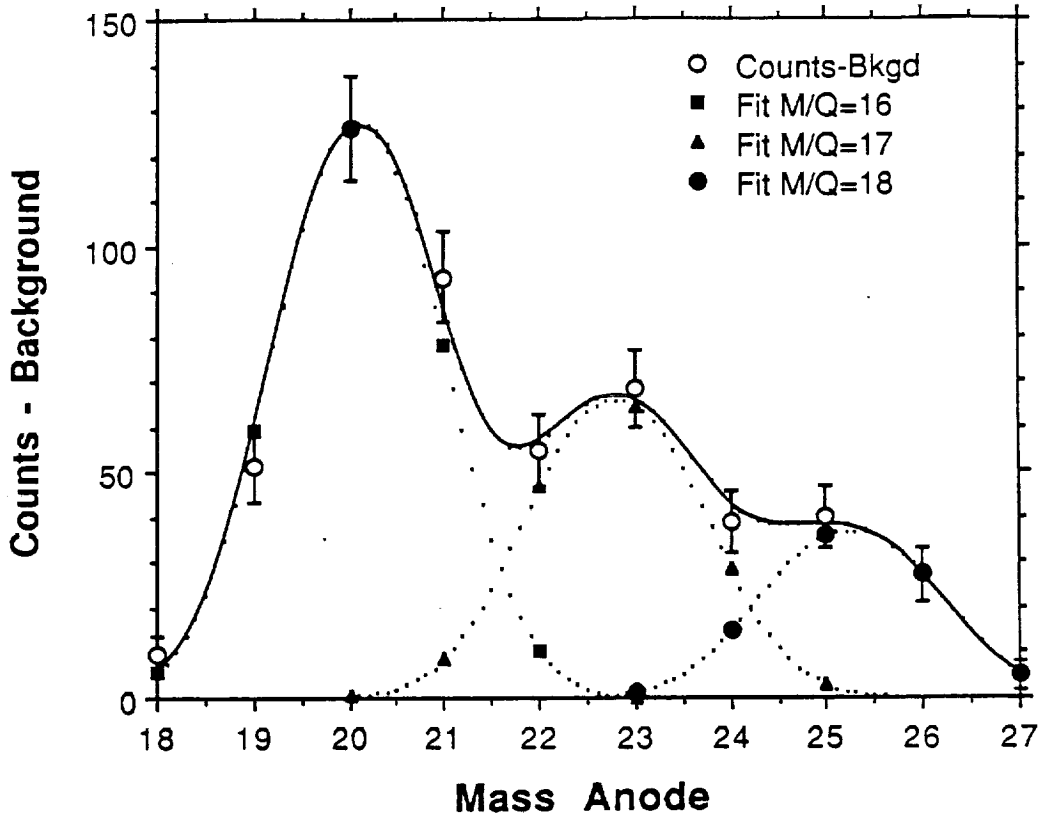
150
100
50
0
Counts - Background
18
19
20
21
22
23
24
25
26
27
Mass Anode
Counts-Bkgd
Fit M/Q=16
Fit M/Q=17
Fit M/Q=18

Figure 2

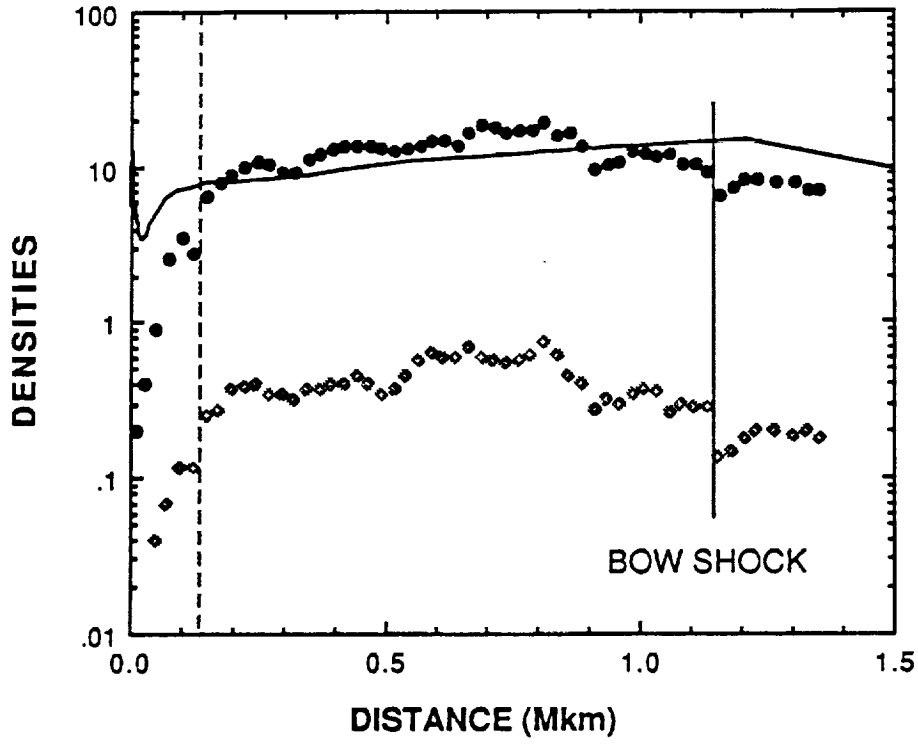

Figure 3

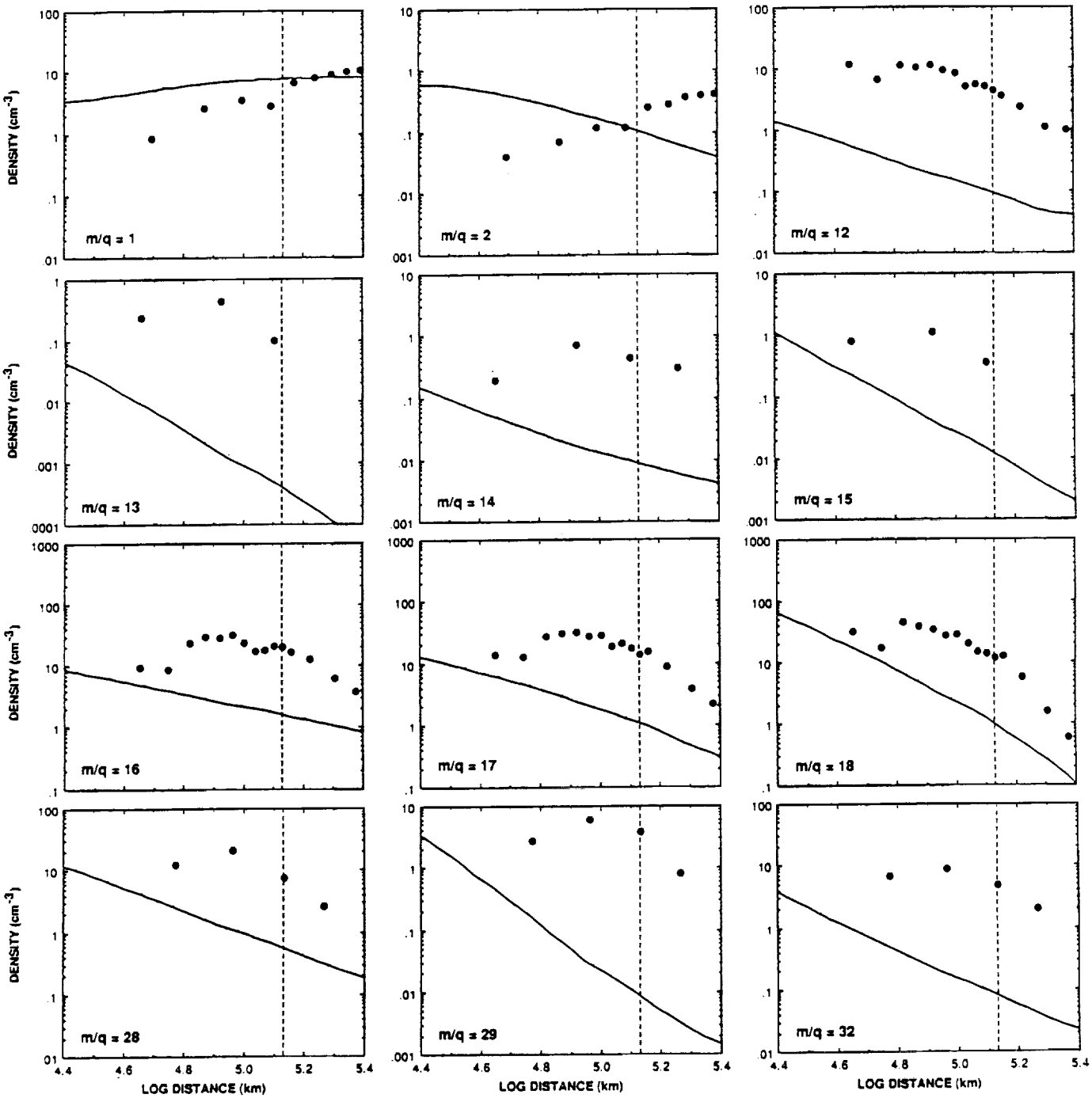
DENSITY (cm^{-3})
m/q = 1
m/q = 2
m/q = 12
m/q = 13
m/q = 14
m/q = 15
m/q = 16
m/q = 17
m/q = 18
m/q = 28
m/q = 29
m/q = 32
LOG DISTANCE (km)
LOG DISTANCE (km)
LOG DISTANCE (km)

Figure 4

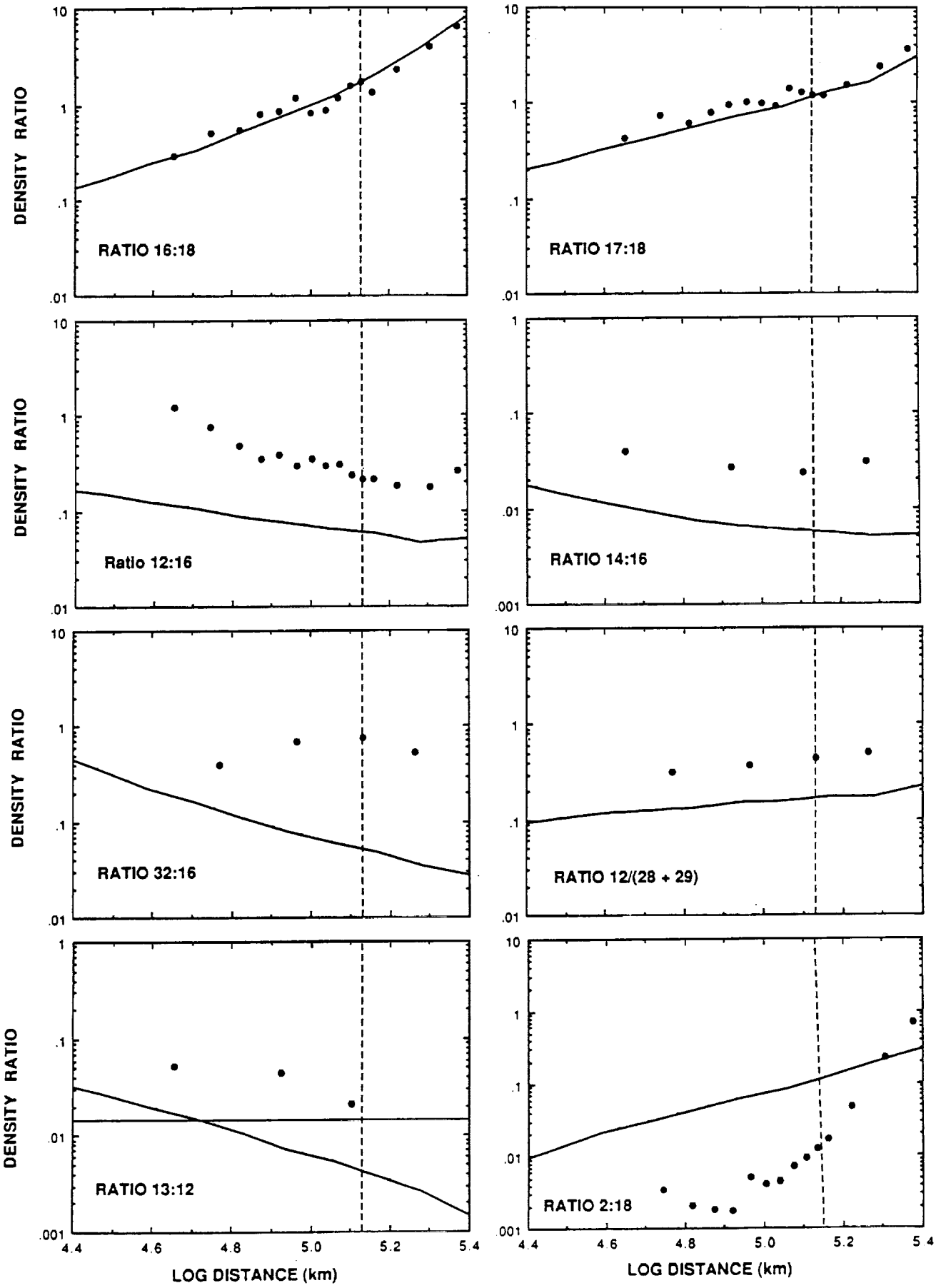
DENSITY RATIO
RATIO 16:18
RATIO 17:18
Ratio 12:16
RATIO 14:16
RATIO 32:16
RATIO 12/(28 + 29)
RATIO 13:12
RATIO 2:18
LOG DISTANCE (km)
LOG DISTANCE (km)

Figure 5

Observations of Solar Wind Ion Charge Exchange in the Comet Halley Coma

S. A. FUSELIER AND E. G. SHELLEY

Lockheed Palo Alto Research Laboratory, Palo Alto, CA

B. E. GOLDSTEIN, R. GOLDSTEIN, AND M. NEUGEBAUER

Jet Propulsion Laboratory, California Institute of Technology, Pasadena, CA

W. -H. IP

Max-Planck-Institut für Aeronomie, Katlenberg-Lindau, FRG

H. BALSIGER

Physikalisches Institut, Universität Bern, Bern, Switzerland

H. RÈME

Centre d'Étude Spatiale des Rayonnements, Toulouse, France

Giotto Ion Mass Spectrometer/High Energy Range Spectrometer (IMS/HERS) observations of solar wind ions show charge exchange effects and solar wind compositional changes in the coma of comet Halley. As the comet was approached, the He^{2+} to proton density ratio increased until about 1 hour before closest approach after which time it decreased. Abrupt increases in this ratio were also observed in the beginning and near the end of the so-called Mystery Region (8.6 to 5.5×10^5 km from the comet along the spacecraft trajectory). These abrupt increases in the density ratio were well correlated with enhanced fluxes of keV electrons as measured by the Giotto plasma electron spectrometer. The general increase and then decrease of the He^{2+} to proton density ratio is quantitatively consistent with a combination of the addition of protons of cometary origin to the plasma and loss of plasma through charge exchange of protons and He^{2+}. In general agreement with the solar wind proton and He^{2+} observations, solar wind oxygen and carbon ions were observed to charge exchange from higher to lower charge states with decreasing distance to the comet. The more abrupt increases in the He^{2+} to proton and the He^{2+} to O^{6+} density ratios in the mystery region require a change in the solar wind ion composition in this region while the correlation with energetic electrons indicates processes associated with the comet.

INTRODUCTION

Soon after the spacecraft encounters with comet Halley, it was reported that a considerable amount of solar wind He^{2+} was charge exchanged to He^+ in the comet coma [*Balsiger et al.*, 1986; *Shelley et al.*, 1986]. Specifically, it was reported that inside the magnetic pile-up boundary (1.35×10^5 km from the nucleus along the Giotto trajectory), over 30% of the solar wind He^{2+} distribution was charge exchanged to He^+. This result

is illustrated in Figure 1, which shows the time profile of the ratio of M/Q=4 to He^{2+} + M/Q=4 densities. This time profile is similar to the one reported by *Shelley et al.* [1986, Figure 3] except that here, the contribution of cometary H_2^+ to the M/Q=2 mass peak has been removed (see *Fuselier et al.* [1988]). Because of the relatively high concentrations, the M/Q=4 mass peak is thought to contain mainly He^+ charge exchanged from solar wind He^{2+} near the comet (within 10^6 km from the nucleus), Figure 1 is expected to reasonably represent the fraction of charge exchanged solar wind He^{2+} as a function of distance from the comet along the Giotto spacecraft trajectory. This figure clearly shows that the charge exchanged fraction increased rather abruptly from <10% to over 40% after the magnetic pile-up boundary (MPB). (Model results will be discussed in a later section.)

Solar wind ion charge exchange with cometary neutrals in the comet coma was predicted prior to the spacecraft encounters with comet Halley [e.g., *Ip and Axford,* 1982]. However, charge exchange effects were expected to be important at distances less than about 10^4 km from the nucleus along the comet-sun line for a Halley-type comet [*Ip and Hsieh,* 1982]. The observations of significant charge exchange of solar wind He^{2+} at the magnetic pile-up boundary (Figure 1) correspond to a distance that is approximately an order of magnitude further from the comet nucleus than predicted.

Thus far, direct observations of charge exchange of solar wind ions have been limited to charge exchange of He^{2+} to He^+ in the comet Halley coma and possibly considerably tailward of the nucleus [Milhalov et al., 1987]. Although the charge exchange cross section for He^{2+} in H_2O is not known, it is probably on the order of 3×10^{-16} cm^2 for typical He^{2+} energies near the magnetic pile-up boundary [*Fite et al.*, 1962; *Koopman,* 1968]. Cross sections for other solar wind minor ions (e.g. O^{7+}, O^{6+}, etc.) in H_2O are also poorly known; however, they may be as much as an order of magnitude larger than that for He^{2+} and nearly equal to the cross section for H^+ in H_2O [*Koopman,* 1968; *Spjeldvik,* 1979]. Since such a large fraction of He^{2+} is charge exchanged in the vicinity of the

magnetic pile-up boundary (Figure 1), it follows that an even larger fraction of other solar wind ions should be charge exchanged in that region of the comet Halley coma. The larger cross sections of these other solar wind ions should also result in observable charge exchange effects further from the comet.

In this paper, we present observations of solar wind electrons and ions in the coma of comet Halley. These observations have potentially important consequences for charge exchange near the magnetic pile-up boundary and other locations throughout the comet Halley coma.

Ion observations in this paper were from the Giotto Ion Mass Spectrometer/High Energy Range Spectrometer (IMS/HERS) [*Balsiger et al.*, 1987]. This instrument cycled through four modes during the Halley encounter. The two modes of interest here measured the three dimensional velocity distributions of protons and solar wind ions with mass per charge (M/Q)=2 to 4 amu/e. Each individual mode required four seconds (one spacecraft spin) to complete an energy and angle scan and the modes were repeated sequentially every 16 seconds. The field-of-view of this instrument extended from 15 to 75° relative to the spacecraft spin axis (which was also approximately the spacecraft velocity vector relative to the comet) and ion energies from 10 eV/e to ~4 keV/e were measured.

For protons and He^{2+}, the moment calculations have been revised from previous work to include an estimate of the percentage of ions outside of the HERS field-of-view. In this procedure, the distribution was assumed to be gyrotropic in the plasma rest frame and the measured phase space density at each velocity and pitch angle was weighted by the inverse fraction of phase space sampled at that pitch angle. This procedure gave reliable estimates of the density as long as the bulk of the distribution was in the field-of-view. For protons and He^{2+}, the bulk of the distribution was in the HERS field-of-view from upstream of the shock (~10^6 km) to well inside the magnetic pile-up boundary (~10^4 km) [*Goldstein et al.*, 1991].

Electron observations in this paper were from the Electron Electrostatic Analyzer (RPA1-EESA) [*Rème et al.*, 1986]. This instrument measured a full 3-dimensional electron distribution from 10 eV to 30 keV every 2 seconds. Here, 4 second averages of these data were used.

OBSERVATIONS

Figure 2 shows the M/Q=2 to proton density ratio at 64 s resolution from 1830 UT to near closest approach to the comet. The distance to the comet along the spacecraft trajectory is shown above the density ratio profile and some of the major regions and boundaries are shown in the figure. The dashed line in this figure will be discussed in detail in the model section.

Upstream from the shock (1830-1922 UT), the M/Q=2 mass peak is dominated by solar wind He^{2+} and the M/Q=2 to proton density ratio shows rapid fluctuations ranging from 1.8 to 3.8%. These fluctuations are due in part to M/Q=2 counting statistics and the fact that the M/Q=2 ions were systematically measured 4 s before the protons. The magnitude of the fluctuations gives some indication of the uncertainty in the measured density ratio in this region. Downstream from the shock (1922 - 2400 UT), the average density ratio increases from about 2.5% to ~4% before decreasing near closest approach. More abrupt, longer lasting deviations are superposed on this trend with the two most notable deviations occurring at the beginning and near the end of the mystery region. After 2310 UT, both the M/Q=2 distribution and the proton distribution are contaminated by a substantial fraction of cometary ions. The M/Q=2 mass peak contains a significant fraction of cometary H_2^+ [*Fuselier et al.*, 1988] and the proton peak contains a significant fraction of cometary pick up protons. While it would be extremely difficult to separate the cometary and solar wind protons, the slight difference in the mass per charge of solar wind He^{2+} and cometary H_2^+ has been used to separate these two species [*Fuselier et al.*, 1988]. Using the density estimates for solar wind He^{2+} inside 2310 UT from Fuselier et

al., 5 min averages of the He^{2+} to proton density ratio are shown by the filled circles connected by the solid line in Figure 2. As can be seen, the He^{2+} to proton density ratio actually reaches a peak at about 2310 UT and decreases significantly thereafter.

In addition to protons and He^{2+}, the Giotto IMS/HERS sensor measured solar wind ions in the mass per charge range from 2 to 4. Figure 3 shows two mass spectra from M/Q=2 to 4 in the solar wind (upper panel) and near the comet (lower panel). Long averaging times were required to obtain good counting statistics for solar wind ions other than He^{2+}. Plotted is the countrate multiplied by $(M/Q)^4$ normalized to the peak countrate as a function of IMS/HERS mass channel. Error bars are one sigma based on counting statistics only. The Y-axis is roughly proportional to flux relative to the M/Q=2 ion flux (primarily He^{2+} in the solar wind and a mixture of He^{2+} and H_2^+ near the comet). In the solar wind spectrum, the O^{7+}, C^{5+}, and Ne^{8+} fluxes are about 0.5% of the solar wind He^{2+} flux while the O^{6+} and C^{4+} fluxes are about 1% of He^{2+}. In addition, there is a relatively small amount of M/Q=4 and slightly larger M/Q ions (probably of solar wind origin and consisting mainly of Si^{7+} with contributions from multiply charge iron ions).

The spectrum in the lower panel of Figure 3 near the comet shows considerable change from the solar wind spectrum. Solar wind O^{7+}, O^{6+}, and Ne^{8+} fluxes are all reduced relative to the M/Q=2 flux. The most dramatic change occurs in the M/Q=4 flux. It is now well above background at a few percent of the M/Q=2 flux.

Besides M/Q=2, the relatively good counting statistics for O^{6+}, the second most abundant solar wind minor ion, and M/Q=4 ions allow us to construct density profiles for these ion species with the time resolution needed to distinguish some features in the cometary coma. Figure 4 shows density profiles for these two ion species from the upstream solar wind to near closest approach. A variety of averaging intervals were used based on counting statistics of the individual ion species. For example, one hour averages were used in the solar wind and after 2200 UT and half hour averages were used between the shock and the end of the mystery region. Because of the 4 keV/e upper energy

per charge cutoff of the IMS/HERS detector, a fraction of the higher mass per charge solar wind ion distributions were outside the energy per charge range of the instrument. This energy per charge cutoff had the greatest effect on the M/Q=4 densities in the solar wind, where the solar wind velocity was relatively high. Because mass loading caused the solar wind velocity to decrease from about 400 km/s far from the comet to near zero near the comet, the upper energy per charge cutoff of the HERS detector had less effect on M/Q=4 densities closer to the comet. It is estimated that 47% of the distribution was above 4 keV/e from 1600-1700 UT, 20% from 1700-1800 UT and about 9% from 1800-1900 UT. After 1930 UT, the solar wind velocity had decreased enough so that a negligible amount of M/Q=4 solar wind ion distribution was above the 4 keV/e cutoff. For other solar wind ions, such as C^{4+} and O^{5+}, the upper energy per charge cutoff had much less effect on the density. It is estimated that less than 5% of the solar wind C^{4+} and O^{5+} distributions were above the 4 keV/e cutoff from 1600-1700 UT. This percentage decreased as the comet was approached.

Despite the long averaging times, some general trends can be seen in Figure 4. The O^{6+} density profile is similar to the proton and M/Q=2 density profiles [see *Goldstein et al.*, 1987; 1991]. In particular, it shows a factor of two increase in density between 2000 and 2200 UT associated with the mystery region. In contrast, The M/Q=4 density is at detection threshold ($\sim 10^{-3}$ cm^{-3}) in the solar wind and increases sharply after 2200 UT [see also, *Shelley et al.*, 1986].

Although the densities of other solar wind ions were extremely low, a general trend towards lower charge states was seen in the comet coma. Table 1 lists density ratios for Oxygen and Carbon charge states for the 2 hours prior to the crossing of the cometary bow shock ($\sim 10^6$ from the comet) and for the 2 hours before closest approach (~few x 10^5 km from the comet). Whereas the O^{7+} to O^{6+} density ratio decreased with decreasing distance to the comet, the O^{5+} to O^{6+} density ratio increased with decreasing distance. Also, the C^{4+} to C^{5+} ratio increased with decreasing distance to the comet. Although

the uncertainties are quite large, the general trend in Table 1 was toward lower charge states as the comet was approached.

CHARGE EXCHANGE

The observations in Figures 1 through 4 and Table 1 are qualitatively consistent with charge exchange of solar wind ions in the comet Halley coma. Figure 1 shows that He^{2+} was charge exchanged to He^{+} as the comet was approached. Figure 2 shows a general increase in the He^{2+} to proton density ratio as the comet was approached. This density ratio was affected by solar wind composition changes, addition of cometary protons, and charge exchange losses. The addition of comeatry protons would cause the He^{2+} to proton density ratio to decrease with decreasing distance to the comet. It is clear from Figure 2 that the presence of cometary protons does not have an effect before 2310 UT, when the density ratio began to decrease. The increase in the He^{2+} to proton density ratio from 1830 UT to 2310 UT could be due to a slow change in the solar wind composition (i.e., unrelated to the presence of the comet). However, the slow change in composition would not account for the increase in the M/Q = 4 ion density (interpreted as He^{+}) as the comet was approached (Figure 4). Charge exchange of He^{2+} and protons can account for the increase in the He^{2+} to proton density ratio in Figure 2 since, as discussed in the introduction, the charge exchange cross section for protons is believed to be ten times higher than that for He^{2+}. Charge exchange of He^{2+} to He^{+} also accounts for the increase in the M/Q=4 ion density as the comet was approached. Although there are several other possible sources for the M/Q=4 mass peak (see Figure 3), the total density of the solar wind ions between M/Q=2 to 4 is only a few percent of the He^{2+} density. Therefore, these ions cannot contribute significantly to the M/Q=4 ion density near the comet and the major contribution to the M/Q=4 mass peak appears to be He^{+} charge exchanged from solar wind He^{2+} [see also, *Shelley et al.*, 1986]. Superposed on the charge exchange loss of

He^{2+} and protons are possible solar wind composition changes (for example from 2120 to 2150 UT in Figure 1) which will be discussed in more detail in the next two sections.

Figure 3 and Table 1 are also consistent with charge exchange as the comet was approached. In Figure 3, there is evidence for a loss of solar wind minor ions such as O^{7+} and Ne^{8+} close to the comet. In Table 1, there is a general trend to lower oxygen and carbon charge states as the comet was approached. Since all charge states of solar wind oxygen have approximately the same charge exchange cross section [*Spjeldvik*, 1979], the general trend to lower charge states indicates that multiply charged ions undergo charge exchange as the solar wind approaches the comet.

MODEL FOR PROTON AND He^{2+} CHARGE EXCHANGE

Unfortunately, the very low densities of the solar wind minor ions between M/Q=2 and 4 allow only a qualitative comparison with predictions from solar wind ion charge exchange. However, the proton, M/Q=2, and M/Q=4 densities are large enough to allow some quantitative comparison with predictions from solar wind ion charge exchange. Comparison between the observations and a simple model for the solar wind interaction have already been made [*Shelley et al.*, 1986]. Shelley et al. concluded that the helium observations in the comet coma were inconsistent with present models of the solar wind interaction with the comet. They suggested that model results and observations would be in better agreement if the He^{2+} to He^{+} charge exchange cross section in H_2O was substantially larger than the $\sim 3 \times 10^{-16}$ cm^2 assumed in their model and/or if the flow field in the comet coma was substantially different than assumed in their model.

Given a cometary flow model, the ratio of the He^{2+} and proton densities can be determined along the Giotto trajectory. This ratio will depend on the ratio of the charge exchange cross sections of He^{2+} and protons and on the production rate of cometary H^{+} from H_2O. Since the proton charge exchange cross section in H_2O at the energies of interest here is reasonably well known and the production of H^{+} can be modeled, the profile of the

He^{2+} to proton density ratio is a function of the He^{2+} charge exchange cross section. In this section, we use a cometary flow model to predict the He^{2+} to proton density ratio and compare this prediction to the observations. Through this comparison, we estimate the charge exchange cross section for He^{2+} in H_2O.

The model charge exchange calculations were made using the procedure outlined in *Ip* [1989]. The MHD flow dynamics of the comet-solar wind interaction were separated from the photochemistry and the charge exchange process. In doing this, the continuity equation

$$\frac{1}{A}\frac{d}{ds}(n_j v_j A) = q_j - s_j \qquad (1)$$

for the j^{th} species can be integrated. Here, v_j is the flow velocity along the stream line, n_j is the number density, q_j is the production rate, s_j is the loss rate, and A is the cross section of the stream tube. The flow field model determines the values of v_j for each stream line and the cross section of the stream line. Here, we use the Fedder et al. 2-D flow model [*Fedder et al.*, 1986].

To compute the net production rate for cometary H^+ (q_H-s_H in Equation 1), we assume a coma model of water vapor and its photodissociation fragments (OH, O, and H). The production rate for hydrogen ions is then given by,

$$\dot{n}(H^+) = n(H)\,(1/t_i + \sum_j n_j \sigma_j(H) < v_j >) \qquad (2)$$

Here the ionization time (t_i), which includes photoionization and charge exchange with solar wind protons, is assumed to be 10^6 seconds. The cross section $\sigma_j(H)$ in the second term refers to the interaction between H^+ and the neutral gas and $<v_j>$ is the root-mean-square of the plasma flow speed v_p and the thermal speed (δv_j) of the j^{th} species.

The loss term in (1) is dominated by the charge exchange process. Although charge exchange cross sections for different reactions should vary with the flow speed, in the present approximation we assume the the charge exchange rate for protons is constant with energy.

The dashed line in Figure 2 shows the results from the model. In the model, the initial density ratio was 2.5%, the He^{2+} charge exchange cross section was $\sigma = 3\times10^{-16}$ cm^2, and the H^+ charge exchange cross section was 5×10^{-15} cm^2. The general trend of the observed density ratio is reproduced, indicating that the charge exchange cross section for He^{2+} is about a factor of 10 lower than that for H^+. Increasing the He^{2+} charge exchange cross section by a factor of 10 would result in a He^{2+} to proton density ratio that neither has an initial increase with decreasing distance nor has a decrease in the last hour before closest approach.

Since the densities are computed individually in the model, the He^+ to total Helium ion density ratio can be directly compared with the observations in Figure 1. The percent charge exchanged He^{2+} predicted from the model (solid line connected by x's in Figure 1) is clearly in good agreement with the observations up to the magnetic pile-up boundary. This is again consistent with a He^{2+} charge exchange cross section of $\sim3\times10^{-16}$ cm^2 for this region. After the magnetic pile-up boundary, the predicted percentage is about a factor of 4 below the observed percentage.

Thus, while the general trend in Figures 1 and 2 are reproduced with the expected cross sections, the model underestimates the density ratio in the mystery region and near the magnetic pile-up boundary. and it also underestimates the percent charge exchanged He^{2+} near the magnetic pile-up boundary. In the next section, we address the discrepancy between observations and predictions in the mystery region by considering why the density ratio changes rather abruptly. The deviation between observations and predictions is left for the final discussion secion.

MYSTERY REGION

The mystery region is a region of increased density, increased flow speed, decreased ion temperature, and increased electron temperature relative to the rest of the region downstream from the Giotto bowshock crossing [*Goldstein et al.*, 1986; *Rème et al.*, 1986; *Rème*, 1990]. Figure 2 also shows that the M/Q=2 to proton density ratio deviates from its relatively smooth, increasing trend in this region. In this section, we will discuss the possible origins of these deviations and other properties of the mystery region.

Figure 5 shows the density profiles for electrons from 10 eV to 3.5 keV, protons, M/Q=2 ions (primarily solar wind He^{2+}), solar wind O^{6+}, and electrons from 0.8 to 3.5 keV. The proton and electron density profiles in the top two panels show both qualitative and quantitative agreement throughout this time interval. The mystery region extends from the sharp density increase at 2022 UT to the sharp decrease in the M/Q=2 ion density and the 0.8 to 3.5 keV electron density at 2152 UT.

The horizontal bars in Figure 5 show the time intervals when the M/Q=2 to proton density ratio in Figure 2 deviated from its smooth trend. Of particular interest is the interval from 2115 to 2150 UT. As can be seen in Figure 5 at 2120 UT, the increase in the M/Q=2 to proton density ratio in Figure 2 is associated with a drop in both the electron and proton number densities. The M/Q=2 number density did not decrease from 2115 to 2125 UT, in fact, it increased somewhat. The net result was an abrupt increase in the M/Q=2 to proton density ratio. It is also interesting to note that the changes in the M/Q=2 to proton density ratio in the period from 2115 to 2150 UT are associated with a decrease in the solar wind O^{6+} density and an increase in the electron density above 800 eV (see the bottom two panels in Figure 5). The half hour averages of the O^{6+} density do not allow us to determine if a similar decrease in that density is associated with the first interval of increased M/Q=2 to proton density ratio from 2013 to 2021 UT. However,

it is clear that the increase in the M/Q=2 to proton density ratio is associated with increased electron density above 800 eV from 2037 to 2105 UT. The energetic electron density increases in the mystery region are unique. From the bow shock to the mystery region and after the mystery region to closest approach, the energetic electron density was $\sim 3\text{-}4 \times 10^{-4}$ cm^{-3} (see Figure 5 from 2000 to 2040 UT and *Rème et al.* [1986]).

DISCUSSION

In most regions of the comet Halley coma, we have attempted to interpret the IMS/HERS observations in terms of charge exchange with cometary neutrals. The increase in the He^+ density with decreasing distance to the comet in Figure 1, the general increasing M/Q=2 to H^+ density ratio in Figure 2, and the trend to lower charge states for multiply charged Oxygen and Carbon in Table 1 are all considered as evidence for this charge exchange process.

While we can find substantial qualitative evidence for charge exchange in the comet Halley coma, quantitative comparisons between the observations and predictions from cometary models is clearly lacking in the mystery region and the region near and inside the magnetic pile-up boundary.

To the properties of the mystery region that have been known previously [e.g., *Goldstein et al.*, 1986; *Rème et al.*, 1990], we add that there are solar wind composition changes in parts of this region. The He^{2+} to proton density ratio shows two deviations in its increasing trend in this region (see Figure 2). The second of these deviations occurs within the last 30 minutes of the mystery region and is associated with a decrease in the proton density and a possible slight increase in the M/Q=2 density (see Figure 5). Also, it is associated with a decrease in the O^{6+} density and the largest fluxes of energetic electrons observed during the encounter.

The general increase in all solar wind ion densities and the change in the He^{2+} to proton density ratio are strong indicators that the mystery region is dominated by solar

wind plasma with different characteristics from the plasma in other parts of the coma. While it is tempting to interpret this region as simply a separate solar wind plasma that has convected into the Halley coma, the observation of keV electrons in this region indicates that there is also an additional interaction related to the presence of the comet. It is also interesting to note that the second increase in the He^{2+} to proton density ratio (from 2115 to 2150 UT in Figure 5) results primarily from the decrease in the proton density and there is a simultaneous decrease in the O^{6+} density. As pointed out in the introduction, H^+ and O^{6+} both have charge exchange cross sections that are an order of magnitude larger than that for He^{2+}. This observation suggests that enhanced charge exchange may be occurring in the parts of the mystery region where the He^{2+} to H^+ density ratio is elevated and keV electrons are present. The possible causes of this enhanced charge exchange and the relation, if any, with the keV electrons are not known at this time. Also, it has been noted that the transition from the mystery region back into lower density plasma (at 2150 UT in Figure 5) may have been seen by other spacecraft that encountered comet Halley and by the International Cometary Explorer (ICE) spacecraft at comet Giacobini-Zinner [*Rème et al.*, 1986; *Rème*, 1990].

Thus, while the observations in Figures 2 and 5 indicate that the mystery region is likely a separate solar wind plasma that has convected into comet coma, some of the features in this region and possibly its boundaries indicate that additional and different interactions between this plasma and the comet coma are taking place.

Another important region where the cometary models fail to predict the amount of charge exchange is the region from 2310 UT to closest approach, or the region near and inside the magnetic pile-up boundary. Figure 1 shows that the amount of charge exchanged He^{2+} to He^+ increases dramatically across the magnetic pile-up boundary. This amount is much larger than that predicted by previous models [*Shelley et al.*, 1986] and by the model used in this paper. In addition, the predicted He^{2+} to H^+ density ratio is clearly too low (Figure 2).

The difference between the predicted and observed density ratios indicates that either there is too little He^{2+} or too much H^+ present in the vicinity of the magnetic pile-up boundary. As pointed out by *Shelley et al.* [1986] the sharp increase in the percent charge exchanged He^{2+} at the Magnetic Pile-up Boundary (Figure 1) is not the result of a rapid increase in the He^+ density but a rapid decrease in the He^{2+} density. These results taken together suggest that the charge exchange of He^{2+} relative to H^+ is underestimated in the cometary models. An overestimate of the the production of cometary H^+ could also help explain the differences between predictions and observations in Figure 2 in the vicinity of the Magnetic Pile-up Boundary but obviously do not affect the results in Figure 1.

A possibility already discussed by *Shelley et al.* [1986] is that the He^{2+} cross section could be about a factor of 3 to 10 times larger than the 3×10^{-16} cm^2 value used in the models. This is clearly not the case prior to 2310 UT, where the predicted density ratio using this cross section agrees well with the observations. One possibility is that the cross section for He^{2+} increases with decreasing energy faster than that for H^+. (The H^+ cross section has been shown to increase with decreasing energy for energies below 100 eV [*Koopman* 1968].) Armed with such a free parameter, the density ratio profile in Figure 2 could be reproduced exactly, but the understanding of the density ratio decrease after 2310 UT would not be improved. Also, this possibility would not explain the rather abrupt increase in the percent charge exchanged He^{2+} in Figure 1 because the He^{2+} flow velocity decreases smoothly across the magnetic pile-up boundary and the thermal speed does not change at all across this boundary [*Fuselier et al.*, 1987]. One thing that does change rather abruptly in the vicinity of the magnetic pile-up boundary is the flow direction [*Fuselier et al.*, 1987].

It is possible that a combination of rapid slowing and deflection of the solar wind plasma incident along the sun-comet line, followed by a re-acceleration along the flanks of the comet could explain both the large amount of charge exchange and the relatively

smooth velocity profile observed by Giotto [*Shelley et al.*, 1986; *Wallis*, 1990]. However, the present computer models cannot be used to predict such a possibility. Thus, we must conclude that present computer models allow us to qualitatively understand the charge exchange of solar wind ions in the outer reaches of the coma and help to distinguish real charge exchange effects from changes in the solar wind composition (for example in the mystery region). The quantitative understanding of the observations of charge exchange in the inner coma (i.e. in the region just before and inside the magnetic pile-up boundary in Figures 1 and 2) remains poor.

Acknowledgments. The authors acknowledge the contributions of the entire IMS team. Research at Lockheed was funded by NASA under contract NAS5-4336. Work at the Centre d'Ètude Spatiale des Rayonnements was supported by CNES under grant number 1212.

REFERENCES

Balsiger, H., K. Altwegg, F. Buhler, J. Geiss, A. G. Ghielmetti, B. E. Goldstein, R. Goldstein, W. T. Huntress, W.-H. Ip, A. J. Lazarus, A. Meier, M. Neugebauer, U. Rettenmund, H. Rosenbauer, R. Schwenn, R. D. Sharp, E. G. Shelley, E. Ungstrup, and D. T. Young, Ion composition and dynamics at comet Halley, *Nature*, *321*, 330-334, 1986.

Balsiger, H., K. Altwegg, J. Benson, F. Buhler, J. Fischer, J. Geiss, B. E. Goldstein, R. Goldstein, P. Hemmerich, G. Kulzer, A. J. Lazarus, A. Meier, M. Neugebauer, U. Rettenmund, H. Rosenbauer, K. Sager, T. Sanders, R. Schwenn, E. G. Shelley, D. Simpson, and D. T. Young, The ion mass spectrometer on Giotto, *J. Phys. E: Sci. Instrum.*, *20*, 759-767, 1987.

Fedder, J. A., J. G. Lyon, J. L. Giuliani Jr., ,*EOS Trans. AGU*, *67*, 17, 1986.

Fuselier, S. A., E. G. Shelley, H. Balsiger, J. Geiss, B. E. Goldstein, R. Goldstein, W. -H. Ip, Cometary H_2^+ and solar wind He^{2+} dynamics across the Halley cometopause, *Geophys. Res. Lett.*, *15*, 549-552, 1988.

Goldstein, B. E., M. Neugebauer, H. Balsiger, J. Drake, S. A. Fuselier, R. Goldstein, W.-I. Ip, U. Rettenmund, H. Rosenbauer, R. Schwenn, and E. G. Shelley, Giotto-IMS observations of ion flow velocities and temperatures outside the contact surface of comet Halley, Proceedings of the 20th ESLAB Symposium on the Exploration of Halley's Comet, *ESA SP-250, 1*, 229-233, 1986, *Astron. and Astrophys., 187*, 174-178, 1987.

Goldstein, B. E., R. Goldstein, M. Neugebauer, S. A. Fuselier, E. G. Shelley, H. Balsiger, G. Kettmann, W.-H. Ip, H. Rosenbauer, and R. Schwenn, Observations of plasma parameters in the coma of P/Halley by the Giotto ion mass spectrometer, *J. Geophys. Res.*, submitted, 1991.

Ip, W.-H., On charge exchange effect in the vicinity of the cometopause of comet Halley, *Astrophys. J., in press*, 1989.

Ip, W.-H., and K. C. Hsieh, Production of energetic neutrals in cometary comae via solar wind interaction, in *Cometary Exploration I*, ed. T. I. Gombosi, Hungarian Academy of Sciences, 265-270, 1982.

Ip, W.-H., and W. I. Axford, Theories of physical processes in the cometary comae and ion tails, in *Comets*, ed. L. L. Wilkening, The University of Arizona Press, Tucson, 588-634, 1982.

Koopman, D. W., Light ion charge exchange in atmospheric gases, *Phys. Rev., 166*, 57-62, 1968.

Mihalov, J. D., H. R. Collard, D. S. Intriligator, and A. Barnes, Observations by Pioneer 7 of He^+ in the distant coma of Halley's comet, *Icarus, 71*, 192-197, 1987.

Rème, H., Cometary plasma observations between the shock and the contact surface, *J. Geophys. Res.*, in press, 1990.

Rème, H., F. Cotin, A. Cros, J. L. Médale, J. A Sauvaud, C. d'Uston, A. Korth, A. K. Richter, A. Loidl, K. A. Anderson, C. W. Carlson, D. W. Curtis, R. P. Lin, and D. A. Mendis, The Giotto RPA-Copernic plasma experiment, *ESA SP-177*, 33-52, 1986.

Rème, H., J. A Sauvaud, C. d'Uston, A. Cros, K. A. Anderson, C. W. Carlson, D. W. Curtis, R. P. Lin, A. Korth, A. K. Richter, and D. A. Mendis, General Features of the comet Halley - solar wind interaction from plasma measurements, *ESA SP-250, 1,* 29-34, 1986, *Astron. and Astrophys., 187,* 33-38, 1987.

Shelley, E. G., S. A. Fuselier, J. F. Drake, W.-I. Ip, H. Balsiger, B. E. Goldstein, R. Goldstein, M. Neugebauer, Charge exchange of solar wind ions in the comet Halley coma, Proceedings of the 20th ESLAB Symposium on the Exploration of Halley's Comet, *ESA SP-250, 1,* 285-289, 1986, *Astron. and Astrophys., 187,* 304-306, 1987.

Spjeldvik, W. N., Expected charge states of energetic ions in the magnetosphere, *Space Science Reviews, 23,* 499-538, 1979.

Wallis, M. K., Charge exchange regime in the plasma flow as source of cometosheath and Halley's plasma tail, *J. Geophys. Res.,* in press, 1990.

Table 1. Solar wind Oxygen and Carbon density ratios

Time (UT)	O^{7+}/O^{6+}	O^{5+}/O^{6+}	C^{4+}/C^{5+}
1705-1913	0.35±0.14	0.24±0.20	0.42±0.44
2200-2400	0.17±0.31	0.59±0.81	0.74±0.92

Fig. 1. Observed (+'s) and modeled (x's) M/Q=4 to He^{2+} + M/Q=4 density ratio versus distance from the comet along the Giotto trajectory. The abrupt increase at the magnetic pile-up boundary (MPB) is interpreted as a large increase in the percent He^{2+} charge exchange to He^{+}.

Fig. 2. M/Q=2 to H^{+} density ratio versus time or distance from the comet (solid line). The filled circles connected by the solid line are the ratios after the cometary H_2^{+} contribution to the M/Q=2 mass peak is removed. The Dashed line show a fit to the observed ratio from the charge exchange model.

Fig. 3. Mass spectra from M/Q=2 to 4 far from the comet (upper panel) and near the comet (lower panel). The vertical axis is proportional to the flux normalized by the He^{2+} flux. Near the comet, the relative fluxes of all multiply charged solar wind species are reduced except for M/Q=4 when compared to the mass spectrum further away.

Fig. 4. Densities versus time for M/Q=4 ions (dashed line) and solar wind O^{6+} (solid line).

Fig. 5. Electron, proton, He^{2+}, O^{6+}, and electron $\geq$1 keV densities for a time period centered on the mystery region. The bars in the figure identify the intervals when the He^{2+} to H^{+} density ratio in Figure 2 are elevated. These intervals are correlated with enhanced energetic electron flux. The second interval is also correlated with a decrease in the H^{+} and O^{6+} densities.

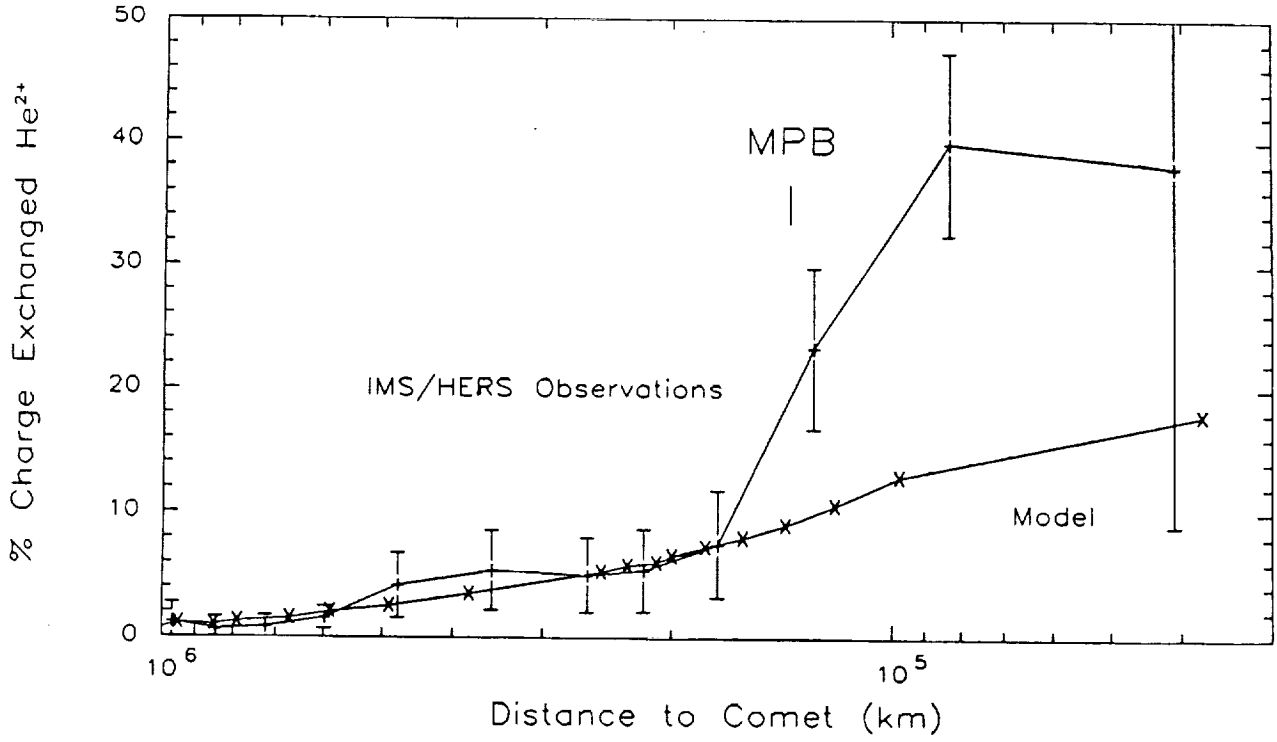
50
40
30
20
10
0
% Charge Exchanged He^{2+}
MPB
IMS/HERS Observations
Model
10^6
10^5
Distance to Comet (km)

Figure 1

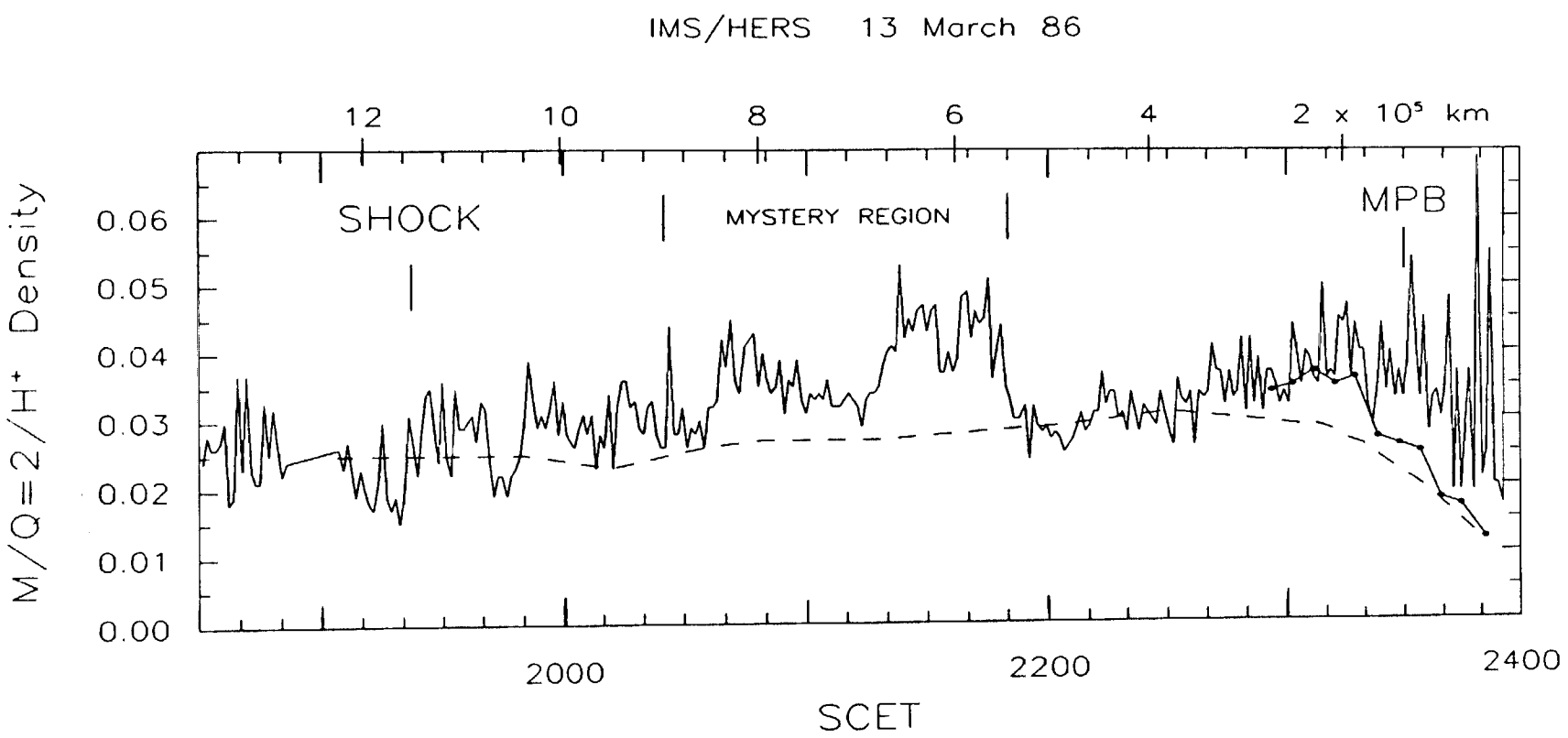
IMS/HERS 13 March 86
12
10
8
6
4
2 x 10⁵ km
SHOCK
MYSTERY REGION
MPB
M/Q=2/H⁺ Density
0.06
0.05
0.04
0.03
0.02
0.01
0.00
2000
2200
2400
SCET

Figure 2

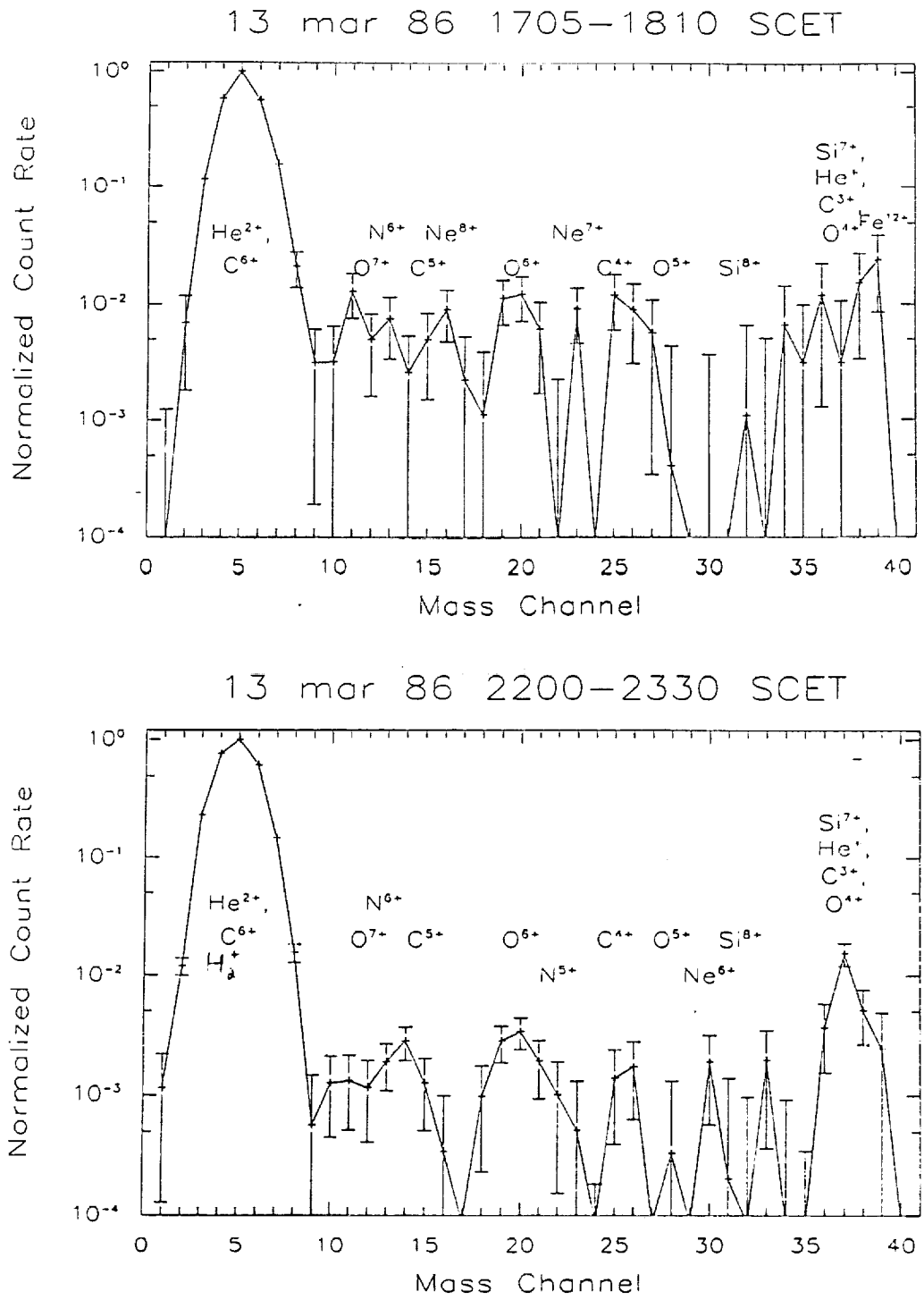
13 mar 86 1705–1810 SCET
Normalized Count Rate
Mass Channel
He2+, C6+
N6+ Ne8+
O7+ C5+
O6+
Ne7+
C4+ O5+
Si8+
Si7+, He+, C3+ O4+ Fe12+
13 mar 86 2200–2330 SCET
Normalized Count Rate
Mass Channel
He2+, C6+ H2+
N6+
O7+ C5+
O6+
N5+
C4+ O5+
Ne6+
Si8+
Si7+, He+, C3+, O4+

Figure 3

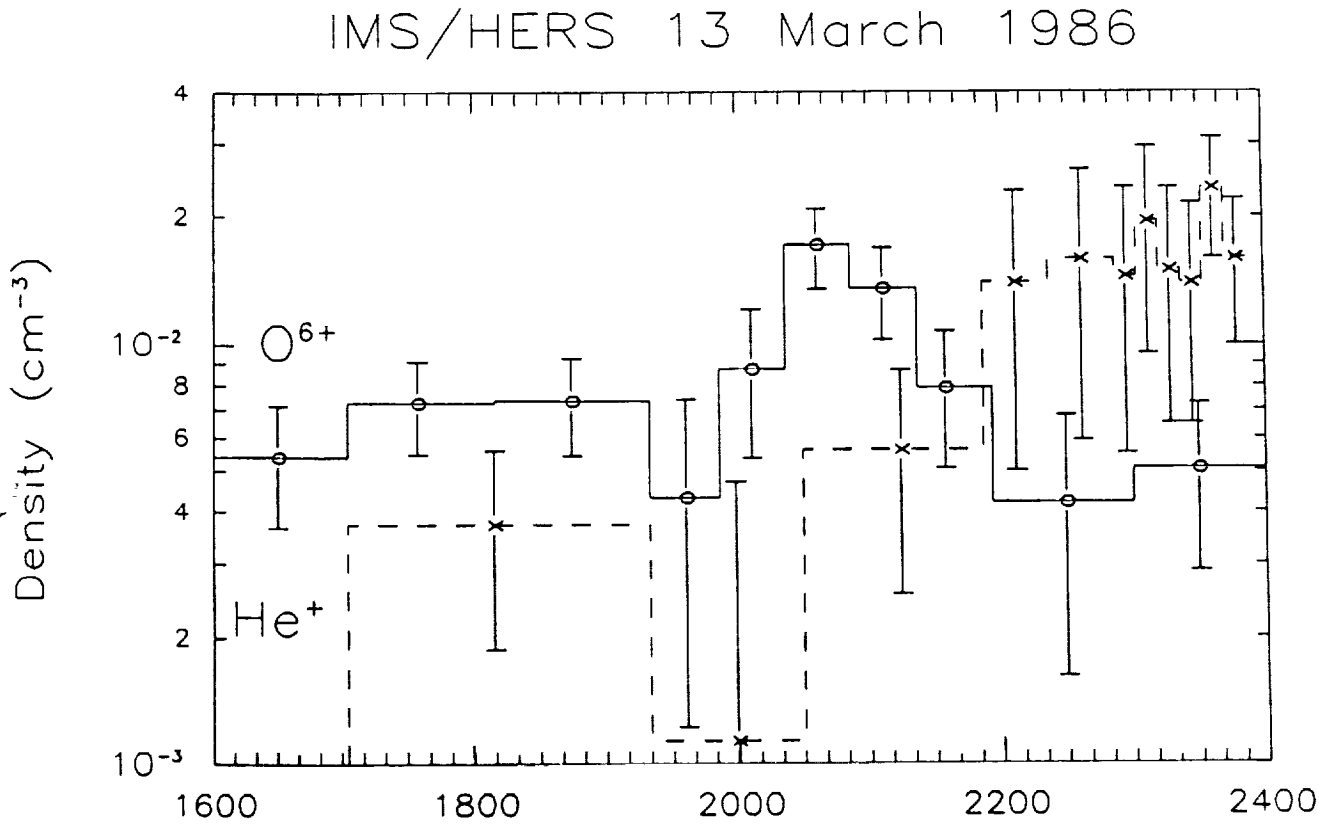
IMS/HERS 13 March 1986
Density (cm⁻³)
4
2
10⁻²
8
6
4
2
10⁻³
O⁶⁺
He⁺
1600
1800
2000
2200
2400

Figure 4

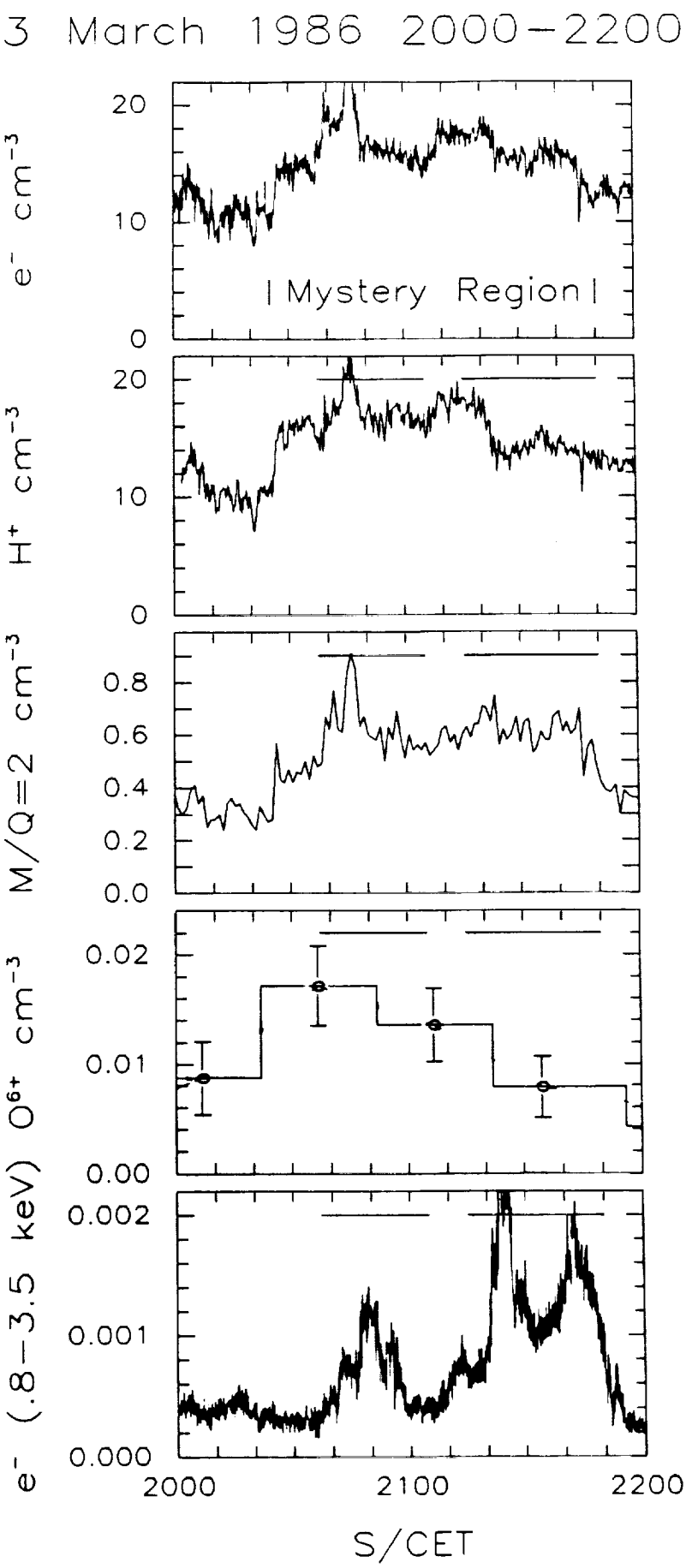
13 March 1986 2000–2200 SCET
e⁻ cm⁻³
20
10
0
Mystery Region
H⁺ cm⁻³
20
10
0
M/Q=2 cm⁻³
0.8
0.6
0.4
0.2
0.0
O⁶⁺ cm⁻³
0.02
0.01
0.00
e⁻ (.8–3.5 keV)
0.002
0.001
0.000
2000
2100
2200
S/CET

Figure 5

OBSERVATIONS OF PLASMA DYNAMICS IN THE COMA OF P/HALLEY BY THE GIOTTO ION MASS SPECTROMETER

B. E. Goldstein, R. Goldstein, M. Neugebauer

Jet Propulsion Laboratory
4800 Oak Grove Drive
Pasadena, CA 91109 USA

S. A. Fuselier, E. G. Shelley

Lockheed Palo Alto Research Laboratory

H. Balsiger

University of Bern

G. Kettmann, W.-H. Ip, H. Rosenbauer, R. Schwenn

Max-Planck Institut für Aeronomie

Submitted to Journal of Geophysical Research
December 26, 1990

ABSTRACT

Observations in the coma of P/Halley by the Giotto Ion Mass Spectrometer (IMS) are reported. The High Energy Range Spectrometer (HERS) of the IMS obtained measurements of protons and alpha particles from the far upstream region to the near ionopause region, and of ions from mass 12 to 32 at distances of about 250,000 km to 40,000 km from the nucleus. Plasma parameters from the High Intensity Spectrometer (HIS) of the IMS obtained between 150,000 to 5000 km from the nucleus are also be discussed. The distribution functions of water group ions (water group will be used to refer to ions of 16 to 18 m/q, where m is in AMU and q is in unit charges) are observed to be spherically symmetric in velocity space, indicating strong pitch angle scattering. The discontinuity known as the magnetic pile-up boundary (MPB) is apparent only in proton, alpha, and magnetometer data, indicating that it is a tangential discontinuity of solar wind origin. HERS observations show no significant change in the properties of the heavy ions across the MPB. A comparison of the observations to an MHD model (Wegmann *et al.*, 1987) is made. The plasma flow directions at all distances greater than 30,000 km from the nucleus are in agreement with MHD calculations. However, despite the agreement in flow direction, within 200,000 km of the nucleus the magnitude of the velocity is lower than predicted by the MHD model and the density is much larger (a factor of 4). Within 30,000 km of the nucleus there are large theoretical differences between the MHD model flow calculations for the plane containing the magnetic field and for the plane perpendicular to the magnetic field. The observations agreed much better with the pattern calculated for the plane perpendicular to the magnetic field. The data obtained by the High Energy Range Spectrometer (HERS) of the IMS that are published herein have also been provided to the International Halley Watch archive.

INTRODUCTION

The Giotto spacecraft of the European Space Agency approached Halley's comet at a speed of 68.4 km/sec, with an angle between the spacecraft velocity in the comet frame and the sun-comet line of 107°, and with closest approach occurring at 00:03 UT on March 14, 1986. Among the investigations on the spacecraft was the Ion Mass Spectrometer (IMS). The major focus of this paper is the presentation of heavy ion plasma parameters and particle distributions obtained by the HERS. Also presented are improved estimates of proton and alpha particle parameters obtained by the HERS. The proton, alpha particle, and heavy ion observations are also compared to the predictions of an MHD model. Recent compositional results of data from the High Energy Range Spectrometer (HERS) of the IMS (Neugebauer *et al.*, 1990) have recently been accepted for publication.

DESCRIPTION OF INSTRUMENT AND METHOD OF ANALYSIS

The HERS measured positive ions for energies up to about 4 keV, depending on the mass being observed and the view direction. The instrument had a fan-like field of view that rotated about the spin axis; the inner edge (the edge towards the comet direction) of the fan was 15° from the spin axis, while the outer edge was 75° from the spin axis. The instrument had 4 modes (proton, light, medium, and

heavy); each mode was measured once every 4 spins, so that measurements of different species were obtained at 16 second intervals. The HERS sensor had energy windows that were of constant width in momentum per unit charge (rather than constant width in the logarithm of energy per unit charge as for a conventional electrostatic analyzer). Further description of the experiment is provided in Balsiger *et al.* (1986a); first results are reported in Balsiger *et al.* (1986b).

A number of different methods have been used to analyze Giotto HERS data. The consequence of constant momentum width windows is that, although good energy resolution is obtained for heavy ions, the energy window for alpha particles is 64 eV full width at half maximum, and for protons is twice as wide. Two problems result if a straightforward moment analysis is used: 1) the thermal broadening along the line of sight is overestimated, and 2) for low proton and alpha particle velocities, the bulk flow speed is overestimated due to the low energy cutoff (10 eV) of the instrument not being properly taken into account. Additionally, there is a cone of 15° half-angle centered on the cometary direction in which the HERS sensor does not obtain measurements. Goldstein *et al.* (1987, Figs. 1 and 3) used fits to a Maxwell-Boltzmann distribution integrated over the instrument response to estimate proton and alpha velocities, whereas the heavy ion velocities were calculated from a moment technique. Since that time, we have recalibrated the proton mode of the flight spare, and obtained an improved understanding of the instrument response to low energy protons. In the present paper, we obtain estimates of plasma parameters by assuming that distributions are spherically symmetric in velocity space. The density in a shell is then computed by averaging over the observations within the shell. The velocity of the distribution (i.e., center of the shells) is adjusted using an iterative least squares technique to reduce the error in a fitting parameter. This fitting parameter is the first moment of the distribution obtained by integrating over the instrument field of view, and it is compared to the first moment obtained by integrating the assumed distribution over the instrument field of view. This procedure corrects for errors if a portion of a spherical shell is out of the field of view; however, it can not compensate for an entire shell being out of the field of view. This happens in the cold, dense region of the inner coma when the bulk velocity relative to the spacecraft is nearly from the ram direction. In Figure 1 we have plotted the velocity of water group ions in instrument coordinates obtained by the HERS sensor as estimated from model fits to the HERS data. The datum points represent data averaged over time periods ranging from approximately two minutes when close to the comet to eight minutes when far from the comet. The measurements obtained by the HERS sensor should include all velocity shells up until about 23:38 (102,000 km from the comet), after this time it can not be said with complete assurance that none of the cold plasma has been missed because the estimated velocities fall very close to the boundary of the 15° half-angle cone. When the center of the distribution falls well within the 15° half-angle cone (i.e., the last four points starting at 23:44:51 UT, within 75,000 km of the nucleus), then the cold core of the distribution is definitely not seen by the HERS sensor. The estimate of plasma direction may also be verified by comparison to data from the High Intensity Spectrometer (HIS) of the IMS (see Fig. 6 below). Improved density and compositional measurements obtained by the HERS experiment have recently been submitted for publication

(Neugebauer *et al.*, 1990); similar field of view effects apply to these densities and abundances as well. The data obtained by the High Energy Range Spectrometer (HERS) of the IMS that are published herein have also been provided to the International Halley Watch archive.

REVISED PROTON AND ALPHA PARTICLE MEASUREMENTS

The general features of the outer cometosheath have been described by Balsiger *et al.* (1986), Neubauer *et al.* (1986), Johnstone *et al.* (1986), Goldstein *et al.* (1987), Glassmeier *et al.* (1987), Rème *et al.* (1987), and others. In particular, Goldstein *et al.* (1987) have published earlier HERS alpha particle analyses, and HERS parameters for all species including protons have been submitted to the National Space Science Data Center. Our newly reduced proton and alpha particle measurements using the revised techniques just discussed in this paper have been submitted to the NSSDC and the International Halley Watch archives. We publish these revised estimates herein. Due to the upper energy limit of the HERS sensor, and counting statistics, only H^+, m/q=2, and m/q=4 observations were obtained at distances greater than 250,000 km. The m/q=2 particles are either He^{++} or H_2^+, and the m/q=4 particles are He^+. Shelley *et al.* (1987) have discussed the conversion of He^{++} to He^+. Fuselier *et al.* (1988, 1990).have investigated the pick-up of H_2^+; the m/q=2 species is composed almost entirely of He^{++} until after 23:30 UT (125,000 km from the nucleus). The plasma parameters are shown in Figure 2 for the period 19:00 UT to 24:00 UT. The speed (km/sec) in a comet centered frame is shown in the upper panel, the next panel shows number density (cm^{-3}, alpha particle densities are multiplied by 10), the next shows log temperature (°K), and the lowest panel shows pressure (dynes/cm^2). Proton parameters are shown as solid lines, alpha particles parameters as dashed lines, and water group parameters as dotted lines. The water group temperature does not include contributions from particles in velocity shells with radii greater than 100 km/sec. It can be seen that there is excellent agreement between the proton and He^{++} speeds until about 21:45; after this time there is an increasing divergence of the estimates. As mentioned, the instrument has a rather broad energy acceptance for protons, and we interpret this difference as most likely to be due to poor velocity resolution for protons. The alpha velocity should be better determined than the proton velocity in this region.

HEAVY ION DISTRIBUTIONS

The general characteristics of heavy ion distributions should depend upon the injection of pick-up ions, their scattering in pitch angle and energy, adiabatic (de)compression as the plasma is compressed(expands) and loss by recombination or charge exchange. At distances for which HERS could obtain measurements, recombination is unimportant (Ip,1989), but the data provide support for the importance of scattering in pitch angle and loss by charge exchange. To demonstrate the importance of pitch angle scattering, we show in Figure 3 contours of common logarithm of phase space density of water group ions for a 5 minute averaging period centered at 23:27:39 UT. For this period the average location for a picked-up ring-beam distribution was at a pitch angle of 71.7° from the magnetic field direction with a velocity amplitude of 29.6 km/sec. The

expected location for the pick-up beam is indicated by the cross. It can be seen that the pick-up location is within the region (dark grey) of maximum phase space density. There is also evidence for considerable scattering in pitch angle; a shell (light grey region) has been formed that includes the pick-up location. Although pitch angle scattering is clearly very important, it is not sufficiently rapid to obliterate the peak in the vicinity of the pick-up location. It can be seen that diffusion not only in pitch angle, but also in velocity, has occurred with the particles being scattered to lower velocities than the pick up velocity. Yoon (1990) and Yoon and Ziebbell (1990) have discussed mechanisms that cause diffusion in energy.

To investigate the evolution of the distribution as the comet is approached, we show the water group ion densities in two different formats. In Fig.4 are shown the phase space densities averaged over spherical velocity shells with the bottom line being the earliest data and the top line being the latest. The leftmost value plotted (smallest value of shell radius) varies from case to case because of poor counting statistics when the phase space volume of the shell is small. Comparison with the water group speed in the comet frame (vertical arrows marked on plots) shows that the peak of the distribution appears at (or just below) the local pick-up velocity. There are no observations at the last time shown (23:52 UT) for the lowest velocity shells because the cold distribution has moved into the unobserved cone in the ram direction (see Fig. 1).

At 254,000 km (23:00:30) there are higher densities in the region 50 to 60 km/sec radii than in the lower velocity shells (the apparently larger value in the 10-20 km/sec radii may be counting statistics as the volume of this portion of phase space is relatively small). The enhancement in the 50 to 60 km/sec radii region is reasonably good agreement with a pick-up velocity of 63 km/sec (plasma velocity in the comet frame) at this time; the center of the distribution (shell radii of 50 km/sec or less) has not been filled in by energy diffusion. As the comet is approached, the pick-up velocity decreases and the number of neutrals being ionized increases; for these reasons one would expect that the density in intermediate shells should increase, and then the density in the lowest velocity shells should increase later to even larger values. As expected, the peak of the distribution moves to lower velocities at later times. These changes are shown more quantitatively in Figure 5. At the highest energy shells shown (radii of 50-60 km/sec) the phase space density decreases from 23:05 to 23:14, whereas in the next highest velocity shells (radii of 40-50 km/sec) the phase space density is are simultaneously increasing. The phase space densities in these shells is roughly constant from 23:10 to 23:40 (220,000 to 95,000 km), and then decreases rapidly due to charge exchange in the near vicinity of the comet (after about 23:45 UT, within 95,000 km). The other, lower velocity, shells, (with the exception of 0 to 10 km/sec) all show a pattern of increasing flux as the comet is approached, followed by a decrease during later times. The shells from 30-40 km/sec show a possible modest decrease from 23:25 to 23:40, before the precipitous decrease after 23:40 caused by charge exchange. It could be argued that a similar decrease occurs in the 40-50 km/sec shells from about 23:20 to 23:40, although the data are somewhat scattered and could equally well be argued to show no change during this period. The cause of the drop in the 30-40 km/sec shell radius region from 23:25 to 23:40 is unclear. Charge exchange might be occurring, although the neutral densities in

these regions are low. Adiabatic compression due to flow deceleration would affect the distribution function, by increasing the local spatial density, but moving particles to shells with larger velocity radii. However, as the phase space density in the 20-30 km/sec region was equal to or greater than the value in the 30-40 km/sec region, the net effect of adiabatic compression would be to increase the phase space densities in the 30-40 km/sec shell region during the period 23:20 to 23:40. Diffusion in energy space would also tend to decrease phase space densities in peak regions (radii of 30 km/sec or less during this period), and increase it at greater distances. Thus, the flat behavior of the 50-60 km/sec region from 23:20 to 23:40, the decrease in the 30-40 km/sec region, and the debatable behavior in the 40-50 km/sec region may result from a balance of several processes. Detailed comparisons with theoretical models will be required to further understand these behaviors.

MAGNETIC PILE-UP BOUNDARY (MPB, OR "COMETOPAUSE")

At 135,000 km from the nucleus (23:30:00 UT), the spacecraft passed through a discontinuity designated as the magnetic pile-up boundary (Neubauer, 1987). A somewhat similar boundary observed by the plasma experiment on the VEGA spacecraft (Gringauz *et al.*, 1986) was referred to as a "cometopause" and was interpreted as a region in which a rapid build-up of cometary ions occurs. Neubauer (1987) concluded that the MPB had to be either a tangential discontinuity, or a slowly propagating rotational discontinuity with strongly differing plasma properties on either side. The plasma distribution from just before the MPB shown in Fig. 3 has no strong anisotropy; nor is there a strong anisotropy in the distribution (not shown) just after the MPB. The MPB has been of some interest because of interpretations that it might be due to a rapid charge exchange of plasma ions with neutrals with a run-away rapid growth due to deceleration of the flow by the pick-up process. Our data, however, do not show any remarkable changes in the properties of the heavy ion distributions across the pile-up boundary (Figs. 4,5), but do show a discontinuity in the properties of the protons and alpha particles (Fig.2, see also Fig. 2 of Goldstein *et al.* (1987) and Fig. 4 of Neugebauer *et al.* (1990)).

If the MPB is a tangential discontinuity, there should be no flow across it. The normal to the discontinuity is (.097, .993, -.059) in HSE coordinates (Neubauer, 1987); i.e., the normal is almost exactly in the y-direction. We compute (Table 1) the HSE velocity difference in km/sec, $\Delta V = V_{outside} - V_{inside}$, across the interface using HERS proton, alpha particle, and water group data, and HIS water group data. Also shown in Table 1 is the angle, θ, between the velocity difference and the normal to the discontinuity. If the MPB is a tangential discontinuity, then for an ideal MHD fluid ΔV_y should be zero and θ should be 90°. Because of time variations in the data, we have taken both 2.5 and 5 minute averages on either side. Because the HERS water group parameters were not available at 2.5 minute intervals upstream of the MPB the 5 minute value upstream was used for both the 2.5 and 5 minute cases. Upstream 2.5 minute averages were not available for HERS water group data because it was necessary to have longer integration periods further from the comet, and the MPB happened to be a location where the integration period was changed in the analysis. It can be seen that the alpha

particle and proton velocity differences are at a substantial angle to the normal to the discontinuity, about 65° to 70°. The fact that this angle is not 90° (as would be expected for a tangential discontinuity) might be attributable both to error in determination of the normal to the discontinuity (λ_2/λ_3 was 12.5, Neubauer, 1987), and, more likely, to errors in measurement of both proton and alpha particle velocities. The water group ΔV_z estimates from HIS and HERS disagree by about 4 km/sec; the cause of this is unknown and may reflect measurement error. The ΔV_y component (i.e., the normal component, which should be zero for a tangential discontinuity) of the alpha velocity changes in sign according to whether 2.5 or 5 minute averages are used. Both HIS and HERS find a decrease of 2.5 to 3 km/sec in the y-component of the water group velocity as the spacecraft crosses the MPB. Since the ΔV_y result does not depend upon averaging period, and both experiments agree, we believe this result is probably real, but are not absolutely certain because of the unexplained disagreement in the ΔV_z estimate.

TABLE 1

ANGLES BETWEEN COMETOPAUSE NORMALS AND VELOCITY CHANGES

	ΔV_x	ΔV_y	ΔV_z	θ
protons, 5 minute averages	7.9	3.4	-8.2	67
protons, 2.5 minute averages	9.8	3.7	-5.4	65
alphas, 5 minute averages	8.7	-9.5	-13.5	65
alphas, 2.5 minute averages	7.5	4	-14.5	71
water group, HERS, 5 minute avg.	-4.5	-2.5	3.5	60
water group, HERS, 2.5 minute avg.	-3.0	-3.0	3.0	48
water group, HIS, 5 minute avg.	-2.0	-2.8	-1.1	36
water group, HIS, 2.5 minute avg.	-2.9	-3.0	-1.0	42

The 2.5 minute averages of proton and alpha particle densities before the MPB are 5.9 cm^{-3} and 0.21 cm^{-3}, respectively, whereas after the MPB the corresponding values are 2.8 cm^{-3} and 0.13 cm^{-3}. The sharp drop in both alpha and proton densities at the MPB support Neubauer's suggestion that the MPB is a tangential discontinuity, and are inconsistent with his alternative suggestion that the MPB is a slowly propagating rotational discontinuity. The tangential discontinuity hypothesis, however, appears to be inconsistent with the marginal evidence for normal flow of water group ions across the boundary. One explanation might be

the presence of multi-fluid (proton and water group) waves as proposed by Sauer and Motschmann (1989).

We have attempted to verify the pressure balance across the tangential discontinuity. However, this requires estimating perpendicular and parallel temperatures for the water group ions; accurate values are necessary as the water group dominates the plasma pressure. Unfortunately, the variation (due to counting statistics and background) between estimates of the pressures made using different techniques is so large that it precludes an accurate estimate of the pressure change across the MPB.

COMPARISON TO MHD MODELS

Wegmann *et al.* (1987) and Schmidt and Wegmann (1990) have undertaken a numerical MHD model of the dynamical flow and chemical reactions of the plasma at Comet Halley. The dynamics are treated with a three dimensional single fluid model, while the compositional variations are computed in a two dimensional axially symmetric flow field. The Schmidt and Wegmann paper uses a grid refined by a factor of two over that used by Wegmann *et al.* , and corrects an error in the calculation of the ion temperature. A comparison between the large scale flow direction observed by the IMS and the MHD calculations of Wegmann *et al.* (1987) is shown in Fig. 6. The data are plotted in aberrated solar wind coordinates. We have defined these coordinates with the x axis pointing opposite to the direction of the upstream solar wind flow (taken to be {-365.,-17,17} km/sec in Halley solar ecliptic coordinates), with the y axis in the plane containing the spacecraft-comet velocity difference in the approximate direction of the HSE y coordinate. In these aberrated coordinates the angle between the upstream direction and the comet-spacecraft velocity difference is 103° (rather than the 107° angle between the HSE x-axis and the velocity difference), and there is a rotation of roughly 11° in the y-z plane from the HSE y-z components. The units of the axes are megameters. The spacecraft trajectory is shown as the sloping line. At large distances from the comet the best velocity measurements obtained by the experiment are given by alpha particle data; these data are plotted as vectors extending upwards from the trajectory. Closer to the comet the HERS instrument obtains water group data; these data are shown as the lines extending downwards from the trajectory. Finally, closest to the comet the best data are water group data obtained by the HIS sensor and are shown as lines extending upwards from the trajectory. The HIS velocity vectors shown are based upon the same data set described by Kettmann et al. (1990), but are rotated into aberrated coordinates (two different methods of data reduction were used by them; the data shown in Fig. 7 are that from their method of ignoring the innermost angular channel during the last ten minutes before encounter). The alpha particle data may be distinguished from the HIS data due to their separation by a gap in the upwards pointing lines. Different scales are used for plotting the alpha particle velocities and the water group velocities. The short vertical line in the lower center of the figure is the length of a 100 km/sec alpha particle vector in the plot, and is also the length of a 20 km/sec water group vector (both HIS and HERS). It can be seen that there is generally good agreement between the flow directions predicted by the model and the observations. One

exception to this rule is the strong deflection observed just inside the bow shock that is not predicted by the MHD model (which does not resolve the shock well)

In Fig. 7 is shown a comparable plot of the HIS data for the region within 30,000 km of the nucleus; the units of the axes are 10^4 km and the vertical line in the lower center of the figure denotes a vector that is 10 km/sec in magnitude. The data are compared to the calculation of Wegmann *et al.* (1987) for the flow in the plane perpendicular to the magnetic field, and it can be seen that overall there is good agreement (except close to the comet). By contrast, Wegmann *et al.* (1987) have also presented the flow in the plane containing the magnetic field. In this plane the recombining plasma can flow down along field lines towards the comet, and the flow close to the comet is actually converging towards the comet rather than diverging from it. (This would be the case if the interplanetary magnetic field were in the ecliptic plane and if the comet had been approached in a trajectory lying in the ecliptic.) The Wegmann *et al.* calculations would also predict an ionopause elliptical (rather than circular) in cross-section, with the greater width in the direction not confined by draped magnetic fields. This might account for a tilt of the ionopause surface reported by Neubauer (1987, see Fig. 4). The plasma velocity observations do not agree at all (comparison not shown) with the flow pattern predicted by Wegmann *et al.* (1987) for the plane containing the magnetic field.

Which case should apply is problematic. Neubauer (1987) reports that the angle of the magnetic field out of the ecliptic plane is large and variable close to the comet. This suggests that the situation should be a compromise between the two cases reported by Wegmann *et al.* (1987); however, as mentioned earlier, the flow pattern observations agree very well with the calculation for the flow in the plane perpendicular to the magnetic field.

It may also be noted that the flow directions observed by the HIS angle analyzer within about 10,000 km of the comet do not agree with reasonable expectations. This is in part due to observational difficulties; the plasma is flowing past at 68 km/sec in the spacecraft frame and we are trying to measure a small deviation from this value. A further problem is that as the comet is approached the plasma gets colder, and eventually most of it lies in the field of view of the innermost angle analyzer. However, as the count rate became higher, some problem with this angular channel became apparent (Kettmann *et al.*, 1990), so the data that we present here are derived ignoring this channel. This means that we do not have a good measurement of the velocity component in the ram direction from HIS angle analyzer alone during the last several minutes. It is possible that recently completed reductions and analyses of the HIS mass analyzer calibrations may allow use of the mass analyzer data to resolve these ambiguities in the future.

In Fig. 8 are shown comparisons to other parameters of the MHD model of Schmidt and Wegmann (1990). The plasma parameters plotted are proton density, alpha particle velocity, water group density, velocity, and temperature as measured by the HERS, and water group velocity and temperature as measured by HIS. Comparing first the velocity prediction of the Schmidt and Wegmann paper to the alpha observations, we notice that there is excellent agreement in the outer portions of the comet (R greater than 250,000 km). At 250,000 km there is

good agreement between both the prediction, the alpha particle velocity, and the water group velocities that the HERS detector observed beginning at that distance. However, at about 200,000 km a very noticeable difference has developed between the observation of the water group ions and the predictions of the model (we do not compare to the alpha velocities, which disagree with the water velocities, because the water group dominates the mass and the alpha velocity determination becomes less reliable as the comet is approached). Simultaneously, a large increase in the ion density above the values predicted by the model is observed.

It is not surprising that the model would simultaneously underestimate the density and overestimate the velocity. If too much pick-up plasma were added to the flow, conservation of momentum would require a reduction in the flow velocity. Alternatively, if for some reason the model gives too low a flow velocity, there would be greater time for addition of mass to the flow. For example, an underestimate of the neutral ionization rate might cause these disagreements. The MHD calculation assumed a single fluid, whereas the cometary plasma is composed of both solar wind protons and cometary pick-up ions. However, throughout the region where the disagreement occurs (250,000 to 25,000 km), the plasma mass density is strongly dominated by the pick-up ions, so it does not seem likely that relative velocity differences between solar wind and pick-up ions could explain the discrepancy. Temporal variation in the upstream solar wind density and velocity might also cause errors in the prediction.

Another noteworthy disagreement between the model and the observations is the apparent increase in observed HIS ion temperature above predicted values within 10,000 km of the nucleus, and below predicted values for distances between 16,000 to 250,000 km from the comet. The measured temperatures in the region close to the comet are in agreement with similar temperatures reported by Schwenn et al. (1987) from IMS-HIS mass analyzer data, and by Lämmerzahl et al. (1987) from neutral mass spectrometer data. A one dimensional MHD model of the inner coma (Cravens, 1989) does predict a region of increased temperature due to ion-neutral friction in the collisionally coupled region external to the ionopause. The region in which the temperatures measured by HERS and HIS are lower than the model (16,000 km to 250,000 km from the nucleus) can be explained by two possibilities. First, the two fluid nature of the plasma might result in some of the internal kinetic energy of the flow being maintained as a relative drift between solar wind ions and cometary ions. Although we did not regard such a two fluid effect as a likely explanation of the density/velocity discrepancy, the temperature of the plasma is much more sensitive to such effects. Second, the HERS temperatures were calculated using a cut-off for velocity shells with radii greater than 100 km/sec, and the HIS temperatures were calculated from Maxwell-Boltzmann fits to the total distribution. It is possible that there might be a hot unobserved or unmodelled shell at larger energies, and that the measured temperatures are too low. However, even at distances less than 30,000 km the disagreement is quite striking, and at such distances the mass and temperature should be dominated by the cold pick-up plasma. So, we do not believe that observational errors account for the disagreement.

ACKNOWLEDGEMENTS

The research at JPL was done under a contract between the California Institute of Technology and the National Aeronautics and Space Administration under the the sponsorship of the Magnetospheric Physics program. Research at Lockheed was supported by NASA through contract NASW-4336. The work was also supported by the Swiss National Science Foundation and the German Bundesministerium für Forschung and Technologie.

REFERENCES

Balsiger, H., K. Altwegg, F. Buehler, J. Fischer, J. Geiss, A. Meier, U. Rettenmund, H. Rosenbauer, R. Schwenn, J. Benson, P. Hemmerich, K. Sager, G. Kulzer, M. Neugebauer, B. E. Goldstein, R. Goldstein, E. G. Shelley, T. Sanders, D. Simpson, A. J. Lazarus, D. T. Young, in The Giotto Mission-Its Scientific Investigations, ESA-SP1077, eds. R. Reinhard, B. Battrick, p. 129, 1986a.

Balsiger, H., K. Altwegg, F. Buehler, J. Geiss, A. G. Ghielmetti, B. E. Goldstein, R. Goldstein, W. T. Huntress, W.-H. Ip, A. J. Lazarus, A. J. Meier, M. Neugebauer, U. Rettenmund, H. Rosenbauer, R. Schwenn, R. D. Sharp, E. G.Shelley, E. G. Ungstrup, D. T. Young, *Nature, 321,* 330, 1986b.

Coates, A. J., B. Wilken, A. D. Johnstone, K. Jockers, K.-H. Glassmeier, and D. E. Huddleston, Bulk Properties and Velocity Distributions of Water Group Ions at Comet Halley: Giotto Measurements, *J. Geophys. Res., 95,* 10249, 1990.

Cravens, T. E., A magnetohydrodynamical model of the inner coma of Comet Halley, *J. Geophys. Res., 94,* 15025, 1989.

Fuselier, S. A., E. G. Shelley, B. E. Goldstein, R. Goldstein, M. Neugebauer, W.-H. Ip, H. Balsiger, and H. Rème, Observations of Solar Wind Ion Exchange in the Comet Halley Coma, draft manuscript, 1990.

Fuselier, S. A., E. G. Shelley, H. Balsiger, J. Geiss, B. E. Goldstein, R. Goldstein, and W.-H. Ip, Cometary H_2^+ and Solar Wind He^{2+} Dynamics Across the Halley Cometopause, *Geophys. Res. Letts., 15,* 549, 1988.

Glassmeier, K. H., F. M. Neubauer, M. H. Acuña, and F. Mariani, Low-frequency magnetic field fluctuations in comet P/Halley's magnetosheath: Giotto observations, *Astron. Astrophys., 187,* 65, 1987.

Goldstein, B. E., M. Neugebauer, H. Balsiger, J. Drake, S. A. Fuselier, R. Goldstein, W.-H. Ip, U. Rettenmund, H. Rosenbauer, R. Schwenn, and E. G. Shelley, Giotto-IMS observations of ion-flow velocities and temperatures outside the magnetic cavity of comet P/Halley, *Astron. Astrophys., 187,* 174, 1987.

Gringauz, K. I., T. I. Gombosi, M. Tatrallyay, M. I. Verigin, A. P. Remizov, A. K. Richter, I. Apathy, I. Szemerey, A. V. Dyachkov, O. V. Balakina, A. F. Nagy, *Geophys. Res. Letts., 13,* 613, 1986.

Ip, W.-H., On charge exchange effect in the vicinity of the cometopause of Comet Halley, *Astrophys. J., 343,* 946, 1989.

Kettmann, G., W.-H. Ip, H. Balsiger, B. E. Goldstein, A. Meier, H. Rosenbauer, R. Schwenn, and E. G. Shelley, Cometary Ion Flow Variations at Comet P/Halley as Observed by the Giotto IMS Experiment, *Annales Geophysicae, 8,* 229, 1990.

Lämmerzahl, P., D. Krankowsky, R. R. Hodges, U. Stubbemann, J. Wowries, I. Herrwerth, J. J. Berthelier, J. M. Illiano,P. Eberhardt, U. Dolder, W. Schulte, and J. H. Hoffman, Expansion velocity and temperatures of gas and ions measured in the coma of comet P/Halley, *Astron. Astrophys., 187,* 169, 1987.

Neubauer, F. M., K. H. Glassmeier, M. Pohl, J. Raeder, M. H. Acuna, L. F. Burlaga, N. F. Ness, G. Musmann, F. Mariani, Mk. K. Wallis, E. Ungstrup, H. U. Schmidt, First results from the Giotto magnetometer experiment at comet Halley, *Nature, 321,* 352, 1986.

Neubauer, F. M., Giotto magnetic-field results on the boundaries of the pile-up region and the magnetic cavity, *Astron. Astrophys., 187,* 73, 1987.

Neugebauer, M., F. M. Neubauer, H. Balsiger, S. A. Fuselier, B. E. Goldstein, R. Goldstein, F. Mariani, H. Rosenbauer, R. Schwenn, and E. G. Shelley, The variation of protons, alpha particles and the magnetic field across the bow shock of comet Halley, *Geophys. Res. Letts., 14,* 995, 1987.

Neugebauer, M., R. Goldstein, B. E. Goldstein, S. A. Fuselier, H. Balsiger, and W.-H. Ip, Densities and Abundances of Hot Cometary Ions in the Coma of P/Halley, accepted for publication, *Astrophys. J.,* 1990.

Sauer, K., and U. Motschmann, Plasma Boundaries at Comet Halley, preprint, Institut für Kosmosforschung, Berlin, 1989.

Schmidt, H. U., and R. Wegmann, A MHD Model of Cometary Plasma and Comparison with Observations, to appear in the Proceedings of the 1989 Chapman Conference in Guildford, 1990.

Schwenn, R., W.-H. Ip, H. Rosenbauer, H. Balsiger, F. Bühler, R. Goldstein, A. Meier, and E. G. Shelley, Ion temperature and flow profiles in comet P/Halley's close environment, *Astron. Astrophys., 187,* 160, 1987.

Shelley, E. G., S. A. Fuselier, H. Balsiger, J. F. Drake, J. Geiss, B. E. Goldstein, R. Goldstein, W.-H. Ip, A. J. Lazarus, and M. Neugebauer, *Astron. Astrophys., 187,* 304, 1987.

Wegmann, R., H. U. Schmidt, W. F. Huebner, and D. C. Boice, Cometary MHD and Chemistry, *Astron. Astrophys., 187,* 339, 1987.

Yoon, P. H., Kinetic Instability Associated with Spherical Shell Distribution of Cometary Pickup Ions, *Geophys. Res. Letts., 17,* 1033, 1990.

Yoon, P. H., and L. F. Ziebbel, Development of Pitch Angle Anisotropy and Velocity Diffusion of Pickup Ion Shell Distribution by Solar Wind Turbulence, *J. Geophys. Res., 95,* 17085, 1990.

FIGURE CAPTIONS

Fig. 1 The velocity measured by HERS in instrument coordinates. The direction from the comet is downwards (along the vertical axis of the plot). The line at an angle of 15° from the comet direction represents the inner edge of the HERS sensor field of view. The modelling procedure used to estimate the bulk velocities can not compensate for velocity shells of cold pick-up ions that are entirely within the unobserved cone. Thus, the estimates do not approach the ram velocity (i.e., the vertical axis) as the comet is approached. The observation points are indicated by + symbols on the curve and are average values centered at the times (UT) given in the box on the plot. The first datum (23:13:40) is the leftmost point in the plot.

Fig. 2. Plasma parameters obtained by the HERS for the period 19:00 UT to 24:00 UT. The solid lines are proton data, the dashed lines are alpha particle data, and the dotted lines are water group data. The speed (km/sec) in a comet centered frame is shown in the upper panel, the next panel shows number density (cm^{-3}, the scale on the left is for protons and for alpha particles multiplied by 10, the scale on the right is for the water group ions), the next panel shows log temperature (K), and the lowest panel shows pressure ($dynes/cm^2$). The ion temperature does not include contributions from particles in velocity shells with radii greater than 100 km/sec.

Fig. 3. Contours of common logarithm of phase space density in units of $cm^{-6}sec^3$ of mass 17 ions for a 5 minute averaging period centered at 23:27:39 UT. The cross is at the location where new pick-up ions are created.

Fig. 4. Phase space densities (arbitrary units) of spherical velocity shells with the bottom line being the earliest data and the top line being the latest. The times shown on the figure are UT. The vertical arrows indicate the average pick up velocity during the period of measurement.

Fig. 5. Average phase space densities (units of $cm^{-6}sec^3$) in velocity space of spherical shells 10 km/sec in thickness. The data are similar to those shown in Fig. 4 except that the velocity space intervals are 10 km/sec, and the time centers of the averaging intervals are different. The format allows numerical values to be ascertained without ambiguity.

Fig. 6. A comparison in aberrated HSE coordinates between the large scale flow direction observed by the IMS (HERS and HIS) and the MHD calculations of Wegmann *et al.* (1987, see their Fig. 3b). The units of the axes are 10^6 km. See text for interpretation of magnitude of vectors.

Fig. 7. A comparison in aberrated HSE coordinates between the large scale flow direction observed by the HIS and the MHD calculations of Wegmann *et al.* (1987, see their Fig. 4b). The units of the axes are 10^4 km. The vertical line in the lower center of the figure is the length of a 10 km sec velocity vector.

Fig. 8. A comparison between flow parameters measured by the IMS and the MHD calculations of Schmidt and Wegmann (1990). N, v, and T_i, are the number density, the velocity, and the ion temperature of the calculation (medium thickness lines), N_W, V_W, and T_W, are the number density, velocity, and temperature of water group ions as measured by the HERS sensor (heaviest lines), and (thinnest lines) N_p is proton number density, V_a is the velocity of the alpha particles, V_h and T_h are the velocity and temperature of the water group ions as measured by the HIS sensor.

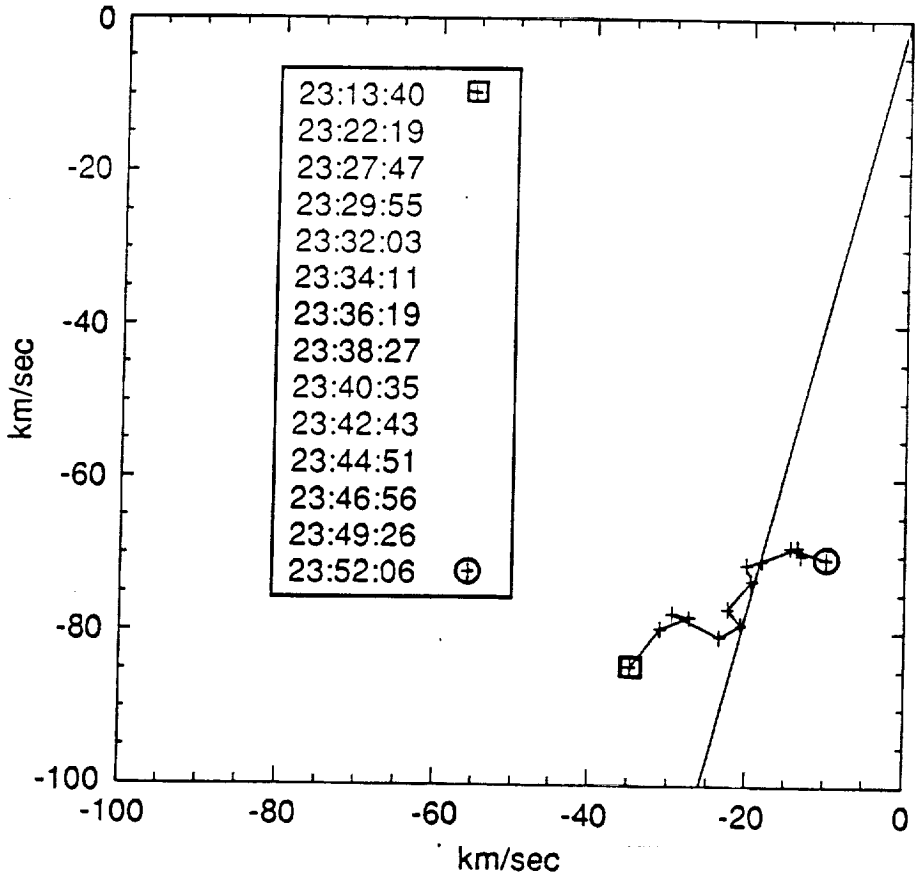
23:13:40
23:22:19
23:27:47
23:29:55
23:32:03
23:34:11
23:36:19
23:38:27
23:40:35
23:42:43
23:44:51
23:46:56
23:49:26
23:52:06
0
-20
-40
-60
-80
-100
km/sec
-100
-80
-60
-40
-20
0
km/sec

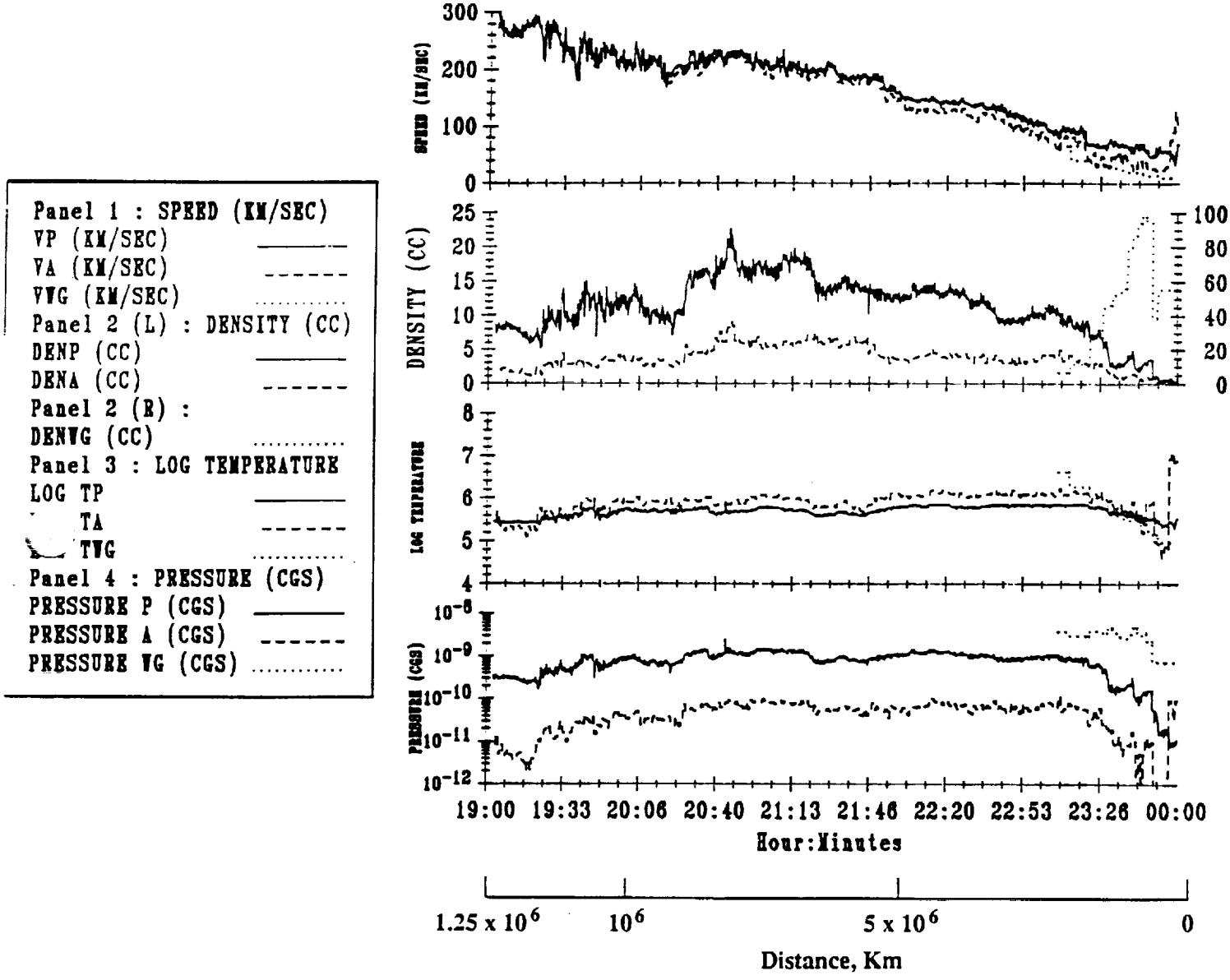
Panel 1 : SPEED (KM/SEC)
VP (KM/SEC)
VA (KM/SEC)
VVG (KM/SEC)
Panel 2 (L) : DENSITY (CC)
DENP (CC)
DENA (CC)
Panel 2 (R) :
DENVG (CC)
Panel 3 : LOG TEMPERATURE
LOG TP
TA
TVG
Panel 4 : PRESSURE (CGS)
PRESSURE P (CGS)
PRESSURE A (CGS)
PRESSURE VG (CGS)
SPEED (KM/SEC)
300
200
100
0
DENSITY (CC)
25
20
15
10
5
0
100
80
60
40
20
0
LOG TEMPERATURE
8
7
6
5
4
PRESSURE (CGS)
10^{-8}
10^{-9}
10^{-10}
10^{-11}
10^{-12}
19:00 19:33 20:06 20:40 21:13 21:46 22:20 22:53 23:26 00:00
Hour:Minutes
1.25×10^6
10^6
5×10^6
0
Distance, Km

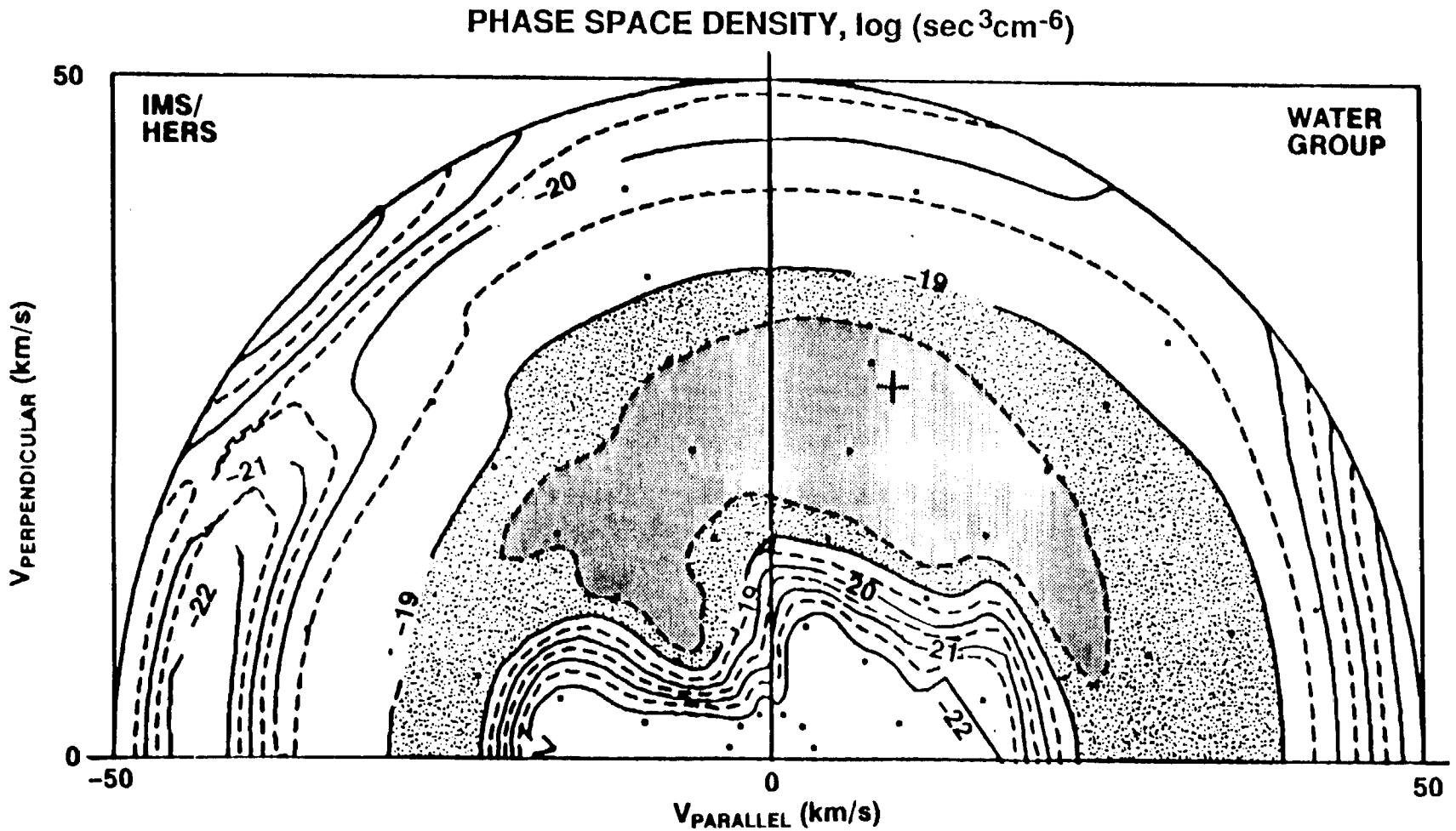
PHASE SPACE DENSITY, log (sec^{3}cm^{-6})
IMS/
HERS
WATER
GROUP
-20
-19
-21
-22
-19
-19
-20
-21
-22
50
0
-50
0
50
$V_{PERPENDICULAR}$ (km/s)
$V_{PARALLEL}$ (km/s)

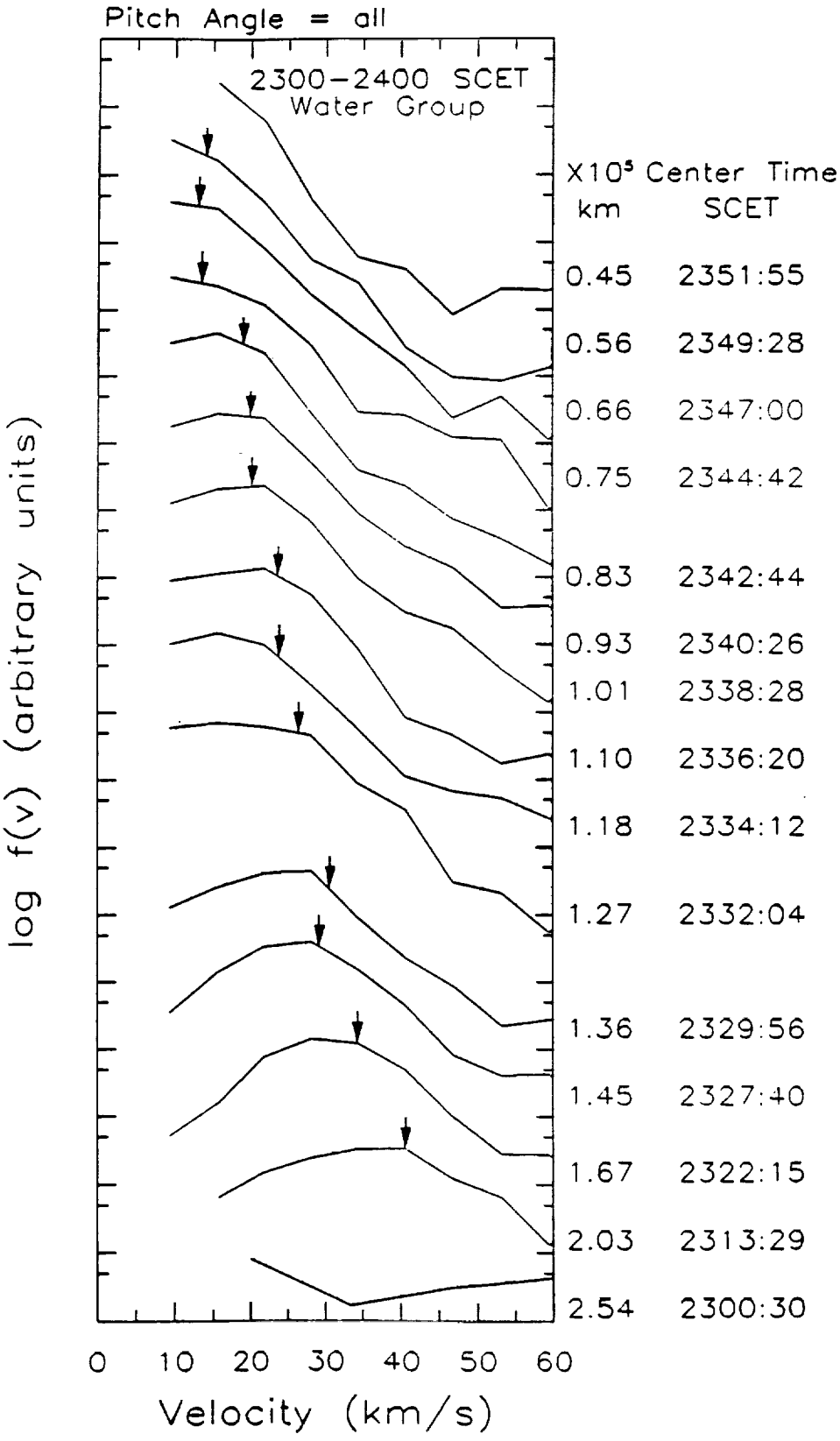
Pitch Angle = all
2300–2400 SCET
Water Group
X10⁵ km
Center Time SCET
0.45 2351:55
0.56 2349:28
0.66 2347:00
0.75 2344:42
0.83 2342:44
0.93 2340:26
1.01 2338:28
1.10 2336:20
1.18 2334:12
1.27 2332:04
1.36 2329:56
1.45 2327:40
1.67 2322:15
2.03 2313:29
2.54 2300:30
log f(v) (arbitrary units)
0 10 20 30 40 50 60
Velocity (km/s)

IMS/HERS 13 Mar 1986

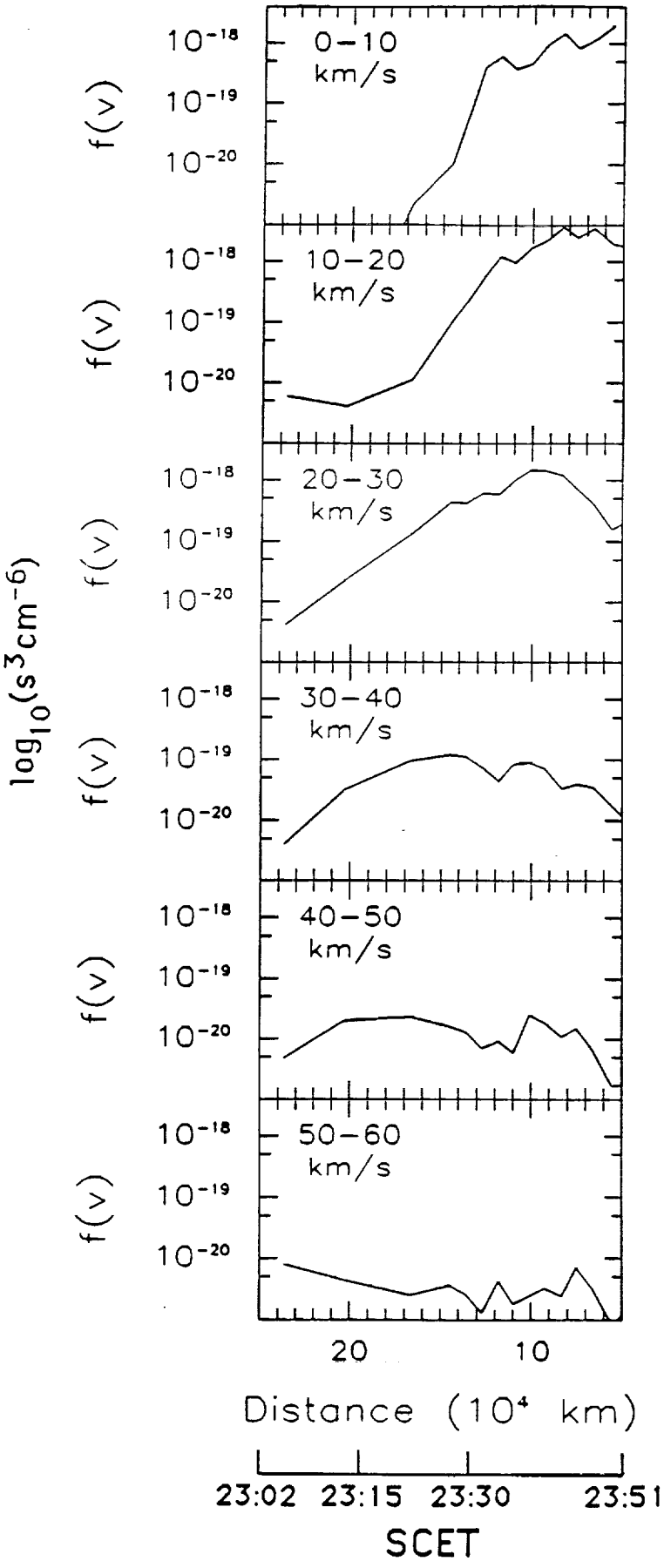

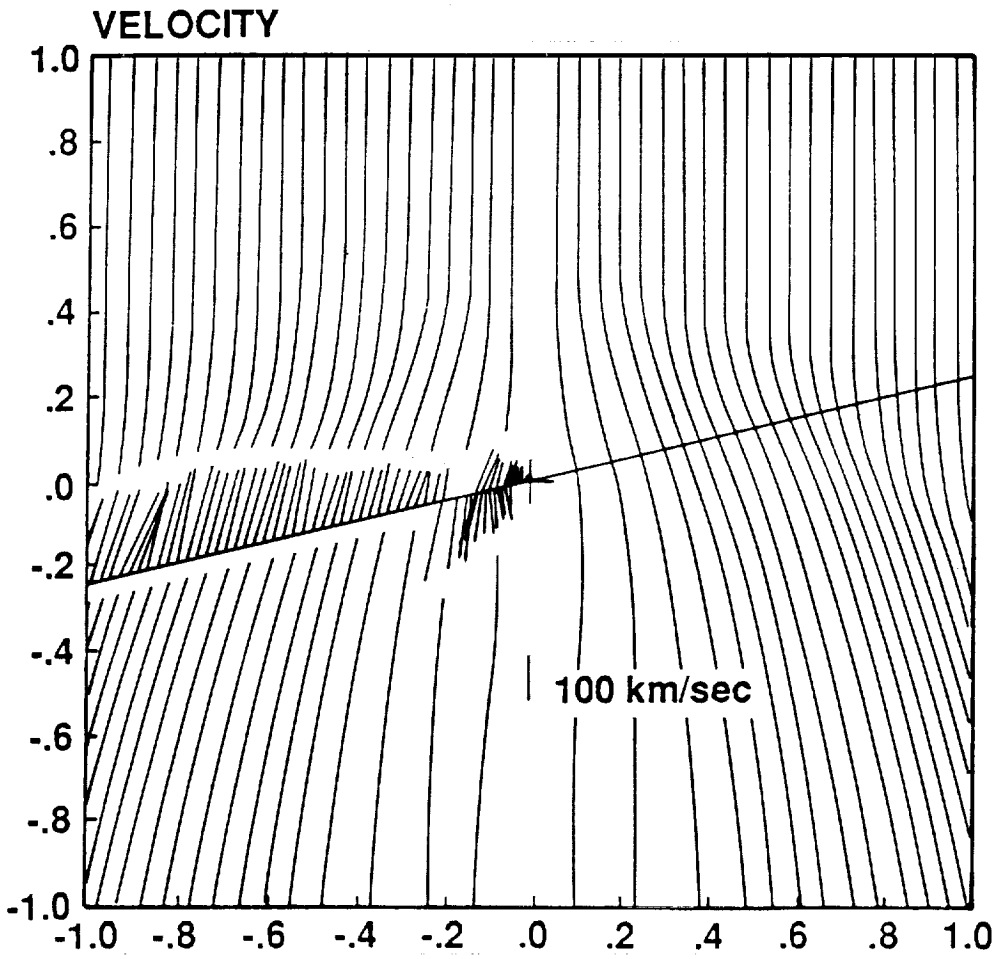
VELOCITY
1.0
.8
.6
.4
.2
.0
-.2
-.4
-.6
-.8
-1.0
-1.0 -.8 -.6 -.4 -.2 .0 .2 .4 .6 .8 1.0
100 km/sec

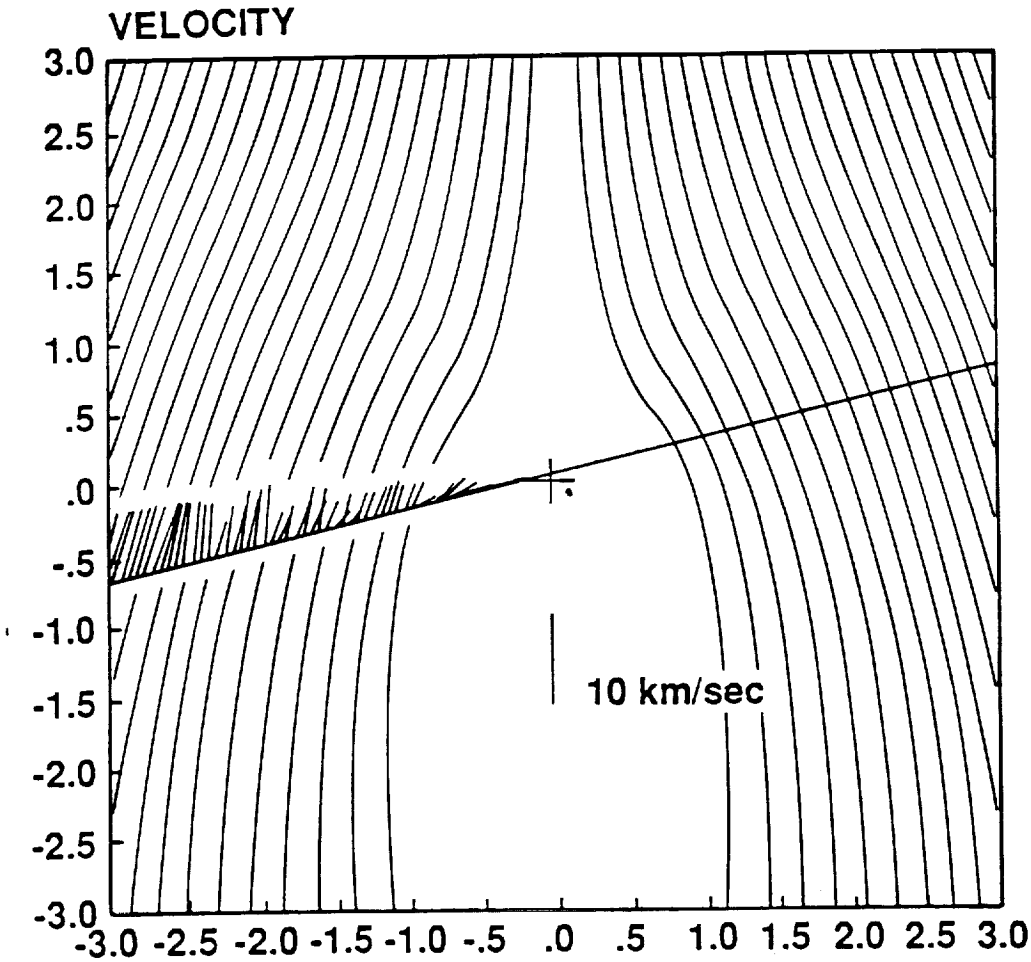
VELOCITY
3.0
2.5
2.0
1.5
1.0
.5
.0
-.5
-1.0
-1.5
-2.0
-2.5
-3.0
-3.0 -2.5 -2.0 -1.5 -1.0 -.5 .0 .5 1.0 1.5 2.0 2.5 3.0
10 km/sec

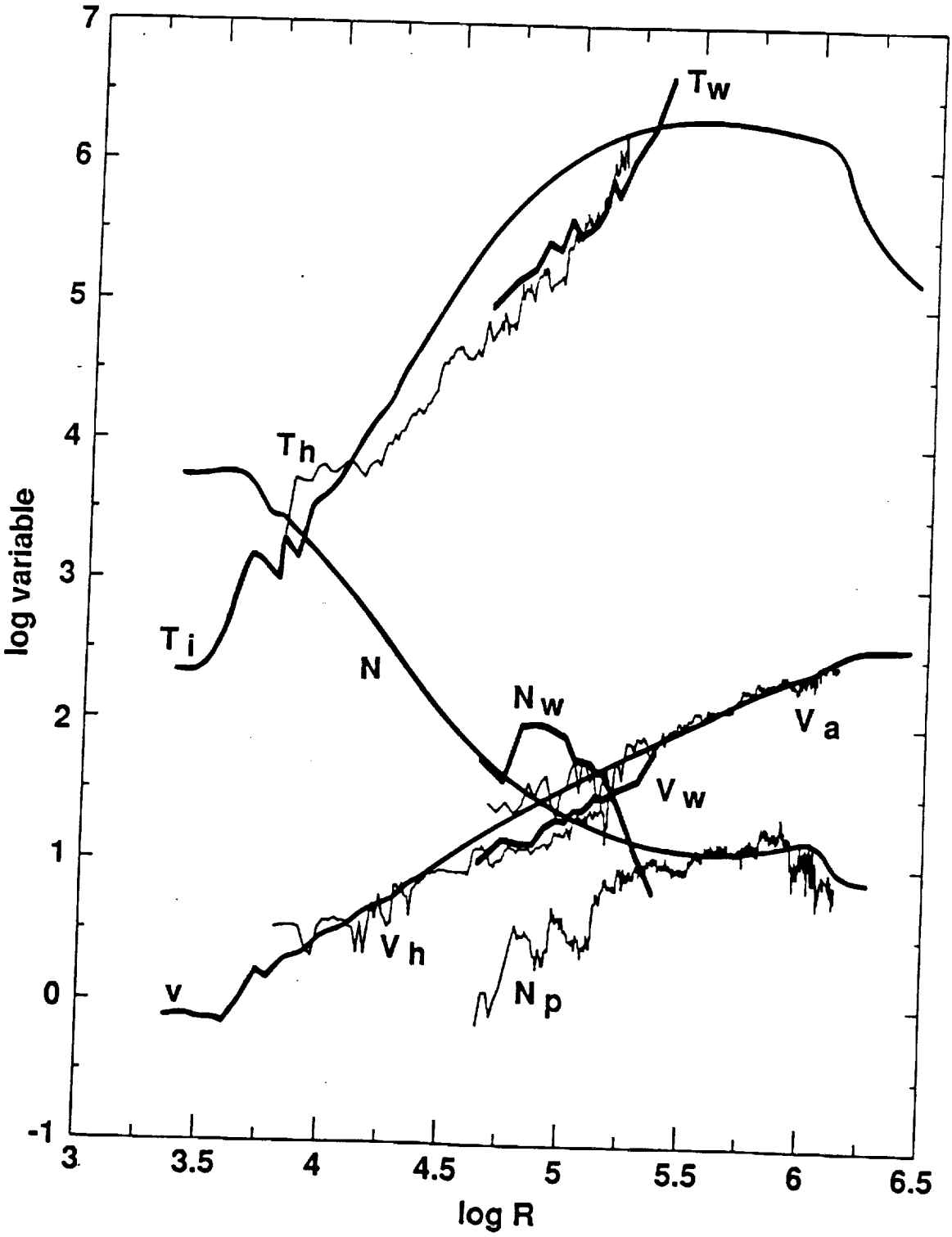
7
6
5
4
3
2
1
0
-1
3
3.5
4
4.5
5
5.5
6
6.5
log variable
log R
Tw
Th
Ti
N
Nw
Va
Vw
Vh
v
Np

Interpretation of the ion mass spectra in the mass range 25-35 obtained in the inner coma of Halley's comet by the HIS-sensor of the GIOTTO IMS Experiment

J. Geiss[1], K. Altwegg[1], E. Anders[1], H. Balsiger[1], W.-H. Ip[2], A. Meier[1], M. Neugebauer[3], H. Rosenbauer[2], E.G. Shelley[1,4]

[1]Physikalisches Institut, University of Bern, 3012 Bern, Switzerland
[2]Max-Planck-Institut für Aeronomie, D-3411 Katlenburg-Lindau, Federal Republic of Germany
[3]Jet Propulsion Laboratory and California Institute of Technology, Pasadena, California 91109, USA
[4]Permanent address: Lockheed Palo Alto Research Laboratory, Palo Alto, California 94304, USA

Running title:

Ion mass spectra in the inner coma of Halley's comet by GIOTTO IMS

Proofs and offprint requests to be sent to:

J. Geiss

Key word codes:

03.03.1, 03.07.1, 03.11.1, 19.06.1

Section 10:

The solar system

To be published in the Main Journal

Summary

The IMS-HIS double-focussing mass spectrometer that flew on the GIOTTO spacecraft covered the mass per charge range from 12 to 56 (AMU/e). By comparing flight data, calibration data and results of model calculations of the ion population in the inner coma, the absolute mass scale is established, and ions in the mass range 25 to 35 are identified. Ions resulting from protonation of molecules with high proton affinity are relatively abundant, enabling us to estimate relative source strengths for H_2CO, CH_3OH, HCN, and H_2S, providing for the first time a positive in situ measurement of methanol. Also upper limits for NO and some hydrocarbons are derived.

Key words: cometary atmosphere, mass spectrometry, ion spectra, molecular processes

1. Introduction

The composition of gases in the coma of comets can be studied by spectroscopy at various wave lengths of electromagnetic radiation, by mass spectrometric analysis of the neutral component, and by ion mass spectrometry. All these methods have their advantages and limitations, and it is their combination that has led to the advances in cometary chemistry that we have witnessed since the flight of spacecraft into the coma of Halley's comet.

In this paper, we use the data obtained by the HIS sensor of the IMS experiment (Balsiger et al., 1986) on the spacecraft GIOTTO during its passage through the inner coma of Halley's comet. The HIS is a double-focussing magnetic mass spectrometer with 9 channel electron multipliers (CEMs) arranged in a specially designed distributor, called an "Igel", at its exit (cf. Balsiger et al., 1986). It provides information on the mass/charge ratio, the velocity and the angles of incidence of the ions. Among the GIOTTO instruments, the capabilities of the HIS are unique for investigating the ion composition in the region between the cometopause (Gringauz et al., 1986) and the ionopause (Neubauer et al., 1986; Neubauer, 1987; Balsiger et al., 1986a) of Halley's coma.

The HIS, of course, also works in the low temperature (200-300 K) region inside the ionopause, but it is not simple to reduce the four-dimensional representation of these data (i.e. mass/charge, velocity and two angles of incidence) to a one-dimensional mass spectrum giving quantitative ion abundances, because the spectrometer response is not strictly a separable function of these four parameters. Thus, the

apparent mass/charge ratio depends somewhat on the velocity and direction of incidence. We have developed a method by which quantitative M/Q spectra are derived, using a scheme of adding CEM count rates combined with a fitting routine based on laboratory calibration data (Meier, 1988).

In contrast to previous attempts to reproduce the IMS mass spectra by ion-chemical modelling (e.g. Wegmann et al., 1987; cf. Schmidt et al., 1988), we use a model which concentrates on the ion mass range between 25 and 35 AMU/e in order to obtain better estimates of the parent molecule abundances which contribute to this ion mass range.

2. Experimental Results

The HIS sensor took data in two modes, the H- and the N-mode (Balsiger et al., 1986; Meier, 1988). Results obtained in the H-mode for the mass range 12 to 35 at nine distances from the nucleus are shown in Figs. 1 and 2. Each spectrum represents the data of one spin period, corresponding to a traversal of 273 km. The distances from the nucleus given in the figures are determined at the centers of the respective spin periods. The HIS instrument scans the voltage of the energy analyzer in 64 steps, covering the energy range appropriate for rammed cold ions with mass/charge 12 to 56. In the innermost part of the coma a countrate vs. measurement step plot represents a mass spectrum, because all cold ions have the same velocity in the instrument frame of reference, i.e. the ram velocity (68.4 km/s). The H- and N-mode are different in so far that in the H-mode all masses with the same

angle and velocity are measured by the same CEM, whereas in the N-mode different masses are deflected to different CEMs. Hence the H-mode is well suited to get full survey mass spectra (by plotting countrates vs. measurement step). However, the assignment of mass in the measurement step/CEM-matrix is dependent on ion speed, temperature and angle, and the detailed response of the matrix bins to each ion beam had to be carefully calibrated. Thus, for the purposes of this paper, we use the H-mode to give an overview of the spectra as a function of distance from the nucleus. The N-mode data are then used to derive relative ion abundances based on the calibrated response function.

Up to about mass 20, the identification of the ionic masses does not pose a problem, thus there is no uncertainty in the mass scale given in Fig. 1. This is supported by the fact that the calibration data predict the position of H_3O^+ where the highest ion peak is actually found. From this part of the spectrum, we can determine velocity and angle of incidence of the ions. If we then assume that the velocities and the flow directions are the same for all masses, we can assign an accurate mass scale to the higher masses as well. In Fig. 2, we give the H-mode spectra thus obtained for the ions in the range M/Q = 25-35.

The data displayed in Figs. 1 and 2 divide naturally into three spatial regions as can be recognized in the patterns of the spectra.

I. 1215 km - 3289 km. This region lies well inside the contact surface (Neubauer et al., 1986; Neubauer, 1987; Balsiger et al., 1986a). Here the counts are fairly evenly distributed in azimuth indicating that the flow direction coincides with the spin axis. The

ion temperature is less than 500 K. The M/Q patterns of the five spectra are fairly similar and indicate a good tuning of the instrument and a good mass resolution for the regular flow velocity encountered here.

II. 4365 - 6554 km. This region lies mainly outside the contact surface (at 4660 km, Neubauer, 1987). The counts are unevenly distributed over azimuth in this region, indicating a flow with a velocity component coming from the solar direction. This is consistent with expectation since bulk flow of the ions should follow roughly the contours of the contact surface. The 4365 km spectrum contains data from inside the contact surface. It was here that the HERS sensor detected hot cometary ions which may be due to the double charge-exchange mechanism (Goldstein et al., 1987; Eviatar et al., 1989). The flow conditions and distribution functions in region II are significantly different from those in region I. The poor mass definition and resolution shown for the region II spectra in Figs. 1 and 2 results from the fact that they were generated using the flow conditions prevailing in region I.

III. 9814 km. This spectrum is typical of the region outside ~7500 km. The azimuthal anisotropy is still observed, compatible with the expected flow pattern around the contact surface. The spectrum is similar to those in region I, with the exception of the strong count rate at M/Q = 32. The latter may result from a change in chemical composition with distance (i.e. there is a slow build-up of S^+; cf. section 4).

3. Interpretation of the spectra

This paper is concerned primarily with the ion mass range 25 to 35 AMU/e (Fig. 2) focussing on region I, i.e. the low temperature gas inside the contact surface. Here, photodissociation, photoionization, ion-molecule reactions, and dissociative recombination dominate the chemistry. The dominance of water vapor in the neutral gas together with its high proton affinity (PA) results in H_3O^+ being by far the most abundant ion. Thus, this ion governs the direction that the ion-molecule reactions take (Aikin, 1974). As a consequence, the PA of the molecules or radicals in the inner coma (Table 1) is the most important chemical parameter (Huntress, 1977), determining what the main ionized species are for a particular parent molecule.

Molecules (M) having a higher PA than water (cf. Table 1) react readily with H_3O^+ abstracting a proton:

$$H_3O^+ + M \rightarrow H_2O + MH^+ \ . \qquad (k1)$$

Consequently, the resulting MH^+ ions (Table 2, column 3) are very abundant relative to their parent molecules. For molecules containing H, C, and O, reactions with H_3O^+ have the effect of transforming a molecular mass spectrum dominated by even numbers into an ion mass spectrum dominated by odd numbers.

On the other hand, ions M^+ produced by simple photoionization (emission of an electron) from a molecule having a PA lower than water fall into two categories. If they react with water (e.g. CO^+, cf. Table 1)

$$M^+ + H_2O \rightarrow \text{products} \qquad (k2)$$

they will have a low abundance (Table 2, column 5). If they do not react with water (e.g. NO^+; cf. Table 1), they will have a rather long lifetime, governed in most cases by dissociative recombination, and thus they will accumulate towards a relatively high abundance (Table 2, column 4).

While these simple systematics are qualitatively valid, ion-molecule reactions with species other than the most abundant H_2O and H_3O^+ must be taken into account for a quantitative analysis. For this purpose, we have developed a numerical method which is simple, yet adequate for treating the radial evolution of ion abundances in the inner coma (Appendix A). The 21 neutral and 40 ion species listed in Table 3 were included in the calculations for the present paper. The parent molecules selected fall into three categories: (1) Those which could reasonably be expected and are essential to obtain an adequate fit to the data (e.g. H_2O, CO), (2) those which have been previously reported but cannot be positively confirmed or excluded by the data (e.g. N_2), and (3) theoretically possible molecules for which the data provide abundances (H_2CO, CH_3OH, NCN, H_2S) or meaningful upper limits (e.g. NO, hydrocarbons). Photodissociation and photoionization of all neutral species, dissociative recombination of the ions, and about 280 ion-molecule reactions were taken into account. Information on the rate constants that were used is given in Appendix B. While the expansion velocity could be introduced into the program as a function of radial distance, for the purpose of this paper, which deals with the coma inside the contact surface, the expansion velocity was assumed to be a constant 900 m/s (cf. Lämmerzahl et al., 1987). The program allows for molecular point sources (near the nucleus) and for extended sources. We have used a point source for H_2O with a strength

corresponding to a H_2O density of 5×10^7 cm^{-3} at 1000 km from the nucleus (Krankowsky et al., 1986). Strengths of point sources or extended sources for the other neutral species given in Table 3 could be freely chosen. Many numerical integrations varying these source strengths were carried out in order to study the influence of individual components and combinations of components.

As discussed above, the mass scale can be influenced by various parameters including angle of incidence and ion speed. The results can be summarized as follows: With the mass scale given in Fig. 2, we find a reasonable set of molecular abundances that can reproduce the observed ion mass spectra in the mass per charge range 25 to 35. We have not been able to find an alternative mass assignment that could do this. For instance, a shift of all peaks by one unit to higher M/Q values could not be ruled out absolutely by the calibration data alone. However, we would have no explanation for a high abundance at M/Q = 34 along with a low abundance at M/Q = 35; e.g. H_2S would produce the opposite effect. Also, a relatively high flux of M/Q = 29 ions could not be explained: HCO^+ has to be lower than CO^+, and $C_2H_5^+$ or N_2H^+ react with H_2O with high rate constants.

A shift of all peaks by one unit to lower M/Q values would be difficult to reconcile with the calibration data. Moreover, it would again be difficult to find a chemical interpretation (cf. Table 2). For instance, it would be hard to explain the high abundance at M/Q = 30 that results with this mass scale.

On the other hand, the mass scale given in Fig. 2 results in relative abundance peaks inside the contact surface at the four mass

numbers corresponding to the products of H_3O^+ listed in column 3 of Table 2. In other words, the pattern in the mass range 25 to 35 finds a natural explanation. A careful comparison of this mass scale with the calibration data implies that the average arrival direction of the ions was ~0.3 degrees away from the optical axis of the entrance deflector of the HIS sensor and that the ions had an average radial speed of 900 m/s. These parameters also fit the lower mass ions given in Fig. 1, for which the mass assignment is not in question.

With the adopted mass scale, we interpret the spectra obtained between 1215 km and 3289 km as follows:

1. Because of their high proton affinity, H_2CO and CH_3OH dominate the mass range 25 to 35, being the parent molecules of the two most abundant ions (CH_3O^+ and $CH_3OH_2^+$).

2. The minimal ion abundances at masses 27, 29, and 34 are consistent with prediction. All ions listed in Tables 2 and 3 with these masses ($C_2H_3^+$, HCN^+, $C_2H_5^+$, N_2H^+, HCO^+, H_2S^+), and also $H_2O_2^+$, react with water.

3. The peak height at mass 28 is consistent with the HCN/H_2O abundance ratio of 0.001 derived by Schloerb et al. (1987) from radio frequency observations. CO^+ also contributes to the mass 28 peak but is not dominant.

4. The hydrocarbons C_2H_n are difficult to determine from the ion spectra. At this time, only upper limits can be given. The small peak at mass 26, if real, would be due to $C_2H_2^+$, rather than CN^+, since the latter is readily destroyed by water (Tables 1 and 2).

For the purpose of deriving molecular abundances, we have computed ion mass spectra as a function of distance from the nucleus, varying the proportions of the assumed parent molecules to optimize the fit. In Fig. 3, we compare such a computed spectrum, based on the abundances indicated, with the observed spectra at two radial distances straddling that of the computation. It is evident that the fit is quite reasonable. The sensitivity of the fit to variations in the parent molecule source strengths was investigated in order to establish ranges or limits.

As noted in Fig. 3, contributions from extended sources were assumed for some molecules. For these we assume an exponential depletion length of 10^4 km, originating at the nucleus. Such extended sources are indicated by the comprehensive CN-observations of A'Hearn et al. (1986) and Hoban et al. (1988), as well as by the mass spectrometer results for neutral CO (Eberhardt et al., 1987). While the need to include both point and extended sources is clearly indicated, both from the previous work and our data, the distance between the two experimental spectra given in Fig. 3 is too small for arriving at a reliable quantitative separation between them. For this, a complete investigation of the radial evolution of each ion in question would be required.

We emphasize that the molecular abundances shown in Fig. 3 are not unique in giving a reasonable agreement between theoretical and experimental spectra, considering the uncertainties in the experimental data and in the reaction rate constants. Definite abundance estimates can be obtained, however, for molecules having high PAs, because the ions resulting from their protonation dominate the mass

spectra. This is evident from Table 4 where the relative contributions to some relevant mass numbers are listed.

4. Molecular Abundances

Below, we give abundance estimates derived from a comparison of the results of the model calculations with the measured spectra in region I. We do not distinguish between point sources and extended sources for most molecular species. Some of the abundances might be improved by applying a more refined fitting programme to the data and by comparing experimental and theoretical ion abundances over the whole length of the trajectory inside the contact surface. However, we are confident that the resultant improvements would not materially alter the conclusions, and thus the added complexity of the modeling is not justified for the purposes of this paper.

Ammonia. NH_3 can be estimated from the NH_4^+/H_3O^+ ratio (Ip, 1986). Allen et al. (1987), using IMS data, applied this method to derive a NH_3/H_2O abundance ratio of .01 to .02; however, they neglected reactions of H_3O^+ with molecules heavier than water. Ip et al. (1990) pointed out that even relatively rare HCN influences the ammonia abundance thus derived. Now that we find a few to several percent of molecules with higher PA than water, we obtain a reduction of H_3O^+, which in turn somewhat reduces the estimate on the NH_3/H_2O ratio. The question of whether or not the ratio thus obtained is compatible with the NH_3/H_2O value of 0.003 derived from the NH_2 emission (Wyckoff et al., 1988) will be discussed in a separate paper.

Formaldehyde. The mass 31 ion rate falls off less rapidly than R^{-1} between 1215 km and 9814 km (cf. Fig. 2) in spite of the relatively short photo lifetime of H_2CO (cf. Table 2). From this, we derive a H_2CO source which is at least partly extended with an integrated strength (relative to water) of about one percent at 1500 km, rising to a few percent at the ionopause. The mass spectra measured in region II suggest that the source extends even farther out. Our results are in agreement with data obtained by other instruments. H_2CO has been found with the IKS infrared spectrometer on the VEGA 1 spacecraft (Combes et al., 1988; Mumma and Reuter, 1989). Polymeric formaldehyde has been inferred from the spectra obtained by the ion energy spectrometer PICCA onboard the GIOTTO spacecraft (Mitchell et al, 1987; Huebner, 1987) . Krankowsky (1990) found the formaldehyde molecule with the GIOTTO NMS mass spectrometer. He estimated a H_2CO abundance relative to water of 4.5 percent, including a contribution from an extended source.

Methanol. The peak at mass 33 could be protonated methanol or hydrazine. Stief and deCarlo (1965) and Delsemme (1975) have proposed that the 3360 Angström emission observed in comets is due to a NH radical, the precursor of which is hydrazine. Under the thermodynamic conditions in the solar nebula or the proposed sub-nebula (Fegley and Prinn, 1988), N_2H_4 would not be produced in significant amounts. Calculations show that the equilibrium ratio N_2H_4/N_2 for these two sites is only 2×10^{-38} and 3×10^{-29} at 300 K or 4×10^{-20} and 3×10^{-11} at 1500 K. The equilibrium ratio CH_3OH/CO is higher, especially in a sub-nebula environment. Also, there has been no mentioning of hydrazine production in interstellar clouds, whereas some ammonia and methanol are produced according to ion molecule reaction calculations (cf. Prasad

and Huntress, 1980; Leung et al., 1984). Moreover, if we wanted to identify the mass 33 peak with $N_2H_5^+$, we would have to postulate $N_2H_4/NH_3 \geq 1$ which seems implausible. Thus, we propose that the mass 33 peak is essentially due to $CH_3OH_2^+$ which leads to an estimate of the methanol/ water ratio of .003 to .015. This is the first in situ measurement of CH_3OH in a comet. However, methanol has also recently been found in comet Austin by millimeter observations (Colom et al., 1990).

Nitrous Oxide. The count rate at mass 30 places an upper limit of .005 on NO/H_2O. NO is usually not mentioned among possible cometary constituents. Since, however, theory indicates that NO is produced in dense interstellar clouds (Prasad and Huntress, 1980), it may be well to mention this NO abundance limit for Halley's coma.

Hydrogen Cyanide. The peak at mass 28 is probably mainly due to H_2CN^+. Although CO is the second most abundant molecule in Halley's coma (Eberhardt et al., 1987), the contribution of CO^+ is minor, because this ion reacts readily with water (cf. Tables 1, 2, and 4). If we assume that also C_2H_4 does not contribute very much, then we have enough H_2CN^+ to account for the $HCN/H_2O \sim .001$ abundance ratio derived from radio frequency observations (Schloerb et al., 1987) or from the CN emission (A'Hearn et al., 1986). Our estimate for the HCN abundance is higher than the one given by Ip et al. (1990).

Hydrocarbons. Since C_2H_6, C_2H_4, and C_2H_2 have PAs lower than water, they do not form ions with prominent abundances. However, the count rates at masses 25 and 26 indicate that some hydrocarbon ions are present in the mass range considered. While a careful analysis of

the abundances - particularly at even mass number - might produce some definite hydrocarbon estimates, we simply mention that as a result of our present modelling effort the sum of the abundances of acetylene and ethylene are at most one or two percent relative to water.

H_2S and S. The inclusion of S, H_2S and related ions was intended to allow for studying their contribution in the mass range considered. We defer a more complete discussion of the sulfur containing species to a later publication and discuss here only the abundance of H_2S, which has just been detected in comet Austin by millimeter observation (Colom et al., 1990). For comet Halley's coma, Marconi et al. (1990) derived a *lower* limit of 0.5 percent for the H_2S/H_2O ratio. However, their conclusion is based on a dissociation time for H_2S of $\sim$300 sec, which we consider to be erroneous for two reasons: (1) The photolysis of H_2S leads to SH which in turn dissociates in 118 sec (0.9 AU; Kim and A'Hearn, 1990) to give S. From atomic sulfur, S^+ is produced at a relatively high rate (Table B1). Thus, not only H_3S but also S^+ carries significant information on the occurrence of H_2S. Our model calculations clearly show that H_2S with a half percent abundance and a lifetime of only $\sim$300 sec would lead to a much higher ion abundance at mass 32 than we actually observe (cf. Fig. 3). (2) Using the cross section data given by Lee et al. (1967), Kim and A'Hearn (1990) have derived a photodissociation time for H_2S of 3200 sec (0.9 AU), a result we have confirmed. With this longer dissociation time, we have consistency between the masses 35 and 32 in the ion spectra and obtain a H_2S source strength (point source and/or extended source) of 0.001 to 0.004 relative to H_2O.

There is a significant change in the appearance of ion mass spectra in region II relative to region I (Figs. 1 and 2). As pointed out in Section 2, the distribution functions of the ions have changed significantly from the quiet flow encountered in region I. This makes it difficult to identify changes in ion abundances with the methods used in this paper, since these methods are based on the assumption of quiet flow conditions appropriate to region I.

While the perturbations in the spectra observed in the mass range 16-20 in region II have again disappeared in region III (Fig. 1), the high count rate at M/Q = 32 remains (Fig. 2). A slow build-up of M/Q = 32 actually begins between 2000 and 3000 km. Thus, this general increase in M/Q = 32 with increasing distance could be due to the S^+ ion. However, quantitative interpretation of the spectra in regions II and III needs further analyses, which we leave to future publications.

5. Discussion

The ions CH_3O^+ and $CH_3OH_2^+$ are derived from formaldehyde and methanol, respectively. Judging from ion-molecule reaction systematics, it seems improbable that heavier gaseous aldehydes, ketones or alcohols contribute significantly to these ions. Thus, we propose that both H_2CO and CH_3OH are present in the gas phase with the relative abundances indicated in Section 4. This observation neither precludes nor supports the possibility that H_2CO and/or CH_3OH are present in some polimerized form in the solid (Vanysek and Wikramasinghe, 1975; Huebner, 1987; Mitchell et al., 1987). The radial decrease of CH_3O^+ is less

than expected for a point source, indicating that H_2CO is released from grains over times of the order of hours.

The analysis offered here underlines that carbon in Halley's comet exists largely in oxidized form - at least the portion of it that is released into the gas phase within the first one or two hours.

Krankowsky et al. (1986a) have shown that the dominating peaks in the 40-50 mass region occur at M/Q = 45 and M/Q = 47, and they identify them as HCS^+ and H_3CS^+, respectively. We note that protonized *acetaldehyde* (CH_3CHO) and *ethylalcohol* (C_2H_5OH) may significantly contribute to these mass peaks.

Acknowledgements

The authors wish to acknowledge advice and comments by Drs. M.F. A'Hearn, M. Coplan, E.E. Ferguson, E. Herbst, and E. Kopp. They thank Mrs. Graziella Troxler for preparing the manuscript. This work was supported by the Swiss National Science Foundation. The research at JPL was done under a contract between the California Institute of Technology and NASA under the sponsorship of the Magnetospheric Physics program. The research at Lockheed was supported by NASA through contract NASW-4336 and Lockheed Independent Research. This paper was completed while E. Shelley worked as a Visiting Professor at the University of Bern, supported by the Bern Government, and while J. Geiss was a Visitor at the Institute of Science and Technology and the Space Physics Group of the University of Maryland in College Park and a National Academy/National Research Council Senior Associate at the NASA Goddard Space Flight Center, Greenbelt, MD.

Appendix A

The chemistry in the ionosphere - the region well inside the contact surface - of Halley's comet is dominated by photodissociation, photoionization, ion-molecule reactions, and dissociative recombination. Since these reactions and in particular the ion-molecule reactions connect a great variety of species in a rather non-systematic way, a large matrix of non-linear differential equations results.

The ionosphere is characterized by a steady expansion velocity of ∿0.9 km/s which is roughly equal for ions and neutrals (Krankowsky et al., 1986; Lämmerzahl et al., 1987) and by low kinetic temperatures (200-300 K; Balsiger et al., 1986a). Thus, the rate constants for ion- molecule reactions measured in the laboratory can be used.

We found reactions between neutrals (molecules or radicals) to be of minor importance for the species considered here; thus, we have neglected this type of reaction. In fact, the most important change in neutral abundances comes from photodissociation (and ionization) and this has been taken into account.

The ion abundances originally obtained from photoionization are thoroughly changed by ion-molecule reactions. On the other hand, for the neutral partners the relative importance of these ractions is small because of the relatively low abundance of the ions. Thus, we have neglected the changes in neutral abundances due to ion-molecule reactions. The types of reactions included in our model are given in the following equations (reactants or products for which the changes due to the reaction are taken into account in our calculations are underlinded):

$$\underline{A} + h\nu \rightarrow \underline{B} + \underline{C} + \ldots\ldots \quad (1)$$

$$\underline{A} + h\nu \rightarrow \underline{B^+} + \underline{e^-} + \underline{C} + \ldots\ldots \quad (2)$$

$$A + \underline{B^+} \rightarrow C + \underline{D^+} \quad (3)$$

$$\underline{B^+} + \underline{e^-} \rightarrow C + D \quad (4)$$

It is seen that with the simplifications introduced here, the first three types of equations are linear.

The set of differential equations corresponding to the reaction equations (1) to (4) is solved by stepwise integration over r, the distance from the nucleus. The relation between time t and r is given by the expansion velocity v(r) which was taken to be constant at 900 m/s. A backward integration scheme was chosen for the destruction terms, but not for the production terms which were treated according to the forward method. In this way, the differential equations are decoupled, and a matrix conversion procedure is avoided.

The reaction rates of equations (1) to (4) form one-, two- or three-dimensional arrays of real numbers. Since many elements in these arrays are empty, we have the code first establish arrays with integers 0 or 1 depending on whether the corresponding element in the real number array vanishes or not. These integer number arrays are interrogated at each integration step. Empty elements of the arrays are skipped; thus, a large number of useless real number multiplications are avoided. These simplifications led to a program which can be used in an interactive mode on a modest PC and the numbers of species and reactions considered can be easily changed.

Appendix B

A large number of photodissociation, photoionization, ion-molecule reaction and recombination rates are used in this investigation. However, only a part of these rates have a major influence on the relative abundances of ions and molecules discussed in Section 4. Therefore, we present in this paper the numerical values only for these important rate constants. References are given for the others.

Photodissociation and Photoionization

Rates corresponding to quiet solar conditions at 0.9 AU were used. Photoionization is of major importance for molecules that do not react with H_3O^+. The rate constants for the ions listed in column 4 of Table 2 are given in Table B1.

Ion-Molcule Reactions

Rate constants were taken from the following compilations: Anicich and Huntress (1986), Allen et al. (1987), Prasad and Huntress (1980), Giguere and Huebner (1978), Huebner and Giguere (1980). The most important rate constants, i.e. those for reactions with H_2O and H_3O^+, are given in Table 1. Atomic sulphur was introduced as a possible source of S^+ ions (cf. text); however, reactions of ions with S were not included.

Dissociative Recombination

Dissociative recombination is usually the dominant destruction mechanism for ions that do not react with water. The corresponding rates, evaluated at 273 K, are given in Table B2. Rates not found in the literature were estimated.

References

Adams, N.G., Smith, D.: 1988, Chemical Phys. Lett. 144, 11

A'Hearn, M.F., Hoban, S., Birch, P.V., Bowers, C., Martin, R., Klinglesmith, D.A.: 1986, Nature 324 649

Aikin, A.C.: 1974, Astrophys. J. 193, 263

Allen, M., Delitsky, M., Huntress, W.T., Yung, Y., Ip, W.-I., Schwenn, R., Rosenbauer, H., Shelley, E., Balsiger, H., Geiss, J.: 1987, Astron. Astrophys. 187, 502

Anicich, V.G. and Huntress, W.T.: 1986, Astrophys. J. Suppl. 62, 553

Ausloos, P.: 1974, Interaction Between Ions and Molecules, Plenum Press, New York and London, p. 415

Balsiger, H., Geiss, J., Young, D.T., Rosenbauer, H., Schwenn, R., Ip, W.-H., Ungstrup, E., Neugebauer, M., Goldstein, R., Goldstein, B.E., Huntress, W.T., Shelley, E.G., Sharp, R.D., Johnson, R.G., Lazarus, A.J., Bridge, H.S.: 1986, ESA-SP 169, 93

Balsiger, H., Altwegg, K., Bühler, F., Geiss, J., Ghielmetti, A.G., Goldstein, B.E., Goldstein, R., Huntress, W.T., Ip, W.-H., Lazarus, A.J., Meier, A., Neugebauer, M., Rettenmund, U., Rosenbauer, H., Schwenn, R., Sharp, R.D., Shelley, E.G., Ungstrup, E., Young, D.T.: 1986a, Nature 321, 330

Colom, P., Despoir, D., Bockelee-Morvan, D., Crovisier, J., Paubert, G.: 1990, to be published in the Proceedings of the Workshop "Observations of Recent Comets", Albuquerque, New Mexico, USA, June 1990

Combes, M., Moroz, V.I., Crovisier, J., Encrenaz, T., Bibring, J.-P., Grigoriev, A.V., Sanko, N.F., Coron, N., Crifo, J.F., Gispert, R., Bockelée-Morvan, D., Nikolsky, Yu. V., Krasnopolsky, V.A., Owen, T., Emerich, C., Lamarre, J.M., Rocard, F.: 1988, The 2.5 to 12 μm spectrum of comet Halley from the IKS-VEGA experiment, Icarus 76, 404

Delsemme, A.H.: 1975, Icarus 24, 95

Eberhardt, P., Krankowsky, D., Schulte, W., Dolder, U., Lämmerzahl, P., Berthelier, J.J., Woweries, J., Stubbemann, U., Hodges, R.R., Hoffman, J.H., Illiano, J.M.: 1987a, Astron. Astrophys. 187, 481

Eviatar, A., Goldstein, R., Young, D.T., Balsiger, H., Rosenbauer, H., Fuselier, S.A.: 1989, Astrophys. J. 339, 545

Fegley, B. Jr., Prinn, R.G.: 1988, in The Formation and Evolution of Planetary Systems, Eds. H.A. Weaver, F. Paresce, L. Danly, Cambridge U. Press, Cambridge

Giguere, P.T., Huebner, W.F.: 1978, Astrophys. J. 223, 638

Goldstein, R., Young, D.T., Balsiger, H., Bühler, F., Goldstein, B.E., Neugebauer, M., Rosenbauer, H., Schwenn, R., Shelley, E.G.: 1987, Astron. Astrophys. 187, 220

Gringauz, K.I., Gombosi, T.I., Tátrallyay, M., Verigin, M.I., Remizov, A.P., Richter, A.K., Apàthy, I., Szemerey, I., Dyachkov, A.V., Balakina, O.V., Nagy, A.F.: 1986, Geophys. Res. Lett. 7, 613

Heppner, R.A., Walls, F.L., Armstrong, W.T., Dunn, G.H.: 1976, Phys. Rev. A, 13, 1000

Hoban, S., Samarasinha, N.H., A'Hearn, M.F., Klinglesmith, D.A.: 1988, Astron. Astrophys. 195, 331

Huebner, W.F.: 1987, Science 237, 628

Huebner, W.F., Giguere, P.T.: 1980, Astrophys. J. 238, 753

Huntress, W.T.: 1977, Astrophys. J. Suppl. 33, 495

Ip, W.-I., 1986: Adv. Space Res. 5, 233

Ip, W.-I., Balsiger, H., Geiss, J., Goldstein, B.E., Kettmann, G., Lazarus, A.J., Meier, A., Rosenbauer, H., Schwenn, R., Shelley, E.G.: 1990, Giotto IMS Measurements of the Production Rate of Hydrogen Cyanide in the Coma of Comet Halley, Ann. Geophys., in press

Kim, S.J., A'Hearn, M.F.: 1990, unpublished

Krankowsky, D., Lämmerzahl, P., Herrwerth, I, Woweries, J., Eberhardt, P., Dolder, U., Herrmann, U., Schulte, W., Berthelier, J.J., Illiano, J.M., Hodges, R.R., Hoffman, J.H.: 1986, Nature 321, 326

Krankowsky, D., Eberhardt, P., Berthelier, J.J., Dolder, U., Hodges, R.R., Hoffman, J.H., Illiano, J.M., Lämmerzahl, P., Schulte, W., Stubbemann, U., Woweries, J.: 1986a, Proc. 20th ESLAB Symposium on the Exploration of Halley's Comet, Heidelberg, 27-31 October 1986, ESA SP-250, Vol. I, 381

Krankowsky, D.: 1990, The composition of comets, in Comets in the Post-Halley Era, Eds. R.L. Newburn, J. Rahe, Kluwer Academic Publishers, Dordrecht, p. 1

Lämmerzahl, P., Krankowsky, D., Hodges, R.R., Stubbemann, U., Woweries, J., Herrwerth, I., Berthelier, J.J., Illiano, J.M., Eberhardt, P., Dolder, U., Schulte, W., Hoffman, J.H.: 1987, Astron. Astrophys. 187, 169

Lee, L.C., Wang, X., Suto, M.: 1987, J. Chem. Phys. 86, 4353

Levine, J.S.: 1985, The Photochemistry of Atmospheres, Academic Press, Orlando, Appendix I

Leung, Ch. M., Herbst, E., Huebner, W.F.: 1984, Astrophys. J. Suppl. Ser. 56, 231

Marconi, M.L., Mendis, D.A., Korth, A., Lin, R.P., Mitchell, D.L., Rème, H.: 1990, Astrophys. J. 352, L 17

McGowan, J. Wm., Mitchell, J.B.A.: 1984, Electron-Molecule Interactions and Their Applications, Vol. 2, ed. L.G. Christophorou, Academic Press, Orlando, p. 65

Meier, A.: 1988, Ph.D. Thesis, University of Bern

Mitchell, D.L., Lin, R.P., Anderson, K.A., Carlson, C.W., Curtis, D.W., Korth, A., Rème, H., Sauvaud, J.A., d'Uston, C., Mendis, D.A.: 1987, Science, 237

Mumma, M.J., Reuter, D.: 1989, Astrophys. J. 344, 940

Neubauer, F.M., Glassmeier, K.H., Pohl, M., Raeder, J., Acuna, M.H., Burlaga, L.F., Ness, N.F., Musmann, G., Mariani, F., Wallis, M.K., Ungstrup, E., Schmidt, H.U.: 1986, Nature 321, 352

Neubauer, F.M.: 1987, Astron. Astrophys. 187, 73

Prasad, S.S., Huntress, W.T.: 1980, Astrophys. J. suppl. 43, 1

Radzig, A.A., Smirnow, B.M.: 1980, Reference Data on Atoms, Molecules, and Ions, Springer, Berlin, p. 438

Schloerb, F.P., Kinzel, W.M., Swade, D.A., Irvine, W.M.: 1987, Astron. Astrophys. 187, 475

Schmidt, H.U., Wegmann, R., Huebner, W.F., Boice, D.C.: 1988, Computer Physics Communications 49, North-Holland, Amsterdam, 17

Stief, L.J., deCarlo, V.J.: 1965, Nature 4974, 889

Vanysek, V., Wickramasinghe, N.C.: 1975, Astrophys. Space Sci. 33, L19

Wegmann, R., Schmidt, H.U., Huebner, W.F., Boice, D.C.: 1987, Astron. Astrophys. 187, 339

Wyckoff, S., Tegler, S., Wehinger, P., Spinrad, H., Belton, M.J.S.: 1988, Astrophys. J. 325, 927

Figure Captions

Fig. 1. Nine mass spectra in the AMU/e range 12 to 24 obtained in the H-mode of the HIS sensor. Distances to the nucleus are indicated. The spectra obtained in the three regions of the inner coma described in the text are distinguished by solid lines (region I), dashed lines (region II), and short dashed lines (region III).

Fig. 2. The same spectra as in Fig. 1 for the AMU/e range 25 to 35.

Fig. 3. Relative ion densities derived from the N-mode data at 1485 km (diamonds and bold dashed line) and 1950 km (triangles and fine dashed line) from the nucleus. These experimental spectra are compared with a model ion spectrum (crosses and solid line) which was calculated at the intermediate distance of 1717 km with the molecular abundances shown in the insert. S_p indicates a point source and S_E indicates an extended source ($R^{-2}e^{-R/10000}$).

Table 1. Proton affinities (PA) and rate constants k_1, k_2

	PA (eV)	k_1		PA (eV)	k_2
NH_3	8.9	2.2	C_2H_4 [3]	7.1	< .001
			C_2H_6	6.9	2.95
C_2H_5OH	8.16	2.8	C_2H_2	6.7	.22
CH_3CHO	8.07	3.6	HCO	6.6	3.0
CH_3OH	7.9	2.8	OH	6.18	2.89
N_2H_4	7.9 [1]		CO	6.15	2.6
HCOOH	7.81	2.7	CH_4	5.7	2.5
H_2CO	7.5	3.4 [2]	CO_2	5.68	2.2
HCN	7.43	4.0	NO	5.5	--
H_2S	7.4	1.9	CH_3	5.4	≤ .01
			N_2	5.1	2.5
			CN	∿5	3.2
H_2O	7.20		O_2	4.38	< .001
			H_2	4.38	7.3

Proton Affinities from Radzig and Smirnow (1980) and Ausloos (1974)

Rate constants k_1 and k_2, defined in the text, in 10^{-9} cm^3 s^{-1} from Anicich and Huntress (1986)

[1] from dissociation constant

[2] the reverse reaction has a rate of $\sim.23\times10^{-9}$ cm^3 s^{-1}

[3] $k_1 = .06\times10^{-9}$ cm^3 s^{-1}

Table 2. Inner coma: Ions in the 25-35 mass range[1]

Parent Molecules	Photo lifetime[2] (s)	Ions in Relation to Abundances of Parent Molecules: Major Ions Produced by H_3O^+	Long-lived[3] Ions Produced by Photons	Minor Ions Destroyed by H_2O
H_2S (34)	3.2×10^3	H_3S^+ (35)		H_2S^+ (34) HS^+ (33)
CH_3OH (32)	3.1×10^3	$CH_3OH_2^+$ (33)		CH_3OH^+ (32)
S (32)	9×10^5		S^+ (32)	
H_2CO (30)	2.9×10^3	CH_3O^+ (31)		H_2CO^+ (30)
NO (30)	2.4×10^5		NO^+ (30)	
C_2H_6 (30)	4.9×10^4			$C_2H_6^+$ (30) $C_2H_7^+$ (31)
C_2H_4 (28)	1.9×10^4		$C_2H_4^+$ (28)[6]	$C_2H_5^+$ (29)[6]
CO (28)	1.3×10^6			CO^+ (28) HCO^+ (29)
N_2 (28)	8.1×10^5			N_2^+ (28) N_2H^+ (29)
HCN (27)	7.7×10^5	H_2CN^+ (28)		HCN^+ (27) CN^+ (26)
C_2H_2 (26)	2.6×10^4		C_2H^+ (25)[4] $C_2H_2^+$ (26)[5,6]	$C_2H_3^+$ (27)[6]

1] Mass numbers in parenthesis

2] 0.9 AU; data from Levine (1985); Kim and A'Hearn (1990)

3] Not destroyed by H_2O

4] Possibly also produced by He^+ near and outside the contact surface

5] Slowly reacting with H_2O (cf. Table 1)

6] Various hydrocarbons may contribute to this ion

Table 3. Molecules and Ions Included in the Coma Model Calculations

Molecules

H, H_2, O, OH, H_2O

C, CH_4, C_2H_2, C_2H_4, C_2H_6

N, NH_3, HCN, N_2, NO

CO, H_2CO, CH_3OH, CO_2

S, H_2S

Ions

H^+, H_2^+, O^+, OH^+, H_2O^+, H_3O^+

C^+, CH_2^+, CH_3^+, CH_4^+, CH_5^+

C_2H^+, $C_2H_2^+$, $C_2H_3^+$, $C_2H_4^+$, $C_2H_5^+$, $C_2H_6^+$, $C_2H_7^+$

N^+, NH^+, NH_2^+, NH_3^+, NH_4^+

HCN^+, H_2CN^+, N_2^+, N_2H^+, NO^+

CO^+, HCO^+, H_2CO^+, H_3CO^+, CH_3OH^+, $CH_3OH_2^+$

CO_2^+, HCO_2^+

S^+, HS^+, H_2S^+, H_3S^+

Table 4. Relative contributions of ions to some important mass numbers. These percentages refer to the theoretical ion mass spectrum shown in Fig. 3.

Mass-28	Mass-30	Mass-31	Mass-32	Mass-33
H_2CN^+ = 69%	NO^+ = 87%	H_3CO^+ = 100%	CH_3OH^+ = 62%	$CH_3OH_2^+$ = 99%
CO^+ = 20%	H_2CO^+ = 12%		S^+ = 38%	SH^+ = 1%
$C_2H_4^+$ = 11%	$C_2H_6^+$ = 1%			

Table B1. Photoionization rates at 0.9 AU

Molecule	Ion	Rate 10^{-7} s^{-1}
H_2O	H_2O^+	4.1
CO	CO^+	3.8
NO	NO^+	16.0
C_2H_2	$C_2H_2^+$	9.6
C_2H_2	C_2H^+	.9
C_2H_4	$C_2H_4^+$	7.2
C_2H_4	$C_2H_2^+$	2.5
S	S^+	12.0

Data are for quiet solar condition (Levine, 1985; Appendix I) at 0.9 AU

Table B2. Dissociative recombination rates with electrons at 273 K

Ion	k (10^{-7} cm^3 s^{-1})	
NH_4^+	15.9	(a)
H_3O^+	10	(a,b)
C_2H^+	5.7	(a)
$C_2H_2^+$	5.7	(a)
$C_2H_4^+$	10	(d)
H_2CN^+	3.5	(c)
NO^+	4.6	(a)
CH_3O^+	10	(d)
$CH_3OH_2^+$	8.8	(c)
H_3S^+	3.7	(c)

(a) McGowan and Mitchell (1984)
(b) Heppner et al. (1976)
(c) Adams and Smith (1988)
(d) estimate

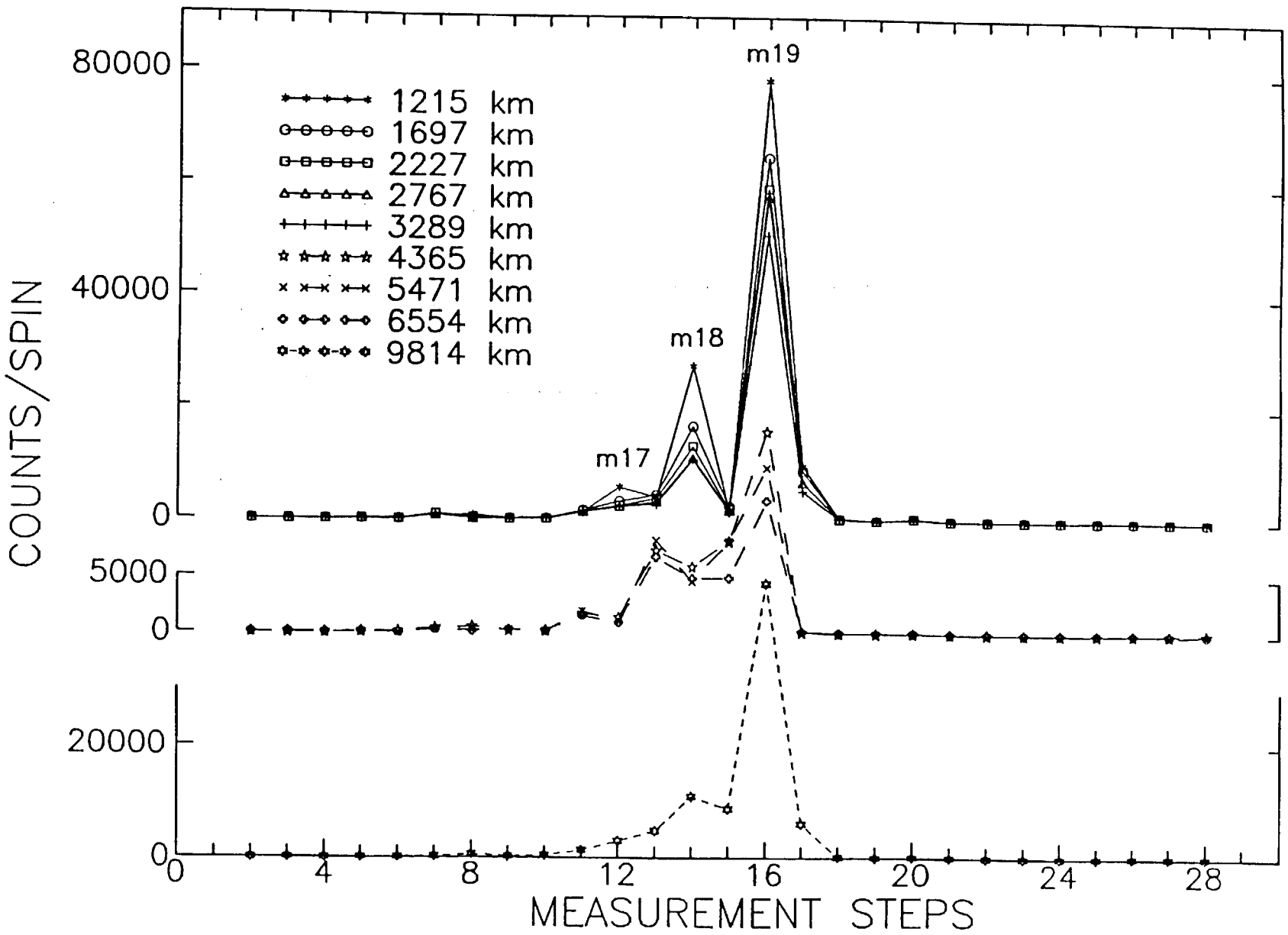
80000
40000
0
5000
0
20000
0
0
4
8
12
16
20
24
28
COUNTS/SPIN
MEASUREMENT STEPS
m17
m18
m19
1215 km
1697 km
2227 km
2767 km
3289 km
4365 km
5471 km
6554 km
9814 km

Fig. 1

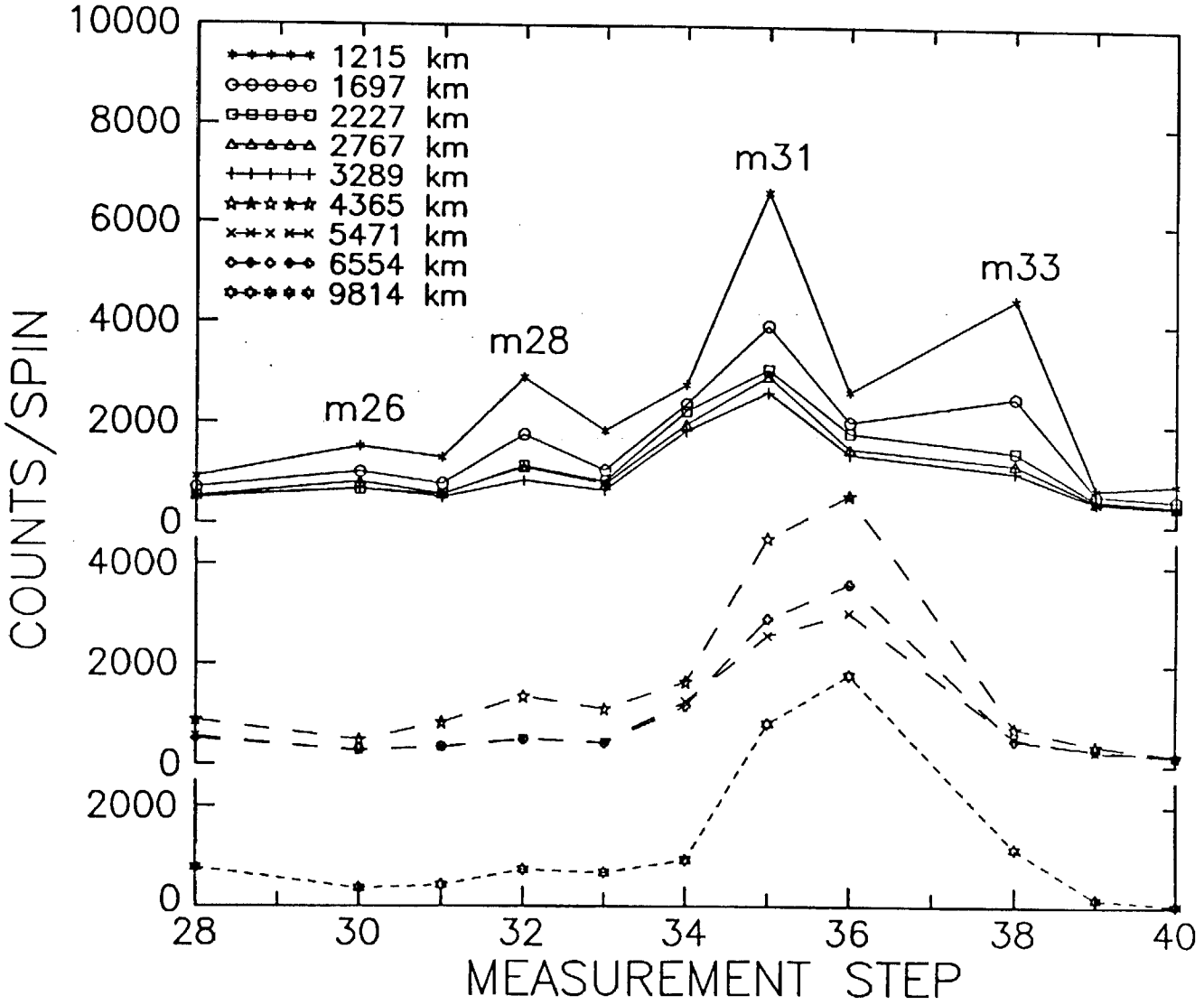
10000
8000
6000
4000
2000
0
4000
2000
0
2000
0
COUNTS/SPIN
1215 km
1697 km
2227 km
2767 km
3289 km
4365 km
5471 km
6554 km
9814 km
m26
m28
m31
m33
28
30
32
34
36
38
40
MEASUREMENT STEP

Fig. 2

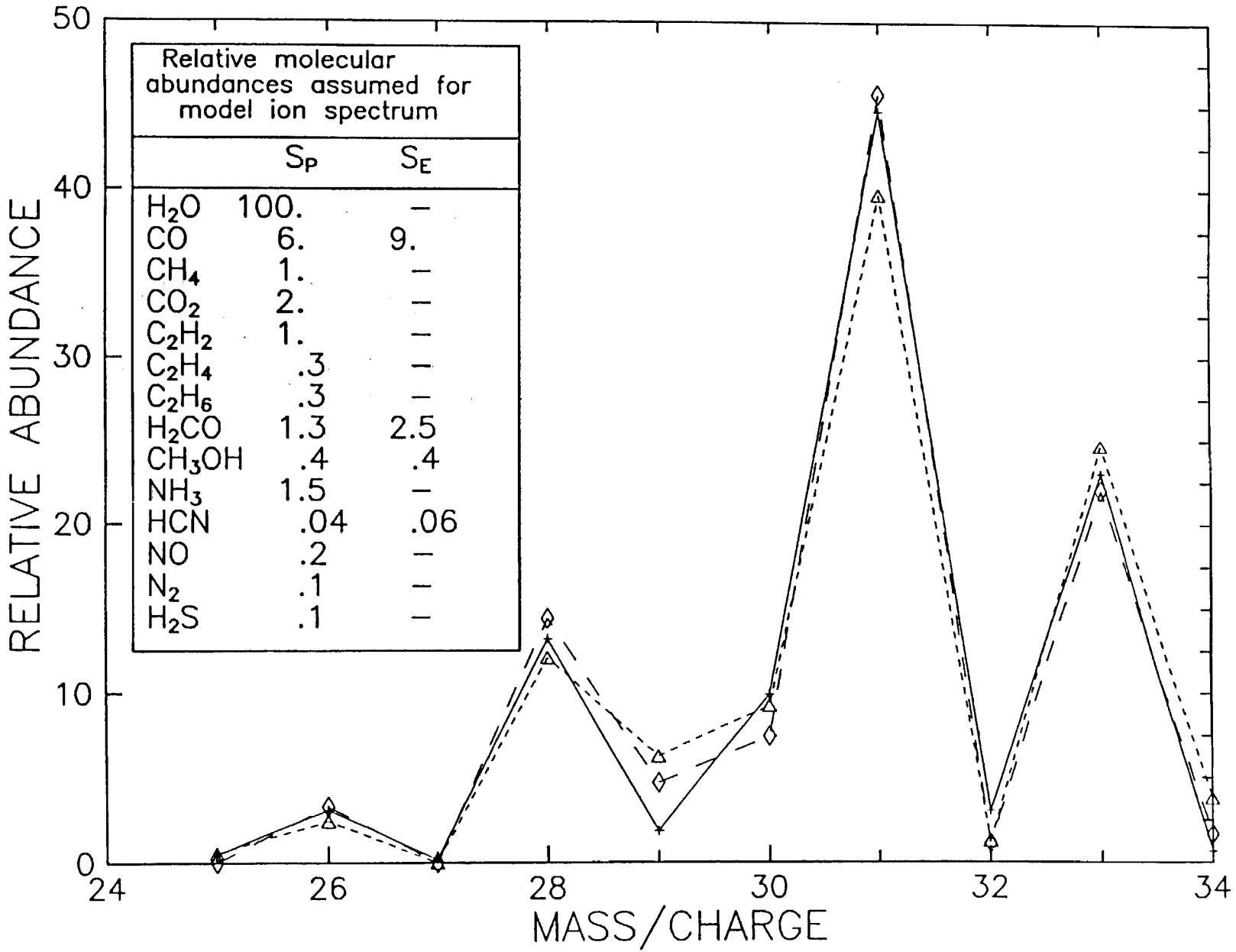
Relative molecular abundances assumed for model ion spectrum
S_P S_E
H_2O 100. –
CO 6. 9.
CH_4 1. –
CO_2 2. –
C_2H_2 1. –
C_2H_4 .3 –
C_2H_6 .3 –
H_2CO 1.3 2.5
CH_3OH .4 .4
NH_3 1.5 –
HCN .04 .06
NO .2 –
N_2 .1 –
H_2S .1 –
RELATIVE ABUNDANCE
0
10
20
30
40
50
24
26
28
30
32
34
MASS/CHARGE

Fig. 3